Role of Androgen Receptor in Hypothalamic Regulation of Metabolism and Reproduction

by

Alexandra Louise Cara

A dissertation submitted in partial fulfillment
of the requirements for the degree of
Doctor of Philosophy
(Molecular and Integrative Physiology)
in the University of Michigan
2021

Doctoral Committee:

Professor Carol F. Elias, Chair
Professor Suzanne M. Moenter
Professor Martin G. Myers, Jr
Professor Diane Robins

Alexandra Louise Cara

acara@umich.edu

ORCID iD: 0000-0002-2140-2573

DEDICATION

To my parents, Martha and John, for nurturing my love of science as a child, and my family for their support.

And to the mice whose lives were sacrificed for these studies, for without research animals, the advancement of science and medicine would not be possible. We owe countless lives to their contribution.

ACKNOWLEDGEMENTS

The Elias lab, thank you for your support, friendship, and camaraderie.

My advisor Carol. I am so lucky to have you guide me through my PhD. And my committee, Sue, Martin, and Didi, for believing in me when I didn't believe in myself.

My PhD cohort – Liz, Jon, Natalie, Sammi, Ian, Thomas. Thank you for being there when I needed a beer after a long day in lab.

Our collaborators in the Moenter lab, especially Dr. Laura Burger and Beth Wagenmaker for assistance with experimental design and analysis.

Thanks to Dr. Karel de Gendt and Dr. S. Marc Breedlove for the AR^{flox} mouse line, Dr. Rich Auchus and the Metabolomics Core for consultation and hormone assays, and Wendy Rosebury-Smith and the In-Vivo Animal Core for histology assistance and tissue processing.

The work presented in this dissertation was conducted at The University of Michigan, Ann Arbor, on land that was stewarded by Niswi Ishkodewan Anishinaabeg: The Council of Three Fires (Ojibwe, Odawa, and Potawatomi), and their neighbors, the Seneca, Delaware, Shawnee, and Wyandot nations.

TABLE OF CONTENTS

LIST OF TABLES

TABLE

LIST OF FIGURES

FIGURE

ABSTRACT

Androgens are steroid hormones that have sex-specific effects on regulation of metabolic and reproductive physiology. Androgens primarily act upon nuclear hormone receptors, including androgen receptors (AR), or estrogen receptors (ERs) after conversion to estradiol by aromatase. Adult males typically have higher levels of circulating androgens. However, imbalance of androgens outside the homeostatic range has both reproductive and metabolic deficits for both sexes. For example, hypoandrogenism in males and hyperandrogenism in females can result in infertility, obesity, and increased risk of diabetes. While many tissues express AR and are sensitive to the effects of androgens, the brain is a key androgen responsive organ. In adults, AR is expressed in many brain regions, including those that are involved in regulation of reproduction, metabolism, behavior, cognition, mood, and autonomic processes. Yet, characterization of AR expression has been lacking in the female and prepubertal brain. Here, we present a comprehensive neuroanatomical characterization of *Ar* mRNA expression in the mouse brain of both sexes, and compare adult and prepubertal expression. We found that expression of *Ar* undergoes dynamic change during a critical window of prepubertal development in male and female mice. Furthermore, we describe brain regions that may preferentially respond to androgens, rather than estrogens. For example, the ventral premammillary nucleus (PMv) shows dense expression of AR-immunoreactivity in both sexes, yet it is relatively low in ERs and aromatase. To identify neuronal populations that are targets of androgen action, we compared areas of dense AR expression, including the PMv and arcuate nucleus (ARH), with known neuronal populations in these nuclei.

AR was found to be coexpressed in PMv and ARH leptin receptor (LepRb) neurons, which are crucial in regulation of energy homeostasis and exert permissive effects on fertility. We hypothesized that androgens acting via AR in LepRb cells contribute to the regulation of reproduction and metabolism at the hypothalamic level, and that loss of AR from LepRb cells would disrupt reproductive and metabolic homeostasis. We found that deletion of AR from LepRb cells ($LepRb^{\Delta AR}$) results in sex-specific changes in the neuroendocrine reproductive axis, locomotor activity, and body composition. We observed that loss of negative feedback actions of sex steroids induces an exaggerated rise in luteinizing hormone in $LepRb^{\Delta AR}$ male mice and in follicle stimulating hormone in $LepRb^{\Delta AR}$ female mice. Furthermore, female $LepRb^{\Delta AR}$ mice show increased lean mass, while male $LepRb^{\Delta AR}$ mice display increased ambulatory activity. Subsequently, we tested if deletion of AR from LepRb neurons would protect female mice from hyperandrogenism-induced reproductive deficits. Female mice exposed to androgen excess during late prenatal development exhibit disrupted estrous cycles, infertility, and mild metabolic changes during adulthood. This phenotype replicates many features of polycystic ovary syndrome (PCOS), which is also partly characterized by androgen excess. We found that female mice with deletion of AR in LepRb neurons had improved estrous cycles with prenatal androgenization compared to their AR-intact littermates. Our findings highlight that LepRb neurons represent an important target of androgen action in the brain, and contribute to sex-specific differences in the neuroendocrine reproductive axis and some aspects of metabolic regulation. Furthermore, LepRb neurons may be involved in the pathogenesis of PCOS. These studies further elucidate the specific targets of androgens in the brain, and open the possibility of additional mechanistic study into the physiologic actions of androgens, especially in females.

CHAPTER 1

Introduction

Biology of androgens

Androgens are a class of steroid hormones that are traditionally known for their role as male sex hormones which promote male traits, including development of male reproductive organs, secondary sex characteristics, and reproductive physiology. However, a contemporary understanding of androgens includes important roles in female physiology as well. Hormones classified as androgens include testosterone (T) and dihydrotestosterone (DHT), while dehydroepiandrosterone (DHEA), dehydroepiandrosterone sulfate (DHEA-S), and androstenedione (A4) are considered as androgenic pro-hormones. The predominant circulating androgen in males is testosterone (T), which is primarily produced in Leydig cells. Testicular T production is responsible for relatively higher levels of circulating androgens in males compared to females.

Androgens are also produced by the ovary and adrenal gland (1). Ovarian androgens are synthesized by theca cells, with A4 and T serving as precursors for estrogen synthesis in granulosa cells (17β-estradiol, or E2, and estrone, or E1)(2). In humans, the adrenal gland is responsible for production of androgenic precursors, including DHEA, DHEA-S, and A4, with minor production of T and 11-oxyandrogens (11-OH-testosterone and 11-OH-androstenedione)(3,4). Peripheral

tissues also contribute to androgen synthesis. For example, adipose tissue expresses steroidogenic enzymes capable of steroid conversion, androgen synthesis, and inactivation (5,6).

Androgens in circulation

Androgens in circulation are primarily bound to sex-hormone binding globulin (SHBG), which in humans, is primarily produced by the liver (7,8). A majority of T and DHT are transported while bound to SHBG (~45-80%), which binds testosterone with high affinity, albeit at low capacity. A smaller fraction of T is bound to lower affinity, but higher capacity, serum proteins, including albumin, corticosteroid-binding globulin, and orosomucoid (9-11). The rodent liver does not produce SHBG past the prenatal period, however, androgen binding protein (ABP), an SHBG homologue, is produced by the testes (12,13). Only approximately 1-2% of T in circulation remains unbound (9,10). It has been traditionally thought that when bound to carrier proteins in circulation, androgens are unable to exert biologic effects via hormone receptors, and were considered biologically inactive. This so called "free hormone hypothesis" predicted that once reaching target tissues, T would dissociate from binding proteins, and become bioavailable for binding to receptors or enzymes for conversion (14,15). However, this hypothesis is disputed. Multiple mechanisms of bound-T uptake and intracellular signaling have been described (11). SHBG-bound T can be internalized via endocytosis mediated by membrane proteins such as megalin. Upon internalization, vesicles containing SHBG-bound T fuse with lysosomes, and T dissociates from SHBG. Free T can then diffuse to the cytoplasm, and interact with androgen receptors (AR) (16,17). In addition to hormone binding sites, SHBG has a binding site that interacts with membrane SHBG-receptors. The ligand-bound SHBG and membrane receptor complex can then activate G-protein coupled intracellular signaling (18,19). Additionally, extracellular matrix

associated proteins, including fibulins, can interact with ligand-bound SHBG. Matrix proteins may provide scaffolding to facilitate interaction with other membrane receptors, or may sequester ligand-bound SHBG extracellularly (20). Each of these mechanisms provides additional complexity to regulate tissue access to androgens and their bioavailability to AR.

Levels of circulating androgens are dependent on sex and age. Following testis differentiation and maturation in fetal humans, T peaks at 11-17 gestational weeks, then decreases until term (21). Following birth, males experience a surge in luteinizing hormone (LH) which triggers a peak in T lasting up to 12 hours in humans (22). The post-natal hypothalamic-pituitary-gonadal (HPG) axis is transiently reactivated during a short period of time called the "mini-puberty of infancy", that occurs following the removal and inhibitory actions of placental and maternal hormones with birth. Increasing gonadotropin releasing hormone (GnRH) from the hypothalamus results in raised LH, leading to elevated T in male infants between 1 and 3 months of age (23,24). The HPG axis remains quiescent in both sexes through the rest of childhood, until the pubertal transition begins. In humans, circulating T typically reaches adult levels in males by Tanner stage IV or V (25,26), while in adult females, T will remain only a fraction of male levels (adult male range ~222-848 ng/dL total T, adult female T range ~3-52 ng/dL total T) (27,28). Small but significant rises in T have been detected during the mid-follicular and luteal phases of the ovarian cycle (29,30). Male total and free T decline progressively with age (31,32), and lower levels of T are observed post-menopause (30,33)

Steroidogenesis of androgens

Androgens, like other steroid hormones, consist of a four ring, carbon structure backbone derived from cholesterol. Cholesterol is intracellularly synthesized via acetate, stored in intracellular lipid

droplets, or is taken up by circulating lipoproteins (34). Free cholesterol is transported between the outer and inner mitochondrial membranes by steroid acute regulatory protein (StAR). Cholesterol side-chain cleavage enzyme (cytochrome P450 side-chain cleavage enzyme 11a, CYP11A) converts cholesterol to pregnenolone in the first and rate-limiting step of steroidogenesis (35). Pregnenolone is then released to the smooth endoplasmic reticulum to undergo 17α-hydroxylation via 17α-hydroxylase (cytochrome P450c17, CYP17, also performs 17,20 lyase activity) to form 17α-hydroxypregnenolone. CYP17 then converts 17α-hydroxypregnenolone to DHEA, which is then converted to androstenediol (A5) via 17β-hydroxysteroid dehydrogenase (17βHSD), and finally from A5 to T via 3β-hydroxysteroid dehydrogenase (3βHSD) (36). T is primarily synthesized via the so called Δ^5 pathway (Δ^5 indicating the double bond at carbon 5 in pregnenolone, 17α-hydroxypregnenolone, DHEA, and A5). Alternatively, T may be synthesized via the Δ^4 pathway, which proceeds from pregnenolone being converted to progesterone via 3β-hydroxysteroid dehydrogenase (3βHSD). Progesterone is subsequently converted to 17α-hydroxyprogesterone, then to androstenedione (A4) via 17α-hydroxylase/17,20-lyase. A4 is then converted to T via 17βHSD (Figure 1.1).

Differences in expression of steroidogenic enzymes in endocrine tissues results in diverse production of hormones, including androgens. A good example is the adrenal gland, where in humans, only the zona reticularis is capable of producing androgenic precursors (DHEA and DHEA-S) (37). The zona glomerulosa does not express CYP17 (17α-hydroxylase/17,20-lyase), so steroidogenesis proceeds towards corticosteroid and aldosterone production. The zona fasciculata expresses CYP17, but has little 17,20-lyase activity, so progesterone and 17-hydroxyprogesterone are shuttled toward corticosteroid production rather than producing DHEA. The zona reticularis expresses CYP17 which performs both 17α-hydroxylase and 17,20-lyase activity, producing

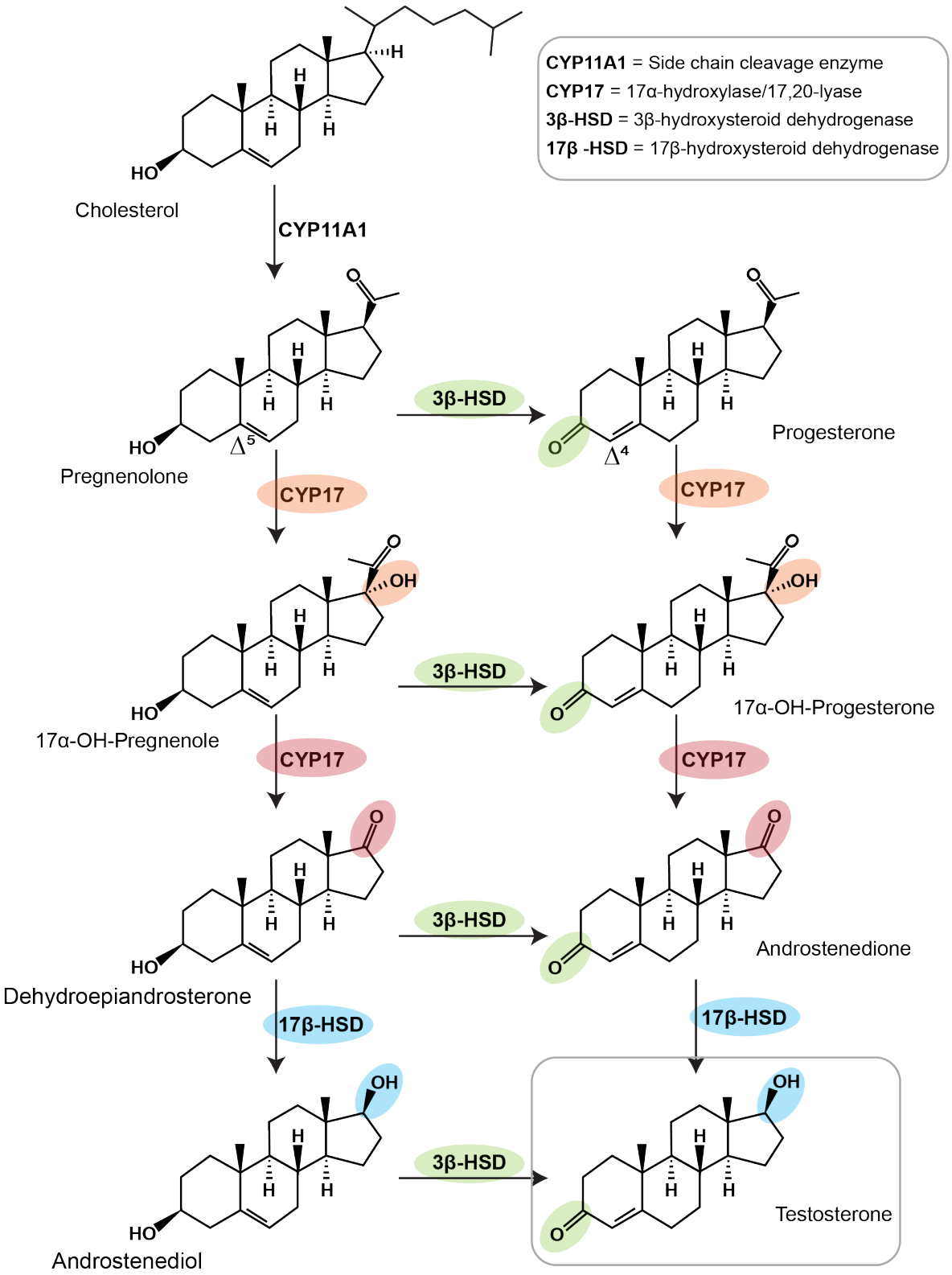

Figure 1.1: Steroidogenesis of Androgens. Synthesis of androgens by key steroidogenic enzymes, beginning with cholesterol.

DHEA. Due to low 3βHSD expression, only small amounts of A4 and T are synthesized by the zona reticularis (35).

Intermediate hormones in the synthesis of T, such as DHEA, have weak androgenic effects and binding to androgen receptors (AR). They are therefore better considered as pro-androgens or androgenic precursors rather than "weak androgens" (37). Notably, the adrenal gland of mice and rats does not express CYP17, and therefore is not capable of producing adrenal androgens (38).

The gonads in mice and rats are the main organ responsible for production of bioactive androgens, such as T and A4. In the testis, 3βHSD and 17βHSD are highly expressed in Leydig cells, ensuring that available DHEA is converted to A4 and T (35). Ovarian androgen production occurs primarily in theca cells, which express all enzymes needed to complete steroidogenesis up to T (1,39). Theca steroidogenic enzymes are regulated via LH, which upon binding to its receptor, initiates a G-protein coupled signal transduction cascade that stimulates CYP11A, CYP17, 3βHSD, and 17βHSD expression (40-43). Theca cells produce A4 and T, which are used as estrogen precursors by granulosa cells (44). This reaction is catalyzed by the enzyme aromatase (cytochrome P450aro, CYP19A1), which eliminates the methyl group (carbon #19, thus forming 18-carbon estrogens) and aromatizes the A ring (45) (Figure 1.2). Aromatase in the granulosa cell is under regulation of follicle-stimulating hormone (FSH) (46,47), and converts T to E2 and A4 to E1. Other tissues also express aromatase, including the placenta, certain brain regions, adipose tissue, and bone (48).

T can be further metabolized to the highly potent androgen DHT via 5α-reductase (5α-R) (Figure 1.2). Three isozymes of 5α-R have been described, each transcribed by three separate genes, i.e.,

type I 5α-reductase encoded by *SRD5A1*, type II 5α-reductase by *SRD5A2*, and type III by *SRD5A3* (49). Tissue expression of each isozyme differs. Type I 5α-R is mostly expressed in the liver, skin (scalp, torso, sebaceous glands), adrenal gland, and kidney, and type II 5α-R is expressed in reproductive tissues (prostate, seminal vesicles, epididymis, testes), skin (face, chest, external genitalia), liver and hair follicles (50). Type III 5α-R has a more ubiquitous expression pattern in a wider variety of tissues, but it rather participates in lipid metabolism, not steroidogenesis (51). DHT is primarily an intracellular metabolite and does not widely circulate in blood. Although, high production of DHT in tissues such as prostate can lead to spillover of DHT into circulation. A key feature of DHT is its inability to be aromatized to estradiol. However, DHT can be converted to estrogenic metabolites, including 3β-androstanediol (3β-diol) via 3βHSD and 3α-androstanediol (3α-diol) via 3αHSD (52,53). Notably, DHT is a potent androgen and binds with high affinity to androgen receptors.

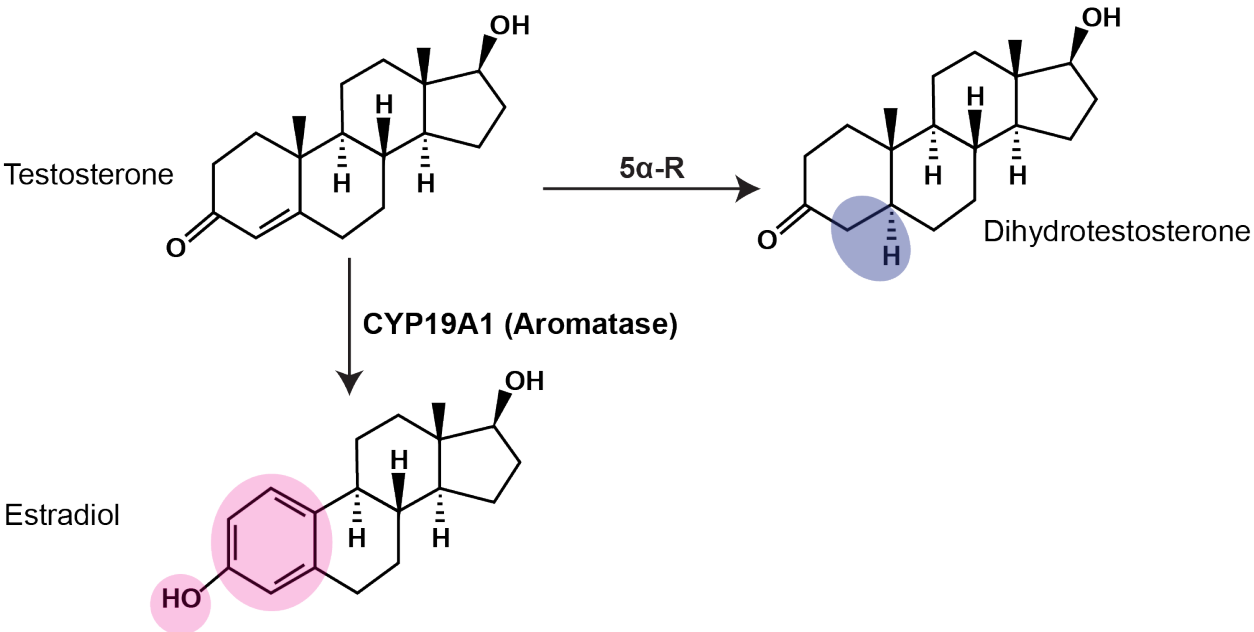

Figure 1.2: Amplification and Diversification of Testosterone. Conversion of testosterone to dihydrotestosterone via 5-alpha-reductase (5α-reductase) to amplify androgenic signaling via androgen receptors, and to estradiol via CYP19A1 (aromatase) to diversify androgen signaling via estrogen receptors.

Androgen Receptors

Androgens exert biologic actions by binding to either androgen receptors (AR) or to estrogen receptors (ERs) after aromatization. AR belongs to a super family of steroid hormone nuclear receptors and is encoded by a single gene (*Ar*) located on the X chromosome. *Ar* is composed of 8 exons which encode 3 functional domains (54,55) (Figure 1.3). The N-terminal domain (exon 1) has transactivation properties, and is required for AR-induced transcription of target genes (56,57). The DNA-binding domain (exons 2 and 3), along with the N-terminal domain, facilitates binding of the receptor to DNA androgen-response elements (ARE) (58), located within promoter or enhancer regions up or downstream of androgen target genes (59). AREs consist of a pair of inverted repeated palindromic sequences separated by three nucleotide spacer (60), which facilitates binding of an AR dimer. The DNA-binding domain is separated from the ligand-binding domain by a hinge region, encoded by part of exon 4. The C-terminal ligand-binding domain (part of exon 4, and exons 5-8) is responsible for ligand interaction and confers specificity of AR for androgens (61). Within the ligand-binding domain is the C-terminal activation function 2 (AF2) sequence, that provides transactivation function in a ligand-dependent manner.

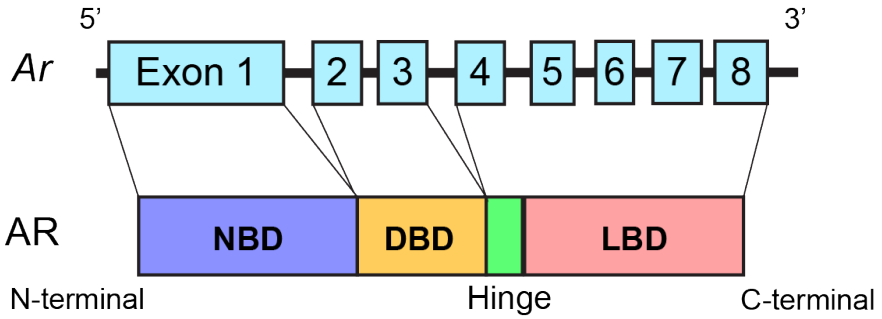

Figure 1.3: Androgen Receptor Gene and Protein Organization. The androgen receptor (*Ar*) gene consists of 8 exons (upper figure). Androgen receptor (AR) protein consists of N-terminal (NTD), DNA (DBD), and ligand-binding domains (LBD), with a hinge region in between the DBD and LBD.

AR shares sequence conservation with progesterone (PR), glucocorticoid (GR), and mineralocorticoid receptors (MR) in the DNA-binding and C-terminal ligand binding domains, yet

relative binding assays demonstrate a high-affinity of AR to endogenous androgens (55). DHT binds much more strongly to AR than T, with a relative binding affinity of 94-180% of T (62,63). However greater concentrations of T can achieve greater AR binding (64).

When in the ligand-unbound state, AR remains in the cytoplasm forming complexes with heat-shock proteins (Hsp). Binding of androgens to the ligand-binding domain induces a conformational change in the receptor, causing dissociation of Hsp and allowing for AR to homodimerize. Homodimeric AR may be phosphorylated and translocated to the nucleus, a process enabled by the nuclear localization signal region spanning between the hinge and DNA-binding region (55). AR then binds to ARE and recruits additional transcriptional co-regulators, either co-activators or co-repressors of gene transcription. Included in the recruited transcriptional machinery are histone acetyltransferases (HAT) that remodel chromatin to an open, accessible state to facilitate transcription of target genes, steroid receptor co-activators (SRC-1), and RNA polymerase II (65). The AF2 region enables the formation of the transcriptional machinery complex at a promoter and enhancer region, allowing for the transcription of AR target genes. Androgens acting on AR may also repress gene expression via the recruitment of a transcriptional repressive complex, consisting of the nuclear receptor corepressor (NCoR) and silencing mediator of retinoid and thyroid receptors (SMRT), and histone deacetylases (HDAC) which causes chromatin to become tightly packed and inaccessible for transcription (66).

In addition to the canonical genomic, transcriptional activity of AR, non-genomic actions of AR signaling have been described. Rapid effects of androgens on cells that cannot be attested to the slower transcription of target genes and translation of proteins have been demonstrated. Ligand-

bound AR can trigger intracellular signaling cascades, such as the PI3K/Akt pathway (67), or the MAPK pathway, by interacting with cellular-Src tyrosine kinase at the inner face of the plasma membrane (68). Membrane-associated AR can also activate G-protein coupled signaling to open membrane calcium channels which increase intracellular calcium, leading to activation of PKC, PKA, and/or MAPK/ERK pathways (69). It has also been suggested that DHT when converted to 3α-diol can bind to γ-aminobutyric acid type A receptors ($GABA_AR$), triggering influx of chloride into cells resulting in hyperpolarization (70,71). Additionally, DHEAS can allosterically antagonize $GABA_AR$, resulting in reduction in $GABA_AR$ currents (72-74). Crosstalk between AR and other signaling pathways have also been described, including growth factor receptor (insulin-like growth factor 1 and epidermal growth factor) signaling (75), MAPK signaling, and cytokine (TNFα , IL-6) signaling pathways (76).

Androgens may also signal via non-AR membrane bound receptors that are unrelated to steroid hormone nuclear receptors. Several multi-functional membrane proteins have been proposed to act as membrane-AR, including transient receptor potential cation channel M8 (TRPM8), G-protein coupled receptors OXER1 and GPCR6A, and the zinc-transporter Zrt Irt-like protein ZIP9 (77,78). While novel membrane androgen receptors are an interesting development, the work in this dissertation focuses only on the classic nuclear AR, whose effects on gene expression have been better described. Additionally, the majority of characterized and validated experimental models of AR deletion involves loss of the classic AR nuclear receptor.

Androgens auto-regulate AR, and depending on the tissue or cell type, may either up or down regulate *Ar* mRNA expression. Castration-induced androgen deprivation results in increased *Ar*

mRNA in the ventral prostate, seminal vesicles, epididymis, kidney (79-81), pre-optic area and pituitary (82) of adult male rats. In contrast, *Ar* mRNA decreases in the hippocampus (83), and shows no change in testis with castration (81). Studies focused on androgen regulated expression of AR protein have also shown increases in AR in prostate and seminal vesicles (79), and decreased AR in efferent ductules and brain (84) with gonadectomy (85,86). The cause for these differences is not yet clear but may reflect differences in tissue-specific regulation of AR expression.

Experimental approaches to investigate actions of androgens on AR

Androgens have a variety of physiologic effects via AR in both male and female tissues. Distinct roles of AR have been elucidated by examining mutation or deletion of androgen steroidogenic enzymes or AR in clinical cases and preclinical animal models. Loss of function mutations in AR lead to either complete or partial androgen insensitivity syndrome (AIS), depending on the location and type of mutation. Features of AIS are replicated in the testicular feminization (Tfm) mouse (87) and rat models (88,89), including feminization of external genitalia and intra-abdominal testes in XY males, and resistance to the effects of androgens. Global loss of AR function due to mutation is useful for examining the overall effect of AR on phenotype, but does not necessarily provide organ, tissue, or cell specificity of AR action. Additionally, AR dysfunction can be induced by a variety of different mutations with differing degrees of severity in phenotype. Experimental female offspring are also extremely difficult to produce, as Ar^{Tfm} males are infertile, and only possess one copy of the mutated AR. Molecular genetic approaches have been utilized to generate global-, tissue-, or cell-specific deletion of AR, or AR "knockouts" (ARKO), to overcome the difficulties of working with Tfm rodent models.

The Cre/loxP technology is the most common method to generate genetically-modified animal models in a conditional fashion. It uses the P1 bacteriophage-derived enzyme cyclization recombination (Cre), which recognizes a pair of inverted 34 base pair loxP (locus of crossing over in P1) sites, resulting in recombination of the "floxed" sequence of DNA (90) (Figure 1.4). Several AR-flox mouse lines have been generated, with loxP sites flanking exon 1 (91-93), exon 2 (94,95), or exon 3 (96,97). Recombination of the floxed sequence in exons 1 or 2 results in premature stop codons in *Ar* mRNA, and lack of transcription of remaining exons, leading to loss of AR protein expression (98). The AR-flox model recombining exon 3, however, results in an in-frame mutation where AR protein is expressed, can bind to ligand, but does not express a portion of the DNA-binding domain, and therefore is unable to induce gene transcription but can still elicit non-genomic actions (96). Of note, excision of exon 2 does not eliminate AR signaling via novel membrane bound AR (77,78). Therefore, rapid membrane effects via androgens may still be possible.

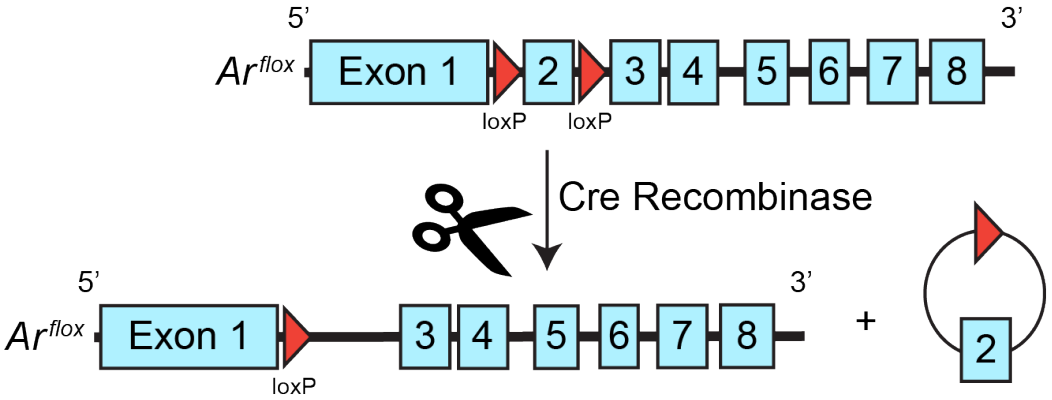

Figure 1.4: Cre-mediated Recombination of Exon 2 of the Mouse Androgen Receptor. Exon 2 of *Ar*^{flox} mouse is flanked by two loxP sites, which are recognized by the enzyme Cre recombinase. Presence of Cre results in recombination, and excision of the target gene plus one loxP site.

To drive tissue- or cell-specific deletion of target floxed genes, Cre can be conditionally expressed by insertion of the Cre transgene under control of tissue or cell-specific promoters. Global, or body-wide ARKO are generated using strong, widely-expressed promoters to drive Cre

expression, including the human cytomegalovirus (CMV), beta-actin, or phosphoglycerate kinase 1 (PGK) promoters. Tissue-specific Cre expression and subsequent ARKO have been generated for many tissues, including testes (Leydig and Sertoli cells), ovary (granulosa and theca cells), pituitary, brain, muscle, adipose, bone, liver, and skin. Effects of ARKO in various tissues will be discussed further below.

Physiologic effects of androgens

Development and Sexual differentiation:

Sex differentiation of the reproductive tract is one of the earliest effects of androgens acting on AR. Prior to sex differentiation, embryos contain two undifferentiated duct systems, Wolffian and Müllerian, which give rise to either the male or female reproductive tract, respectively (99,100). After differentiation of testes from bipotential gonads, fetal Leydig cells begin secreting A4, which is converted to T by fetal Sertoli cells (101,102). T then diffuses to nearby AR-expressing Wolffian ducts, where it promotes differentiation into seminal vesicles, vas deferens, and epididymis (103,104). Anti-Müllerian hormone (AMH) produced by Sertoli cells promotes regression of Müllerian ducts so that only Wolffian ducts will be present in differentiated males (105-107). Conversion of T to DHT via 5αR is required for virilization of the external genitalia, including penis and scrotum development, urogenital sinus development into prostate, and male-typical urethra (108,109). The requirement of androgens for the development of the male-typical reproductive tract and external genitalia has been clearly demonstrated by studies using mutations in AR. For example, Tfm rodents and 46,XY patients with complete AIS display feminized external genitalia, with a short, blind-ended vagina, small phallus, absence of epididymis, vas deferens, seminal vesicles, and prostate. Global ARKO males display similar phenotype to Tfm

males, with overall feminized appearance of external genitalia and lack of secondary and accessory reproductive organs (94,96).

Male Reproductive Function:

The role of androgens and AR are crucial for male reproductive physiology, especially in the testes where androgenic actions are critical for proper spermatogenesis and androgen production. Overall, with mutation of AR (Tfm) or global ARKO, testes are small and remain intra-abdominal, leading to infertility (94,96). However, androgens acting via AR play different roles in cells of the testes, including Sertoli and Leydig cells. Sertoli cells are the nurse cells of the testis, whose primary role is to nourish and provide support for developing germ cells, maintaining the blood-testis barrier, making up part of the seminiferous tubules along with peritubular myoid cells, and secreting AMH during sex differentiation. AR expression in Sertoli cells is stimulated by FSH and androgens produced in nearby Leydig cells (110). Transgenic AMH-Cre mice have been used to drive Sertoli cell-specific ARKO (SCARKO), as AMH is expressed early in testicular development and is exclusive to immature Sertoli cells. SCARKO mice display reduced testis mass and are infertile due to arrest of spermatogenesis during meiosis at the pachytene spermatocyte stage (94,111,112). The blood-testis barrier is also disrupted in SCARKO mice, due to decreased expression of tight junction related components (113,114). However, the ability for Sertoli cells to secrete AMH and trigger sexual differentiation of the reproductive tract is not impaired, and SCARKO mice develop a male typical reproductive tract, accessory organs, external genitalia, with the exception of the seminiferous tubules, which are smaller and do not develop a lumen.

Androgens are also important for Leydig cell function. Leydig cells are interspersed throughout the interstitial space surrounding the seminiferous tubules and are the primary cell responsible for producing T. LH stimulates T production by the Leydig cell, which feeds back to AR expressed in Leydig cells in an autocrine manner (115,116). AR is essential for promoting maturation and development of Leydig cells in adult males (117,118), but is dispensable for fetal Leydig cells, whose function is androgen independent. Leydig cell-specific ARKO (LCARKO) mice that have been generated using Cre-driven by the AMH-receptor 2 (*Amhr2*) promoter display infertility, decreased mass of testes and epididymis, arrested spermatogenesis at the spermatocyte stage, and reduced levels of T (119,120). However, *Amhr2* is expressed in cells other than Leydig (121,122), limiting the conclusions that can be drawn from this line.

Androgens acting via AR are required for the maintenance and homeostasis of adult male accessory glands, including the epididymis, vas deferens, seminal vesicles and prostate, which are highly androgen dependent (123). Loss of androgens via castration or pharmacologic blockade of AR results in decreased mass of seminal vesicles (124), and atrophy and deterioration of prostate gland structures via apoptosis (125,126).

Sufficient levels of androgens are required to maintain male reproductive function and secondary sex characteristics. Hypoandrogenism in males, or androgen deficiency, is generally defined as total T levels below the lower end of the reference range in eugonadal males (below ~300-350 ng/dL)(127,128). While male androgen levels naturally decline with age (129), primary hypogonadism (defect in testicular T production) or secondary hypogonadism (defect in hypothalamic GnRH or pituitary LH/FSH production) can result in clinical androgen deficiency.

Androgen deprivation therapy for the treatment of androgen-dependent cancers (i.e., prostate cancer) will also result in hypoandrogenism, and can be achieved via orchidectomy, GnRH agonists or antagonists, or AR antagonists (130). Hypoandrogenism in males can cause decreased sperm production and infertility, regression or lack of development of secondary sex characteristics, and reduced libido or sexual dysfunction, (127,131,132).

Since males typically have a high concentration of circulating androgens, symptoms of elevated androgens beyond the typical male range may not be readily apparent (133). Endogenous androgen excess in males is uncommon and may be attributed to androgen-secreting adrenal or testicular tumors, or congenital adrenal hyperplasia. It may manifest as precocious puberty, increased body and muscle mass, gynecomastia, or acne (134-136). Male androgen excess may also be attributed to abuse of anabolic steroids or misuse of T prescriptions. Supraphysiologic doses of T may be used for their desired anabolic effects in skeletal muscle, to stimulate erythropoiesis, and gain advantage in competitive sports. However, long-term exogenous androgen excess in males leads to suppression of the HPG axis due to constant negative feedback, causing decreased spermatogenesis and infertility (137).

Female Reproductive Function:

Androgens also play an important role in female reproduction, including ovarian folliculogenesis, particularly during early follicle growth (138). In ovaries, AR is expressed in granulosa, theca, stromal cells, and oocytes (139-142). Developing follicles begin expressing AR at the primary stage, with expression increasing during transition to secondary and pre-antral, reaching a peak in small antral follicles. Androgens acting via AR reduce atresia and enhance expression of FSH

receptors, which promotes growth of pre-antral follicles (143). Mouse models of ARKO have been useful in dissecting the populations of AR expressing cells required for these effects. Female Tfm and global ARKO mice display reduced fertility, which is attributed to decreased ovarian follicle counts and premature ovarian insufficiency (92,95,97,144). Ovaries from granulosa cell-specific ARKO (GCARKO) mice show an increase in preantral and unhealthy atretic follicles, leading to subfertility and premature ovarian insufficiency (145,146). The phenotype of GCARKO mice closely mimics that of the global ARKO, indicating that many of the negative effects on fertility are due to loss of AR in granulosa cells. Contrarily, loss of AR specific to theca cells (ThARKO) does not result in any changes to fertility, pubertal onset, or serum T or E2 (147).

AR is expressed throughout the female reproductive tract, including the Fallopian tube epithelium (148,149), uterine endometrium and myometrium (150), vaginal stroma and epithelium (151,152). Cyclic changes in ovarian estradiol levels induce changes in AR expression in the female reproductive tract. For example, estradiol upregulates AR in the uterus and vagina (153,154). Experimental reduction in estradiol via ovariectomy results in decreased *Ar* mRNA in the mouse uterus and vagina, which is restored with administration of estradiol (151). In the uterus, androgens modulate proliferation of the myometrium and endometrium (155). Global loss of AR in mice results in altered uterine morphology, with elongated and smaller diameter uterine horns (156). Androgens also have physiologic effects on vaginal physiology, often in synergy with estrogens. They regulate epithelial function (157), mucin production (158,159), maintenance of innervation (160,161), and local blood flow (162,163). Additionally, vaginal tissues express steroidogenic enzymes needed to synthesize androgens, and can convert DHEA to T and/or DHT, indicating intracrine androgen actions (164). Vestibular glands (major or Bartholin's glands, and minor or

Skene's glands) of the female vulva, which are the equivalent of the male bulbourethral gland, also depend on androgens and AR for proper mucous production and vaginal lubrication (165).

In contrast to the stimulatory role in some tissues of the reproductive tract, androgens negatively impact mammary gland development in an age-specific manner. During embryonic development, androgens acting via AR promote the regression of primordial mammary tissues in males (166), while development of mammary tissue continues in females that do not produce androgens during embryogenesis. Postnatally, AR is expressed in epithelial and stromal cells of the mammary glands (167). Androgens inhibit mammary gland maturation by suppressing E2-induced epithelial proliferation and breast development during puberty (168,169).

While androgen levels in females are typically much lower than males, hypoandrogenism can have negative effects on female fertility and sexual health (170). Female androgen insufficiency can be caused by age (menopause), primary or secondary hypogonadism, adrenal insufficiency (leading to loss of androgenic precursors DHEA and DHEAS), oral contraceptive pills, premature ovarian insufficiency, or oophorectomy (171). However, since accurate female androgen levels are difficult to obtain without liquid chromatography and mass spectrometry (LC/MS)-based methods (172,173), there is no set of clinical guidelines to define female androgen deficiency. Nonetheless, supplementation of DHEA for those with low functional ovarian reserve undergoing *in vitro* fertilization treatments has proven beneficial for some patients (174).

Elevated androgens, however, prove much more consequential for female reproductive health. Androgen excess in females can be a result of androgen-secreting adrenal or ovarian tumors,

Cushing's syndrome, adrenal hyperplasia, pregnancy, or drug induced androgen excess, but most commonly, polycystic ovary syndrome (PCOS) (175,176). Consequences of hyperandrogenism in females include excessive male pattern body and facial hair growth (hirsutism), androgenic alopecia, increased acne, oligo or anovulation, subfertility or infertility, insulin resistance, abdominal obesity, increased risk of type 2 diabetes, dyslipidemia, increased risk of cardiovascular disease, and increased depression and anxiety. Levels of total T in female hyperandrogenism are elevated relative to the typical range of female values, but usually do not reach that of the typical adult male range, i.e., male total T = ~222 – 848 ng/dL, female total T = ~3 – 52 ng/dL, PCOS total T = ~23 – 138 ng/dL (28). In certain cases of severe biochemical hyperandrogenism caused by androgen producing tumors, female total T may overlap with the typical adult male range, i.e., androgen producing tumor average female total T range = ~185 – 410 ng/dL (177). Androgenic precursors such as DHEA/DHEA-S and A4 may also be elevated, depending on the origin of hyperandrogenism (ovarian vs adrenal), and pre vs post-menopausal status. For example, post-menopausal patients with PCOS may show greater relative elevations in A4, rather than T (176).

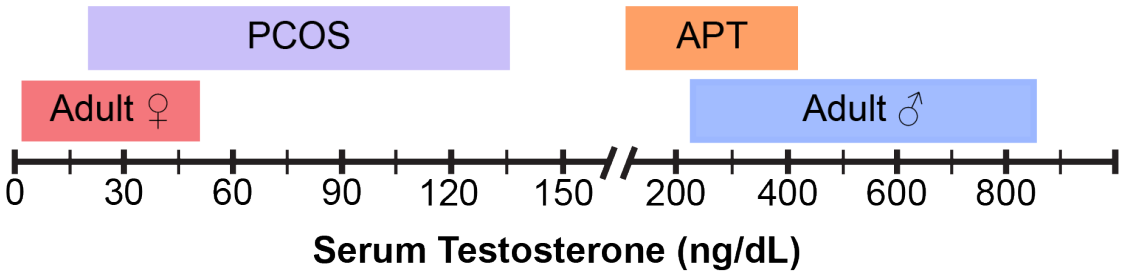

Figure 1.5: Adult serum testosterone levels. Range of typical total testosterone for adult males and females, and female polycystic ovary syndrome (PCOS) and androgen producing tumor (APT).

Since AR is expressed in multiple reproductive and HPG axis tissues, increases in female androgens can have diverse physiologic outcomes. For example, despite being a heterogeneous syndrome, many patients with PCOS exhibits similar neuroendocrine and ovarian changes. GnRH

neurons display continuous increased pulse frequency (178-181), which preferentially drives pituitary LH over FSH production (182,183). Increased LH pulse frequency and amplitude drives increased ovarian androgen production by theca cells. Excessive androgen action on AR drives proliferation of preantral follicles and depletes the primordial follicle pool (184,185). Smaller, non-dominant follicles also inappropriately respond to LH and undergo premature luteinization (186). Without a rise in FSH during the follicular phase, no dominant follicle is selected, resulting in early antral follicle arrest. Without ovulation of a mature follicle, no corpus luteum is formed and progesterone remains low. Lack of a drop in progesterone during the late luteal phase needed to trigger shedding of the endometrium, along with chronic E2 stimulation, results in a buildup of endometrial tissue (187,188). Elevated androgens also reduce hypothalamic sensitivity to progesterone, decreasing progesterone-mediated negative feedback action on GnRH pulses (189). These effects together lead to a vicious cycle of increased GnRH, LH, and ovarian androgens.

Effects in metabolic regulation

Androgens have notable effects on the regulation of energy balance and body composition through sex-specific actions on a variety of metabolic tissues. Male ARKO mice develop obesity later in life due to decreased energy expenditure and reduced brown adipose tissue thermogenesis, insulin resistance, impaired glucose tolerance, and accumulation of triglycerides in skeletal muscle and liver (190-192). Male global ARKO mice replicate phenotypes seen in human males with hypoandrogenism, including increased adiposity, and decreased muscle mass and bone density (193).

Interestingly, elevated androgens in females usually promote metabolic dysfunction similar to androgen deficiency in males. Female hyperandrogenism can decrease insulin sensitivity in

muscle, liver, and adipose tissue, diminish liver glycogen synthesis, promote visceral adipose accrual by increasing adipocyte size and inhibiting lipolysis, and cause beta cell dysfunction via increased basal hypersecretion of insulin, and inadequate or exaggerated glucose-induced insulin secretion (194-197). Overall, these impairments increase the risk of type 2 diabetes and metabolic syndrome.

The metabolic changes seen in hypoandrogenic males and hyperandrogenic females highlights the impact of sex-specific changes in androgen levels in multiple organs (197,198). To dissect out the role of androgens acting via AR on different metabolic organs, several tissue-specific ARKO models have been generated. For example, liver-specific ARKO results in hepatic steatosis and insulin resistance in high-fat diet fed male mice (199), indicating that androgens prevent excess lipid accumulation under normal physiologic conditions. Lack of AR in white adipose tissue, results in decreased body weight and hyperinsulinemia early in life in male mice. Eventually, these mice develop deficiencies in insulin secretion and become hyperglycemic (200).

Skeletal muscle is a major target of androgenic action, with general anabolic effects. Certain skeletal muscles display greater dependence on androgens than others. For example, muscles responsible for control of the penis (e.g., levator ani) that are innervated by the sexually-dimorphic spinal nucleus of the bulbocavernosus (SNB) are highly androgen dependent (201-203). AR is expressed in myofibers, satellite cells (muscle stem cells), fibroblasts, and mesenchymal stem cells (204,205). Deletion of AR from satellite cells results in decreased grip strength, decreased mass of androgen-dependent muscles (levator ani), and fiber type switching in the soleus muscle in male

mice (206). Additionally, decreased muscle strength and maximal force production in the hindlimbs was also observed in male myofiber-specific ARKO mice (207).

Androgens also contribute to pancreatic endocrine function. Beta cells, the endocrine component of the pancreas responsible for producing insulin, express AR, and DHT can enhance glucose-stimulated insulin secretion (GSIS) in beta cell cultures (208). Loss of androgens or AR in male rodents can lead to impaired glucose homeostasis, as castration and/or ARKO in male rodents leads to a reduction in beta cell mass, impaired insulin secretion, and glucose intolerance (209,210). Furthermore, male mice with deletion of AR from beta cells display impaired glucose tolerance and reduced insulin secretion in response to glucose (208).

Brain as a Link for Sex-Specific Androgen Actions in Reproduction and Metabolism

While the effects of androgens acting on AR are important for homeostasis of peripheral tissues, androgens can impact reproduction and energy homeostasis via direct actions in the brain. The brain is a highly androgen-sensitive organ. AR is expressed throughout the hypothalamus, telencephalon, thalamus, and brainstem of both sexes (211-216). In males, T during a critical window of prenatal brain development is necessary for permanent organizational changes which masculinize and defeminize the brain, leading to male-typical behaviors and physiology later in life (217). However, in rodents, the majority of these effects is attributed to androgens acting via estrogen receptors (ERα, ERβ) after aromatization, as mice with deletion of both ERα and ERβ fail to display male-typical sexual behavior (mounting) during adulthood (218). Loss of aromatase expression also results in reduced male-typical behavior (219). While estrogens play a dominant

role in the organization of a male-typical brain, loss or mutation of AR also results in reduction or abolition of male-typical sexual behavior and aggression (220-223).

While AR may not play a significant role in the organizational programming of the brain, it is required for executing male-typical behaviors in mature rodents. Interestingly, primates do not show the same dependence on estrogens for brain sexual differentiation as do rodents, and androgens acting via AR are the dominant mechanism driving male-typical differentiation in primates (224,225). In addition to deficits in behaviors, neuron-specific ARKO (NARKO) mice show disruption in growth, with decreased body mass and serum insulin-like growth factor 1 (IGF1), and disrupted HPG axis (226). Female NARKO mice show altered ovarian follicle dynamics due to dysregulated kisspeptin and LH release (227).

AR contributes to negative feedback regulation of the HPG axis. GnRH neurons located in the hypothalamus release GnRH at the median eminence, which is transported through the pituitary portal vessels to gonadotropes in the anterior pituitary gland. GnRH stimulates gonadotropes to release LH and FSH, which in turn stimulate Leydig and Sertoli cells, respectively. T produced by Leydig cells circulates back to the hypothalamus and pituitary gland and exerts negative feedback, which maintains levels of gonadotropins and T within homeostatic range.

At the level of the hypothalamus, T decreases GnRH pulse frequency, which in turn results in decreased LH pulse frequency, amplitude, and mean serum LH (228,229). These effects are demonstrated through castration, which removes negative feedback from the gonads. Castration leads to increased GnRH neuron firing rate, increased GnRH release at the median eminence, and

increased LH pulse frequency, which can be reversed by treatment with T (230-233). Negative feedback actions of androgens are mediated via both androgenic and estrogenic pathways (AR and ER), as both DHT and estradiol reduce serum LH and increase LH interpulse-interval in castrated male sheep (234,235). However, only estradiol reduces GnRH neuron firing in castrated male mice (236). The contribution of both AR and ER in the hypothalamus and pituitary in HPG axis negative feedback likely represents redundant mechanisms to ensure proper control. However, GnRH neurons themselves do not express detectable levels of either AR or ERα (237-239), so the negative feedback effect of T is likely via neurons upstream of GnRH neurons.

Kisspeptin is one of the most potent stimulators of GnRH release via signaling through the G-protein coupled receptor GPR54 (aka, Kiss1R) (240). Kisspeptin neurons are located in the forebrain, including the anteroventral periventricular nucleus (AVPV) and the arcuate nucleus of the hypothalamus (ARH), where kisspeptin is coexpressed with neurokinin and dynorphin (KNDy) (241). Notably, kisspeptin neurons are sensitive to sex steroids, and express ERα and/or AR (242,243). Androgens influence *Kiss1* mRNA expression in both the AVPV and ARH. For example, castration of male mice leads to increased *Kiss1* in the ARH (242). In addition to influencing gene expression, androgens can modulate kisspeptin neuronal activity. In male mice, DHT inhibits long-term episodic activity in ARH kisspeptin neurons (244). Although the role of estrogens in both negative and positive feedback actions is well described in females, the role of androgens acting upon AR is poorly understood. Nonetheless, female mice with neuron-specific ARKO display reduced *Kiss1* mRNA in the AVPV, but increased *Kiss1* in the ARH during proestrus (227), indicating that androgens acting via AR may regulate *Kiss1* expression in females

as well. These studies reflect the importance of neuronal AR in regulating neuroendocrine output upstream of GnRH neurons.

In addition to kisspeptin-expressing neurons, multiple other pathways converge upon GnRH and/or kisspeptin neurons in HPG axis regulation. One of such critical inputs is the melanocortin system. The hypothalamic melanocortin system consists mainly of two distinct groups of neurons in the ARH, i.e., neurons that coexpress pro-opiomelanocortin (POMC) and cocaine- and amphetamine-regulated transcript (CART), and those that coexpress neuropeptide Y (NPY) and agouti-related peptide (AgRP) (245-247). POMC/CART and NPY/AgRP neurons are the first order neurons that sense metabolic signals, including leptin, insulin, and ghrelin. Leptin increases activity of POMC/CART neurons, but inhibits NPY/AgRP neurons, resulting in an overall anorectic effect which decreases food intake and increases energy expenditure (248-250). In addition to regulating energy homeostasis, melanocortin neurons also modulate the reproductive axis via direct actions in kisspeptin neurons (251-255). Activation of NPY/AgRP neurons or fibers results in inhibition of kisspeptin neurons (256), and decreased LH pulse frequency (257). Conversely, kisspeptin stimulates POMC neurons, and indirectly inhibits NPY/AgRP neurons (258).

While metabolic cues have well-described effects on the reproductive neuroendocrine axis, gonadal hormones can act to modulate overall hypothalamic sensitivity to metabolic hormones, including leptin and insulin. For example, gonadal hormones modulate patterns of food intake and energy expenditure in a sex-specific manner (259-261). These effects are mediated in part through direct actions on POMC and/or NPY/AgRP neurons, as a subset of each neuronal population

coexpress AR. Castration-induced loss of androgens results in decreased *Pomc* mRNA in the male rodent and primate ARH, which is restored by T treatment (262-264). Additionally, treatment of neonatal female mice with DHT results in decreased POMC immunoreactivity and reduced projections from the ARH, resulting in increased food intake (265). However, species differences are conspicuous. Whereas sheep display a high coexpression of AR in POMC and NPY/AgRP neurons (266), only a small subset of POMC neurons (~3%) coexpress AR in the rat (267). Exposure to prenatal androgen excess increases the proportion of NPY/AgRP-AR positive neurons in female mice, and the number and projections of NPY/AgRP neurons in ewes (266,268). This suggests that, at least in rodents, the effects of androgens on energy expenditure via melanocortin neurons is mediated by estrogens after aromatization, as POMC neurons express ERs (269,270). Moreover, androgens can influence POMC and/or NPY/AgRP neurons via upstream AR-expressing neurons. For instance, leptin exerts sexually dimorphic trophic effects on NPY/AgRP fiber innervation during postnatal development (271). Yet, NPY/AgRP neurons express virtually no detectable AR or ERα (260,271), indicating that other AR-positive neurons mediate these effects.

The ventral premammillary nucleus (PMv) is another key site for the metabolic control of reproduction. Interestingly, the PMv shows dense expression of AR in both sexes, but is relatively low in ERs (211,272). Furthermore, the PMv has virtually no aromatase expression (273), suggesting preferential regulation by androgens acting via AR. In addition to receiving signals conveying reproductive status, the PMv also integrates signals conveying energy balance, and environmental cues, such as pheromones (274), and photoperiod in seasonal breeders (275). PMv neurons express a variety of receptors, including receptors for leptin, insulin, ghrelin, sex steroids,

and melanocortins (272,276-279). Neurons of the PMv project directly to GnRH neuronal cell bodies and terminals in the median eminence (280-283), as well as to kisspeptin neurons (281,284-286). The PMv facilitates leptin's permissive actions on puberty and fertility, as re-expression of the leptin receptor (LepRb) in LepRb-null mice is sufficient for pubertal progression and fertility in females (283). AR is coexpressed in LepRb PMv neurons of male mice (287), but the role of androgen actions in PMv neurons has not been determined.

Current Gap in Knowledge

Despite the wealth of knowledge on the physiologic effects of androgens in various organs and tissues, the action of androgens via AR in the brain has remained largely unexplored. The brain is a highly heterogeneous tissue, therefore, the neuronal-specific AR knockout models cannot distinguish the effects of androgens on different brain nuclei, cell types, and function. Furthermore, many studies investigating the role of androgens in the brain have either neglected to include female subjects, examined only adult animals, or focused on the role of aromatized T acting on ERs.

AR is highly expressed in the hypothalamus, particularly in the ARH and PMv (211). These hypothalamic nuclei contain key neuronal populations associated with the neuroendocrine reproductive axis and the metabolic control of reproduction, such as LepRb (277). LepRb neurons respond to leptin, which signals the amount of energy stored in the form of lipids (288,289). Therefore, leptin indicates that enough energy is available to conduct energetically-demanding processes, such as pregnancy and lactation, territoriality in males, and gametogenesis in both sexes (290,291). Lack of either leptin or LepRb results in obesity, diabetes, and infertility (292). This phenotype is reminiscent of global or neuronal ARKO mice, which develop increased adiposity

later in life, glucose intolerance, and insulin resistance (192,293). Whether AR/LepRb neurons mediate the sex-specific actions of androgens in reproduction and/or metabolism remains unknown.

Hypothesis and Objectives

I *hypothesize* that subpopulations of hypothalamic LepRb neurons coexpressing AR play a crucial role in androgenic actions in reproductive and metabolic regulation, and mediate the deficits caused by hyperandrogenism in female mice.

The overall *objective* of this dissertation is to examine the role of androgens acting on AR in the brain, and to determine whether LepRb neurons relay the androgenic actions in reproductive and/or metabolic function. To accomplish this objective, we performed three independent studies described in separate chapters.

In chapter 2, we present a systematic evaluation of AR distribution in the brain of prepubertal and adult mice of both sexes. We found high expression of *Ar* mRNA in multiple brain regions, including the hypothalamus. Of interest are areas which are also dense in LepRb, such as the ARH and PMv (Cara et al, *J Neuroendocrinol*, 2021, re-submitted following revision).

In chapter 3, we assessed if the direct actions of androgens via AR in LepRb cells impact metabolism and/or reproduction. We generated a LepRb-specific ARKO mouse model, and performed a comprehensive analysis of the reproductive and metabolic phenotype of male and female mice (Cara et al, *Endocrinology*, 2020).

In chapter 4, we assessed if deletion of AR from LepRb cells protects female mice from the consequences of exposure to androgen excess during late embryonic development. We used a well-characterized mouse model of prenatal androgen excess that replicates many features of PCOS (Cara et al, *in preparation*).

Finally, in the fifth chapter, I discuss the findings in an integrative perspective, highlighting the strengths and weaknesses, and proposing future studies needed to further advance the understanding of the role of androgens in the central control of reproduction and metabolism.

References

1. Miller WL, Geller DH, Rosen M. Ovarian and Adrenal Androgen Biosynthesis and Metabolism. In: Azziz R, Nestler JE, Dewailly D, eds. Androgen Excess Disorders in Women: Polycystic Ovary Syndrome and Other Disorders. Totowa, NJ: Humana Press; 2007:19-33.

2. Walters KA, Paris VR, Aflatounian A, Handelsman DJ. Androgens and ovarian function: translation from basic discovery research to clinical impact. Journal of Endocrinology 2019; 242:R23

3. Turcu AF, Rege J, Auchus RJ, Rainey WE. 11-Oxygenated androgens in health and disease. Nature Reviews Endocrinology 2020; 16:284-296

4. Rainey WE, Carr BR, Sasano H, Suzuki T, Mason JI. Dissecting human adrenal androgen production. Trends in endocrinology and metabolism: TEM 2002; 13:234-239

5. Bélanger C, Luu-The V, Dupont P, Tchernof A. Adipose Tissue Intracrinology: Potential Importance of Local Androgen/Estrogen Metabolism in the Regulation of Adiposity. Horm Metab Res 2002; 34:737-745

6. Quinkler M, Sinha B, Tomlinson JW, Bujalska IJ, Stewart PM, Arlt W. Androgen generation in adipose tissue in women with simple obesity--a site-specific role for 17beta-hydroxysteroid dehydrogenase type 5. The Journal of endocrinology 2004; 183:331-342

7. Pugeat M, Nader N, Hogeveen K, Raverot G, Déchaud H, Grenot C. Sex hormone-binding globulin gene expression in the liver: Drugs and the metabolic syndrome. Molecular and cellular endocrinology 2010; 316:53-59

8. Khan MS, Knowles BB, Aden DP, Rosner W. Secretion of testosterone-estradiol-binding globulin by a human hepatoma-derived cell line. J Clin Endocrinol Metab 1981; 53:448-449

9. Södergård R, Bäckström T, Shanbhag V, Carstensen H. Calculation of free and bound fractions of testosterone and estradiol-17 beta to human plasma proteins at body temperature. J Steroid Biochem 1982; 16:801-810

10. Dunn JF, Nisula BC, Rodbard D. Transport of Steroid Hormones: Binding of 21 Endogenous Steroids to Both Testosterone-Binding Globulin and Corticosteroid-Binding Globulin in Human Plasma. The Journal of Clinical Endocrinology & Metabolism 1981; 53:58-68

11. Goldman AL, Bhasin S, Wu FCW, Krishna M, Matsumoto AM, Jasuja R. A Reappraisal of Testosterone's Binding in Circulation: Physiological and Clinical Implications. Endocrine Reviews 2017; 38:302-324

12. Sullivan PM, Petrusz P, Szpirer C, Joseph DR. Alternative processing of androgen-binding protein RNA transcripts in fetal rat liver. Identification of a transcript formed by trans splicing. J Biol Chem 1991; 266:143-154

13. Hagenäs L, Ritzén EM, Plöen L, Hansson V, French FS, Nayfeh SN. Sertoli cell origin of testicular androgen-binding protein (ABP). Molecular and cellular endocrinology 1975; 2:339-350

14. Mendel CM. The free hormone hypothesis: a physiologically based mathematical model. Endocr Rev 1989; 10:232-274

15. Laurent MR, Hammond GL, Blokland M, Jardí F, Antonio L, Dubois V, Khalil R, Sterk SS, Gielen E, Decallonne B, Carmeliet G, Kaufman J-M, Fiers T, Huhtaniemi IT, Vanderschueren D, Claessens F. Sex hormone-binding globulin regulation of androgen bioactivity in vivo: validation of the free hormone hypothesis. Scientific Reports 2016; 6:35539

16. Hammes A, Andreassen TK, Spoelgen R, Raila J, Hubner N, Schulz H, Metzger J, Schweigert FJ, Luppa PB, Nykjaer A, Willnow TE. Role of Endocytosis in Cellular Uptake of Sex Steroids. Cell 2005; 122:751-762

17. Adams JS. "Bound" to Work: The Free Hormone Hypothesis Revisited. Cell 2005; 122:647-649

18. Rosner W, Hryb DJ, Khan MS, Nakhla AM, Romas NA. Sex hormone-binding globulin mediates steroid hormone signal transduction at the plasma membrane. J Steroid Biochem Mol Biol 1999; 69:481-485

19. Hryb DJ, Khan MS, Romas NA, Rosner W. The control of the interaction of sex hormone-binding globulin with its receptor by steroid hormones. Journal of Biological Chemistry 1990; 265:6048-6054

20. Ng KM, Catalano MG, Pinós T, Selva DM, Avvakumov GV, Munell F, Hammond GL. Evidence that fibulin family members contribute to the steroid-dependent extravascular sequestration of sex hormone-binding globulin. J Biol Chem 2006; 281:15853-15861

21. Mason KA, Schoelwer MJ, Rogol AD. Androgens During Infancy, Childhood, and Adolescence: Physiology and Use in Clinical Practice. Endocr Rev 2020; 41

22. Corbier P, Dehennin L, Castanier M, Mebazaa A, Edwards DA, Roffi J. Sex differences in serum luteinizing hormone and testosterone in the human neonate during the first few hours after birth. J Clin Endocrinol Metab 1990; 71:1344-1348

23. Renault CH, Aksglaede L, Wøjdemann D, Hansen AB, Jensen RB, Juul A. Minipuberty of human infancy - A window of opportunity to evaluate hypogonadism and differences of sex development? Annals of pediatric endocrinology & metabolism 2020; 25:84-91

24. Winter JSD. Hypothalamic—pituitary function in the fetus and infant. Clinics in Endocrinology and Metabolism 1982; 11:41-55

25. Kushnir MM, Blamires T, Rockwood AL, Roberts WL, Yue B, Erdogan E, Bunker AM, Meikle AW. Liquid chromatography-tandem mass spectrometry assay for androstenedione, dehydroepiandrosterone, and testosterone with pediatric and adult reference intervals. Clin Chem 2010; 56:1138-1147

26. Van Leeuwen AM, Bladh ML. Davis's Comprehensive Handbook of Laboratory & Diagnostic Tests with Nursing Implications. F.A. Davis Company.

27. Taieb Jl, Mathian B, Millot Fo, Patricot M-C, Mathieu E, Queyrel N, Lacroix I, Somma-Delpero C, Boudou P. Testosterone Measured by 10 Immunoassays and by Isotope-Dilution Gas Chromatography–Mass Spectrometry in Sera from 116 Men, Women, and Children. Clinical Chemistry 2003; 49:1381-1395

28. Handelsman DJ, Hirschberg AL, Bermon S. Circulating Testosterone as the Hormonal Basis of Sex Differences in Athletic Performance. Endocrine Reviews 2018; 39:803-829

29. Skiba MA, Bell RJ, Islam RM, Handelsman DJ, Desai R, Davis SR. Androgens During the Reproductive Years: What Is Normal for Women? The Journal of Clinical Endocrinology & Metabolism 2019; 104:5382-5392

30. Rothman MS, Carlson NE, Xu M, Wang C, Swerdloff R, Lee P, Goh VHH, Ridgway EC, Wierman ME. Reexamination of testosterone, dihydrotestosterone, estradiol and estrone levels across the menstrual cycle and in postmenopausal women measured by liquid chromatography–tandem mass spectrometry. Steroids 2011; 76:177-182

31. Harman SM, Metter EJ, Tobin JD, Pearson J, Blackman MR. Longitudinal Effects of Aging on Serum Total and Free Testosterone Levels in Healthy Men. The Journal of Clinical Endocrinology & Metabolism 2001; 86:724-731

32. Feldman HA, Longcope C, Derby CA, Johannes CB, Araujo AB, Coviello AD, Bremner WJ, McKinlay JB. Age trends in the level of serum testosterone and other hormones in middle-aged men: longitudinal results from the Massachusetts male aging study. J Clin Endocrinol Metab 2002; 87:589-598

33. Nanba AT, Rege J, Ren J, Auchus RJ, Rainey WE, Turcu AF. 11-Oxygenated C19 Steroids Do Not Decline With Age in Women. J Clin Endocrinol Metab 2019; 104:2615-2622

34. Gwynne JT, Strauss JF, III. The Role of Lipoproteins in Steroidogenesis and Cholesterol Metabolism in Steroidogenic Glands*. Endocrine Reviews 1982; 3:299-329

35. Miller WL, Auchus RJ. The molecular biology, biochemistry, and physiology of human steroidogenesis and its disorders. Endocr Rev 2011; 32:81-151

36. Payne AH, Hales DB. Overview of steroidogenic enzymes in the pathway from cholesterol to active steroid hormones. Endocr Rev 2004; 25:947-970

37. Turcu A, Smith JM, Auchus R, Rainey WE. Adrenal androgens and androgen precursors-definition, synthesis, regulation and physiologic actions. Comprehensive Physiology 2014; 4:1369-1381

38. van Weerden WM, Bierings HG, Van Steenbrugge GJ, De Jong FH, Schröder FH. Adrenal glands of mouse and rat do not synthesize androgens. Life Sciences 1992; 50:857-861

39. Kaaijk EM, Sasano H, Suzuki T, Beek JF, van der Veen F. Distribution of steroidogenic enzymes involved in androgen synthesis in polycystic ovaries: an immunohistochemical study. Molecular human reproduction 2000; 6:443-447

40. Erickson GF, Ryan KJ. Stimulation of testosterone production in isolated rabbit thecal tissue by LH/FSH, dibutyryl cyclic AMP, PGF2α, and PGE2. Endocrinology 1976; 99:452-458

41. Bogovich K, Richards JS. Androgen Biosynthesis in Developing Ovarian Follicles Evidence that Luteinizing Hormone Regulates Thecal 17α-Hydroxylase and C17–2o-Lyase Activities*. Endocrinology 1982; 111:1201-1208

42. Magoffin DA, Weitsman SR. Differentiation of ovarian theca-interstitial cells in vitro: regulation of 17 alpha-hydroxylase messenger ribonucleic acid expression by luteinizing hormone and insulin-like growth factor-I. Endocrinology 1993; 132:1945-1951

43. Magoffin DA, Weitsman SR. Insulin-like growth factor-I stimulates the expression of 3β-hydroxysteroid dehydrogenase messenger ribonucleic acid in ovarian theca-interstitial cells. Biology of reproduction 1993; 48:1166-1173

44. Hillier SG, Whitelaw PF, Smyth CD. Follicular oestrogen synthesis: the 'two-cell, two-gonadotrophin' model revisited. Molecular and cellular endocrinology 1994; 100:51-54

45. Simpson ER, Mahendroo MS, Means GD, Kilgore MW, Hinshelwood MM, Graham-Lorence S, Amarneh B, Ito Y, Fisher CR, Michael MD, et al. Aromatase cytochrome P450, the enzyme responsible for estrogen biosynthesis. Endocr Rev 1994; 15:342-355

46. Stocco C. Aromatase expression in the ovary: hormonal and molecular regulation. Steroids 2008; 73:473-487

47. Erickson GF, Hsueh AJW. Stimulation of Aromatase Activity by Follicle Stimulating Hormone in Rat Granulosa Cells in Vivo and in Vitro*. Endocrinology 1978; 102:1275-1282

48. Blakemore J, Naftolin F. Aromatase: Contributions to Physiology and Disease in Women and Men. Physiology 2016; 31:258-269

49. Azzouni F, Godoy A, Li Y, Mohler J. The 5 alpha-reductase isozyme family: a review of basic biology and their role in human diseases. Advances in urology 2012; 2012:530121

50. Thigpen AE, Silver RI, Guileyardo JM, Casey ML, McConnell JD, Russell DW. Tissue distribution and ontogeny of steroid 5 alpha-reductase isozyme expression. The Journal of clinical investigation 1993; 92:903-910

51. Cantagrel V, Lefeber DJ, Ng BG, Guan Z, Silhavy JL, Bielas SL, Lehle L, Hombauer H, Adamowicz M, Swiezewska E, De Brouwer AP, Blümel P, Sykut-Cegielska J, Houliston S, Swistun D, Ali BR, Dobyns WB, Babovic-Vuksanovic D, van Bokhoven H, Wevers RA, Raetz CRH, Freeze HH, Morava É, Al-Gazali L, Gleeson JG. SRD5A3 Is Required for Converting Polyprenol to Dolichol and Is Mutated in a Congenital Glycosylation Disorder. Cell 2010; 142:203-217

52. Erskine MS, Hippensteil M, Kornberg E. Metabolism of dihydrotestosterone to 3 alpha-androstanediol in brain and plasma: effect on behavioural activity in female rats. The Journal of endocrinology 1992; 134:183-195

53. Picciarelli-Lima P, Oliveira AG, Reis AM, Kalapothakis E, Mahecha GA, Hess RA, Oliveira CA. Effects of 3-beta-diol, an androgen metabolite with intrinsic estrogen-like effects, in modulating the aquaporin-9 expression in the rat efferent ductules. Reproductive biology and endocrinology : RB&E 2006; 4:51

54. Davey RA, Grossmann M. Androgen Receptor Structure, Function and Biology: From Bench to Bedside. Clin Biochem Rev 2016; 37:3-15

55. Gao W, Bohl CE, Dalton JT. Chemistry and structural biology of androgen receptor. Chem Rev 2005; 105:3352-3370

56. Alen P, Claessens F, Verhoeven G, Rombauts W, Peeters B. The androgen receptor amino-terminal domain plays a key role in p160 coactivator-stimulated gene transcription. Mol Cell Biol 1999; 19:6085-6097

57. Grad JM, Lyons LS, Robins DM, Burnstein KL. The Androgen Receptor (AR) Amino-Terminus Imposes Androgen-Specific Regulation of AR Gene Expression via an Exonic Enhancer. Endocrinology 2001; 142:1107-1116

58. Scheller A, Hughes E, Golden KL, Robins DM. Multiple Receptor Domains Interact to Permit, or Restrict, Androgen-specific Gene Activation *. Journal of Biological Chemistry 1998; 273:24216-24222

59. Verrijdt G, Tanner T, Moehren U, Callewaert L, Haelens A, Claessens F. The androgen receptor DNA-binding domain determines androgen selectivity of transcriptional response. Biochemical Society Transactions 2006; 34:1089-1094

60. Verrijdt G, Haelens A, Claessens F. Selective DNA recognition by the androgen receptor as a mechanism for hormone-specific regulation of gene expression. Molecular genetics and metabolism 2003; 78:175-185

61. Tan MHE, Li J, Xu HE, Melcher K, Yong E-l. Androgen receptor: structure, role in prostate cancer and drug discovery. Acta Pharmacologica Sinica 2015; 36:3-23

62. Ojasoo T, Delettré J, Mornon JP, Turpin-VanDycke C, Raynaud JP. Towards the mapping of the progesterone and androgen receptors. Journal of Steroid Biochemistry 1987; 27:255-269

63. Raynaud JP, Bouton MM, Moguilewsky M, Ojasoo T, Philibert D, Beck G, Labrie F, Mornon JP. Steroid hormone receptors and pharmacology. Journal of Steroid Biochemistry 1980; 12:143-157

64. Grino PB, Griffin JE, Wilson JD. Testosterone at high concentrations interacts with the human androgen receptor similarly to dihydrotestosterone. Endocrinology 1990; 126:1165-1172

65. Shang Y, Myers M, Brown M. Formation of the Androgen Receptor Transcription Complex. Molecular cell 2002; 9:601-610

66. Gritsina G, Gao WQ, Yu J. Transcriptional repression by androgen receptor: roles in castration-resistant prostate cancer. Asian journal of andrology 2019; 21:215-223

67. Sun M, Yang L, Feldman RI, Sun X-m, Bhalla KN, Jove R, Nicosia SV, Cheng JQ. Activation of Phosphatidylinositol 3-Kinase/Akt Pathway by Androgen through Interaction of p85α, Androgen Receptor, and Src *. Journal of Biological Chemistry 2003; 278:42992-43000

68. Liao RS, Ma S, Miao L, Li R, Yin Y, Raj GV. Androgen receptor-mediated non-genomic regulation of prostate cancer cell proliferation. Translational andrology and urology 2013; 2:187-196

69. Foradori CD, Weiser MJ, Handa RJ. Non-genomic actions of androgens. Frontiers in Neuroendocrinology 2008; 29:169-181

70. Frye CA, Van Keuren KR, Erskine MS. Behavioral effects of 3 alpha-androstanediol. I: Modulation of sexual receptivity and promotion of GABA-stimulated chloride flux. Behavioural brain research 1996; 79:109-118

71. Frye CA, Duncan JE, Basham M, Erskine MS. Behavioral effects of 3 alpha-androstanediol. II: Hypothalamic and preoptic area actions via a GABAergic mechanism. Behavioural brain research 1996; 79:119-130

72. Sachidanandan D, Bera AK. Inhibition of the GABAA Receptor by Sulfated Neurosteroids: A Mechanistic Comparison Study between Pregnenolone Sulfate and Dehydroepiandrosterone Sulfate. Journal of Molecular Neuroscience 2015; 56:868-877

73. Majewska MD, Demirgören S, Spivak CE, London ED. The neurosteroid dehydroepiandrosterone sulfate is an allosteric antagonist of the GABAA receptor. Brain Res 1990; 526:143-146

74. Sullivan SD, Moenter SM. Neurosteroids Alter γ-Aminobutyric Acid Postsynaptic Currents in Gonadotropin-Releasing Hormone Neurons: A Possible Mechanism for Direct Steroidal Control. Endocrinology 2003; 144:4366-4375

75. Culig Z, Hobisch A, Cronauer MV, Radmayr C, Trapman J, Hittmair A, Bartsch G, Klocker H. Androgen receptor activation in prostatic tumor cell lines by insulin-like growth factor-I, keratinocyte growth factor, and epidermal growth factor. Cancer research 1994; 54:5474-5478

76. Kaarbø M, Klokk TI, Saatcioglu F. Androgen signaling and its interactions with other signaling pathways in prostate cancer. BioEssays : news and reviews in molecular, cellular and developmental biology 2007; 29:1227-1238

77. Thomas P. Membrane Androgen Receptors Unrelated to Nuclear Steroid Receptors. Endocrinology 2019; 160:772-781

78. Mohandass A, Krishnan V, Gribkova ED, Asuthkar S, Baskaran P, Nersesyan Y, Hussain Z, Wise LM, George RE, Stokes N, Alexander BM, Cohen AM, Pavlov EV, Llano DA, Zhu MX, Thyagarajan B, Zakharian E. TRPM8 as the rapid testosterone signaling receptor: Implications in the regulation of dimorphic sexual and social behaviors. The FASEB Journal 2020; 34:10887-10906

79. Shan L-X, Rodriguez MC, Jänne OA. Regulation of androgen receptor protein and mRNA concentrations by androgens in rat ventral prostate and seminal vesicles and in human hepatoma cells. Molecular endocrinology 1990; 4:1636-1646

80. Quarmby VE, Yarbrough WG, Lubahn DB, French FS, Wilson EM. Autologous down-regulation of androgen receptor messenger ribonucleic acid. Molecular endocrinology 1990; 4:22-28

81. Blok L, Bartlett J, Vreis JB-D, Themmen A, Brinkmann A, Weinbauer G, Nieschlag E, Grootegoed J. Effect of testosterone deprivation on expression of the androgen receptor in rat prostate, epididymis and testis. International journal of andrology 1992; 15:182-198

82. Burgess LH, Handa RJ. Hormonal regulation of androgen receptor mRNA in the brain and anterior pituitary gland of the male rat. Molecular Brain Research 1993; 19:31-38

83. Kerr JE, Allore RJ, Beck SG, Handa RJ. Distribution and hormonal regulation of androgen receptor (AR) and AR messenger ribonucleic acid in the rat hippocampus. Endocrinology 1995; 136:3213-3221

84. Oliveira CA, Mahecha GAB, Carnes K, Prins GS, Saunders PTK, França LR, Hess RA. Differential hormonal regulation of estrogen receptors ERalpha and ERbeta and androgen receptor expression in rat efferent ductules. Reproduction 2004; 128:73-86

85. Lu SF, McKenna SE, Cologer-Clifford A, Nau EA, Simon NG. Androgen receptor in mouse brain: sex differences and similarities in autoregulation. Endocrinology 1998; 139:1594-1601

86. Lynch CS, Story AJ. Dihydrotestosterone and estrogen regulation of rat brain androgen-receptor immunoreactivity. Physiol Behav 2000; 69:445-453

87. Lyon MF, Hawkes SG. X-linked gene for testicular feminization in the mouse. Nature 1970; 227:1217-1219

88. Yarbrough WG, Quarmby VE, Simental JA, Joseph DR, Sar M, Lubahn DB, Olsen KL, French FS, Wilson EM. A single base mutation in the androgen receptor gene causes androgen insensitivity in the testicular feminized rat. J Biol Chem 1990; 265:8893-8900

89. Bardin CW, Bullock L, Schneider G, Allison JE, Stanley AJ. Pseudohermaphrodite rat: end organ insensitivity to testosterone. Science 1970; 167:1136-1137

90. Santoro SW, Schultz PG. Directed evolution of the site specificity of Cre recombinase. Proceedings of the National Academy of Sciences 2002; 99:4185-4190

91. Kato S. Androgen receptor structure and function from knock-out mouse. Clinical pediatric endocrinology 2002; 11:1-7

92. Shiina H, Matsumoto T, Sato T, Igarashi K, Miyamoto J, Takemasa S, Sakari M, Takada I, Nakamura T, Metzger D, Chambon P, Kanno J, Yoshikawa H, Kato S. Premature ovarian failure in androgen receptor-deficient mice. Proceedings of the National Academy of Sciences of the United States of America 2006; 103:224-229

93. Holdcraft RW, Braun RE. Androgen receptor function is required in Sertoli cells for the terminal differentiation of haploid spermatids. Development 2004; 131:459-467

94. De Gendt K, Swinnen JV, Saunders PT, Schoonjans L, Dewerchin M, Devos A, Tan K, Atanassova N, Claessens F, Lecureuil C, Heyns W, Carmeliet P, Guillou F, Sharpe RM, Verhoeven G. A Sertoli cell-selective knockout of the androgen receptor causes spermatogenic arrest in meiosis. Proceedings of the National Academy of Sciences of the United States of America 2004; 101:1327-1332

95. Hu YC, Wang PH, Yeh S, Wang RS, Xie C, Xu Q, Zhou X, Chao HT, Tsai MY, Chang C. Subfertility and defective folliculogenesis in female mice lacking androgen receptor. Proceedings of the National Academy of Sciences of the United States of America 2004; 101:11209-11214

96. Notini AJ, Davey RA, McManus JF, Bate KL, Zajac JD. Genomic actions of the androgen receptor are required for normal male sexual differentiation in a mouse model. J Mol Endocrinol 2005; 35:547-555

97. Walters K, Allan C, Jimenez M, Lim P, Davey R, Zajac J, Illingworth P, Handelsman D. Female mice haploinsufficient for an inactivated androgen receptor (AR) exhibit age-dependent defects that resemble the AR null phenotype of dysfunctional late follicle development, ovulation, and fertility. Endocrinology 2007; 148:3674-3684

98. Walters KA, Simanainen U, Handelsman DJ. Molecular insights into androgen actions in male and female reproductive function from androgen receptor knockout models. Human Reproduction Update 2010; 16:543-558

99. Wilson CA, Davies DC. The control of sexual differentiation of the reproductive system and brain. Reproduction 2007; 133:331

100. Wilson J, George F, Griffin J. The hormonal control of sexual development. Science 1981; 211:1278-1284

101. Shima Y, Miyabayashi K, Haraguchi S, Arakawa T, Otake H, Baba T, Matsuzaki S, Shishido Y, Akiyama H, Tachibana T, Tsutsui K, Morohashi K. Contribution of Leydig and Sertoli cells to testosterone production in mouse fetal testes. Molecular endocrinology 2013; 27:63-73

102. O'Shaughnessy PJ, Baker PJ, Heikkilä M, Vainio S, McMahon AP. Localization of 17beta-hydroxysteroid dehydrogenase/17-ketosteroid reductase isoform expression in the developing mouse testis--androstenedione is the major androgen secreted by fetal/neonatal leydig cells. Endocrinology 2000; 141:2631-2637

103. Welsh M, Saunders PTK, Marchetti NI, Sharpe RM. Androgen-Dependent Mechanisms of Wolffian Duct Development and Their Perturbation by Flutamide. Endocrinology 2006; 147:4820-4830

104. Hannema SE, Hughes IA. Regulation of Wolffian Duct Development. Hormone Research in Paediatrics 2007; 67:142-151

105. Allard S, Adin P, Gouedard L, di Clemente N, Josso N, Orgebin-Crist MC, Picard JY, Xavier F. Molecular mechanisms of hormone-mediated Mullerian duct regression: involvement of beta-catenin. Development 2000; 127:3349-3360

106. Josso N, Belville C, di Clemente N, Picard J-Y. AMH and AMH receptor defects in persistent Müllerian duct syndrome. Human Reproduction Update 2005; 11:351-356

107. Welsh M, Saunders PT, Sharpe RM. The critical time window for androgen-dependent development of the Wolffian duct in the rat. Endocrinology 2007; 148:3185-3195

108. Hiort O. The differential role of androgens in early human sex development. BMC Med 2013; 11:152

109. Butler CM, Harry JL, Deakin JE, Cooper DW, Renfree MB. Developmental expression of the androgen receptor during virilization of the urogenital system of a marsupial. Biology of reproduction 1998; 59:725-732

110. Verhoeven G, Cailleau J. Follicle-stimulating hormone and androgens increase the concentration of the androgen receptor in Sertoli cells. Endocrinology 1988; 122:1541-1550

111. Chang C, Chen YT, Yeh SD, Xu Q, Wang RS, Guillou F, Lardy H, Yeh S. Infertility with defective spermatogenesis and hypotestosteronemia in male mice lacking the androgen receptor in Sertoli cells. Proceedings of the National Academy of Sciences of the United States of America 2004; 101:6876-6881

112. Lim P, Robson M, Spaliviero J, McTavish KJ, Jimenez M, Zajac JD, Handelsman DJ, Allan CM. Sertoli cell androgen receptor DNA binding domain is essential for the completion of spermatogenesis. Endocrinology 2009; 150:4755-4765

113. Meng J, Holdcraft RW, Shima JE, Griswold MD, Braun RE. Androgens regulate the permeability of the blood–testis barrier. Proceedings of the National Academy of Sciences of the United States of America 2005; 102:16696-16700

114. Wang R-S, Yeh S, Chen L-M, Lin H-Y, Zhang C, Ni J, Wu C-C, di Sant'Agnese PA, deMesy-Bentley KL, Tzeng C-R, Chang C. Androgen Receptor in Sertoli Cell Is Essential for Germ Cell Nursery and Junctional Complex Formation in Mouse Testes. Endocrinology 2006; 147:5624-5633

115. O'Hara L, McInnes K, Simitsidellis I, Morgan S, Atanassova N, Slowikowska-Hilczer J, Kula K, Szarras-Czapnik M, Milne L, Mitchell RT, Smith LB. Autocrine androgen action is essential for Leydig cell maturation and function, and protects against late-onset Leydig cell apoptosis in both mice and men. FASEB journal : official publication of the Federation of American Societies for Experimental Biology 2015; 29:894-910

116. O'Shaughnessy PJ, Mitchell RT, Monteiro A, O'Hara L, Cruickshanks L, der Grinten HC-v, Brown P, Abel M, Smith LB. Androgen receptor expression is required to ensure development of adult Leydig cells and to prevent development of steroidogenic cells with adrenal characteristics in the mouse testis. BMC developmental biology 2019; 19:8

117. O'Shaughnessy PJ, Johnston H, Willerton L, Baker PJ. Failure of normal adult Leydig cell development in androgen-receptor-deficient mice. Journal of cell science 2002; 115:3491-3496

118. Murphy L, Jeffcoate IA, O'Shaughnessy PJ. Abnormal Leydig cell development at puberty in the androgen-resistant Tfm mouse. Endocrinology 1994; 135:1372-1377

119. Xu Q, Lin H-Y, Yeh S-D, Yu IC, Wang R-S, Chen Y-T, Zhang C, Altuwaijri S, Chen L-M, Chuang K-H, Chiang H-S, Yeh S, Chang C. Infertility with defective spermatogenesis and steroidogenesis in male mice lacking androgen receptor in Leydig cells. Endocrine 2007; 32:96-106

120. Tsai M-Y, Yeh S-D, Wang R-S, Yeh S, Zhang C, Lin H-Y, Tzeng C-R, Chang C. Differential effects of spermatogenesis and fertility in mice lacking androgen receptor in individual testis cells. Proceedings of the National Academy of Sciences 2006; 103:18975-18980

121. Ohyama K, Ohta M, Hosaka YZ, Tanabe Y, Ohyama T, Yamano Y. Expression of anti-Müllerian hormone and its type II receptor in germ cells of maturing rat testis. Endocrine journal 2015; 62:997-1006

122. Baarends WM, Hoogerbrugge JW, Post M, Visser JA, De Rooij DG, Parvinen M, Themmen AP, Grootegoed JA. Anti-müllerian hormone and anti-müllerian hormone type II receptor messenger ribonucleic acid expression during postnatal testis development and in the adult testis of the rat. Endocrinology 1995; 136:5614-5622

123. Prins G, Lindgren M. Accessory Sex Glands in the Male. Vol 12015:773-804.

124. Chandolia RK, Weinbauer GF, Behre HM, Nieschlag E. Evaluation of a peripherally selective antiandrogen (Casodex) as a tool for studying the relationship between testosterone and spermatogenesis in the rat. J Steroid Biochem Mol Biol 1991; 38:367-375

125. Wright AS, Thomas LN, Douglas RC, Lazier CB, Rittmaster RS. Relative potency of testosterone and dihydrotestosterone in preventing atrophy and apoptosis in the prostate of the castrated rat. The Journal of clinical investigation 1996; 98:2558-2563

126. Kyprianou N, Isaacs JT. Activation of programmed cell death in the rat ventral prostate after castration. Endocrinology 1988; 122:552-562

127. Dandona P, Rosenberg MT. A practical guide to male hypogonadism in the primary care setting. International journal of clinical practice 2010; 64:682-696

128. Carnegie C. Diagnosis of hypogonadism: clinical assessments and laboratory tests. Reviews in urology 2004; 6 Suppl 6:S3-8

129. Handelsman DJ, Sikaris K, Ly LP. Estimating age-specific trends in circulating testosterone and sex hormone-binding globulin in males and females across the lifespan. Annals of clinical biochemistry 2016; 53:377-384

130. Sun M, Choueiri TK, Hamnvik OP, Preston MA, De Velasco G, Jiang W, Loeb S, Nguyen PL, Trinh QD. Comparison of Gonadotropin-Releasing Hormone Agonists and Orchiectomy: Effects of Androgen-Deprivation Therapy. JAMA oncology 2016; 2:500-507

131. Kelleher S, Conway AJ, Handelsman DJ. Blood Testosterone Threshold for Androgen Deficiency Symptoms. The Journal of Clinical Endocrinology & Metabolism 2004; 89:3813-3817

132. Bhasin S, Cunningham GR, Hayes FJ, Matsumoto AM, Snyder PJ, Swerdloff RS, Montori VM. Testosterone Therapy in Adult Men with Androgen Deficiency Syndromes: An Endocrine Society Clinical Practice Guideline. The Journal of Clinical Endocrinology & Metabolism 2006; 91:1995-2010

133. Kuhn JM, Laudat MH, Wolf LM, Luton JP. Male hypertestosteronemia. Presse medicale (Paris, France : 1983) 1987; 16:675-679

134. Degitz K, Placzek M, Arnold B, Schmidt H, Plewig G. Congenital adrenal hyperplasia and acne in male patients. British Journal of Dermatology 2003; 148:1263-1266

135. Djaladat H, Nichols C, Daneshmand S. Androgen-Producing Testicular Germ Cell Tumors. Journal of Clinical Oncology 2011; 29:e634-e635

136. Fung LC, Honey RJDA, Gardiner G. Testicular seminoma presenting withfeatures of androgen excess. Urology 1994; 44:927-929

137. Handelsman DJ. Androgen Misuse and Abuse. Endocr Rev 2021;

138. Lebbe M, Woodruff TK. Involvement of androgens in ovarian health and disease. Molecular human reproduction 2013; 19:828-837

139. Pelletier G, Labrie C, Labrie F. Localization of oestrogen receptor alpha, oestrogen receptor beta and androgen receptors in the rat reproductive organs. Journal of Endocrinology 2000; 165:359

140. Weil SJ, Vendola K, Zhou J, Adesanya OO, Wang J, Okafor J, Bondy CA. Androgen Receptor Gene Expression in the Primate Ovary: Cellular Localization, Regulation, and Functional Correlations. The Journal of Clinical Endocrinology & Metabolism 1998; 83:2479-2485

141. Horie K, Takakura K, Fujiwara H, Suginami H, Liao S, Mori T. Immunohistochemical localization of androgen receptor in the human ovary throughout the menstrual cycle in relation to oestrogen and progesterone receptor expression. Human reproduction (Oxford, England) 1992; 7:184-190

142. Rice S, Ojha K, Whitehead S, Mason H. Stage-Specific Expression of Androgen Receptor, Follicle-Stimulating Hormone Receptor, and Anti-Müllerian Hormone Type II Receptor in Single, Isolated, Human Preantral Follicles: Relevance to Polycystic Ovaries. The Journal of Clinical Endocrinology & Metabolism 2007; 92:1034-1040

143. Sen A, Prizant H, Light A, Biswas A, Hayes E, Lee H-J, Barad D, Gleicher N, Hammes SR. Androgens regulate ovarian follicular development by increasing follicle stimulating hormone receptor and microRNA-125b expression. Proceedings of the National Academy of Sciences 2014; 111:3008-3013

144. Yeh S, Tsai MY, Xu Q, Mu XM, Lardy H, Huang KE, Lin H, Yeh SD, Altuwaijri S, Zhou X, Xing L, Boyce BF, Hung MC, Zhang S, Gan L, Chang C. Generation and characterization of androgen receptor knockout (ARKO) mice: an in vivo model for the study of androgen functions in selective tissues. Proceedings of the National Academy of Sciences of the United States of America 2002; 99:13498-13503

145. Sen A, Hammes SR. Granulosa cell-specific androgen receptors are critical regulators of ovarian development and function. Molecular endocrinology 2010; 24:1393-1403

146. Walters KA, Middleton LJ, Joseph SR, Hazra R, Jimenez M, Simanainen U, Allan CM, Handelsman DJ. Targeted Loss of Androgen Receptor Signaling in Murine Granulosa Cells of Preantral and Antral Follicles Causes Female Subfertility1. Biology of reproduction 2012; 87

147. Ma Y, Andrisse S, Chen Y, Childress S, Xue P, Wang Z, Jones D, Ko C, Divall S, Wu S. Androgen Receptor in the Ovary Theca Cells Plays a Critical Role in Androgen-Induced Reproductive Dysfunction. Endocrinology 2016; 158:98-108

148. Maclean A, Bunni E, Makrydima S, Withington A, Kamal AM, Valentijn AJ, Hapangama DK. Fallopian tube epithelial cells express androgen receptor and have a distinct hormonal responsiveness when compared with endometrial epithelium. Human Reproduction 2020; 35:2097-2106

149. Shao R, Ljungström K, Weijdegård B, Egecioglu E, Fernandez-Rodriguez J, Zhang F-P, Thurin-Kjellberg A, Bergh C, Billig H. Estrogen-induced upregulation of AR expression and enhancement of AR nuclear translocation in mouse fallopian tubes in vivo. American Journal of Physiology-Endocrinology and Metabolism 2007; 292:E604-E614

150. Mertens HJ, Heineman MJ, Koudstaal J, Theunissen P, Evers JL. Androgen receptor content in human endometrium. European journal of obstetrics, gynecology, and reproductive biology 1996; 70:11-13

151. Pelletier G, Luu-The V, Li S, Labrie F. Localization and estrogenic regulation of androgen receptor mRNA expression in the mouse uterus and vagina. The Journal of endocrinology 2004; 180:77-85

152. Baldassarre M, Perrone A, Giannone F, Armillotta F, Battaglia C, Costantino A, Venturoli S, Meriggiola C. Androgen receptor expression in the human vagina under different physiological and treatment conditions. International journal of impotence research 2012; 25

153. Xu J, Li M, Zhang L, Xiong H, Lai L, Guo M, Zong T, Zhang D, Yang B, Wu L, Tang M, Kuang H. Expression and regulation of androgen receptor in the mouse uterus during early pregnancy and decidualization. Molecular reproduction and development 2015; 82:898-906

154. Kowalski AA, Vale-Cruz DS, Simmen FA, Simmen RCM. Uterine Androgen Receptors: Roles in Estrogen-Mediated Gene Expression and DNA Synthesis1. Biology of reproduction 2004; 70:1349-1357

155. Nantermet PV, Masarachia P, Gentile MA, Pennypacker B, Xu J, Holder D, Gerhold D, Towler D, Schmidt A, Kimmel DB, Freedman LP, Harada S-i, Ray WJ. Androgenic Induction of Growth and Differentiation in the Rodent Uterus Involves the Modulation of Estrogen-Regulated Genetic Pathways. Endocrinology 2005; 146:564-578

156. Walters KA, McTavish KJ, Seneviratne MG, Jimenez M, McMahon AC, Allan CM, Salamonsen LA, Handelsman DJ. Subfertile female androgen receptor knockout mice exhibit defects in neuroendocrine signaling, intraovarian function, and uterine development but not uterine function. Endocrinology 2009; 150:3274-3282

157. Witherby S, Johnson J, Demers L, Mount S, Littenberg B, Maclean CD, Wood M, Muss H. Topical Testosterone for Breast Cancer Patients with Vaginal Atrophy Related to Aromatase Inhibitors: A Phase I/II Study. The Oncologist 2011; 16:424-431

158. Kennedy TG. Vaginal Mucification In The Ovariectomized Rat In Response T 5α-Pregnane-3,20-Dione, Testosterone and 5α-Androstan-17β-ol-3-one: Test for Progestogenic Activity. Journal of Endocrinology 1974; 61:293

159. Kennedy TG, Armstrong DT. Induction of vaginal mucification in rats with testosterone and 17β-hydroxy-5α-androstan-3-one. Steroids 1976; 27:423-430

160. Pelletier G, Ouellet J, Martel C, Labrie F. Androgenic Action of Dehydroepiandrosterone (DHEA) on Nerve Density in the Ovariectomized Rat Vagina. The Journal of Sexual Medicine 2013; 10:1908-1914

161. Pessina MA, Hoyt RF, Jr., Goldstein I, Traish AM. Differential Effects of Estradiol, Progesterone, and Testosterone on Vaginal Structural Integrity. Endocrinology 2006; 147:61-69

162. Traish AM, Kim SW, Stankovic M, Goldstein I, Kim NN. Testosterone Increases Blood Flow and Expression of Androgen and Estrogen Receptors in the Rat Vagina. The Journal of Sexual Medicine 2007; 4:609-619

163. Traish AM, Kim NN, Huang YH, Min K, Munarriz R, Goldstein I. Sex steroid hormones differentially regulate nitric oxide synthase and arginase activities in the proximal and distal rabbit vagina. International Journal of Impotence Research 2003; 15:397-404

164. Cellai I, Di Stasi V, Comeglio P, Maseroli E, Todisco T, Corno C, Filippi S, Cipriani S, Sorbi F, Fambrini M, Petraglia F, Scavello I, Rastrelli G, Acciai G, Villanelli F, Danza G, Sarchielli E, Guarnieri G, Morelli A, Maggi M, Vignozzi L. Insight on the Intracrinology of Menopause: Androgen Production within the Human Vagina. Endocrinology 2020; 162

165. Goldstein A, Pukall CF, Goldstein I. Female sexual pain disorders : evaluation and management. Second edition. ed. Hoboken, NJ: Wiley-Blackwell.

166. Liao DJ, Dickson RB. Roles of androgens in the development, growth, and carcinogenesis of the mammary gland. The Journal of Steroid Biochemistry and Molecular Biology 2002; 80:175-189

167. Pelletier G. Localization of androgen and estrogen receptors in rat and primate tissues. Histology and histopathology 2000; 15:1261-1270

168. Peters AA, Ingman WV, Tilley WD, Butler LM. Differential Effects of Exogenous Androgen and an Androgen Receptor Antagonist in the Peri- and Postpubertal Murine Mammary Gland. Endocrinology 2011; 152:3728-3737

169. Dimitrakakis C, Zhou J, Wang J, Belanger A, LaBrie F, Cheng C, Powell D, Bondy C. A physiologic role for testosterone in limiting estrogenic stimulation of the breast. Menopause (New York, NY) 2003; 10:292-298

170. Shohat-Tal A, Sen A, Barad DH, Kushnir V, Gleicher N. Genetics of androgen metabolism in women with infertility and hypoandrogenism. Nature Reviews Endocrinology 2015; 11:429-441

171. Burger HG. Androgen production in women. Fertility and sterility 2002; 77:3-5

172. Handelsman DJ, Wartofsky L. Requirement for mass spectrometry sex steroid assays in the Journal of Clinical Endocrinology and Metabolism. J Clin Endocrinol Metab 2013; 98:3971-3973

173. Pugeat M, Plotton I, Perrière ABdl, Raverot G, Déchaud H, Raverot V. MANAGEMENT OF ENDOCRINE DISEASE Hyperandrogenic states in women: pitfalls in laboratory diagnosis. European Journal of Endocrinology 2018; 178:R141

174. Gleicher N, Kim A, Weghofer A, Shohat-Tal A, Lazzaroni E, Lee HJ, Barad DH. Starting and resulting testosterone levels after androgen supplementation determine at all ages in vitro fertilization (IVF) pregnancy rates in women with diminished ovarian reserve (DOR). Journal of assisted reproduction and genetics 2013; 30:49-62

175. Azziz R, Nestler J, Dewailly D. Androgen Excess Disorders in Women: Polycystic Ovary Syndrome and Other Disorders.

176. Elhassan YS, Idkowiak J, Smith K, Asia M, Gleeson H, Webster R, Arlt W, O'Reilly MW. Causes, Patterns, and Severity of Androgen Excess in 1205 Consecutively Recruited Women. J Clin Endocrinol Metab 2018; 103:1214-1223

177. Sharma A, Kapoor E, Singh RJ, Chang AY, Erickson D. Diagnostic Thresholds for Androgen-Producing Tumors or Pathologic Hyperandrogenism in Women by Use of Total Testosterone Concentrations Measured by Liquid Chromatography-Tandem Mass Spectrometry. Clinical Chemistry 2018; 64:1636-1645

178. Burt Solorzano CM, Beller JP, Abshire MY, Collins JS, McCartney CR, Marshall JC. Neuroendocrine dysfunction in polycystic ovary syndrome. Steroids 2012; 77:332-337

179. Sullivan SD, Moenter SM. Prenatal androgens alter GABAergic drive to gonadotropin-releasing hormone neurons: implications for a common fertility disorder. Proceedings of the National Academy of Sciences of the United States of America 2004; 101:7129-7134

180. Dulka EA, Moenter SM. Prepubertal Development of Gonadotropin-Releasing Hormone Neuron Activity Is Altered by Sex, Age, and Prenatal Androgen Exposure. Endocrinology 2017; 158:3943-3953

181. Roland AV, Moenter SM. Prenatal androgenization of female mice programs an increase in firing activity of gonadotropin-releasing hormone (GnRH) neurons that is reversed by metformin treatment in adulthood. Endocrinology 2011; 152:618-628

182. Fauser BC, Pache TD, Lamberts SW, Hop WC, de Jong FH, Dahl KD. Serum bioactive and immunoreactive luteinizing hormone and follicle-stimulating hormone levels in women with cycle abnormalities, with or without polycystic ovarian disease. J Clin Endocrinol Metab 1991; 73:811-817

183. Yen SS, Vela P, Rankin J. Inappropriate secretion of follicle-stimulating hormone and luteinizing hormone in polycystic ovarian disease. J Clin Endocrinol Metab 1970; 30:435-442

184. Franks S, Mason H, Willis D. Follicular dynamics in the polycystic ovary syndrome. Molecular and cellular endocrinology 2000; 163:49-52

185. Azziz R, Carmina E, Chen Z, Dunaif A, Laven JSE, Legro RS, Lizneva D, Natterson-Horowtiz B, Teede HJ, Yildiz BO. Polycystic ovary syndrome. Nature Reviews Disease Primers 2016; 2:16057

186. Willis DS, Watson H, Mason HD, Galea R, Brincat M, Franks S. Premature response to luteinizing hormone of granulosa cells from anovulatory women with polycystic ovary syndrome: relevance to mechanism of anovulation. J Clin Endocrinol Metab 1998; 83:3984-3991

187. Holm M, Kim JL, Lillienberg L, Storaas T, Jogi R, Svanes C, Schlunssen V, Forsberg B, Gislason T, Janson C, Toren K, Rhine Study Group NE. Incidence and prevalence of chronic bronchitis: impact of smoking and welding. The RHINE study. Int J Tuberc Lung Dis 2012; 16:553-557

188. Wagley A, Hardiman P. Menstrual Dysfunction and Endometrial Neoplasia in the Polycystic Ovary Syndrome and Other Androgen Excess Disorders. In: Azziz R, Nestler JE, Dewailly D, eds. Androgen Excess Disorders in Women: Polycystic Ovary Syndrome and Other Disorders. Totowa, NJ: Humana Press; 2007:303-318.

189. Pastor CL, Griffin-Korf ML, Aloi JA, Evans WS, Marshall JC. Polycystic ovary syndrome: evidence for reduced sensitivity of the gonadotropin-releasing hormone pulse generator to inhibition by estradiol and progesterone. J Clin Endocrinol Metab 1998; 83:582-590

190. Fan W, Yanase T, Nomura M, Okabe T, Goto K, Sato T, Kawano H, Kato S, Nawata H. Androgen Receptor Null Male Mice Develop Late-Onset Obesity Caused by Decreased Energy Expenditure and Lipolytic Activity but Show Normal Insulin Sensitivity With High Adiponectin Secretion. Diabetes 2005; 54:1000-1008

191. Sato T, Matsumoto T, Yamada T, Watanabe T, Kawano H, Kato S. Late onset of obesity in male androgen receptor-deficient (AR KO) mice. Biochem Biophys Res Commun 2003; 300:167-171

192. Lin HY, Xu Q, Yeh S, Wang RS, Sparks JD, Chang C. Insulin and leptin resistance with hyperleptinemia in mice lacking androgen receptor. Diabetes 2005; 54:1717-1725

193. Zarotsky V, Huang M-Y, Carman W, Morgentaler A, Singhal PK, Coffin D, Jones TH. Systematic literature review of the risk factors, comorbidities, and consequences of hypogonadism in men. Andrology 2014; 2:819-834

194. Polderman KH, Gooren LJ, Asscheman H, Bakker A, Heine RJ. Induction of insulin resistance by androgens and estrogens. J Clin Endocrinol Metab 1994; 79:265-271

195. Diamond MP, Grainger D, Diamond MC, Sherwin RS, Defronzo RA. Effects of methyltestosterone on insulin secretion and sensitivity in women. J Clin Endocrinol Metab 1998; 83:4420-4425

196. Corbould A. Effects of androgens on insulin action in women: is androgen excess a component of female metabolic syndrome? Diabetes/Metabolism Research and Reviews 2008; 24:520-532

197. Schiffer L, Kempegowda P, Arlt W, O'Reilly MW. Mechanisms in Endocrinology: The sexually dimorphic role of androgens in human metabolic disease. Eur J Endocrinol 2017; 177:R125-R143

198. Escobar-Morreale HF, Alvarez-Blasco F, Botella-Carretero JI, Luque-Ramirez M. The striking similarities in the metabolic associations of female androgen excess and male androgen deficiency. Human reproduction (Oxford, England) 2014; 29:2083-2091

199. Lin HY, Yu IC, Wang RS, Chen YT, Liu NC, Altuwaijri S, Hsu CL, Ma WL, Jokinen J, Sparks JD, Yeh S, Chang C. Increased hepatic steatosis and insulin resistance in mice lacking hepatic androgen receptor. Hepatology 2008; 47:1924-1935

200. McInnes KJ, Smith LB, Hunger NI, Saunders PT, Andrew R, Walker BR. Deletion of the androgen receptor in adipose tissue in male mice elevates retinol binding protein 4 and reveals independent effects on visceral fat mass and on glucose homeostasis. Diabetes 2012; 61:1072-1081

201. Johansen JA, Breedlove SM, Jordan CL. Androgen receptor expression in the levator ani muscle of male mice. J Neuroendocrinol 2007; 19:823-826

202. Cheung AS, Cunningham C, Ko D-K, Ly V, Gray H, Hoermann R, Strauss BJG, Bani Hassan E, Duque G, Ebeling P, Pandy MG, Zajac JD, Grossmann M. Selective Loss of Levator Ani and Leg Muscle Volumes in Men Undergoing Androgen Deprivation Therapy. The Journal of Clinical Endocrinology & Metabolism 2018; 104:2229-2238

203. Antonio J, Wilson JD, George FW. Effects of castration and androgen treatment on androgen-receptor levels in rat skeletal muscles. Journal of Applied Physiology 1999; 87:2016-2019

204. Sinha-Hikim I, Taylor WE, Gonzalez-Cadavid NF, Zheng W, Bhasin S. Androgen receptor in human skeletal muscle and cultured muscle satellite cells: up-regulation by androgen treatment. J Clin Endocrinol Metab 2004; 89:5245-5255

205. Monks DA, O'Bryant EL, Jordan CL. Androgen receptor immunoreactivity in skeletal muscle: enrichment at the neuromuscular junction. J Comp Neurol 2004; 473:59-72

206. Dubois V, Laurent MR, Sinnesael M, Cielen N, Helsen C, Clinckemalie L, Spans L, Gayan-Ramirez G, Deldicque L, Hespel P, Carmeliet G, Vanderschueren D, Claessens F. A satellite cell-specific knockout of the androgen receptor reveals myostatin as a direct androgen target in skeletal muscle. FASEB journal : official publication of the Federation of American Societies for Experimental Biology 2014; 28:2979-2994

207. Chambon C, Duteil D, Vignaud A, Ferry A, Messaddeq N, Malivindi R, Kato S, Chambon P, Metzger D. Myocytic androgen receptor controls the strength but not the mass of limb muscles. Proceedings of the National Academy of Sciences 2010; 107:14327-14332

208. Navarro G, Xu W, Jacobson DA, Wicksteed B, Allard C, Zhang G, De Gendt K, Kim SH, Wu H, Zhang H, Verhoeven G, Katzenellenbogen JA, Mauvais-Jarvis F. Extranuclear Actions of the Androgen Receptor Enhance Glucose-Stimulated Insulin Secretion in the Male. Cell metabolism 2016; 23:837-851

209. Harada N, Yoda Y, Yotsumoto Y, Masuda T, Takahashi Y, Katsuki T, Kai K, Shiraki N, Inui H, Yamaji R. Androgen signaling expands beta-cell mass in male rats and beta-cell androgen receptor is degraded under high-glucose conditions. American journal of physiology Endocrinology and metabolism 2018; 314:E274-E286

210. Dubois V, Laurent MR, Jardi F, Antonio L, Lemaire K, Goyvaerts L, Deldicque L, Carmeliet G, Decallonne B, Vanderschueren D, Claessens F. Androgen Deficiency Exacerbates High-Fat Diet-Induced Metabolic Alterations in Male Mice. Endocrinology 2016; 157:648-665

211. Simerly RB, Chang C, Muramatsu M, Swanson LW. Distribution of androgen and estrogen receptor mRNA-containing cells in the rat brain: an in situ hybridization study. J Comp Neurol 1990; 294:76-95

212. Brock O, De Mees C, Bakker J. Hypothalamic expression of oestrogen receptor alpha and androgen receptor is sex-, age- and region-dependent in mice. J Neuroendocrinol 2015; 27:264-276

213. Roselli CE, Klosterman S, Resko JA. Anatomic relationships between aromatase and androgen receptor mRNA expression in the hypothalamus and amygdala of adult male cynomolgus monkeys. J Comp Neurol 2001; 439:208-223

214. Wood RI, Newman SW. Androgen receptor immunoreactivity in the male and female Syrian hamster brain. J Neurobiol 1999; 39:359-370

215. Veney SL, Rissman EF. Immunolocalization of androgen receptors and aromatase enzyme in the adult musk shrew brain. Neuroendocrinology 2000; 72:29-36

216. Shah NM, Pisapia DJ, Maniatis S, Mendelsohn MM, Nemes A, Axel R. Visualizing sexual dimorphism in the brain. Neuron 2004; 43:313-319

217. Wallen K, Baum MJ. 69 - Masculinization and Defeminization in Altricial and Precocial Mammals: Comparative Aspects of Steroid Hormone Action. In: Pfaff DW, Arnold AP, Fahrbach SE, Etgen AM, Rubin RT, eds. Hormones, Brain and Behavior. San Diego: Academic Press; 2002:385-423.

218. Ogawa S, Chester AE, Hewitt SC, Walker VR, Gustafsson JA, Smithies O, Korach KS, Pfaff DW. Abolition of male sexual behaviors in mice lacking estrogen receptors alpha and beta (alpha beta ERKO). Proceedings of the National Academy of Sciences of the United States of America 2000; 97:14737-14741

219. Honda S, Harada N, Ito S, Takagi Y, Maeda S. Disruption of sexual behavior in male aromatase-deficient mice lacking exons 1 and 2 of the cyp19 gene. Biochem Biophys Res Commun 1998; 252:445-449

220. Ohno S, Geller LN, Young Lai EV. Tfm mutation and masculinization versus feminization of the mouse central nervous system. Cell 1974; 3:235-242

221. Sato T, Matsumoto T, Kawano H, Watanabe T, Uematsu Y, Sekine K, Fukuda T, Aihara K-i, Krust A, Yamada T, Nakamichi Y, Yamamoto Y, Nakamura T, Yoshimura K, Yoshizawa T, Metzger D, Chambon P, Kato S. Brain masculinization requires androgen receptor function. Proceedings of the National Academy of Sciences of the United States of America 2004; 101:1673-1678

222. Juntti SA, Tollkuhn J, Wu MV, Fraser EJ, Soderborg T, Tan S, Honda S, Harada N, Shah NM. The androgen receptor governs the execution, but not programming, of male sexual and territorial behaviors. Neuron 2010; 66:260-272

223. Raskin K, de Gendt K, Duittoz A, Liere P, Verhoeven G, Tronche F, Mhaouty-Kodja S. Conditional Inactivation of Androgen Receptor Gene in the Nervous System: Effects on Male Behavioral and Neuroendocrine Responses. The Journal of Neuroscience 2009; 29:4461-4470

224. McCarthy MM. Sexual differentiation of the brain in man and animals: of relevance to Klinefelter syndrome? American journal of medical genetics Part C, Seminars in medical genetics 2013; 163c:3-15

225. McGivern R. Androgen Receptors in the Brain: A behavioral perspective. 2002:326-346.

226. Davey RA, Clarke MV, Russell PK, Rana K, Seto J, Roeszler KN, How JMY, Chia LY, North K, Zajac JD. Androgen Action via the Androgen Receptor in Neurons Within the Brain Positively Regulates Muscle Mass in Male Mice. Endocrinology 2017; 158:3684-3695

227. Walters KA, Edwards MC, Tesic D, Caldwell ASL, Jimenez M, Smith JT, Handelsman DJ. The Role of Central Androgen Receptor Actions in Regulating the Hypothalamic-Pituitary-Ovarian Axis. Neuroendocrinology 2018; 106:389-400

228. Tilbrook AJ, de Kretser DM, Cummins JT, Clarke IJ. The negative feedback effects of testicular steroids are predominantly at the hypothalamus in the ram. Endocrinology 1991; 129:3080-3092

229. Jackson GL, Kuehl D, Rhim TJ. Testosterone inhibits gonadotropin-releasing hormone pulse frequency in the male sheep. Biology of reproduction 1991; 45:188-194

230. Levine JE, Duffy MT. Simultaneous measurement of luteinizing hormone (LH)-releasing hormone, LH, and follicle-stimulating hormone release in intact and short-term castrate rats. Endocrinology 1988; 122:2211-2221

231. Roselli CE, Resko JA. Regulation of hypothalamic luteinizing hormone-releasing hormone levels by testosterone and estradiol in male rhesus monkeys. Brain Res 1990; 509:343-346

232. Plant TM. Effects of orchidectomy and testosterone replacement treatment on pulsatile luteinizing hormone secretion in the adult rhesus monkey (Macaca mulatta). Endocrinology 1982; 110:1905-1913

233. Tilbrook AJ, de Kretser DM, Clarke IJ. Seasonal changes in the negative feedback regulation of the secretion of the gonadotrophins by testosterone and inhibin in rams. The Journal of endocrinology 1999; 160:155-167

234. Tilbrook AJ, Clarke IJ. Negative Feedback Regulation of the Secretion and Actions of Gonadotropin-Releasing Hormone in Males. Biology of reproduction 2001; 64:735-742

235. Scott CJ, Kuehl DE, Ferreira SA, Jackson GL. Hypothalamic sites of action for testosterone, dihydrotestosterone, and estrogen in the regulation of luteinizing hormone secretion in male sheep. Endocrinology 1997; 138:3686-3694

236. Pielecka J, Moenter SM. Effect of steroid milieu on gonadotropin-releasing hormone-1 neuron firing pattern and luteinizing hormone levels in male mice. Biology of reproduction 2006; 74:931-937

237. Huang X, Harlan RE. Absence of androgen receptors in LHRH immunoreactive neurons. Brain Res 1993; 624:309-311

238. Lehman MN, Karsch FJ. Do gonadotropin-releasing hormone, tyrosine hydroxylase-, and beta-endorphin-immunoreactive neurons contain estrogen receptors? A double-label immunocytochemical study in the Suffolk ewe. Endocrinology 1993; 133:887-895

239. Herbison AE, Skinner DC, Robinson JE, King IS. Androgen receptor-immunoreactive cells in ram hypothalamus: distribution and co-localization patterns with gonadotropin-releasing hormone, somatostatin and tyrosine hydroxylase. Neuroendocrinology 1996; 63:120-131

240. Roa J, Vigo E, Castellano JM, Navarro VM, Fernández-Fernández R, Casanueva FF, Dieguez C, Aguilar E, Pinilla L, Tena-Sempere M. Hypothalamic Expression of KiSS-1 System and Gonadotropin-Releasing Effects of Kisspeptin in Different Reproductive States of the Female Rat. Endocrinology 2006; 147:2864-2878

241. Oakley AE, Clifton DK, Steiner RA. Kisspeptin signaling in the brain. Endocr Rev 2009; 30:713-743

242. Smith JT, Dungan HM, Stoll EA, Gottsch ML, Braun RE, Eacker SM, Clifton DK, Steiner RA. Differential Regulation of KiSS-1 mRNA Expression by Sex Steroids in the Brain of the Male Mouse. Endocrinology 2005; 146:2976-2984

243. Ruka KA, Burger LL, Moenter SM. Both Estrogen and Androgen Modify the Response to Activation of Neurokinin-3 and κ-Opioid Receptors in Arcuate Kisspeptin Neurons From Male Mice. Endocrinology 2016; 157:752-763

244. Vanacker C, Moya MR, DeFazio RA, Johnson ML, Moenter SM. Long-Term Recordings of Arcuate Nucleus Kisspeptin Neurons Reveal Patterned Activity That Is Modulated by Gonadal Steroids in Male Mice. Endocrinology 2017; 158:3553-3564

245. Hill JW, Faulkner LD. The Role of the Melanocortin System in Metabolic Disease: New Developments and Advances. Neuroendocrinology 2017; 104:330-346

246. Cone RD. The Central Melanocortin System and Energy Homeostasis. Trends in Endocrinology & Metabolism 1999; 10:211-216

247. Elmquist JK, Horton JD. Control of Appetite/Satiety and Energy Balance. Yamada' s Textbook of Gastroenterology2015:528-537.

248. Cowley MA, Smart JL, Rubinstein M, Cerdan MG, Diano S, Horvath TL, Cone RD, Low MJ. Leptin activates anorexigenic POMC neurons through a neural network in the arcuate nucleus. Nature 2001; 411:480-484

249. Elias CF, Aschkenasi C, Lee C, Kelly J, Ahima RS, Bjorbæk C, Flier JS, Saper CB, Elmquist JK. Leptin Differentially Regulates NPY and POMC Neurons Projecting to the Lateral Hypothalamic Area. Neuron 1999; 23:775-786

250. Baver SB, Hope K, Guyot S, Bjørbaek C, Kaczorowski C, O'Connell KM. Leptin modulates the intrinsic excitability of AgRP/NPY neurons in the arcuate nucleus of the hypothalamus. J Neurosci 2014; 34:5486-5496

251. Navarro VM. Metabolic regulation of kisspeptin — the link between energy balance and reproduction. Nature Reviews Endocrinology 2020; 16:407-420

252. Nestor CC, Qiu J, Padilla SL, Zhang C, Bosch MA, Fan W, Aicher SA, Palmiter RD, Rønnekleiv OK, Kelly MJ. Optogenetic Stimulation of Arcuate Nucleus Kiss1 Neurons Reveals a Steroid-Dependent Glutamatergic Input to POMC and AgRP Neurons in Male Mice. Molecular endocrinology 2016; 30:630-644

253. Manfredi-Lozano M, Roa J, Ruiz-Pino F, Piet R, Garcia-Galiano D, Pineda R, Zamora A, Leon S, Sanchez-Garrido MA, Romero-Ruiz A, Dieguez C, Vazquez MJ, Herbison AE, Pinilla L, Tena-Sempere M. Defining a novel leptin-melanocortin-kisspeptin pathway involved in the metabolic control of puberty. Mol Metab 2016; 5:844-857

254. Egan OK, Inglis MA, Anderson GM. Leptin Signaling in AgRP Neurons Modulates Puberty Onset and Adult Fertility in Mice. J Neurosci 2017; 37:3875-3886

255. Sheffer-Babila S, Sun Y, Israel DD, Liu SM, Neal-Perry G, Chua SC, Jr. Agouti-related peptide plays a critical role in leptin's effects on female puberty and reproduction. American journal of physiology Endocrinology and metabolism 2013; 305:E1512-1520

256. Padilla SL, Qiu J, Nestor CC, Zhang C, Smith AW, Whiddon BB, Rønnekleiv OK, Kelly MJ, Palmiter RD. AgRP to Kiss1 neuron signaling links nutritional state and fertility. Proceedings of the National Academy of Sciences of the United States of America 2017; 114:2413-2418

257. Coutinho EA, Prescott M, Hessler S, Marshall CJ, Herbison AE, Campbell RE. Activation of a Classic Hunger Circuit Slows Luteinizing Hormone Pulsatility. Neuroendocrinology 2020; 110:671-687

258. Fu L-Y, van den Pol AN. Kisspeptin Directly Excites Anorexigenic Proopiomelanocortin Neurons but Inhibits Orexigenic Neuropeptide Y Cells by an Indirect Synaptic Mechanism. The Journal of Neuroscience 2010; 30:10205-10219

259. Clegg DJ, Brown LM, Woods SC, Benoit SC. Gonadal hormones determine sensitivity to central leptin and insulin. Diabetes 2006; 55:978-987

260. Olofsson LE, Pierce AA, Xu AW. Functional requirement of AgRP and NPY neurons in ovarian cycle-dependent regulation of food intake. Proceedings of the National Academy of Sciences 2009; 106:15932-15937

261. Asarian L, Geary N. Modulation of appetite by gonadal steroid hormones. Philos Trans R Soc Lond B Biol Sci 2006; 361:1251-1263

262. Adams LA, Vician L, Clifton DK, Steiner RA. Testosterone regulates pro-opiomelanocortin gene expression in the primate brain. Endocrinology 1991; 128:1881-1886

263. Chowen-Breed J, Fraser HM, Vician L, Damassa DA, Clifton DK, Steiner RA. Testosterone regulation of proopiomelanocortin messenger ribonucleic acid in the arcuate nucleus of the male rat. Endocrinology 1989; 124:1697-1702

264. Chowen-Breed JA, Clifton DK, Steiner RA. Regional specificity of testosterone regulation of proopiomelanocortin gene expression in the arcuate nucleus of the male rat brain. Endocrinology 1989; 124:2875-2881

265. Nohara K, Zhang Y, Waraich RS, Laque A, Tiano JP, Tong J, Munzberg H, Mauvais-Jarvis F. Early-life exposure to testosterone programs the hypothalamic melanocortin system. Endocrinology 2011; 152:1661-1669

266. Sheppard KM, Padmanabhan V, Coolen LM, Lehman MN. Prenatal Programming by Testosterone of Hypothalamic Metabolic Control Neurones in the Ewe. Journal of Neuroendocrinology 2011; 23:401-411

267. Fodor M, Delemarre-van de Waal HA. Are POMC neurons targets for sex steroids in the arcuate nucleus of the rat? Neuroreport 2001; 12:3989-3991

268. Marshall CJ, Prescott M, Campbell RE. Investigating the NPY/AgRP/GABA to GnRH Neuron Circuit in Prenatally Androgenized PCOS-Like Mice. Journal of the Endocrine Society 2020; 4

269. Xu Y, Nedungadi TP, Zhu L, Sobhani N, Irani BG, Davis KE, Zhang X, Zou F, Gent LM, Hahner LD, Khan SA, Elias CF, Elmquist JK, Clegg DJ. Distinct hypothalamic neurons mediate estrogenic effects on energy homeostasis and reproduction. Cell metabolism 2011; 14:453-465

270. Stincic TL, Rønnekleiv OK, Kelly MJ. Diverse actions of estradiol on anorexigenic and orexigenic hypothalamic arcuate neurons. Horm Behav 2018; 104:146-155

271. Kamitakahara A, Bouyer K, Wang CH, Simerly R. A critical period for the trophic actions of leptin on AgRP neurons in the arcuate nucleus of the hypothalamus. J Comp Neurol 2018; 526:133-145

272. Donato J, Elias C. The Ventral Premammillary Nucleus Links Metabolic Cues and Reproduction. Frontiers in endocrinology 2011; 2

273. Stanić D, Dubois S, Chua HK, Tonge B, Rinehart N, Horne MK, Boon WC. Characterization of Aromatase Expression in the Adult Male and Female Mouse Brain. I. Coexistence with Oestrogen Receptors α and β, and Androgen Receptors. PloS one 2014; 9:e90451

274. Donato J, Cavalcante JC, Silva RJ, Teixeira AS, Bittencourt JC, Elias CF. Male and female odors induce Fos expression in chemically defined neuronal population. Physiology & Behavior 2010; 99:67-77

275. Hill JW, Elias CF. Neuroanatomical Framework of the Metabolic Control of Reproduction. Physiological Reviews 2018; 98:2349-2380

276. Elmquist JK, Bjorbaek C, Ahima RS, Flier JS, Saper CB. Distributions of leptin receptor mRNA isoforms in the rat brain. J Comp Neurol 1998; 395:535-547

277. Scott MM, Lachey JL, Sternson SM, Lee CE, Elias CF, Friedman JM, Elmquist JK. Leptin targets in the mouse brain. J Comp Neurol 2009; 514:518-532

278. Zigman JM, Jones JE, Lee CE, Saper CB, Elmquist JK. Expression of ghrelin receptor mRNA in the rat and the mouse brain. Journal of Comparative Neurology 2006; 494:528-548

279. Liu H, Kishi T, Roseberry AG, Cai X, Lee CE, Montez JM, Friedman JM, Elmquist JK. Transgenic Mice Expressing Green Fluorescent Protein under the Control of the Melanocortin-4 Receptor Promoter. The Journal of Neuroscience 2003; 23:7143-7154

280. Leshan RL, Louis GW, Jo YH, Rhodes CJ, Munzberg H, Myers MG, Jr. Direct innervation of GnRH neurons by metabolic- and sexual odorant-sensing leptin receptor neurons in the hypothalamic ventral premammillary nucleus. J Neurosci 2009; 29:3138-3147

281. Rondini TA, Baddini SP, Sousa LF, Bittencourt JC, Elias CF. Hypothalamic cocaine- and amphetamine-regulated transcript neurons project to areas expressing gonadotropin releasing hormone immunoreactivity and to the anteroventral periventricular nucleus in male and female rats. Neuroscience 2004; 125:735-748

282. Boehm U, Zou Z, Buck LB. Feedback Loops Link Odor and Pheromone Signaling with Reproduction. Cell 2005; 123:683-695

283. Donato J, Jr., Cravo RM, Frazao R, Gautron L, Scott MM, Lachey J, Castro IA, Margatho LO, Lee S, Lee C, Richardson JA, Friedman J, Chua S, Jr., Coppari R, Zigman JM, Elmquist JK, Elias CF. Leptin's effect on puberty in mice is relayed by the ventral premammillary nucleus and does not require signaling in Kiss1 neurons. The Journal of clinical investigation 2011; 121:355-368

284. Canteras NS, Simerly RB, Swanson LW. Projections of the ventral premammillary nucleus. Journal of Comparative Neurology 1992; 324:195-212

285. Hahn JD, Coen CW. Comparative study of the sources of neuronal projections to the site of gonadotrophin-releasing hormone perikarya and to the anteroventral periventricular nucleus in female rats. Journal of Comparative Neurology 2006; 494:190-214

286. Ross RA, Leon S, Madara JC, Schafer D, Fergani C, Maguire CA, Verstegen AMJ, Brengle E, Kong D, Herbison AE, Kaiser UB, Lowell BB, Navarro VM. PACAP neurons in the ventral premammillary nucleus regulate reproductive function in the female mouse. eLife 2018; 7:e35960

287. Johnson JA, Calo S, Nair L, IglayReger HB, Greenwald-Yarnell M, Skorupski J, Myers MG, Jr., Bodary PF. Testosterone interacts with the feedback mechanisms engaged by Tyr985 of the leptin receptor and diet-induced obesity. J Steroid Biochem Mol Biol 2012; 132:212-219

288. Frederich RC, Hamann A, Anderson S, Löllmann B, Lowell BB, Flier JS. Leptin levels reflect body lipid content in mice: evidence for diet-induced resistance to leptin action. Nature medicine 1995; 1:1311-1314

289. Zhang Y, Proenca R, Maffei M, Barone M, Leopold L, Friedman JM. Positional cloning of the mouse obese gene and its human homologue. Nature 1994; 372:425-432

290. Allison MB, Myers MG, Jr. 20 years of leptin: connecting leptin signaling to biological function. The Journal of endocrinology 2014; 223:T25-35

291. Elias CF, Purohit D. Leptin signaling and circuits in puberty and fertility. Cell Mol Life Sci 2013; 70:841-862

292. Coleman DL. Obese and diabetes: two mutant genes causing diabetes-obesity syndromes in mice. Diabetologia 1978; 14:141-148

293. Yu IC, Lin HY, Liu NC, Sparks JD, Yeh S, Fang LY, Chen L, Chang C. Neuronal androgen receptor regulates insulin sensitivity via suppression of hypothalamic NF-kappaB-mediated PTP1B expression. Diabetes 2013; 62:411-423

CHAPTER 2

Brain Sites Preferentially Responsive to Androgens During Pubertal Transition in Mice

Abstract

Androgens are steroid hormones that play a critical role in brain development and sexual maturation by acting upon both androgen receptors (AR), and estrogen receptors (ERα/β) after aromatization. The contribution of estrogens from aromatized androgens in brain development and the central regulation of metabolism, reproduction, and behavior is well defined, but the role of androgens acting on AR has been unappreciated. Here we map the sex specific expression of *Ar* in the adult and developing mouse brain. Postnatal days (PND) 12 and 21 were used to target a critical window of prepubertal development. Consistent with previous literature in adults, sex-specific differences in *Ar* expression were most profound in the bed nucleus of the stria terminalis (BST), medial amygdala (MEA), and medial preoptic area (MPO). *Ar* expression was also high in these areas in PND 12 and 21 of both sexes. In addition, we describe extra-hypothalamic and extra-limbic areas which show moderate, consistent, and similar *Ar* expression in both sexes at both prepubertal time points. Briefly, *Ar* expression was also observed in olfactory areas of the cerebral cortex, in the hippocampus, several thalamic nuclei, and cranial nerve nuclei involved in autonomic sensory and motor function. To characterize areas that are preferably responsive to androgens, we mapped the coexpression of AR-immunoreactivity (AR-ir) and aromatase-Cre or ERα-Cre dependent eGFP expression. We found that only BST, MEA, and part of the ventrolateral subdivision of the ventromedial hypothalamus (VMHvl) coexpress AR-ir and aromatase-

Cre;eGFP. Coexpression of AR-ir and ERα-Cre;eGFP was more penetrant, but still restricted to hypothalamic and limbic sites. Our findings indicate that in various brain areas androgens, rather than neuroestrogens or circulating estrogens, play an important role in female neuronal development and physiology.

Introduction

Gonadal steroids, including androgens and estrogens, play a dominant role in the development of sex differences in the brain. During male embryonic development, expression of the *Sry* gene located on the Y chromosome leads to differentiation of bipotental gonads into testes, which begin secreting testosterone (1-4). Embryonic testosterone is locally converted to estradiol by the enzyme P450 aromatase (*CYP19A1*) (5-7), which acts to masculinize and defeminize specific brain nuclei via estrogen receptor alpha (ERα) and estrogen receptor beta (ERβ) (8-11). Both effects take place during the organizational window of development (12-14), when the bipotential brain is most sensitive to the organizational effect of gonadal steroids. Developing females, which lack *Sry*, do not develop testes or produce testosterone, and are protected from maternal estradiol by the presence of alpha-fetoprotein *in utero*, and therefore differentiate toward a feminized brain (15,16). As a result, several adult brain sites display gonadal steroid-dependent sexual dimorphism (17-20).

During puberty, increased activity of hypothalamic gonadotropin releasing hormone (GnRH) neurons drives pituitary synthesis and release of gonadotropins, which induce gonadal steroid secretion and production of mature gametes (21). Testosterone activates developmentally programmed brain circuits to generate male specific behaviors, while cyclical ovarian steroids

have a similar role in females (22). Circulating levels of androgens are higher in males during and after completion of puberty (23-25), while very low levels of androgens are detected during the prepubertal stage in both sexes. In the hypothalamus, however, androgen receptor immunoreactivity (AR-ir) is observed throughout postnatal development. AR-ir is higher in males at postnatal day 5, but comparable at 15 days of age, when increasing numbers of female neurons show AR-ir (26). This is highly relevant as the prepubertal window between postnatal days 12 and 22 accounts for the greatest differences in temporal gene expression (27,28) indicating that active neurodevelopmental changes occur prior to puberty and the activation of the hypothalamic-pituitary-gonadal (HPG) axis, when circulating gonadal steroids are low, particularly in females.

The requirement of gonadal steroids and sexual dimorphism in specific brain nuclei for reproduction has been widely demonstrated (29,30), but the same cannot be said of nonreproductive sex-dependent or sex-associated brain responses and function. Among them, emotion, motivation, addiction, and energy balance are well-defined (31). Notably, sex is one of the most relevant risk factors for a variety of psychiatric and neurologic disorders, most of which show clinical onset in peripubertal stages (32). Whether this is a direct effect of developmental testosterone is not clear. In both sexes many adult brain areas outside reproductive centers are androgen sensitive and express AR (33), but the distribution of *Ar* expression in male and female brain during the prepubertal time window has been poorly defined.

In this study, we performed a comprehensive analysis of *Ar* expression in the mouse brain, expanding upon previous descriptions (26,34-37) to include all main subdivisions (e.g., neocortex, thalamus, brainstem, circumventricular organs) in both sexes. In addition, we mapped the

distribution of *Ar* expression in the developing brain, specifically at postnatal days 12 and 21, which frame a critical window of pubertal development (27,28). Finally, we identify regions that are preferentially responsive to androgens in females, i.e., those that lack the enzyme aromatase and do not express ERα. Our data provides a greater in-depth anatomical map of reproductive and non-reproductive sites of androgen action in the male and female mouse brain, particularly during pubertal transition.

Methods

Animal Ethics

All research animals were acquired, used, and maintained in accordance with the National Research Council *Guide for the Care and Use of Laboratory Animals* (38), the US Public Health Service's Policy on Humane Care and Use of Laboratory Animals, and Guide for the Care and Use of Laboratory Animals, as well as federal, state, and local laws. Procedures and protocols were approved by the University of Michigan Committee on Use and Care of Animals (IACUC, Animal Protocol: PRO8712).

Animals

C57BL/6J (JAX® mice, stock #000664), aromatase-Cre (aro^{Cre}, JAX® mice, B6.129S(SJL)-*Cyp19a1*$^{tm2.1(cre)Shah}$/J, stock #027038, provided by Dr. Nirao Shah, Stanford University, (39)), ROSA26-loxSTOPlox-eGFP-L10a (JAX® mice, B6;129S4-*Gt(ROSA)26Sor*$^{tm9(EGFP/Rpl10aAmc/}$J, stock #024750, (40)), and ERα^{Cre} (JAX® mice, B6N.129S6(Cg)-*Esr1*$^{tm1.1(cre)And}$/J, stock #017911, (41)) mice were housed in an Association for Assessment and Accreditation of Laboratory Animal Care (AAALAC) accredited facility at the University of Michigan Medical School. Mice were

housed in a 12:12 light/dark cycle environment with controlled temperature (21-23°C) and humidity (30-70%). Mice were provided water ad libitum and were fed a phytoestrogen-reduced diet (16% protein, 4.0% fat, 48.5% carbohydrate, Teklad 2916 irradiated global rodent diet, Envigo) or a phytoestrogen-reduced, higher protein and fat diet (19% protein, 9% fat, 44.9% carbohydrate, Teklad 2919 irradiated global rodent diet, Envigo) for breeding and lactating females. Phytoestrogen-reduced diets were used to avoid any effects of exogenous dietary estrogens on AR or aromatase expression in experimental mice. Primers used for genotyping are listed in Table 2.1. Adult male mice were single housed at least one week prior to euthanasia to control for housing status, which may impact testosterone levels (42), and androgen-regulated AR expression (36,37). Adult female mice (group housed) were euthanized during diestrus, after completing at least two estrous cycles. Cycle stage was determined by vaginal lavage with predominately leukocytes (43) and confirmed by uterine weight below 100 mg (44).

Table 2.1: Primers used for genotyping

Mice	Primer Sequence	Size (bp)
aro^{Cre}	WT FOR 5' AAA TGA GGA CAG GCA CCT TG 3' MUT FOR 5' GAA ACA GGG GCA ATG GTG 3' COMM REV 5' CGG ATA AGT AAT GCC CCA GA 3'	Wt: 109 Mutant: 140
R26-loxSTOPlox-eGFP-L10a	FOR 1 5' GAG GGG AGT GTT GCA ATA CC 3' FOR 2 5' TCT ACA AAT GTG GTA GAT CCA GGC 3' REV 5' CAG ATG ACT ACC TAT CCT CCC 3'	Wt: 300 Mutant: 200
ERα^{Cre}	COMM FOR 5' AAC AAA GGC ATG GAG CAT CT 3' WT REV 5' CCA CAG TGT ACG CAG GAG AC 3' MUT REV 5' CGG ACA GAA GCA TTT TCC AG 3'	Wt: 331 Mutant: 470

The aromatase-Cre (aro^{Cre}) mouse line, which contains an IRES-Cre transgene knocked into the 3' UTR region of the *Cyp19a1* locus (39) was crossed with reporter mice that express eGFP-L10a in a Cre-dependent manner to obtain aro$^{Cre;eGFP}$ mice. Aro^{Cre} mice were bred to homozygosity for the Cre allele, as two copies of Cre are required for efficient recombination of floxed genes.

The ERα^{Cre} mouse line, which contains an *attP*-flanked 2A oligopeptide and Cre recombinase knocked into the 3' UTR region of the *Esr1* gene (41), was crossed with reporter mice that express eGFP-L10a to obtain ERα$^{Cre;eGFP}$ mice. ERα^{Cre} mice were heterozygous for the Cre allele.

Sample size was 3-4 animals per sex and per age group (PND 12, PND 21, and adult) for C57BL/6J mice, and 3-4 adult females/group for aro$^{Cre;eGFP}$ and ERα$^{Cre;eGFP}$ mice.

Tissue preparation

Adult (postnatal day (PND) 56-70) and PND 21 mice were deeply anesthetized with isoflurane and transcardially perfused with diethyl pyrocarbonate (DEPC)-treated 0.1M PBS until liver and lungs cleared (about 1 minute), followed by 10% neutral buffered formalin (NBF) for 10 minutes. Brains were dissected and postfixed for 2 h, then transferred to 20% sucrose in DEPC-treated 0.1M PBS overnight for cryoprotection. PND 12 mice were anesthetized with isoflurane and euthanized by decapitation. Brains were dissected and fixed in 10% NBF for 4 h, then transferred to 20% sucrose in 10% NBF for 48-72 h at 4°C. PND 12 and PND 21 brains were embedded in optimal cutting temperature (OCT) compound, frozen on dry ice, and stored at -80°C. Brains from PND 12 and 21 mice were sectioned at 30 µm thickness on the frontal plane into 4-5 series on a cryostat (Leica CM 3050S). Sections were directly collected onto SuperFrost Plus slides (Fisher Scientific) and stored at -20°C. Adult brains were sectioned at 30 µm thickness on the frontal plane into 5 series on a freezing microtome (Leica SM 2010R). Sections were stored at -20°C in DEPC-treated cryoprotectant.

Immunohistochemistry

AR immunoreactivity was visualized using a modified tyramide signal amplification (TSA) method previously described (45). Brain sections were rinsed with 0.1M PBS, incubated in 0.6% hydrogen peroxide for 30 min, rinsed with 0.1M PBS, then blocked with 3% normal donkey serum with 0.25% Triton-X-100 for 1 h at room temperature. Sections were incubated overnight with rabbit anti-AR antibody (1:200, AbCam [EPR1535(2)], Cat #ab133273, RRID: AB_11156085). Sections were rinsed with 0.1M PBS and then incubated for 1 h with biotinylated donkey anti-rabbit IgG (1:500, Jackson ImmunoResearch Laboratories, Cat #711-065-152, RRID: AB_2340593), followed by incubation in avidin-biotin (AB) solution in 0.1M PBS (1:1000, Vector Laboratories) for 1 h. Next, sections were incubated in biotinylated tyramide (1:250, Perkin Elmer) with 0.009% hydrogen peroxide for 10 min, followed by incubation with streptavidin-conjugated AlexaFluor 594 (1:1000, Invitrogen, ThermoFisher) for 1 h. Sections were mounted onto gelatin-coated slides and coverslipped with ProLong Gold Antifade mounting medium (Invitrogen, ThermoFisher).

In situ hybridization

Adult brain sections were mounted onto Superfrost Plus slides (Fisher Scientific) in DEPC-treated 0.1M PBS, air dried overnight at room temperature, and stored at -20°C. For pretreatment, slides were thawed at room temperature for 15-20 min, then fixed with 10% NBF for 15 min. Slides were rinsed with DEPC-treated PBS, then dehydrated with increasing concentrations of ethanol and cleared with xylene. Slides were rehydrated, boiled in sodium citrate (0.01M sodium citrate, pH 6.0 in DEPC-H_2O) in a microwave for 10 min, dehydrated, and air dried for 30 min at room temperature.

To generate a ^{35}S-labelled *Ar* cRNA riboprobe, a cDNA template was first generated by RT-PCR amplification using cDNA obtained from whole mouse hypothalamic RNA (TRIzol Reagent, Ambion, Life Technologies) and the primer pairs FOR 5' CAACCAGATTCCTTTGCTGCC 3' and REV 5' GAGCTTGGTGAGCTGGTAGAA 3' (NCBI accession number NM_013476.4, *M. musculus* androgen receptor (*Ar*), mRNA, target region 3042-3551, product length 510 bp). Linear template PCR products were gel purified according to the manufacturer's protocol (QIAquick Gel Extraction Kit, 28706, Qiagen). To generate an antisense cRNA ^{35}S-*Ar* riboprobe by *in vitro* transcription, the linear template was incubated with ^{35}S-UTP (UTPαS, Perkin Elmer) and T7 RNA polymerase according to the manufacturer's protocol (Promega). Riboprobes were diluted to 10^6 cpm/mL in hybridization buffer (50% formamide, 10mM Tris-HCl, pH 8.0 (Invitrogen), 5mg tRNA, 10mM dithiothreitol (DTT), 10% dextran sulfate, 0.3M NaCl, 1mM EDTA, 1x Denhardt's Solution, 0.1% SDS, 0.1% sodium thiosulfate). Hybridization solution was applied to slides, which were coverslipped and incubated overnight at 57°C. The following morning, slides were treated with RNAse A (Roche Applied Bioscience) for 30 min, then treated with a series of high stringency washes in sodium chloride-sodium citrate buffer (SSC). Slides were dehydrated, air dried, then placed into an X-ray film cassette with Biomax MR film (Carestream) for 1-2 days. Slides were dipped in NTB autoradiographic emulsion (Kodak, VWR), dried, and stored at 4°C in foil-wrapped slide boxes for 5 days per 1 day of film exposure. Slides were developed with GBX (Carestream Dental) developer and fixer, then dehydrated with graded ethanol, cleared with xylene, and coverslipped with DPX mounting media (Electron Microscopy Sciences).

To generate neuroanatomical references, slides with adjacent sections of PND 12 and 21 male and female brains were dipped in 0.25% thionin for 45 s, quickly rinsed in water, dehydrated in

increasing concentration of ethanol, and cleared in xylene. Slides were coverslipped with DPX mounting media.

Microscopy and Image Acquisition

Digital images were acquired using an Axio Imager M2 (Carl Zeiss) with a digital camera (AxioCam, Zeiss) using Zen Pro 2 software (Zeiss). Photomicrographs of films were acquired using a SteREO Discovery.V8 stereomicroscope with a digital camera (AxioCam, Carl Zeiss), using the same magnification, illumination, and exposure time for each image. Dark field photomicrographs for silver grains (hybridization signal) were acquired using the same illumination and exposure time for each section, at 10× magnification.

Illustration

Adobe Photoshop software (Adobe Creative Cloud) was used to prepare digital images, including adjusting resolution to 300 dpi, adjustment of image size, addition of annotation and labels, conversion to greyscale, unsharp mask, and levels. Uniform adjustments were made to every image. Mouse brain coordinates were estimated from Paxinos and Franklin's Mouse Brain in Stereotaxic Coordinates atlas (46). Abbreviations are based on the Allen Mouse Brain Atlas (postnatal day 56, coronal reference atlas, Allen Institute for Brain Science, Allen Mouse Brain Atlas, http://mouse.brain-map.org/static/atlas).

Data Analysis

Estimation of hybridization signal was obtained by analysis of integrated optical density (IOD) using ImageJ software (NIH, http://rsb.info.nih.gov/ij) as previously described (47,48). Briefly,

IOD values were calculated as the total IOD of a constant region of interest (ROI) after subtracting background intensity. Quantification of *Ar* silver grain IOD was performed in one 30-µm thick section, on one hemisphere of each animal (n = 3-4/group), at approximately the same rostrocaudal level.

Statistics

Data are reported as mean ± standard error of the mean (SEM). Analysis was performed using GraphPad Prism software (Version 8). Normal distribution of data was analyzed using Shapiro-Wilk test (significance alpha 0.05). Unpaired *t* test with Welch's correction and Mann-Whitney nonparametric test was used to analyze IOD. Exact *P* values are reported and statistical significance is defined as $P < 0.05$.

Results

Distribution of AR mRNA in adult mouse brain

Ar mRNA expression was visualized using in situ hybridization histochemistry. Hybridization signal on autoradiographic film was evaluated in male and female brain sections (n = 3-4/sex, Figure 2.1A). Adult brains were systematically examined and compared with published data as an initial control (26,36,37). Analysis of AR immunoreactivity was also performed as a control for areas that had not been fully described in previous publications (n = 3-4/sex, Figure 2.2).

Table 2.2: Qualitative expression of Ar mRNA distribution by nuclei in postnatal and adult mouse brain. -, +/-, +, ++, +++, and ++++ represent not detected, very low, low, moderate, high, and very high expression of silver grain deposits corresponding to *Ar* mRNA. The Allen Mouse Brain Atlas was used as a reference for names, abbreviations, and location of nuclei.

	Adult		**Prepubertal**			
	PND 56-70		**PND 12**		**PND 21**	
Brain areas and nuclei	**Male**	**Female**	**Male**	**Female**	**Male**	**Female**
Cerebral Cortex						
Motor (MO)	+/-	+/-	+/-	+/-	+/-	+/-
Olfactory nucleus (Anterior) (AON)	-	-	++	++	++	++
Taenia tecta (TT)	+	+/-	+	+	+	+
Piriform (PIR)	+	+	+	+	+	+
Cingulate (Anterior) (ACA)	+	+	+	+	+	+
Endopiriform (EP)	+/-	+/-	+/-	+/-	+	+/-
Hippocampal Formation						
Induseum griseum (IG)	+	+	+	+	+	+
Field CA1 (CA1)	+++	+++	+++	+++	+++	+++
Field CA2 (CA2)	+++	+++	+++	+++	+++	+++
Field CA3 (CA3)	+	+	+	+	+	+
Dentate gyrus (DG)	+	+	+/-	+/-	+	+
Entorhinal area (ENT)	+/-	+/-	+	+	+/-	+/-
Presubiculum / Subiculum (PRE/SUB)	+	+	+	+	+	+
Cortical subplate and cerebral nuclei						
Septohippocampal nucleus (SH)	+	+	+	+	+	+
Lateral septal nucleus, caudodorsal (LSc)	+++	+	+	+	+	+
Lateral septal nucleus, rostroventral (LSr)	+++	+	+	+	+	+
Bed nucleus of stria terminalis, principal nucleus (BSTpr)	++++	+++	+	+	++++	+++
Cortical amygdalar area (COA)	+++	+++	+	+	+++	+++
Medial amygdalar nucleus, posterodorsal (MEApd)	+++	+	+	+	+++	+++
Posterior amygdala (PA)	+++	+	+++	+	+++	+
Thalamus and Subthalamus						
Ventral posterior complex of the thalamus (VP)	+	+	+	+	+	+
Paraventricular nucleus of the thalamus (PVT)	+	+	+	+	+	+
Nucleus of reuniens (RE)	+/-	+/-	+	+	++	+
Subthalamic/ Parasubthalamic, caudal (STN/PSTN)	++	+	+	+	++	++
Medial geniculate complex (MG)	+	+	+	+	++	+

Hypothalamus						
Medial preoptic area, anterior (MPOa)	+	+	+	+	+	+
Medial preoptic area, posterior (MPOp)	++++	++++	++++	++++	++++	++++
Suprachiasmatic nucleus (SCH)	++	+	+/-	+/-	+	+/-
Paraventricular hypothalamic nucleus (PVH)	+/-	+/-	-	-	-	-
Periventricular hypothalamic nucleus (PV)	+	+/-	-	-	-	-
Subparaventricular zone (SBPV)	+	+	++	++	+	+
Lateral hypothalamic area (LHA)	+/-	+/-	-	-	-	-
Arcuate hypothalamic nucleus (ARH)	++	+	+/-	+/-	+	+
Ventromedial hypothalamic nucleus, ventrolateral (VMHvl)	+	++	+	+	++	+
Tuberal nucleus (TU)	+	+	-	-	+	+
Dorsomedial nucleus of the hypothalamus (DMH)	+	-	-	-	+/-	-
Dorsal premammillary nucleus (PMd)	+	+	++	++	++	++
Ventral premammillary nucleus (PMv)	++++	++++	+++	+++	+++	++
Supramammillary nucleus (SUM)	+	+/-	+	+	+	+/-
Midbrain						
Periaqueductal gray, ventrolateral (PAGvl)	+/-	+/-	+/-	+/-	+	+
Ventral tegmental area (VTA)	+/-	-	-	-	-	-
Red nucleus (RN)	+/-	-	-	-	+/-	-
Dorsal nucleus raphe (DR)	+/-	+/-	+/-	+/-	+	+
Pons and Medulla						
Pontine reticular nucleus (PRN)	+/-	+/-	+/-	+/-	+/-	+/-
Superior olivary complex (SOC)	-	-	+	+	+	+
Principal sensory nucleus of the trigeminal (PSV)	-	-	+	+/-	+	-
Parabrachial nucleus (PB)	+/-	+/-	-	-	-	-
Dorsal tegmental nucleus (DTN)	+	+	+	+	+	+
Facial motor nucleus (VII)	+	+/-	+	+	+	+
Cochlear nuclei (CN)	+/-	-	+	+	+	+
Vestibular Nucleus (VNC)	+/-	-	+	+	+	+
Nucleus ambiguus (AMB)	+/-	+/-	++	++	++	++
Hypoglossal nucleus (XII)	+	+	+	+	++	++
Nucleus of the solitary tract (NTS)	+/-	+/-	+/-	+/-	+/-	+/-
Dorsal motor nucleus of vagus nerve (DMX)	+	+	+	+	++	++
Circumventricular Organs						
Subfornical organ (SFO)	+/-	+	+	+	+/-	+/-
Area postrema (AP)	+/-	+/-	+/-	+/-	+	+

Patterns of hybridization signal were similar between sexes in several subdivisions of the cerebral cortex, including the motor (MO), piriform (PIR), and anterior cingulate (ACA) (Table 2.2). In the hippocampal formation, highest expression was observed in Field CA1 and CA2 (Figure 1A, Bregma -1.34 through -3.52mm), and lowest expression in the entorhinal area (ENT). As previously described for AR-ir (35-37), several cortical subplate and cerebral nuclei displayed apparent sex differences. The lateral septal nucleus (caudodorsal and rostroventral subdivisions, LSc and LSr) (Figure 2.1A, Bregma +0.62, +0.14, -0.22mm), bed nucleus of the stria terminalis (principal, BSTpr) (Figure 1A, Bregma -0.22mm), posterodorsal medial amygdalar nucleus (MEApd, Figure 1A, Bregma -1.34mm), and posterior amygdala (PA, Figure 2.1A, Bregma -2.46mm) showed higher *Ar* mRNA levels in males. The cortical amygdalar area (COA) displayed high *Ar* mRNA in both sexes (Table 2.2).

The thalamus and subthalamus contained low to moderate *Ar* hybridization signal. Conspicuous expression was observed in the paraventricular (PVT), medial geniculate (MG), and subthalamic nuclei (STN) in both sexes (Figure 2.1A, Bregma -1.34 to -3.52, Table 2.2).

Hypothalamic AR-ir expression is fairly well characterized in adult mice, and *Ar* hybridization signal was consistent with previous descriptions (26,34,35,37). In brief, highest expression was seen in the medial preoptic area (MPO, Figure 1A, Bregma +0.14mm), arcuate nucleus (ARH), ventrolateral subdivision of the ventromedial hypothalamic nucleus (VMHvl, Figure 2.1A, Bregma -1.34mm), and ventral premammillary nucleus (PMv, Figure 2.1A, Bregma -2.46mm). Sex differences were apparent in the suprachiasmatic nucleus (SCH) and ARH, with expression higher in male mice. Higher *Ar* hybridization signal was also apparent in the periventricular (PV)

and dorsomedial (DMH) nuclei of the hypothalamus in males. The tuberal nucleus (TU) displayed low *Ar* expression, and the paraventricular hypothalamic nucleus (PVH) displayed very low expression in both sexes (Table 2.2). The supramammillary nucleus (SUM) was observed to have an apparent sex difference, with females exhibiting very low expression, and males with higher but still low *Ar* mRNA (Table 2.2).

In the midbrain, *Ar* mRNA was low in both sexes, and mainly observed in the periaqueductal gray (ventrolateral column, PAGvl) and dorsal raphe nucleus (DR, Figure 2.1A, Bregma -3.52 and -5.02mm). Very low expression was also observed in the ventral tegmental area (VTA) and red nucleus (RN) (Table 2.2).

In the pons and medulla, low *Ar* mRNA expression was observed in the dorsal tegmental (DTN), facial motor (VII), hypoglossal (XII), and dorsal motor nucleus of the vagus nerve (DMX) in both sexes (Figure 2.1A, Bregma -5.02mm). Very low hybridization signal was observed in the parabrachial nucleus (PB) and pontine reticular nucleus (PRN, Table 2.2). *Ar* mRNA was also detected in the nucleus ambiguus (AMB, Figure 2.1A, Bregma -7.08mm), and nucleus of the solitary tract (NTS, Figure 2.1A, Bregma -7.48mm) of both sexes, while the cochlear (CN) and vestibular nuclei (VNC) displayed very low signal in males, but not in females (Table 2.2).

In circumventricular organs, we observed very low to low *Ar* hybridization signal in the subfornical organ (SFO) and area postrema (AP) of both sexes (Table 2.2).

AR-immunoreactivity in adult mouse brain

In the adult brain, our findings thoroughly replicate previous reports by different groups (26,34,36,37). In brief, high AR-ir was observed in the BSTpr, MPO, VMHvl, PMv, and MEApd. In addition, and in agreement with *Ar* mRNA distribution, we found moderate to low AR-ir in the PIR, ACA (Figure 2.2A), CA1 and CA2 (Figure 2.2B), septohippocampal nucleus (SH), LSc (Figure 2.2C), PVT (Figure 2.2D), subparaventricular zone (SBPV, Figure 2.2E), PA, PAGvl (Figure 2.2F), DTN (laterodorsal), and many nuclei of the cranial nerves, including the principal sensory nucleus of the trigeminal nerve (PSV), VII, and medial vestibular nucleus (MV, Figure 2.2G). Scattered AR-ir was also observed in the SFO (Figure 2.2H) and AP.

Prepubertal distribution of *Ar* mRNA

Ar mRNA expression was analyzed in two developmental prepubertal stages, PND 12 and 21 (n = 3-4/sex/age, Figure 2.1B-C). In the cerebral cortex, both male and female mice at PND 12 and PND 21 showed consistent and similar expression between sexes (Table 2.2). The anterior olfactory nucleus (AON) displayed moderate *Ar* hybridization signal, while the taenia tecta (TT), PIR, and ACA displayed low *Ar* hybridization signal (Figure 2.3A-D). The endopiriform (EP) and MO showed very low *Ar* hybridization signal in PND 12 and PND 21 mice (Table 2.2).

In the hippocampal formation, expression level of *Ar* mRNA in prepubertal mice was similar to that observed in adults. Briefly, expression of *Ar* mRNA in both male and female mice was detected in the induseum griseum (IG, Figure 2.3E-F), CA1, CA2 (Figure 2.3G-H), and presubiculum/subiculum (PRE/SUB). Higher expression was observed in CA1 and CA2, while lower expression was found in Field CA3 (CA3, Table 2.2). In the dentate gyrus (DG), lower

expression was observed in PND 12 of male and female mice. The ENT displayed moderate expression at PND 12 in male and females, but expression decreased by PND 21.

Cortical subplate and cerebral nuclei also exhibited consistent *Ar* hybridization signal in prepubertal mice in the SH (Figure 2.3E-F) and PA. The LSc displayed moderate expression in PND 12 (Figure 2.4A-C), and PND 21 (Figure 2.4D-F). *Ar* hybridization signal was higher in PND 12 males compared to females, (Figure 2.4C), and was not different between sexes at PND 21 (Figure 2.4F). The BSTpr showed sex differences at PND 12 (Figure 2.4G-I) with higher *Ar* levels in males, and similar levels between sexes at PND 21 (Figure 2.4J-L), whereas the MEApd showed similar pattern of *Ar* expression in between sexes at PND 12 and PND 21 (Table 2.2). *Ar* mRNA in the COA was similar between sexes, with low expression at PND 12, increasing to high expression by PND 21 (Table 2.2).

In thalamic nuclei, moderate to high levels of *Ar* hybridization signal was observed in the PVT (Figure 2.5A-B), the nucleus of reuniens (RE, Figure 2.5C-D), the ventral posterior complex nuclei (VP, Figure 2.5E-F), the STN (Figure 2.5G-H) and the MG (Table 2.2). No difference between sexes and prepubertal ages was apparent.

In the hypothalamus, the MPO and anteroventral periventricular nucleus (AVPV) showed similar levels of *Ar* in both sexes at PND 12 and PND 21 (Table 2.2). The SCH had similar levels of *Ar* at PND 12 in both sexes (Figure 2.6A-C, E-G), however, expression increased in male mice at PND 21 (Figure 2.6G). The SBPV, although apparently higher in males, did not reach statistical significance when comparing sexes at both prepubertal ages (Figure 2.6D, H). The PMv showed

no difference between sexes at PND 12 and PND 21 (Figure 2.6I-K, M-O), however expression was higher in PND 12 (Figure 2.6K) compared to PND 21 mice (Figure 2.6O). In the dorsal premammillary nucleus (PMd), *Ar* mRNA levels were low to moderate, and no difference between sexes or ages was observed (Figure 2.6L, P). The SUM displayed low *Ar* mRNA expression in both sexes at PND 12, and low expression in males and very low expression in females at PND 21 (Table 2.2). The TU exhibited no detectable *Ar* hybridization signal at PND 12, but low signal was detected at PND 21 (Table 2.2). The PVH had no detectable *Ar* hybridization signal at either PND 12 or 21 (Table 2.2).

In the midbrain, expression of *Ar* hybridization signal was low to very low. The PAG showed low expression which was consistent between sexes, particularly in the caudal ventrolateral column (PAGvl, Figure 2.7A-B, Table 2.2). The DR also showed a low to very low level of *Ar* mRNA expression in PND 12 and PND 21 mice (Table 2.2).

In the pons and medulla, the DTN showed consistent, moderate expression in both sexes and in both prepubertal ages (Figure 2.7A-B, Table 2.2). Low *Ar* mRNA expression was detected in the superior olivary complex (SOC, Figure 2.7C-D), the VII (Figure 2.7E-F), the VNC, and the CN (Table 2.2) in both prepubertal stages of both sexes. Low to moderate *Ar* expression was observed in the AMB (Figure 2.7G-H), the DMX and the XII (Figure 2.7I-J) in males and females. Very low to low levels of *Ar* mRNA were detected in the PRN and the PSV (Table 2.2).

In circumventricular organs, *Ar* mRNA expression was low to very low in the SFO and AP of both sexes at PND 12 and PND 21 (Table 2.2).

Brain sites selectively responsive to androgens

Because this study is focused on brain sites that are selective targets of androgens, we further mapped the areas that express AR, but not the enzyme aromatase or ERα. We chose to examine areas expressing ERα due to the well described role of estrogens in masculinization of the male brain during development (49,50), as well as the major role that estrogens play in female pubertal development (51). We used mouse models of Cre-induced reporter gene expression (aro^{Cre} and $ER\alpha^{Cre}$), previously validated (39,41), to allow well-defined labelling of the neuronal soma. Only adult female mice were assessed for colocalization between Cre-induced reporter expression and AR-ir (n = 3-4/group).

Distribution of aro^{Cre} dependent eGFP-L10a reporter expression was consistent with previous literature (52-55). Briefly, eGFP was mostly restricted to forebrain sites, particularly cerebral nuclei and hypothalamus. Virtually no eGFP-positive neurons were detected in the neocortex, hippocampal formation, thalamus, midbrain, or hindbrain. Highest number of eGFP-positive neurons were observed in the BSTpr and the MEApd (Figure 2.8A-D), and a moderate number in the MPO and the VMHvl (Figure 2.8E-H). Colocalization between aro^{Cre} induced eGFP and AR-ir was mostly observed in the BSTpr and the MEApd. The MPO showed virtually no coexpression of AR-ir and eGFP, whereas the VMHvl showed partial co-localization (Figure 2.8E-H). In the VMHvl, three distinct populations were apparent; those co-expressing AR-ir and aro^{Cre};eGFP, those expressing only AR-ir, and those expressing only aro^{Cre};eGFP. Notably, in the LSc and PMv, two sites of high AR-ir, very few eGFP positive neurons and no colocalization between AR-ir and aro^{Cre}-eGFP was observed (Table 2.3).

Table 2.3: Subjective analysis of colocalization of AR-ir and eGFP in aro^{Cre} and ERα^{Cre} mouse models. +, high colocalization; +/-, partial colocalization; -, virtually no or very few colocalization. Areas not represented had no colocalization.

Brain areas and nuclei	Adult Female (PND 56-70)	
	AR-ir	
	aro^{Cre};eGFP	ERα^{Cre};eGFP
Cortical Subplate and Cerebral Nuclei		
Lateral septal nucleus, caudodorsal (LSc)	-	-
Lateral septal nucleus, rostroventral (LSr)	-	+/-
Bed nucleus of stria terminalis, principal nucleus (BSTpr)	+	+
Medial amygdalar nucleus, posterodorsal (MEApd)	+	+
Hypothalamus		
Medial preoptic area, anterior (MPOa)	-	+/-
Medial preoptic area, posterior (MPOp)	-	+
Periventricular nucleus, anterior (PVa)	-	+/-
Arcuate hypothalamic nucleus (ARH)	-	+/-
Ventromedial nucleus, dorsomedial (VMHdm)	-	-
Ventromedial nucleus, ventrolateral (VMHvl)	+/-	+
Tuberal medial nucleus (TU)	-	+/-
Dorsomedial nucleus of the hypothalamus (DMH)	-	+/-
Lateral hypothalamic area (LHA)	-	+/-
Ventral premammillary nucleus (PMv)	-	+/-
Dorsal premammillary nucleus (PMd)	-	-
Brainstem		
Periaqueductal gray, ventrolateral (PAGvl)	-	+/-
Area Postrema (AP)	-	+/-

We next assessed if brain sites that are direct targets of androgens are also responsive to circulating estrogens via ERα. Here, we also used Cre-induced eGFP-L10a expression driven by the ERα promoter (41) to allow for better cellular definition and to potentially identify cells that express ERα in distinct phases of development. As described before (9,26,56,57), and as expected due to the role of ERα in the organization of sex differences in the brain, eGFP was widespread and densely expressed in multiple brain areas of male and female brains. This was particularly evident in forebrain nuclei, including both sexually dimorphic and non-dimorphic sites. The entire female brain was evaluated and only areas showing some degree of colocalization were documented.

In cerebral nuclei, we found that virtually all AR-ir neurons in the BSTpr and most of the MEApd coexpress ERα^{Cre};eGFP (Figure 2.9A-D, Table 2.3). In the LS, we found that most dual labeled AR-ir and eGFP neurons were distributed in the rostroventral subdivision, whereas the caudodorsal subdivision showed segregated populations. In the hypothalamus, the posterior MPO has near complete colocalization, whereas about half of AR-ir neurons in the anterior MPO colocalized with eGFP. We also found clear differences in the VMH, where most of AR-ir neurons in the ventrolateral subdivision co-express eGFP, but not those in the dorsomedial subdivision, which are almost exclusively AR-ir (Figure 2.9E-F). There was also moderate co-expression of eGFP and AR-ir in the PMv, and distinct groups of AR-ir or eGFP positive neurons were observed (Figure 2.9G-H).

In the brainstem, partial colocalization was observed in the PAGvl and in the AP. In cranial nerve nuclei, including VII, VNC, DMX (Figure 2.9I-J) and AMB (Figure 2.9K-L), there were two distinct populations; neurons that expressed AR-ir, or those that expressed ERα^{Cre}-eGFP.

Discussion

In this study, we characterized the expression of *Ar* mRNA in the brain of adult and two prepubertal time points of male and female mice. We show that at PND 12 and 21, before the activation of the HPG axis, many brain nuclei express high levels of *Ar* in both sexes. Additionally, we highlight specific nuclei and subpopulations of neurons that are selectively responsive to androgens. Mouse models carrying Cre-induced reporter genes for aromatase and ERα were used to allow for better cellular (cytoplasmic boundaries) delimitation and to take advantage of the

possibility of identifying cells that express aromatase or ERα in different phases of development. We focused on ERα due to the well described role of estrogens in masculinization of the male brain during prenatal development (49,50), and in female pubertal development and fertility (51,58). Further studies will be necessary to evaluate if the identified brain sites are responsive to alternative estrogens receptors.

Systematic characterization of AR expression during prepubertal development is essential for understanding how androgens can shape brain organization and activation of neural circuits. While circulating androgens are low in the prepubertal period, we show that AR is highly expressed in many areas of the brain in both sexes during this time window. The exact role of AR in brain development in general, and in specific neuronal subpopulations is not well described. It has been demonstrated that gonadal hormones during puberty can further organize and refine neural circuits (59,60). During adolescence, pruning and remodeling of synapses, morphology, density, and sexual dimorphism of dendritic spines occurs throughout the brain. In many brain sites, this fine remodeling is orchestrated by gonadal hormones, particularly androgens (61-65). Thus, increased AR expression during the prepubertal window in both sexes plays a key role in the continuous developmental process towards the adult brain. Sex differences in circulating steroids during pubertal transition would ultimately determine the circuitry, morphology, and neurochemical fate of the subpopulations of neurons.

Sex differences in AR expression are most apparent in areas related to male sexual behavior and reproduction, including the well characterized BSTpr, MPO, MEApd, and LS (26,35,66,67). Differences were also observed during development, with similar *Ar* expression at PND 12

between males and females (e.g., BSTpr and LS), and higher *Ar* in males at PND 21, in agreement with previous reports showing greater hypothalamic AR-ir in prepubertal male mice (26). Nonetheless AR is still prevalent in the female brain and is expressed in a multitude of different brain nuclei.

While the role that AR plays in the prepubertal and adult female brain is not fully understood, models of female androgen excess demonstrate that prenatal and prepubertal androgen exposure has the potential to heavily impact female physiology. For example, polycystic ovary syndrome (PCOS) is partly characterized by female androgen excess, and can significantly impact fertility, body weight and insulin sensitivity (68-70). PCOS-like features can be replicated in mice, with one prepubertal model inducing androgen excess beginning at PND 19 (71) and another at PND 21 (72). This peripubertal androgenization model induces changes upon multiple tissues, including the brain, eliciting well described effects on reproduction and metabolism (73,74). The exact brain sites associated with the consequences of hyperandrogenism in females have not been fully determined. Defining selective and non-selective brain sites responsive to androgens is an important first step for a better mechanistic understanding of the pathological origins of diseases of androgen excess.

Brain AR expression and distribution have been previously characterized in the rat (67,75), hamster (76), musk shrew (77), and monkey (78). These findings, however, are not directly translatable to the mouse due to species differences. For example, AR is abundant in the dorsomedial VMH (VMHdm) of adult male rats (20,67,75), but much less so in adult male mice. It is important to be aware of species differences, particularly in the mouse, which is a frequently

used model organism in studies using genetic and molecular tools. Furthermore, because the number of neurons necessary for a specific function may not be determined *a priori*, moderate and low AR expression in extra-hypothalamic and extra-limbic areas is not irrelevant or less important. Consistent with this concept, *Ar* expression in cranial nerve nuclei of both sexes during pre-pubertal development is particularly interesting. Many nuclei along the olfactory and auditory pathways express AR, but studies exploring the role of androgenic signaling in cranial nerve nuclei have been limited (79,80). Androgens promote neuronal survival and axon regeneration in cranial nerve motor nuclei in male and female rats (81,82). In the spinal cord, however, androgens acting on AR protect against motor neuron death in the spinal nucleus of the bulbocavernosus (SNB) during postnatal development in males, resulting in a male-biased sex difference in cell number and morphology (83,84). It remains to be determined as to why circulating androgens induce sexual dimorphism in some areas of the brain, but not others, and why specific nuclei preferentially respond to androgens, rather than estrogens, to promote neuronal survival, and if these events occur before puberty when androgens are low but AR expression is present in many nuclei of both sexes. Answers to these questions may require a closer look into the regulation of AR signaling complexity, including the role of alternative ligands and ligand-independent signaling properties (85).

While this study examines the distribution of AR in male and female prepubertal mice, we have not systemically mapped ERα or other estrogen receptors in the same experimental groups. Instead, we have examined AR immunoreactivity in neurons coexpressing an $ER\alpha^{Cre}$ reporter gene. The advantage of this model is that cells are labelled permanently from the time of promoter expression, allowing for the visualization of all neurons that have expressed Cre during

development. It is highly possible however, that subpopulations of cells only transiently express ERα, inflating the number of cells expressing the reporter gene in adult mice. Additional studies will be necessary to define specific time points of postnatal development in which subpopulations of neurons are engaged by selective gonadal steroids.

Gonadal hormones are not the only factor that contribute to sex differences in the brain. Sex chromosome genes, autosome genes whose expression are mediated by sex-steroid receptors, epigenetics, environmental factors and exposures, factors which regulate the sensitivity of a brain region to sex steroids, and brain immune cells all contribute to brain sex differentiation (86). Yet, it is clear that androgens play a very important, arguably dominant role in sex differentiation in rodents, and their unknown role in female brain remains to be fully determined. In the attempt to decrease this gap, we focused our analysis on the female brain. Our findings indicate that in various brain areas androgens, rather than neuroestrogens or circulating estrogens, play an important role in female neuronal development and physiology. They also highlight the need for greater investigation into the variety of actions of androgens throughout the male and female brain, particularly during prepubertal development. Future studies targeting specific brain sites are warranted.

References

1. Koopman P, Münsterberg A, Capel B, Vivian N, Lovell-Badge R. Expression of a candidate sex-determining gene during mouse testis differentiation. Nature 1990; 348:450-452

2. Sinclair AH, Berta P, Palmer MS, Hawkins JR, Griffiths BL, Smith MJ, Foster JW, Frischauf A-M, Lovell-Badge R, Goodfellow PN. A gene from the human sex-determining region encodes a protein with homology to a conserved DNA-binding motif. Nature 1990; 346:240-244

3. Rhoda J, Corbier P, Roffi J. Gonadal Steroid Concentrations in Serum and Hypothalamus of the Rat at Birth: Aromatization of Testosterone to 17β-Estradiol*. Endocrinology 1984; 114:1754-1760

4. Weisz J, Ward IL. Plasma Testosterone and Progesterone Titers of Pregnant Rats, Their Male and Female Fetuses, and Neonatal Offspring*. Endocrinology 1980; 106:306-316

5. Naftolin F, MacLusky N. Aromatization hypothesis revisited. Sexual differentiation: Basic and clinical aspects: Raven Press New York; 1984:79-91.

6. McEwen BS, Lieberburg I, Chaptal C, Krey LC. Aromatization: Important for sexual differentiation of the neonatal rat brain. Hormones and Behavior 1977; 9:249-263

7. Naftolin F, Ryan KJ, Davies IJ, Reddy VV, Flores F, Petro Z, Kuhn M, White RJ, Takaoka Y, Wolin L. The Formation of Estrogens by Central Neuroendocrine Tissues. In: Greep RO, ed. Proceedings of the 1974 Laurentian Hormone Conference. Vol 31. Boston: Academic Press; 1975:295-319.

8. McCarthy MM, Schlenker EH, Pfaff DW. Enduring consequences of neonatal treatment with antisense oligodeoxynucleotides to estrogen receptor messenger ribonucleic acid on sexual differentiation of rat brain. Endocrinology 1993; 133:433-439

9. Shughrue PJ, Lane MV, Merchenthaler I. Comparative distribution of estrogen receptor-α and -β mRNA in the rat central nervous system. Journal of Comparative Neurology 1997; 388:507-525

10. Ogawa S, Chan J, Chester AE, Gustafsson J-Å, Korach KS, Pfaff DW. Survival of reproductive behaviors in estrogen receptor β gene-deficient (βERKO) male and female mice. Proceedings of the National Academy of Sciences 1999; 96:12887-12892

11. Wersinger SR, Sannen K, Villalba C, Lubahn DB, Rissman EF, De Vries GJ. Masculine Sexual Behavior Is Disrupted in Male and Female Mice Lacking a Functional Estrogen Receptor α Gene. Hormones and Behavior 1997; 32:176-183

12. Arnold AP, Gorski RA. Gonadal Steroid Induction of Structural Sex Differences in the Central Nervous System. Annual Review of Neuroscience 1984; 7:413-442

13. Arnold AP, Breedlove SM. Organizational and activational effects of sex steroids on brain and behavior: A reanalysis. Hormones and Behavior 1985; 19:469-498

14. Phoenix CH, Goy RW, Gerall AA, Young WC. Organizing action of prenatally administered testosterone propionate on the tissues mediating mating behavior in the female guinea pig1. Endocrinology 1959; 65:369-382

15. Keller M, Pawluski JL, Brock O, Douhard Q, Bakker J. The alpha-fetoprotein knock-out mouse model suggests that parental behavior is sexually differentiated under the influence of prenatal estradiol. Hormones and behavior 2010; 57:434-440

16. Vannier B, Raynaud JP. Effect of estrogen plasma binding on sexual differentiation of the rat fetus. Molecular and cellular endocrinology 1975; 3:323-337

17. Hines M, Allen LS, Gorski RA. Sex differences in subregions of the medial nucleus of the amygdala and the bed nucleus of the stria terminalis of the rat. Brain Res 1992; 579:321-326

18. Lisciotto CA, Morrell JI. Sex differences in the distribution and projections of testosterone target neurons in the medial preoptic area and the bed nucleus of the stria terminalis of rats. Horm Behav 1994; 28:492-502

19. Madeira MD, Ferreira-Silva L, Paula-Barbosa MM. Influence of sex and estrus cycle on the sexual dimorphisms of the hypothalamic ventromedial nucleus: stereological evaluation and Golgi study. J Comp Neurol 2001; 432:329-345

20. Dugger BN, Morris JA, Jordan CL, Breedlove SM. Androgen receptors are required for full masculinization of the ventromedial hypothalamus (VMH) in rats. Horm Behav 2007; 51:195-201

21. Abreu AP, Kaiser UB. Pubertal development and regulation. Lancet Diabetes Endocrinol 2016; 4:254-264

22. Bakker J, Baum MJ. Role for estradiol in female-typical brain and behavioral sexual differentiation. Front Neuroendocrinol 2008; 29:1-16

23. Nilsson ME, Vandenput L, Tivesten A, Norlen AK, Lagerquist MK, Windahl SH, Borjesson AE, Farman HH, Poutanen M, Benrick A, Maliqueo M, Stener-Victorin E, Ryberg H, Ohlsson C. Measurement of a Comprehensive Sex Steroid Profile in Rodent Serum by High-Sensitive Gas Chromatography-Tandem Mass Spectrometry. Endocrinology 2015; 156:2492-2502

24. Gupta D, Attanasio A, Raaf S. Plasma Estrogen and Androgen Concentrations in Children During Adolescence. The Journal of Clinical Endocrinology & Metabolism 1975; 40:636-643

25. Kushnir MM, Blamires T, Rockwood AL, Roberts WL, Yue B, Erdogan E, Bunker AM, Meikle AW. Liquid Chromatography–Tandem Mass Spectrometry Assay for

Androstenedione, Dehydroepiandrosterone, and Testosterone with Pediatric and Adult Reference Intervals. Clinical Chemistry 2010; 56:1138-1147

26. Brock O, De Mees C, Bakker J. Hypothalamic expression of oestrogen receptor alpha and androgen receptor is sex-, age- and region-dependent in mice. J Neuroendocrinol 2015; 27:264-276

27. Hou H, Uusküla-Reimand L, Makarem M, Corre C, Saleh S, Metcalf A, Goldenberg A, Palmert MR, Wilson MD. Gene expression profiling of puberty-associated genes reveals abundant tissue and sex-specific changes across postnatal development. Human Molecular Genetics 2017; 26:3585-3599

28. Han X, Burger LL, Garcia-Galiano D, Sim S, Allen SJ, Olson DP, Myers MG, Jr., Elias CF. Hypothalamic and Cell-Specific Transcriptomes Unravel a Dynamic Neuropil Remodeling in Leptin-Induced and Typical Pubertal Transition in Female Mice. iScience 2020; 23:101563

29. Gorski RA. Sexual Differentiation of the Brain. Hospital Practice 1978; 13:55-62

30. Tsukahara S, Morishita M. Sexually Dimorphic Formation of the Preoptic Area and the Bed Nucleus of the Stria Terminalis by Neuroestrogens. Frontiers in Neuroscience 2020; 14

31. Marrocco J, McEwen BS. Sex in the brain: hormones and sex differences. Dialogues in clinical neuroscience 2016; 18:373-383

32. Altemus M, Sarvaiya N, Neill Epperson C. Sex differences in anxiety and depression clinical perspectives. Front Neuroendocrinol 2014; 35:320-330

33. Wood RI, Newman SW. Androgen and Estrogen Receptors Coexist within Individual Neurons in the Brain of the Syrian Hamster. Neuroendocrinology 1995; 62:487-497

34. Jahan MR, Kokubu K, Islam MN, Matsuo C, Yanai A, Wroblewski G, Fujinaga R, Shinoda K. Species differences in androgen receptor expression in the medial preoptic and anterior hypothalamic areas of adult male and female rodents. Neuroscience 2015; 284:943-961

35. Shah NM, Pisapia DJ, Maniatis S, Mendelsohn MM, Nemes A, Axel R. Visualizing sexual dimorphism in the brain. Neuron 2004; 43:313-319

36. Lu SF, McKenna SE, Cologer-Clifford A, Nau EA, Simon NG. Androgen receptor in mouse brain: sex differences and similarities in autoregulation. Endocrinology 1998; 139:1594-1601

37. Apostolinas S, Rajendren G, Dobrjansky A, Gibson MJ. Androgen receptor immunoreactivity in specific neural regions in normal and hypogonadal male mice: effect of androgens. Brain Res 1999; 817:19-24

38. Council NR. Guide for the Care and Use of Laboratory Animals: Eighth Edition. Washington, DC: The National Academies Press.

39. Unger Elizabeth K, Burke Kenneth J, Yang Cindy F, Bender Kevin J, Fuller Patrick M, Shah Nirao M. Medial Amygdalar Aromatase Neurons Regulate Aggression in Both Sexes. Cell Reports 2015; 10:453-462

40. Krashes MJ, Shah BP, Madara JC, Olson DP, Strochlic DE, Garfield AS, Vong L, Pei H, Watabe-Uchida M, Uchida N, Liberles SD, Lowell BB. An excitatory paraventricular nucleus to AgRP neuron circuit that drives hunger. Nature 2014; 507:238-242

41. Lee H, Kim D-W, Remedios R, Anthony TE, Chang A, Madisen L, Zeng H, Anderson DJ. Scalable control of mounting and attack by Esr1+ neurons in the ventromedial hypothalamus. Nature 2014; 509:627-632

42. Oyegbile TO, Marler CA. Winning fights elevates testosterone levels in California mice and enhances future ability to win fights. Hormones and Behavior 2005; 48:259-267

43. Caligioni C. Assessing Reproductive Status/Stages in Mice. Current protocols in neuroscience / editorial board, Jacqueline N Crawley [et al] 2009:Appendix-4I

44. Silveira MA, Wagenmaker ER, Burger LL, DeFazio RA, Moenter SM. GnRH Neuron Activity and Pituitary Response in Estradiol-Induced vs Proestrous Luteinizing Hormone Surges in Female Mice. Endocrinology 2016; 158:356-366

45. Low KL, Ma C, Soma KK. Tyramide Signal Amplification Permits Immunohistochemical Analyses of Androgen Receptors in the Rat Prefrontal Cortex. J Histochem Cytochem 2017; 65:295-308

46. Paxinos G, Franklin KBJ. Paxinos and Franklin's the mouse brain in stereotaxic coordinates : George Paxinos, Keith B.J. Franklin.

47. Rodrigues BC, Cavalcante JC, Elias CF. Expression of cocaine- and amphetamine-regulated transcript in the rat forebrain during postnatal development. Neuroscience 2011; 195:201-214

48. Cavalcante JC, Bittencourt JC, Elias CF. Female odors stimulate CART neurons in the ventral premammillary nucleus of male rats. Physiology & Behavior 2006; 88:160-166

49. Rissman EF, Wersinger SR, Taylor JA, Lubahn DB. Estrogen Receptor Function as Revealed by Knockout Studies: Neuroendocrine and Behavioral Aspects. Hormones and Behavior 1997; 31:232-243

50. Ogawa S, Chester AE, Hewitt SC, Walker VR, Gustafsson JA, Smithies O, Korach KS, Pfaff DW. Abolition of male sexual behaviors in mice lacking estrogen receptors alpha and beta (alpha beta ERKO). Proceedings of the National Academy of Sciences of the United States of America 2000; 97:14737-14741

51. Mayer C, Acosta-Martinez M, Dubois SL, Wolfe A, Radovick S, Boehm U, Levine JE. Timing and completion of puberty in female mice depend on estrogen receptor α-signaling in kisspeptin neurons. Proceedings of the National Academy of Sciences 2010; 107:22693-22698

52. Tabatadze N, Sato SM, Woolley CS. Quantitative analysis of long-form aromatase mRNA in the male and female rat brain. PloS one 2014; 9:e100628

53. Roselli CE, Abdelgadir SE, Ronnekleiv OK, Klosterman SA. Anatomic distribution and regulation of aromatase gene expression in the rat brain. Biology of reproduction 1998; 58:79-87

54. Wu MV, Manoli DS, Fraser EJ, Coats JK, Tollkuhn J, Honda S, Harada N, Shah NM. Estrogen masculinizes neural pathways and sex-specific behaviors. Cell 2009; 139:61-72

55. Stanić D, Dubois S, Chua HK, Tonge B, Rinehart N, Horne MK, Boon WC. Characterization of Aromatase Expression in the Adult Male and Female Mouse Brain. I. Coexistence with Oestrogen Receptors α and β, and Androgen Receptors. PloS one 2014; 9:e90451

56. Merchenthaler I, Lane MV, Numan S, Dellovade TL. Distribution of estrogen receptor α and β in the mouse central nervous system: In vivo autoradiographic and immunocytochemical analyses. Journal of Comparative Neurology 2004; 473:270-291

57. Saito K, He Y, Yan X, Yang Y, Wang C, Xu P, Hinton AO, Shu G, Yu L, Tong Q, Xu Y. Visualizing estrogen receptor-α-expressing neurons using a new ERα-ZsGreen reporter mouse line. Metabolism 2016; 65:522-532

58. Lubahn DB, Moyer JS, Golding TS, Couse JF, Korach KS, Smithies O. Alteration of reproductive function but not prenatal sexual development after insertional disruption of the mouse estrogen receptor gene. Proceedings of the National Academy of Sciences of the United States of America 1993; 90:11162-11166

59. Sisk CL, Zehr JL. Pubertal hormones organize the adolescent brain and behavior. Front Neuroendocrinol 2005; 26:163-174

60. Schulz KM, Zehr JL, Salas-Ramirez KY, Sisk CL. Testosterone programs adult social behavior before and during, but not after, adolescence. Endocrinology 2009; 150:3690-3698

61. Frankfurt M, Gould E, Woolley CS, McEwen BS. Gonadal steroids modify dendritic spine density in ventromedial hypothalamic neurons: a Golgi study in the adult rat. Neuroendocrinology 1990; 51:530-535

62. Gould E, Woolley CS, Frankfurt M, McEwen BS. Gonadal steroids regulate dendritic spine density in hippocampal pyramidal cells in adulthood. J Neurosci 1990; 10:1286-1291

63. Hatanaka Y, Hojo Y, Mukai H, Murakami G, Komatsuzaki Y, Kim J, Ikeda M, Hiragushi A, Kimoto T, Kawato S. Rapid increase of spines by dihydrotestosterone and testosterone in hippocampal neurons: Dependence on synaptic androgen receptor and kinase networks. Brain Res 2015; 1621:121-132

64. Leranth C, Petnehazy O, MacLusky NJ. Gonadal Hormones Affect Spine Synaptic Density in the CA1 Hippocampal Subfield of Male Rats. The Journal of Neuroscience 2003; 23:1588-1592

65. Leranth C, Hajszan T, MacLusky NJ. Androgens Increase Spine Synapse Density in the CA1 Hippocampal Subfield of Ovariectomized Female Rats. The Journal of Neuroscience 2004; 24:495-499

66. Juntti SA, Tollkuhn J, Wu MV, Fraser EJ, Soderborg T, Tan S, Honda S, Harada N, Shah NM. The androgen receptor governs the execution, but not programming, of male sexual and territorial behaviors. Neuron 2010; 66:260-272

67. McAbee MD, DonCarlos LL. Ontogeny of region-specific sex differences in androgen receptor messenger ribonucleic acid expression in the rat forebrain. Endocrinology 1998; 139:1738-1745

68. Huang A, Brennan K, Azziz R. Prevalence of hyperandrogenemia in the polycystic ovary syndrome diagnosed by the National Institutes of Health 1990 criteria. Fertility and sterility 2010; 93:1938-1941

69. Sanchez-Garrido MA, Tena-Sempere M. Metabolic dysfunction in polycystic ovary syndrome: Pathogenic role of androgen excess and potential therapeutic strategies. Mol Metab 2020; 35:100937

70. Dumesic DA, Oberfield SE, Stener-Victorin E, Marshall JC, Laven JS, Legro RS. Scientific Statement on the Diagnostic Criteria, Epidemiology, Pathophysiology, and Molecular Genetics of Polycystic Ovary Syndrome. Endocr Rev 2015; 36:487-525

71. van Houten EL, Kramer P, McLuskey A, Karels B, Themmen AP, Visser JA. Reproductive and metabolic phenotype of a mouse model of PCOS. Endocrinology 2012; 153:2861-2869

72. Caldwell AS, Middleton LJ, Jimenez M, Desai R, McMahon AC, Allan CM, Handelsman DJ, Walters KA. Characterization of reproductive, metabolic, and endocrine features of polycystic ovary syndrome in female hyperandrogenic mouse models. Endocrinology 2014; 155:3146-3159

73. Aflatounian A, Edwards MC, Rodriguez Paris V, Bertoldo MJ, Desai R, Gilchrist RB, Ledger WL, Handelsman DJ, Walters KA. Androgen signaling pathways driving reproductive and metabolic phenotypes in a PCOS mouse model. The Journal of endocrinology 2020; 245:381-395

74. Caldwell ASL, Edwards MC, Desai R, Jimenez M, Gilchrist RB, Handelsman DJ, Walters KA. Neuroendocrine androgen action is a key extraovarian mediator in the development of polycystic ovary syndrome. Proceedings of the National Academy of Sciences of the United States of America 2017; 114:E3334-E3343

75. Simerly RB, Chang C, Muramatsu M, Swanson LW. Distribution of androgen and estrogen receptor mRNA-containing cells in the rat brain: an in situ hybridization study. J Comp Neurol 1990; 294:76-95

76. Wood RI, Newman SW. Androgen receptor immunoreactivity in the male and female Syrian hamster brain. J Neurobiol 1999; 39:359-370

77. Veney SL, Rissman EF. Immunolocalization of androgen receptors and aromatase enzyme in the adult musk shrew brain. Neuroendocrinology 2000; 72:29-36

78. Roselli CE, Klosterman S, Resko JA. Anatomic relationships between aromatase and androgen receptor mRNA expression in the hypothalamus and amygdala of adult male cynomolgus monkeys. J Comp Neurol 2001; 439:208-223

79. Yu WH, McGinnis MY. Androgen receptors in cranial nerve motor nuclei of male and female rats. J Neurobiol 2001; 46:1-10

80. Sar M, Stumpf W. Androgen concentration in motor neurons of cranial nerves and spinal cord. Science 1977; 197:77-79

81. Yu WH. Administration of testosterone attenuates neuronal loss following axotomy in the brain-stem motor nuclei of female rats. J Neurosci 1989; 9:3908-3914

82. Amy Yu W-h. Effect of testosterone on the regeneration of the hypoglossal nerve in rats. Experimental Neurology 1982; 77:129-141

83. Nordeen E, Nordeen K, Sengelaub D, Arnold A. Androgens prevent normally occurring cell death in a sexually dimorphic spinal nucleus. Science 1985; 229:671-673

84. Breedlove SM, Arnold AP. Sexually dimorphic motor nucleus in the rat lumbar spinal cord: response to adult hormone manipulation, absence in androgen-insensitive rats. Brain Res 1981; 225:297-307

85. Davey RA, Grossmann M. Androgen Receptor Structure, Function and Biology: From Bench to Bedside. Clin Biochem Rev 2016; 37:3-15

86. McCarthy MM, Arnold AP. Reframing sexual differentiation of the brain. Nature Neuroscience 2011; 14:677-683

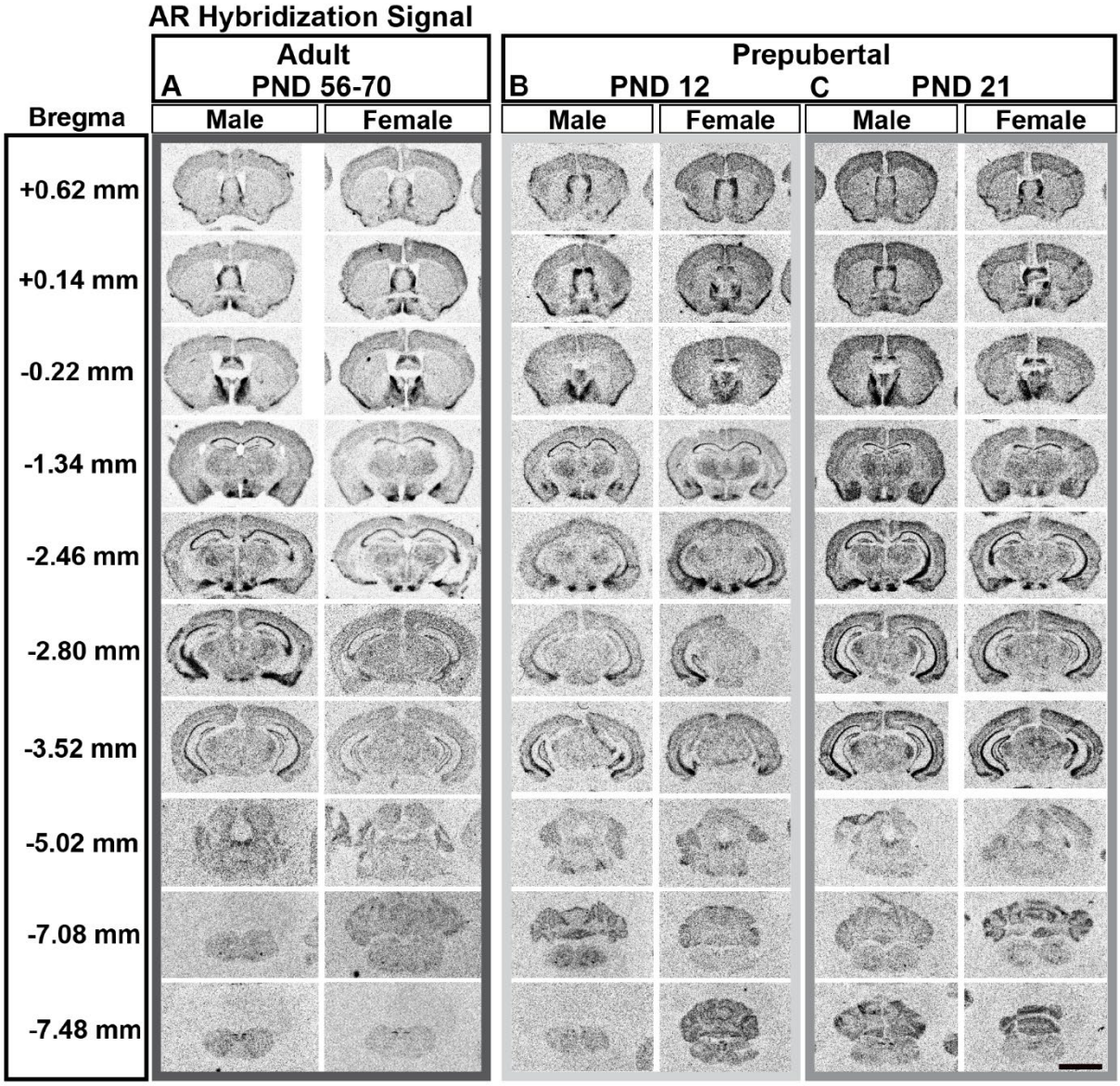

Figure 2.1: *Ar* mRNA hybridization signal expression in male and female postnatal and adult brain. Images from scanned autoradiographic film of adult (postnatal day/PND 56-70, A), and prepubertal (PND 12, B, and PND 21, C) male and female mouse brain. Select coronal sections are shown in rostral to caudal order. Darker signal indicates higher expression of Ar mRNA. Approximate distance from bregma (left column) derived from adult mouse brain (Paxinos and Franklin atlas). Scale bar = 4000 μm.

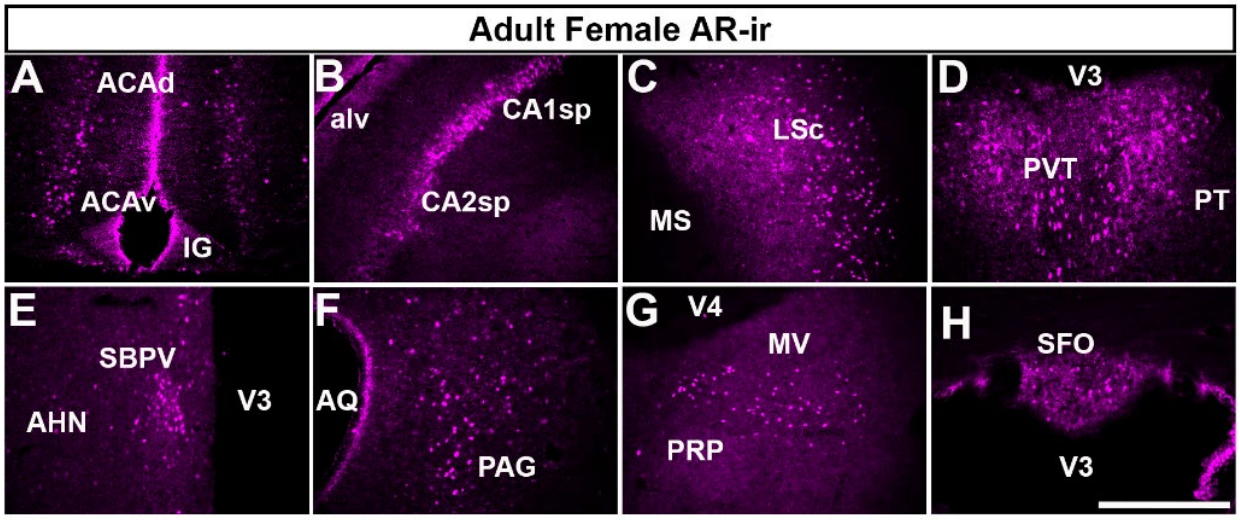

Figure 2.2: AR immunoreactivity (AR-ir) in adult mouse brain. A-H, fluorescent images showing AR-ir in the adult female mouse brain (postnatal day/PND 56-70). AR-ir was observed in virtually all areas where we observed Ar mRNA. Selected areas from (A) cerebral cortex (dorsal and ventral anterior cingulate area, ACAd, ACAv), (B) hippocampal formation (pyramidal layer or sp field CA1 and CA2), (C) cerebral nuclei (lateral septal nucleus, caudodorsal, LSc), (D) thalamus (paraventricular nucleus of the thalamus, PVT), (E) hypothalamus (subparaventricular zone, SBPV), (F) midbrain (periaqueductal gray, PAG), (G) pons/medulla (medial vestibular nucleus, MV), and (H) circumventricular organs (subfornical organ, SFO) are shown. Abbreviations: AHN, anterior hypothalamic nucleus, alv, alveus, AQ, cerebral aqueduct, IG, induseum griseum, MS, medial septal nucleus, PRP, nucleus prepositus, PT, parataenial nucleus, V3, third ventricle, V4, fourth ventricle. Scale bar = 100 μm.

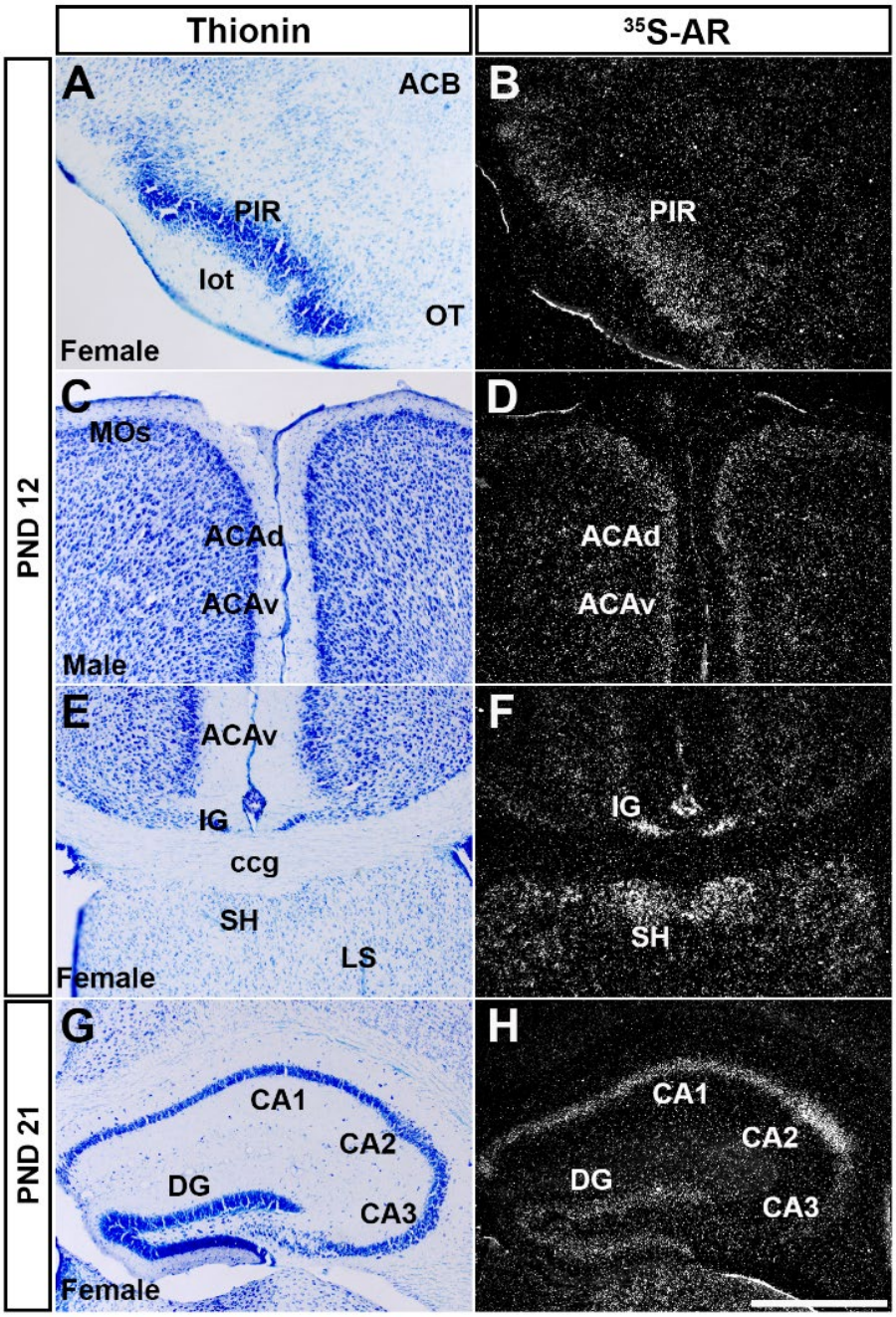

Figure 2.3: *Ar* mRNA expression in cerebral cortex in prepubertal male and female mice. Images showing thionin staining for neuroanatomical reference (left column), silver grains corresponding to *Ar* mRNA (right column). Low AR expression was observed in the piriform area (PIR, A-B), dorsal and ventral anterior cingulate area (ACAd and ACAv, C-D), induseum griseum, septohippocampal nucleus (IG and SH, E-F), and CA3, and high in field CA1 and CA2 (G-H). Abbreviations: ACB, nucleus accumbens, ccg, genu of corpus callosum, DG, dentate gyrus, lot, lateral olfactory tract, LS, lateral septal nucleus, MOs, secondary motor area, OT, olfactory tubercle. Scale bar = 200 μm.

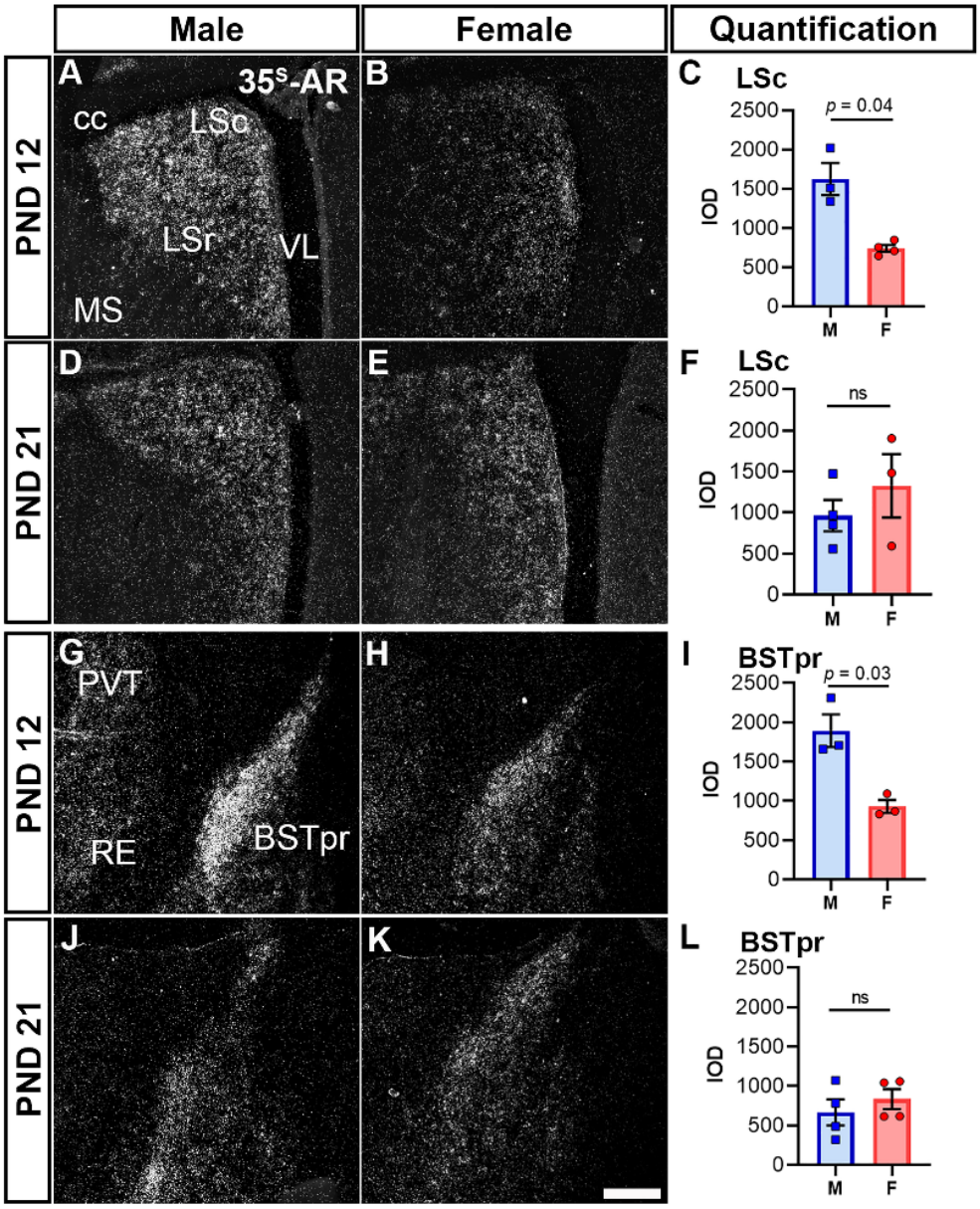

Figure 2.4: *Ar* mRNA expression in cerebral nuclei of male and female prepubertal mice. Silver grain deposition corresponding to *Ar* mRNA hybridization signal in prepubertal (postnatal day (PND) 12 (A-B, G-H), and PND 21 (D-E, J-K) male (A, D, G, J) and female (B, E, H, K) mice. (A-F) Lateral septal nucleus, caudodorsal (LSc) and (G-L) bed nucleus of the stria terminalis, principal nucleus (BSTpr). Bar graphs showing mean ± SEM integrated optical density (IOD) of silver grains (C, F, I, L). IOD was analyzed by *t*-test with Welch's correction for LSc male vs female PND 12 ($P = 0.04$, $n = 3$-4/sex), PND 21 ($P = 0.46$, $n = 3$-4/sex), BST male vs female PND 12 ($P = 0.03$, $n = 3$/sex), and Mann-Whitney nonparametric test for BST male vs female PND 21 ($P = 0.68$, $n = 4$/sex). Abbreviations: cc, corpus callosum, LSr, lateral septal nucleus, rostral (rostroventral), MS, medial septal nucleus, PVT, paraventricular nucleus of the thalamus, RE, nucleus of reuniens, VL, lateral ventricle. Scale bar = 200 µm.

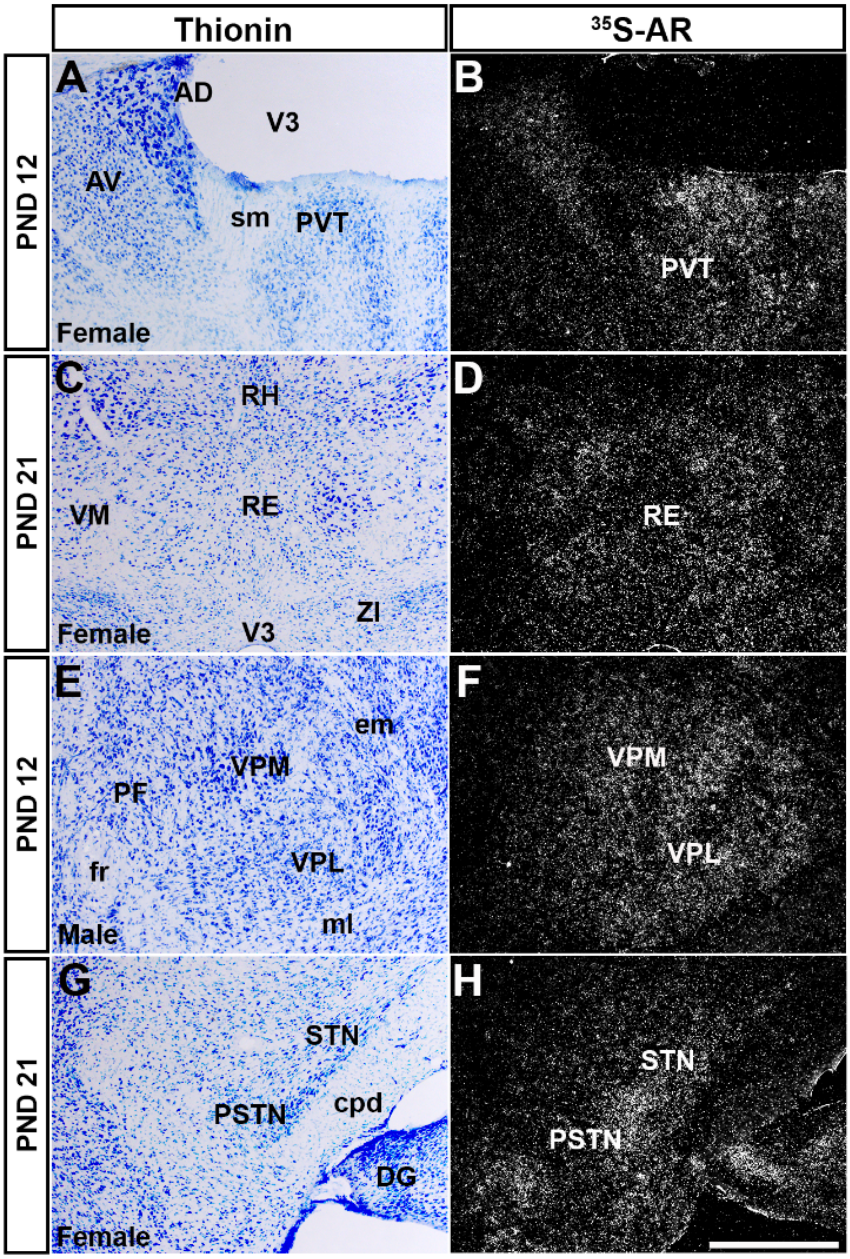

Figure 2.5: *Ar* mRNA expression in thalamic nuclei of male and female prepubertal mice. Images showing thionin staining for neuroanatomical reference (left column), silver grains corresponding to *Ar* mRNA (right column). (A-B) Low silver grain deposition in the paraventricular nucleus of the thalamus (PVT), (C-D) low to moderate in the nucleus of reuniens (RE), (E-F) ventral posterolateral and posteromedial nuclei of the thalamus (VPL and VPM), (G-H) subthalamic and parasubthalamic nuclei (STN and PSTN). Abbreviations: AD, anterodorsal nucleus of the thalamus, AV, anteroventral nucleus of the thalamus, cpd, cerebral peduncle, DG, dentate gyrus, em, external medullary lamina of the thalamus, fr, fasciculus retroflexus, ml, medial lemniscus, PF, parafascicular nucleus, RH, rhomboid nucleus, sm, stria medullaris, VM, ventral medial nucleus of the thalamus, ZI, zona incerta. Scale bar = 200 µm.

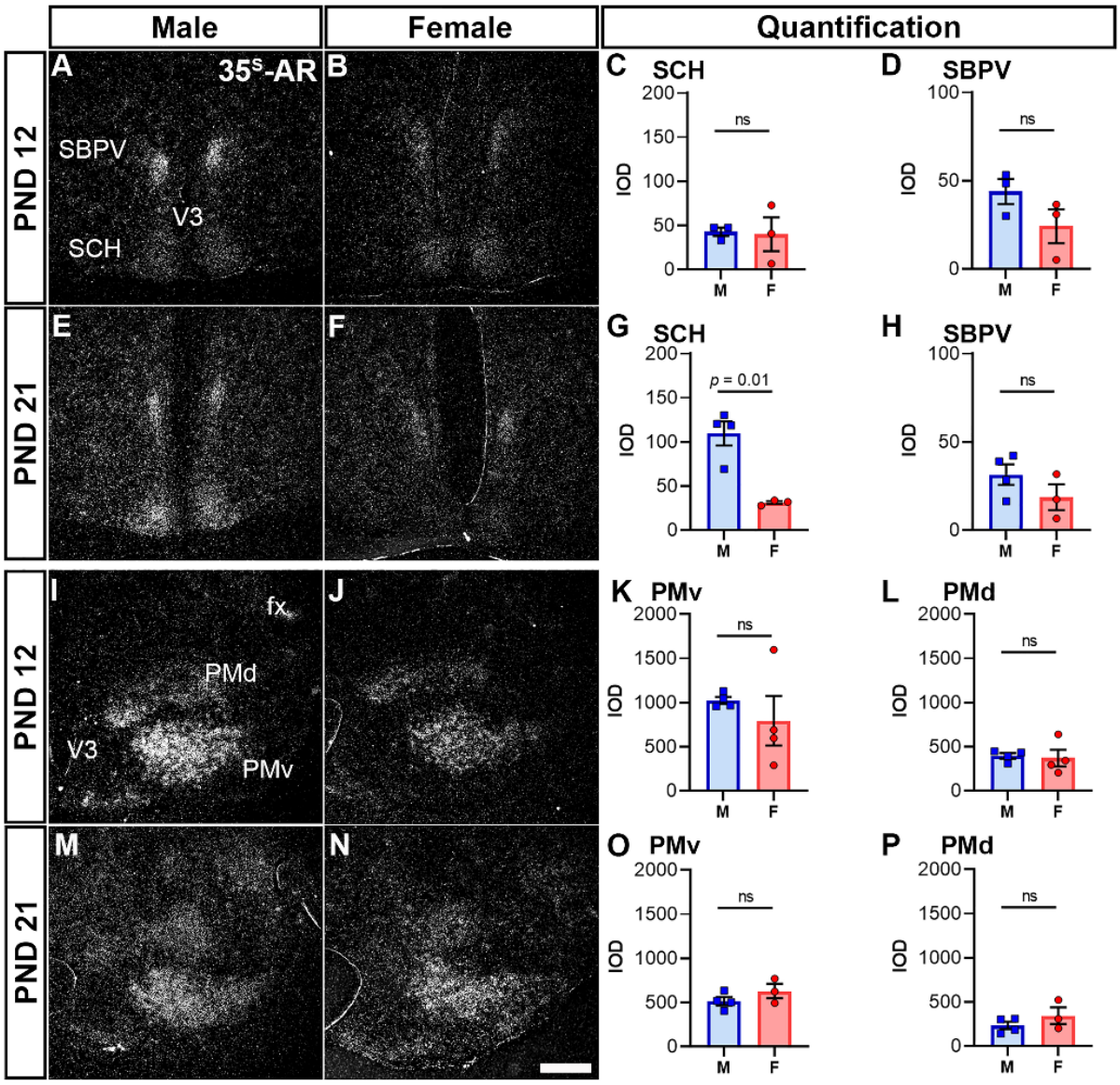

Figure 2.6: *Ar* mRNA expression in hypothalamic nuclei of male and female prepubertal mice. Silver grain deposition corresponding to *Ar* mRNA hybridization signal in prepubertal (postnatal day (PND) 12 (A-B, I-J), and PND 21 (E-F, M-N) male (A, E, I, M) and female (B, F, J, N) mice. (A-H) Suprachiasmatic nucleus (SCH) and subparaventricular zone (SBPV), and (I-P) dorsal and ventral premammillary nuclei (PMd and PMv). Note higher expression of *Ar* in the SCH of males at PND 21 (E). Bar graphs showing mean ± SEM integrated optical density (IOD) of silver grains (C-D, G-H, K-L, O-P). IOD was analyzed by *t*-test with Welch's correction for SCH male vs female PND 21 ($P = 0.01$, $n = 3$-4/sex), SBPV male vs female PND 12 ($P = 0.18$, $n = 3$/sex) and PND 21 ($P = 0.23$, $n = 3$-4/sex), PMv male vs female PND 12 ($P = 0.47$, $n = 3$-4/sex) and PND 21 ($P = 0.30$, $n = 3$-4/sex), PMd male vs female PND 12 ($P = 0.81$, $n = 4$/sex) and PND 21 ($P = 0.37$, $n = 3$-4/sex), and Mann-Whitney nonparametric test for SCH male vs female PND 12 ($P > 0.99$, $n = 3$/sex). Abbreviations: fx, fornix, V3, third ventricle. Scale bar = 200 µm.

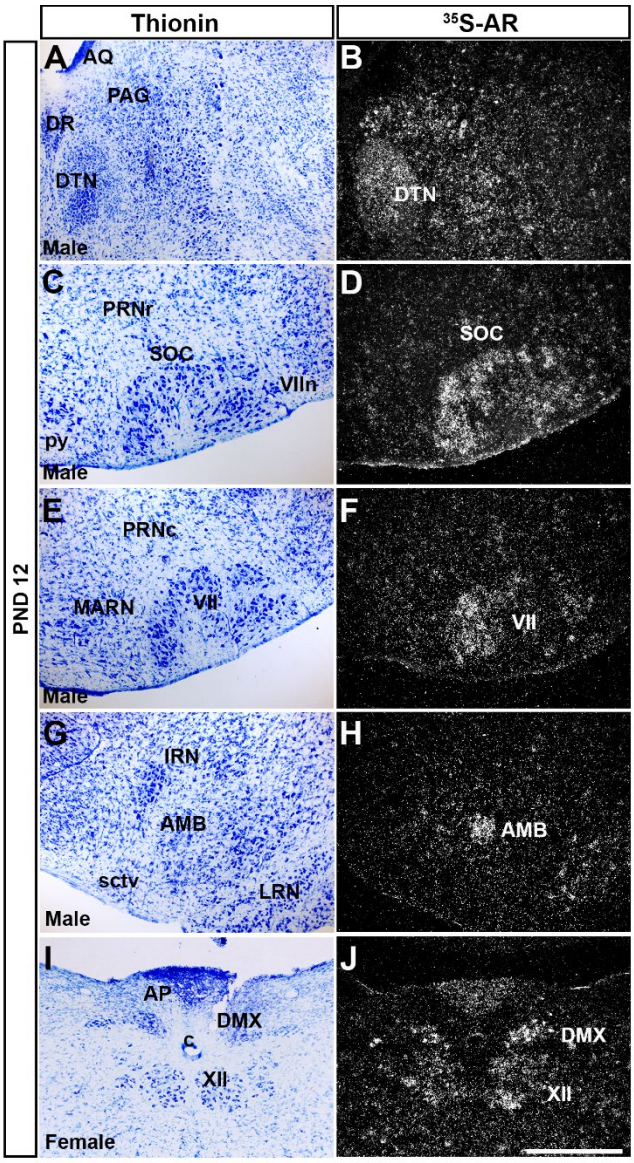

Figure 2.7: *Ar* mRNA expression in brainstem nuclei of prepubertal male and female mice. Images showing thionin staining for neuroanatomical reference (left column), silver grains corresponding to AR mRNA (right column). (A-B) Very low to low silver grain deposition in the periaqueductal gray (PAG), and low in the dorsal tegmental nucleus (DTN). (C-D) Low expression in the superior olivary complex (SOC), (E-F) facial motor nucleus (VII). (G-H) Moderate expression in the nucleus ambiguus (AMB). (I-J) Low to moderate expression in the dorsal motor nucleus of the vagus nerve (DMX) and hypoglossal nucleus (XII). Abbreviations: VIIn, facial nerve, AP, area postrema, AQ, cerebral aqueduct, c, central canal of the spinal cord/medulla, DR, dorsal nucleus raphe, IRN, intermediate reticular nucleus, LRN, lateral reticular nucleus, MARN, magnocellular reticular nucleus, PRNc, pontine reticular nucleus, caudal part, PRNr, pontine reticular nucleus, py, pyramid, sctv, ventral spinocerebellar tract. Scale bar = 200 µm.

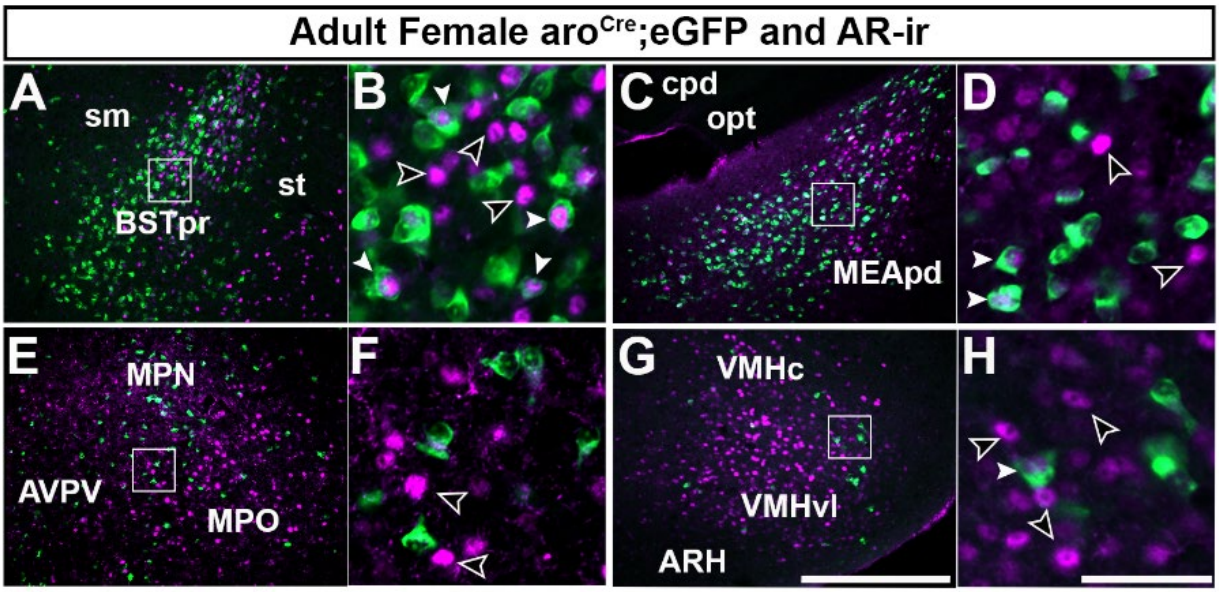

Figure 2.8: Brain areas expressing AR immunoreactivity (AR-ir) and aro^{Cre};eGFP in adult female mice. A-L, fluorescent images showing aro^{Cre};eGFP-L10a reporter mice (green) and AR-ir (purple). B, D, F, and H are higher magnification of highlighted area in A, C, E, and G. Areas with high aro^{Cre};eGFP and AR-ir coexpression include the bed nucleus of the stria terminalis, principal nucleus (BSTpr ,A-B) and medial amygdalar nucleus, posterodorsal (MEApd, C-D). Areas with moderate aro^{Cre};eGFP expression, but high AR expression include the medial preoptic area (MPO, E-F), and ventrolateral ventromedial hypothalamic nucleus (VMHvl, G-H). B, D, F, and H are higher magnification of highlighted areas. Solid white arrows indicate cells that express both AR-ir and aro^{Cre};eGFP, hollow arrows indicate cells that express only AR-ir. Abbreviations: ARH, arcuate hypothalamic nucleus, AVPV, anteroventral periventricular nucleus, cpd, cerebral peduncle, fx, fornix, MPN, medial preoptic nucleus, opt, optic tract, PMv, ventral premammillary nucleus, sm, stria medularis, st, stria terminalis, VMHc, ventromedial hypothalamic nucleus, central part. Scale bar = 100 µm for A, C, E, and G, and 50 µm in B, D, F, and H.

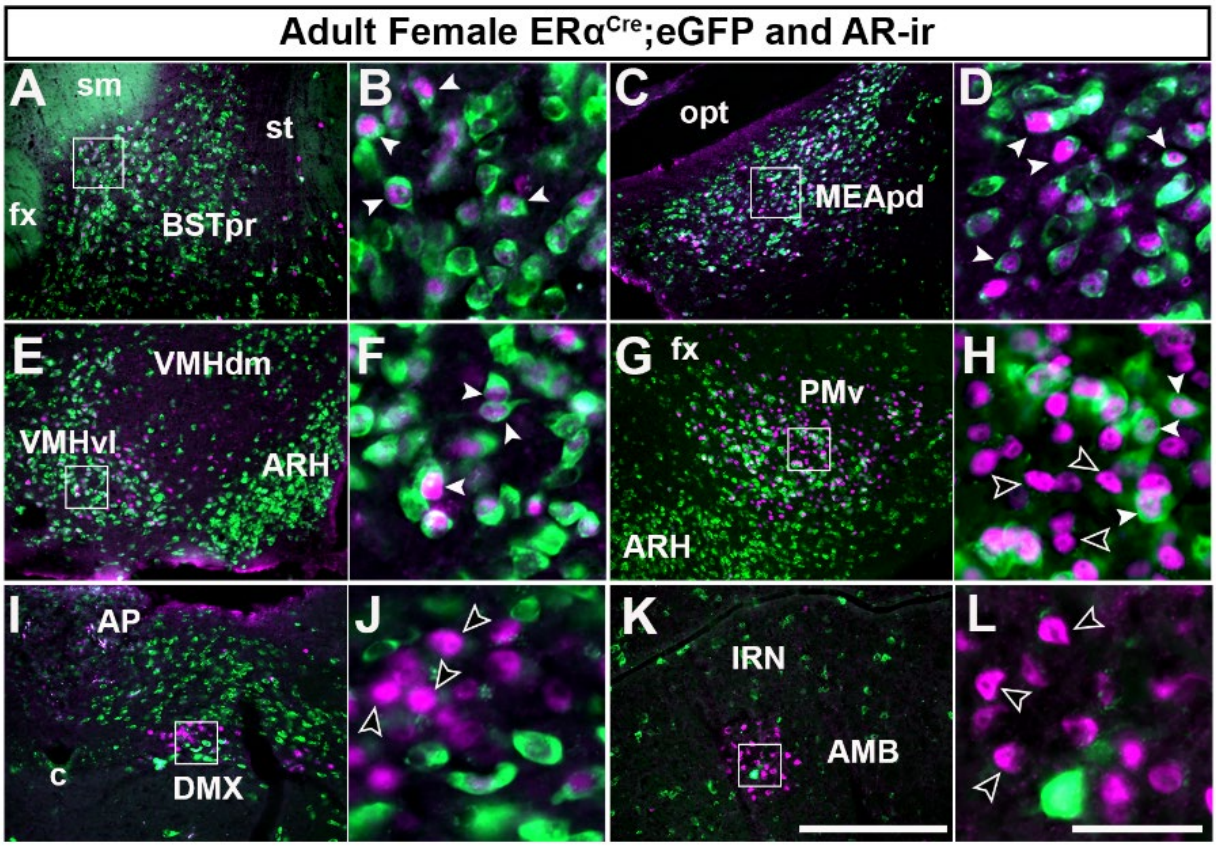

Figure 2.9: Brain areas expressing AR immunoreactivity (AR-ir) and ERα^{Cre};eGFP in adult female mice. A-L, fluorescent images showing AR-ir (purple) and ERα^{Cre};eGFP-L10a expression (green). Areas with high ERα^{Cre};eGFP and AR-ir colocalization include the bed nucleus of the stria terminalis, principal nucleus (BSTpr, A-B) and medial amygdalar nucleus, posterodorsal (MEApd, C-D). Areas with partial ERα^{Cre};eGFP and AR-ir colocalization include the ventrolateral ventromedial hypothalamic nucleus (VMHvl, E-F) and ventral premammillary nucleus (PMv, G-H). The dorsal motor nucleus of the vagus nerve (DMX, I-J) and nucleus ambiguus (AMB, K-L) show distinct AR-ir and ERα^{Cre};eGFP positive cells. B, D, F, H, J, L are higher magnification of highlighted areas. Solid white arrows indicate cells that express both AR-ir and ERα^{Cre};eGFP, hollow arrows indicate cells that express only AR-ir. Abbreviations: AP, area postrema, ARH, arcuate nucleus, c, central canal of the spinal cord/medulla, fx, fornix, IG, induseum griseum, IRN, intermediate reticular nucleus, opt, optic tract, SCH, suprachiasmatic nucleus, sm, stria medularis, st, stria terminalis, V3, third ventricle, VMHdm, ventromedial hypothalamic nucleus, dorsomedial part. Scale bar = 100 µm for A, C, E, G, I, K, and 50 µm for B, D, F, H, J, L.

CHAPTER 3

Lack of AR in LepRb Cells Disrupts Ambulatory Activity and Neuroendocrine Axes in a Sex-Specific Manner in Mice

Abstract

Disorders of androgen imbalance, such as hyperandrogenism in females or hypoandrogenism in males, increase risk of visceral adiposity, type 2 diabetes, and infertility. Androgens act upon androgen receptors (AR) which are expressed in many tissues. In the brain, AR are abundant in hypothalamic nuclei involved in regulation of reproduction and energy homeostasis, yet the role of androgens acting via AR in specific neuronal populations has not been fully elucidated. Leptin receptor (LepRb) expressing neurons co-express AR predominantly in hypothalamic arcuate and ventral pre-mammillary nuclei (ARH and PMv, respectively), with low colocalization in other LepRb neuronal populations, and very low colocalization in the pituitary gland and gonads. Deletion of AR from LepRb expressing cells ($LepRb^{\Delta AR}$) has no effect on body weight, energy expenditure, and glucose homeostasis in male and female mice. However, $LepRb^{\Delta AR}$ female mice show increased body length later in life, whereas male $LepRb^{\Delta AR}$ mice show an increase in spontaneous ambulatory activity. $LepRb^{\Delta AR}$ mice display typical pubertal timing, estrous cycles, and fertility, but increased testosterone levels in males. Removal of sex steroid negative feedback action induced an exaggerated rise in LH in $LepRb^{\Delta AR}$ males and in FSH in $LepRb^{\Delta AR}$ females. Our findings show that AR can directly affect a subset of ARH and PMv neurons in a sex-specific manner and demonstrates specific androgenic actions in the neuroendocrine hypothalamus.

Introduction

Androgens are steroid hormones that play a role in reproductive and metabolic physiology in males and females (1-4). Androgens primarily act upon nuclear hormone receptors to induce gene transcription, resulting in sex-specific differences in reproductive and metabolic physiology. Androgens can act on either estrogen receptors (ERα/β) after conversion to estradiol via the enzyme aromatase, or on androgen receptors (AR) as testosterone or dihydrotestosterone via 5α-reductase (5,6). Many tissues express AR, including gonads, reproductive tract, skeletal muscle, adipose tissue, and the brain. The role of AR in reproductive physiology has been demonstrated using models which lack AR (3) or express a non-functional AR mutant (testicular feminization, Tfm) (7). Global deletion of AR (ARKO) in mice results in male infertility due to lack of proper testicular descent and impaired spermatogenesis (8). These models replicate dysfunctions observed in men with low levels of androgens who experience sexual and reproductive deficits (9). Additionally, female ARKO mice display a subfertile phenotype, with disrupted uterine morphology, fewer corpora lutea, abnormal estrous cycles, and defective folliculogenesis (10). ARKO and Tfm females also display accelerated reproductive senescence (11,12).

In addition to the role that AR plays in the reproductive axis, AR signaling is also required for typical metabolism. Global ARKO male mice display increased body weight, increased adiposity, and glucose intolerance (13,14). Furthermore, liver-specific ARKO males on a high-fat diet show increased body weight and insulin resistance (15), while deletion of AR in beta cells or adipocytes disrupts glucose homeostasis. (16,17).

Androgens via AR exert many effects on peripheral tissues, yet the brain regulates many metabolic and reproductive processes, and abundantly expresses AR. Neuronal deletion of AR has produced controversial data, potentially due to distinct mouse models and different Cre lines used in each study with varying degrees and pattern of AR deletion (18-20). Neuronal ARKO male mice display reduced insulin sensitivity, increased body weight and adiposity later in life in one study (18), and no changes or decreased body weight and length in different studies (19,20). AR is widely expressed in many different areas of the brain, yet the role of AR in specific neuronal populations has not been clearly defined, and it is unclear which populations of neurons mediate androgenic effects.

Several hypothalamic nuclei associated with the control of reproduction and metabolism express leptin receptors (LepRb). Leptin is primarily secreted by white adipocytes in proportion to adipose tissue mass, which signals peripheral energy stores via binding to LepRb (21,22). LepRb expressing neurons in the brain are crucial targets for converging metabolic and reproductive signals, and are required for the central control of metabolism and reproduction (23-28). States of low leptin or leptin resistance are associated with infertility, diabetes, and obesity (29-34). We and others have shown that LepRb cells in the ventral pre-mammillary nucleus (PMv) and in arcuate agouti-related peptide (AgRP) neurons, which co-express LepRb (35), integrate metabolic and reproductive signals required for timing of puberty and fertility (36-40). Therefore, we hypothesized that AR in LepRb cells contributes to the regulation of reproduction and metabolism at the hypothalamic level, and that loss of AR from LepRb cells would disrupt reproductive and metabolic homeostasis. We initially made a whole-body evaluation of LepRb and AR

colocalization and used a Cre-loxP approach to systematically assess the metabolic and reproductive phenotype generated by lack of AR signaling in LepRb cells in male and female mice.

Materials and Methods

Animal Ethics

All research animals were acquired, used, and maintained in accordance with the National Research Council *Guide for the Care and Use of Laboratory Animals* (41), as well as federal, state, and local laws. Procedures and protocols were approved by the University of Michigan Committee on Use and Care of Animals (IACUC, Animal Protocol: PRO00008712).

Animals

LepRb-Cre (LepRb^{Cre}, JAX® mice, B6.129-*Lepr$^{tm3(cre)Mgmj}$*/J, stock #032457 (42,43)), AR-flox (AR^{flox}, 129-*Ar^{tm1Verh}*/Sv, provided by Dr. S. Marc Breedlove, Michigan State University, with permission from Dr. Karel De Gendt, Catholic University of Leuven, Belgium, UFA ID: 16-UFA03327 (8)), ROSA26-loxSTOPlox-eGFP-L10a (JAX® mice, B6;129S4-*Gt(ROSA)26Sor$^{tm9(EGFP/Rpl10aAmc/}$*J, stock #024750, (44)), C57BL/6J (JAX® mice, stock # 000664), and FVB/NJ (JAX® mice, stock #001800) mice were housed in an Association for Assessment and Accreditation of Laboratory Animal Care (AAALAC) accredited facility at the University of Michigan Medical School. Mice were housed in a 12:12 light/dark cycle environment with controlled temperature (21-23°C) and humidity (30-70%). Mice were provided water ad libitum and were fed a phytoestrogen-reduced diet (16% protein, 4.0% fat, 48.5% carbohydrate, Teklad 2916 irradiated global rodent diet, Envigo) or a phytoestrogen-reduced, higher protein and fat diet (19% protein, 9.0% fat, 44.9% carbohydrate, Teklad 2919 irradiated global rodent diet, Envigo)

for breeding and lactating females. Phytoestrogen-reduced diets were used to avoid any effects of exogenous dietary estrogens on reproductive or metabolic physiology of experimental mice.

LepRb-specific deletion of AR (LepRb$^{\Delta AR}$)

A Cre-loxP approach was used to generate mice with deletion of AR in LepRb expressing neurons. *Lepr*^{Cre} mice, which contain an IRES element plus the coding sequences for Cre-recombinase knocked into the LepRb-specific exon of *Lepr* (42) were crossed with mice expressing lox-P sites flanking exon 2 of the *Ar* gene, located on the X chromosome (AR^{flox} mice) (8). Mice were bred to homozygosity or hemizygosity for *Ar*^{flox} (*Ar*$^{fl/fl}$ females and *Ar*$^{fl/Y}$ males), and homozygosity for *Lepr*^{Cre}, as complete Cre-mediated excision of floxed alleles is only accomplished with two copies of Cre under the *Lepr* promoter (45-47). No metabolic or reproductive phenotypes are observed in mice homozygous for *Lepr*^{Cre} (46). Experimental mice (LepRb$^{\Delta AR}$ mice = *Lepr*$^{Cre/Cre}$; *Ar*$^{fl/fl}$ females or *Ar*$^{fl/Y}$ males) were compared to littermates homozygous for the wild-type allele of *Lepr* (AR^{flox} mice = *Lepr*$^{wt/wt}$; *Ar*$^{fl/fl}$ females or *Ar*$^{fl/Y}$ males). For scientific rigor and reproducibility, we performed the same experiment in at least two independent cohorts. Experimental animals were derived from multiple breeding pairs (a minimum of 5, but up to 10 breeding pairs per data set). Each graph shown includes animals derived from different pairs of breeders to account for differences in vivarium conditions. Genotyping was performed on DNA extracted from ear samples or tail tips obtained prior to weaning and at termination of experiments (RED Extract-N-Amp Tissue PCR Kit, Cat #XNAT, MilliporeSigma). Genotyping primers are listed in Table 3.1.

Table 3.1: Primers used for genotyping

Mice	Primer Sequence	Size (bp)
LepRb^{Cre}	Comm FOR 5' TCC AAG AAG CCT CAA GGT TCC A 3' Wt REV 5' TCG TGT TGA AAT TTC TTC TTT CCA GA 3' Cre REV 5' ACG CAC ACC GGC CTT ATT CC 3'	Wt: 300 Mutant: 200
AR^{flox}	mAR28 5' AGC CTG TAT ACT CAG TTG GGG 3' mAR29 5' AAT GCA TCA CAT TAA GTT GAT ACC 3'	Wt: 860 Flox: 930
R26-loxSTOPlox-eGFP-L10a	FOR 1 5' GAG GGG AGT GTT GCA ATA CC 3' FOR 2 5' TCT ACA AAT GTG GTA GAT CCA GGC 3' REV 5' CAG ATG ACT ACC TAT CCT CCC 3'	Wt: 300 Mutant: 200

Immunohistochemistry

To assess where AR and LepRb colocalize, we crossed LepRb^{Cre} mice with reporter mice that express eGFP-L10a in a Cre-dependent manner to obtain LepRb^{Cre} reporter mice (48). Adult male (n = 5/genotype) and female (n = 4/genotype) LepRb^{Cre} and LepRb$^{\Delta AR}$ reporter mice were deeply anesthetized with isoflurane and trans-cardially perfused with 10% neutral buffered formalin for 10 min. Brains were dissected and post-fixed for 2 h, then transferred to 20% sucrose in 0.1M PBS overnight for cryoprotection. Brains were sectioned at 30 µm on a freezing microtome (Leica SM 2010R) into 4-5 series and stored at -20°C in cryoprotectant. AR immunoreactivity was labelled using a modified tyramide signal amplification method previously described (49). Brain sections were rinsed with 0.1M PBS, incubated in 0.6% hydrogen peroxide for 30 mins, rinsed with 0.1M PBS, then blocked with 3% normal donkey serum with 0.25% Triton-X-100 for 1 h at room temperature. Sections were incubated overnight with rabbit anti-androgen receptor antibody (1:200, AbCam [EPR1535(2)], Cat # ab133273, RRID: AB_11156085). Sections were rinsed with 0.1M PBS and then incubated for 1 h with biotinylated donkey anti-rabbit IgG (1:500, Jackson ImmunoResearch Laboratories, Cat # 711-065-152, RRID: AB_2340593), followed by incubation in avidin-biotin (AB) solution in PBS (1:1000, Vector Laboratories) for 1 h. Next, sections were

incubated in biotinylated tyramide (1:250, Perkin Elmer) with 0.009% hydrogen peroxide for 10 mins, followed by incubation with streptavidin-conjugated AlexaFluor 594 (1:1000, Invitrogen, ThermoFisher) for 1 h. Sections were mounted onto gelatin-coated slides and coverslipped with ProLong Gold Antifade mounting medium (Invitrogen, ThermoFisher). The eGFP-L10a reporter did not require additional immunostaining to amplify fluorescent signal.

To assess potential deletion of AR in neuroendocrine tissues, testes, ovaries, and pituitary gland were examined for $LepRb^{Cre}$ mediated eGFP-L10a and AR expression. Fixed frozen gonads and pituitary were cryoprotected and embedded in optimal cutting temperature (OCT) compound (Electron Microscopy Systems). They were sectioned at 30 µm for testes, 12 µm for ovaries, and 14 µm for pituitary on a cryostat (Leica CM 3050S) into 3-5 series on SuperFrost Plus slides (Fisher Scientific) and stored at -20°C. AR staining was performed as described above.

To assess potential compensation of sex steroid receptors in $LepRb^{\Delta AR}$ cells, brain sections from male $LepRb^{Cre}$ and $LepRb^{\Delta AR}$ reporter mice (n = 4/genotype) were stained for ERα immunoreactivity. Brain sections were rinsed with 0.1M PBS, then blocked with 3% normal donkey serum with 0.25% Triton-X-100 for 1 h at room temperature. Sections were incubated overnight in rabbit anti-estrogen receptor α antibody (1:5000, Millipore, Cat # 06-935, RRID: AB_310305). Sections were rinsed with 0.1M PBS and then incubated for 1 h with donkey anti-rabbit AlexaFluor 594 Plus (1:500, Invitrogen ThermoFisher, Cat # A32754, RRID: AB_2762827) for 1 h. Sections were mounted onto gelatin-coated slides and coverslipped with ProLong Gold Antifade mounting medium (Invitrogen, ThermoFisher). Antibodies used are listed in Table 3.2.

Table 3.2: Antibodies

Peptide/Protein Target	Antibody Name	Cat#	Species Raised in	Dilution Used	RRID
Androgen receptor	Recombinant Anti-Androgen Receptor antibody [EPR1535(2)]	AbCam ab133273	Rabbit, Monoclonal	1:200	AB_11156085
Estrogen Receptor α	Anti-Estrogen Receptor α antibody (C1355)	Millipore 06-935	Rabbit, Polyclonal	1:5000	AB_310305
Rabbit IgG	Biotin-SP-conjugated AffiniPure Donkey Anti-Rabbit IgG	Jackson ImmunoResearch 711-065-152	Donkey, Polyclonal	1:500	AB_2340593
Rabbit IgG	Donkey anti-Rabbit IgG AlexaFluor® Plus 594	Invitrogen ThermoFisher, A32754	Donkey, Polyclonal	1:1000	AB_2762827

Metabolic phenotyping

Body weight of experimental and control mice was measured weekly beginning at weaning (post-natal day 21). Body composition (fat and lean mass) was quantified at 15-week old male (n = 10-13 mice/genotype), and female (n = 8-9 mice/genotype) $LepRb^{\Delta AR}$ and AR^{flox} mice using an NMR-based device (Minispec LF 90II, Bruker Optics). Comprehensive Laboratory Monitoring System (CLAMS, Columbia Instruments) unit was used as an indirect calorimeter to measure O2 consumption (VO2), CO2 production (VCO2), as well as food intake and spontaneous motor activity via photo beam sensors. Body composition and CLAMS analysis was performed at the Michigan Mouse Metabolic Phenotyping Center (MMPC). Male (15 weeks of age, n = 10-11 mice/genotype) and female (19-21 weeks of age, n = 8-9 mice/genotype) $LepRb^{\Delta AR}$ and AR^{flox} mice were transferred to the MMPC for CLAMS analysis. Mice were weighed before measurements and individually placed into the sealed chambers with free access to food and water. After 48 h of adaptation, measurements were carried out continuously for 72 h. VO2 and VCO2

were sampled in 10 min intervals and the motor activity was recorded every second in X and Z dimensions. Total energy expenditure was calculated respectively based on the values of VO2 and VCO2. Indirect calorimetry data was normalized to lean body mass (LBM) recorded at the end of the CLAMS run using an NMR-based device (Minispec LF 90II, Bruker Optics). Total energy expenditure was calculated using the following formula: Energy Expenditure = 3.91 x [($VO2_{LBM}$) + 1.1 x ($VCO2_{LBM}$)]/1000.

Glucose levels were measured in blood samples obtained from tail-tip bleeding in male (*n* = 5-8 mice/genotype, 11-15 weeks of age) and female (*n* = 7 mice/genotype, 20-21 weeks of age, after estrous cycle analysis was completed) $LepRb^{\Delta AR}$ and AR^{flox} mice after an overnight fast (approximately 16 h) using a glucometer (OneTouch Ultra, LifeScan Inc). Males were single housed up to 2 weeks prior to and during GTT. After fasting blood glucose was measured, mice received an intraperitoneal bolus of D-glucose in sterile saline (2 mg D-glucose/g body weight) at 0 min, and tail tip blood was collected for glucose levels at 15 min intervals for the first hour, and 30 min intervals for the second hour (2 h total).

An additional group of male (n = 9-10/genotype) and female (n = 7-8/genotype) $LepRb^{\Delta AR}$ and AR^{flox} mice were fed high-fat diet (HFD, Teklad TD.88137, 42% fat, 15.2% protein, 42.7% carbohydrate, Envigo) for 12 weeks beginning at weaning. Mice were weighed weekly, and GTT performed at 16 weeks of age.

Body length was measured as snout to anus distance in isoflurane (Fluriso, VetOne) anesthetized LepRb$^{\Delta AR}$ and AR^{flox} male (*n* = 10-12 mice/genotype) and female (*n* = 14-15 mice/genotype) mice at 15 weeks of age, and at 20 weeks of age as a follow-up for females.

Tissue collection and organ weight

Adult LepRb$^{\Delta AR}$ and AR^{flox} mice were deeply anesthetized with isoflurane and euthanized via decapitation. Females were euthanized during diestrus, as confirmed by the presence of predominantly leukocytes in vaginal smear and a uterine weight of less than 100 mg (50). Trunk blood was collected and allowed to clot for 45 min at room temperature, then centrifuged at 4°C for 20 min at 3,000 x g, followed by collection of serum which was stored at -20°C. Testes and seminal vesicles were dissected and weighed. Femurs were collected from LepRb$^{\Delta AR}$ and AR^{flox} female mice at 20 weeks of age, fixed in 10% neural buffered formalin for 48 h, then transferred to 70% ethanol. Tissue was removed from bone, and femur length was measured using digital calipers. Pituitary gland and whole hypothalamus were quickly collected, frozen on dry ice, and stored at -80°C until RNA extraction.

Reproductive Phenotyping

Timing of pubertal onset was monitored daily beginning at weaning (post-natal day 21) in male (*n* = 14-17 mice/genotype) and female (*n* = 10-12 mice/genotype) LepRb$^{\Delta AR}$ and AR^{flox} mice. Female mice were checked for day of vaginal opening (VO) and day of first estrus, defined by the presence of keratinized epithelial cells in vaginal lavage for two consecutive days following presence of predominantly leukocytes or one day preceded by proestrus (51-53). Male mice were checked daily for completion of balanopreputial separation (BPS) by applying gentle pressure to the

prepuce (54). Estrous cyclicity was analyzed in female mice beginning at 8-10 weeks of age. Vaginal lavage was performed daily for 35 consecutive days and estrous cycle stage determined based on the proportion of leukocytes, epithelial, and keratinized epithelial cells (55). Estrous cycle length was determined by counting the number of days between the first day of estrous in each cycle, and averaged for each female. Percentage of days in each estrous cycle stage was calculated as number of days in each cycle (diestrus, proestrus, or estrus) divided by 35 total days. Number of cycles over the total sampling period were counted as the number of complete estrous cycles in 35 days.

One female LepRb$^{\Delta AR}$ and one AR^{flox} mouse (n = 6 mice/genotype) at 10 weeks of age were trio-mated with a sexually-experienced male C57BL/6J (8-10 weeks of age) mouse. Male LepRb$^{\Delta AR}$ and AR^{flox} mice (n = 7-8 mice/genotype) at 8 weeks of age were trio-bred with two FVB/NJ females (8-10 weeks of age). FVB/NJ female mice were chosen for their high fecundity and high percent of productive matings (56). Trios were allowed to breed until delivery of two consecutive litters per female. Time to first litter and inter-litter interval (latency to birth), and number of pups per litter for females were recorded.

Sex steroid and gonadotropin assays

To assess response of the HPG axis to negative feedback, male LepRb$^{\Delta AR}$ and AR^{flox} mice (n = 7-11 per group) were orchidectomized (ORX), and female LepRb$^{\Delta AR}$ and AR^{flox} mice (n = 5-13) ovariectomized (OVX) under isoflurane anesthesia. One week after gonadectomy, mice were deeply anesthetized with isoflurane, and euthanized via decapitation. Intact female LepRb$^{\Delta AR}$ and AR^{flox} mice were euthanized during diestrus. Trunk blood was collected as described above, and

serum samples were sent to the University of Virginia Ligand Core for the following assays: mouse/rat LH/FSH multiplex (LH reportable range = 0.24 – 30.0 ng/mL, FSH reportable range = 0.48 – 300.0 ng/mL, intra-assay %CV = 4.0-5.4, inter-assay %CV = 8.6 - 8.9), mouse/rat testosterone IBL ELISA (IBL, Cat# IB79174, RRID#: AB_2784504, reportable range = 10.0 - 1600.0 ng/dL, assay sensitivity = 6.6 ng/dL, intra-assay %CV = 5.4 - 6.0, inter-assay %CV = 7.8 - 9.4). ORX LepRb$^{\Delta AR}$ and AR^{flox} males were compared to intact LepRb$^{\Delta AR}$ and AR^{flox} males (*n* = 11-15 per group). An additional group of LepRb$^{\Delta AR}$ and AR^{flox} males (*n* = 8-9 per group) were single housed for at least 2 weeks prior to ORX to control for a group housed setting, which may alter testosterone levels in male mice (57).

For female serum testosterone, Δ-4 steroids analysis via LC/MS/MS was performed at the Michigan Regional Comprehensive Metabolomics Resource Core at the University of Michigan. Mouse serum samples were processed using 30 µL of serum to 100 µL of internal standard and were reconstituted with 100 µL of 40% methanol in water for a sample dilution of 3.33x. This was done to keep processing consistent with sample volume being limited. Samples were extracted using SLE and injection volume was 20 µL. Serum samples with remaining volume were pooled and then processed in 3200 µL aliquots of serum with 100 µL of internal standard and were reconstituted with 100 µL of 40% methanol in water for a sample dilution of 0.5 (2x concentration). This was done because previous lower volume samples showed very few measurable signals. Samples were extracted using SLE and injection volume was 20 µL. Variation was fairly high as signal strength, while quantifiable, was still quite low. This was to be expected and for this reason multiple injections were made and averaged.

Serum IGF1 assay

To assess serum insulin-like growth factor 1 (IGF1) levels in females at 20 weeks of age, trunk blood was collected and serum processed as described above. Serum IGF1 was quantified using a mouse/rat IGF1 Quantikine ELISA Kit (R&D Systems, Cat# MG100, RRID#: AB_884569, assay range = 31.2 - 2,000 pg/mL, assay sensitivity = 8.4 pg/mL, intra-assay %CV = 3.3 - 5.6, inter-assay %CV 4.3 – 9.1) following manufacturer's instructions. Samples were assayed in duplicate.

Quantitative PCR (qPCR)

Pituitary gland and whole hypothalamus from adult, gonad intact, group housed male AR^{flox} (n = 3-4) and $LepRb^{\Delta AR}$ (n = 4) mice were homogenized with Qiazol reagent (Qiagen), and total RNA was isolated using the RNeasy Plus Mini kit (Qiagen), including genomic DNA elimination, following manufacturer's instructions. First-strand cDNA was synthesized using SuperScript® II reverse transcriptase and oligo(dT). Gene expression was quantified in triplicate samples using qPCR with a CFX-384 Bio-Rad Real-Time PCR detection system with SYBR Green® (ThermoFisher) reaction for *Kiss1*, *Tac2*, and *Pdyn*, and TaqMan Gene Expression MasterMix (Applied Biosystems) for *Ar*. Transcript levels were normalized to the housekeeping gene β-actin (*Actb*). mRNA expression of target genes in male AR^{flox} and $LepRb^{\Delta AR}$ mice was determined by a comparative cycle threshold (Ct) and relative (to *Actb*) gene copy number was calculated as $2^{-\Delta\Delta Ct}$, and is presented as the percentage of relative mRNA expression of AR^{flox} mice. Primers used are shown in Table 3.3.

Table 3.3: qPCR Primers

Gene	Primer Sequence	Company	Reference
Ar	FOR 5' CTG CCT TGT TAT CTA GCC TCA 3' REV 5' ATA CTG AAT GAC CGC CAT CTG 3' Probe: /56-FAM/ACC ACA TGC /ZEN/ACA AGC TGC CTC T/3IABkFQ/	IDT	Mm.PT.47.17416675
Kiss1	FOR 5' GCT GCT GCT TCT CCT CTG TG 3' REV 5' TCT GCA TAC CGC GAT TCC TT 3'	IDT	Custom
Tac2	FOR 5' TCT GTG TGG GAT GTA AAG GAG GG 3' REV 5' GAC AGC GCG AAA CAG CAT GG 3'	IDT	Custom
Pdyn	FOR 5' CGT TGC TGT CAA GAT CTG TTG 3' REV 5' AGG CAG TCC GCC ATA ACA TT 3'	IDT	Custom
Actb	FOR 5' GAT TAC TGC TCT GGC TCC TAG 3' REV 5' GAC TCA TCG TAC TCC TGC TTG 3' Probe: 5' CTG GCC TCA /ZEN/CTG TCC ACC TTC C 3'	IDT	Mm.PT.39a.22214843.g
Actb	FOR 5' CAG CCT TCC TTC TTG GGT ATG G 3' REV 5' AGC TCA GTA ACA GTC CGC CT 3'	IDT	Custom

Analysis of Data and Image Production

Digital images were acquired using an Axio Imager M2 (Carl Zeiss) with a digital camera (AxioCam, Zeiss) using Zen Pro 2 software (Zeiss). Colocalization of neurons that express AR-ir and eGFP-L10a was quantified in one section on one side of each animal (n = 4-5 mice/sex) in specific hypothalamic nuclei (medial pre-optic area, MPO, rostral (rARH), mid (mARH), and caudal (cARH) arcuate, dorsomedial nucleus of the hypothalamus, DMH, PMv, nucleus of the solitary tract, NTS). Colocalization of neurons that express ERα-ir and eGFP-L10a was quantified in one section on one side of each animal (n = 4/genotype) in mARH and PMv. Cell counts were performed on images taken at 20× magnification using Photoshop software (Adobe Creative Cloud) Analysis Count Tool. Adobe Photoshop and Illustrator software were used to crop, scale, label, and assemble images into figures.

Statistics

Data are reported as mean ± standard error of the mean (SEM). Data analysis was performed using GraphPad Prism software (Version 8). Data was analyzed for normal distribution using Shapiro-Wilk test (significance level alpha 0.05). Unpaired t-test with Welch's correction was used for day of VO, latency to birth for males, number of pups per litter, percentage of days in diestrus and estrus, femur length, serum IGF1, female serum testosterone, single housed male serum testosterone, female fat mass, female body length, food intake, energy expenditure (male and female, dark, light and 24h), ambulatory activity (male, dark and light phase, female, dark, light, and 24h), fasting blood glucose, area under the curve for GTT, pituitary *Ar* and hypothalamic *Kiss1*, *Tac2*, and *Pdyn* relative gene expression. Non-normal data was analyzed using Mann-Whitney non-parametric test (first estrus, female latency to birth, day of BPS, percentage of days in proestrus, cycle length, number of cycles, testes and seminal vesicle mass, male fat mass, male and female lean mass, male body length, and male 24 h activity). Male serum testosterone values were log transformed prior to analysis by Mann-Whitney non-parametric test for group housed males and unpaired t-test with Welch's correction for single housed males. Analysis for potential outliers was performed using the ROUT method (Q = 1%). Two-way ANOVA with repeated measures and Holm-Sidak correction was used to analyze glucose tolerance test and body weight data. Serum LH and FSH values were analyzed by two-way ANOVA with multiple comparisons and Holm-Sidak correction. Exact *P* values are reported and statistical significance is defined as $P < 0.05$.

Results

High colocalization of AR and LepRb in the arcuate and PMv nuclei

Several populations of LepRb neurons have been described in brain sites that also contain AR. These include the medial pre-optic area (MPO), arcuate nucleus (ARH), dorsomedial nucleus of the hypothalamus (DMH), ventral premammillary nucleus (PMv), and nucleus of the solitary tract (NTS) (43,58,59). Expression of AR in LepRb neurons was observed primarily in the ARH and PMv of both males and females (Figure 3.1A-D), which is consistent with previous studies (60).

Table 3.4: Colocalization quantification of LepRb neurons with AR

	Control Mice					
	Male: LepRb^{Cre}			**Female: LepRb^{Cre}**		
Nucleus	**#LepRb**	**#LepRb+AR**	**%LepRb+AR**	**#LepRb**	**#LepRb+AR**	**%LepRb+AR**
rARH	138.4 ± 6.80	32.2 ± 5.78	23.44 ± 4.07	124 ± 8.90	30.5 ± 6.69	24.28 ± 4.34
mARH	187.4 ± 15.39	54.6 ± 11.61	28.24 ± 4.09	164.0 ± 17.57	49.75 ± 7.75	30.30 ± 3.65
cARH	135.4 ± 8.41	13.4 ± 6.32	10.05 ± 4.55	155.0 ± 14.53	19.0 ± 4.38	11.91 ± 1.76
PMv	228.6 ± 25.05	114 ± 16.65	49.76 ± 3.44	233.0 ± 24.27	84.5 ± 22.05	35.78 ± 7.61
MPO	54.4 ± 7.45	7.6 ± 2.42	13.98 ± 3.49	57.25 ± 6.14	3.5 ± 0.87	6.03 ± 1.02
DMH	221.8 ± 51.78	24.4 ± 5.47	11.92 ± 2.64	253.25 ± 5.92	12.0 ± 0.91	4.76 ± 0.45
NTS	27.0 ± 6.35	2.67 ± 0.88	9.30 ± 1.53	36.75 ± 6.45	2.0 ± 0.0	6.05 ± 1.17

In the mid-ARH, approximately 30% of LepRb cells express AR in both sexes (Figure 3.1K). Most colocalization of AR and LepRb was observed at the mid/tuberal region of the ARH, with fewer LepRb cells co-expressing AR in the caudal and rostral ARH (rARH, ~24%, cARH, ~10-12%, Table 3.4). The PMv has the highest degree of colocalization, with approximately 49% of male and 35% of female LepRb cells expressing AR. Other nuclei, including the MPO (Figure 3.1E-F), DMH (Figure 3.1G-H), and NTS (Figure 3.1I-J) contained less than 15% of LepRb cells co-expressing AR in both sexes.

In the pituitary gland, very few cells express LepRb$^{Cre;eGFPL10a}$ (Figure 3.2A-C), and expression was sporadic and dispersed. qPCR was used to validate that *Ar* transcript levels were not affected in the pituitary gland. *Ar* gene expression levels relative to the housekeeper *Actb* were not significantly different in the pituitary gland of LepRb$^{\Delta AR}$ mice (AR^{flox} relative expression = 100%, SEM = 28.59, LepRb$^{\Delta AR}$ relative expression = 162%, SEM = 19.86, t-test with Welch's correction, $P = 0.12$). In the testis, LepRb$^{Cre;eGFPL10a}$ and AR co-expression was observed in few Leydig cells. Sertoli cells strongly express AR, but do not express LepRb$^{Cre;eGFPL10a}$ (Figure 3.2D-F). LepRb$^{Cre;eGFPL10a}$ cells were virtually absent in ovarian granulosa cells and theca cells, but were observed sporadically in ovarian parenchyma (Figure 3.2G-L). Liver, bone, and muscle were examined for LepRb$^{Cre;eGFPL10a}$, but reporter gene expression was very low or absent in these tissues. This pattern of co-localization between LepRb and AR indicate that the observed phenotype of LepRb$^{\Delta AR}$ mice are primarily due to deletion of AR in LepRb cells in the ARH and PMv. In LepRb$^{\Delta AR}$ mice, less than 4% (approximately 5-6 cells per mouse) of LepRb neurons express AR in the ARH and PMv of LepRb$^{\Delta AR}$ mice, indicating efficient deletion of AR in LepRb cells (Figure 3.3A-E and Table 3.5).

Table 3.5: Colocalization quantification of LepRb neurons with AR in knockout mice (LepRb$^{\Delta AR}$)

	Knockout Mice					
	Male: LepRb$^{\Delta AR}$			**Female: LepRb$^{\Delta AR}$**		
Nucleus	**#LepRb**	**#LepRb+AR**	**%LepRb+AR**	**#LepRb**	**#LepRb+AR**	**%LepRb+AR**
rARH	120 ± 13.85	2.2 ± 0.58	1.75 ± 0.35	139.25 ± 20.17	1.50 ± 0.65	0.99 ± 0.36
mARH	162.8 ± 21.85	5.8 ± 1.36	3.60 ± 0.70	169.25 ± 14.01	1.75 ± 0.85	1.03 ± 0.53
cARH	140 ± 8.44	1.8 ± 0.49	1.34 ± 0.35	144.75 ± 17.38	0.75 ± 0.25	0.58 ± 0.22
PMv	238.4 ± 30.29	6.6 ± 1.72	2.95 ± 0.68	289.5 ± 12.65	3.0 ± 1.22	1.03 ± 0.44

No increase in ERα expression in the ARH and PMv of LepRb$^{\Delta AR}$ mice

Fewer than 20% of LepRb cells in the ARH and PMv have been described to coexpress ERα in male and female mice (61). Neuronal deletion of AR in male mice results in increased ERα expression in the lateral septum and MPO (19). If LepRb cells in the ARH and PMv require androgenic signaling for proper function, we hypothesized that ERα expression would increase in order to compensate for loss of AR. Consistent with previous studies (61), approximately 17% of LepRb cells in the mARH and 5% of LepRb cells in the PMv co-express ERα in LepRb^{Cre} males (Figure 3.3F, H, J). With loss of AR, ERα expression in LepRb cells did not change (Table 3.6). In LepRb$^{\Delta AR}$ males, approximately 10% of LepRb cells coexpress ERα in the mARH and PMv (Figure 3.3G, I, J).

Table 3.6: Colocalization quantification of ERα in LepRb neurons

	Control Mice			Knockout Mice		
	Male: LepRb^{Cre}			Male: LepRb$^{\Delta AR}$		
Nucleus	**#LepRb**	**#LepRb+ERα**	**%LepRb+ERα**	**#LepRb**	**#LepRb+ERα**	**%LepRb+ERα**
mARH	104.5 ± 4.87	18.25 ± 3.52	17.48 ± 3.3	96 ± 18.24	10.25 ± 3.07	12.23 ± 4.60
PMv	209.25 ± 26.41	9.33 ± 2.12	5.40 ± 1.0	191.75 ± 17.92	10 ± 5.74	6.32 ± 4.29

LepRb$^{\Delta AR}$ mice show typical sexual maturation and fertility

To assess if lack of AR in LepRb cells disrupts sexual maturation, we evaluated external markers of puberty onset (VO) and puberty completion (first estrus) beginning at weaning. Female LepRb$^{\Delta AR}$ and control mice had similar day of VO (Figure 3.4A). No difference was seen in the day of first estrus between LepRb$^{\Delta AR}$ and control females (Figure 3.4B). LepRb$^{\Delta AR}$ and control females showed typical estrous cycles (Figure 3.4C), with a similar amount of time in each cycle stage (Figure 3.4D), estrous cycle length (Figure 3.4E), and number of cycles (Figure 3.4F).

LepRb$^{\Delta AR}$ and control females had a similar latency to birth (Figure 3.4G) and number of pups per litter (Figure 3.4H) for two consecutive pregnancies. Male LepRb$^{\Delta AR}$ and control mice had similar day of complete BPS (Figure 3.4I), and showed no difference in the latency to impregnate a female (time from start of mating to birth of pups) when mated with wild-type females (Figure 3.4J).

LepRb$^{\Delta AR}$ male mice show exaggerated response to negative feedback actions of sex steroids

Male LepRb$^{\Delta AR}$ mice display increased serum testosterone (T) compared to control males (AR^{flox} mean T = 90.05 ng/dL, LepRb$^{\Delta AR}$ mean T = 297.5 ng/dL, Mann-Whitney non-parametric test, P = 0.02, Figure 3.5A). Despite increased serum T, male LepRb$^{\Delta AR}$ mice had similar gonadal mass (mass of both testes, AR^{flox} mean = 0.42 g, SEM = 0.04, LepRb$^{\Delta AR}$ mean = 0.47 g, SEM = 0.03, Mann-Whitney non-parametric test, P = 0.45) and seminal vesicle mass (AR^{flox} mean = 0.38 g, SEM = 0.05, LepRb$^{\Delta AR}$ mean = 0.42 g, SEM = 0.04, Mann-Whitney non-parametric test, P = 0.56) compared to control males. Serum LH and FSH were no different between intact LepRb$^{\Delta AR}$ and AR^{flox} male mice (Figure 3.5B-C). Additionally, hypothalamic gene expression of *Kiss1*, *Tac2*, and *Pdyn* relative to the housekeeper *Actb* were not different in gonad intact LepRb$^{\Delta AR}$ and AR^{flox} male mice (*Kiss1* relative expression: AR^{flox} = 100%, SEM = 8.17, LepRb$^{\Delta AR}$ = 81.69%, SEM = 22.09, t-test with Welch's correction, P = 0.48, *Tac2* relative expression: AR^{flox} = 100%, SEM = 8.24, LepRb$^{\Delta AR}$ = 101.7%, SEM = 9.30, t-test with Welch's correction, P = 0.89, *Pdyn* relative expression: AR^{flox} = 100%, SEM = 6.42, LepRb$^{\Delta AR}$ = 85.78%, SEM = 19.78, t-test with Welch's correction, P = 0.53).

LepRb$^{\Delta AR}$ and control mice were orchidectomized (ORX) to remove the predominant source of androgens (testes), resulting in loss of negative feedback to the hypothalamus and pituitary gland.

One week after ORX, AR^{flox} control males showed an expected rise in serum LH, whereas $LepRb^{\Delta AR}$ males showed an exaggerated rise in serum LH (ORX AR^{flox} mean LH = 1.242 ng/mL vs ORX $LepRb^{\Delta AR}$ = 3.265 ng/mL, two-way ANOVA, $P = 0.04$, Figure 3.5B). No difference in FSH levels were detected in ORX between AR^{flox} and $LepRb^{\Delta AR}$ males (Figure 3.5C).

Male mouse social hierarchy may result in differing levels of T among group housed cage mates (57,62). A separate cohort of $LepRb^{\Delta AR}$ and control males were single housed for up to 2 weeks to control for group housed status prior to ORX. Single housed $LepRb^{\Delta AR}$ and control males showed similar intact T levels (AR^{flox} mean T = 303.8 ng/dL, SEM = 107.9, $LepRb^{\Delta AR}$ mean T = 283.5 ng/dL, SEM = 65.66, t-test with Welch's correction, $P = 0.77$, Figure 3.5D). Levels of T in $LepRb^{\Delta AR}$ males were similar between group and single housed mice, whereas T in single housed AR^{flox} males increased to levels comparable to $LepRb^{\Delta AR}$ males. Single housed $LepRb^{\Delta AR}$ and AR^{flox} ORX mice showed elevated gonadotropins, but there was no effect of genotype on LH or FSH. Single housed AR^{flox} males show an increase in LH comparable to $LepRb^{\Delta AR}$ males (ORX AR^{flox} mean LH = 4.26 ng/mL, SEM = 0.83, ORX $LepRb^{\Delta AR}$ mean LH = 4.91 ng/mL, SEM = 1.07, two-way ANOVA with multiple comparisons and Holm-Sidak correction, $P = 0.75$, Figure 3.5E). FSH was no different between ORX males, and FSH levels were comparable to group housed males (ORX AR^{flox} mean FSH = 243.4 ng/mL, SEM = 17.99, ORX $LepRb^{\Delta AR}$ mean FSH = 261.6 ng/mL, SEM = 14.47, two-way ANOVA with multiple comparisons and Holm-Sidak correction, $P = 0.67$, Figure 3.5F).

Serum T did not differ between AR^{flox} and $LepRb^{\Delta AR}$ females (AR^{flox} mean T = 1.95 ng/dL, $LepRb^{\Delta AR}$ mean T = 1.65 ng/dL, t-test with Welch's correction, $P = 0.49$, Figure 3.5G). Levels of

LH in females were mostly below the detectable limit of the LH assay, as samples were collected during diestrus. No differences were detected between intact AR^{flox} and $LepRb^{\Delta AR}$ female FSH. One week after ovariectomy (OVX), serum LH did not differ between OVX AR^{flox} and OVX $LepRb^{\Delta AR}$ females (Figure 3.5H). However, OVX $LepRb^{\Delta AR}$ females display increased FSH compared with OVX AR^{flox} females (OVX AR^{flox} mean FSH =187.75 ng/mL, OVX $LepRb^{\Delta AR}$ mean FSH = 243.59 ng/mL, two-way ANOVA, $P = 0.02$, Figure 3.5I).

$LepRb^{\Delta AR}$ mice show changes in ambulatory activity, lean mass, and body length in a sexually dimorphic manner

To determine whether loss of AR from LepRb cells impacts regulation of energy homeostasis, mice underwent a comprehensive metabolic assessment. Male and female $LepRb^{\Delta AR}$ mice did not display a significant difference in body weight compared to control mice through 14 weeks of age (Figure 3.6A). No difference was observed in fat mass or lean mass in $LepRb^{\Delta AR}$ males compared to control males at 15 weeks of age (Figure 3.6B). $LepRb^{\Delta AR}$ females showed increased lean mass (about 2.5 g), but no change in percentage of lean or fat mass (Figure 3.6C), indicating that $LepRb^{\Delta AR}$ females are larger in size compared to control females. Body length was not different between $LepRb^{\Delta AR}$ males and females compared to controls at 15 weeks of age (males at 15 weeks of age, Figure 3.6D), but showed a trend in females at 15 weeks of age ($P = 0.07$, data not shown). A follow-up assessment showed increase in body length in $LepRb^{\Delta AR}$ females at 20 weeks of age (Figure 3.6D). Despite increased body length, femur length (mean femur length AR^{flox} = 15.90 mm, SEM = 0.11, $LepRb^{\Delta AR}$ = 15.68 mm, SEM = 0.21, t-test with Welch's correction, $P = 0.39$) and serum IGF1 (mean serum IGF1 AR^{flox} = 334.7 ng/mL, SEM = 33.32, $LepRb^{\Delta AR}$ = 258.1

ng/mL, SEM = 50.37, t-test with Welch's correction, $P = 0.23$) were not different between AR^{flox} and $LepRb^{\Delta AR}$ females at 20 weeks of age.

Male and female $LepRb^{\Delta AR}$ mice show similar food intake (Figure 3.6E) and fasting blood glucose (mean male fasting blood glucose AR^{flox} = 110 mg/dL, SEM = 7.30, $LepRb^{\Delta AR}$ = 106 mg/dL, SEM = 5.67, t-test with Welch's correction, $P = 0.70$, mean female fasting blood glucose AR^{flox} = 106 mg/dL, SEM = 7.54, $LepRb^{\Delta AR}$ = 96.8 mg/dL, SEM = 10.3, t-test with Welch's correction, $P = 0.47$). GTT of both $LepRb^{\Delta AR}$ males and females on normal chow diet were similar compared with controls (Figure 3.6F). Area under the curve was used to compare GTT, and was not different between genotypes on same diet (AUC male AR^{flox} = 3.2×10^4 mg/dL*min, SEM = 3.2×10^3, $LepRb^{\Delta AR}$ = 3.0×10^4 mg/dL*min, SEM = 1.9×10^3 , t-test with Welch's correction, $P = 0.62$, AUC female AR^{flox} = 2.8×10^4 mg/dL*min, SEM = 1.8×10^3, $LepRb^{\Delta AR}$ = 2.7×10^4 mg/dl*min, SEM = 3.1×10^3, t-test with Welch's correction, $P = 0.89$).

To determine if latent differences in body weight regulation would be uncovered with nutrient excess, we challenged $LepRb^{\Delta AR}$ and control mice with HFD. Previous studies have demonstrated that ARKO mice on HFD show increase in fat mass (17,63). After 12 weeks of HFD, $LepRb^{\Delta AR}$ and control male and female mice gained a similar amount of weight (Figure 3.6G) and displayed similar levels of fasting blood glucose (mean male HFD fasting blood glucose AR^{flox} = 156 mg/dL, SEM = 13.74, $LepRb^{\Delta AR}$ = 126 mg/dL, SEM = 11.53, t-test with Welch's correction, $P = 0.10$, mean female HFD fasting blood glucose AR^{flox} = 126 mg/dL, SEM = 7.66, $LepRb^{\Delta AR}$ = 113.4 mg/dL, SEM = 5.24, t-test with Welch's correction, $P = 0.18$). $LepRb^{\Delta AR}$ males and females displayed similar glucose tolerance after 12 weeks HFD compared with control mice (Figure 3.6H). Area under the curve was used to compare GTT, and was not different between genotypes

on same diet (AUC HFD male AR^{flox} = 4.6 x 10^4 mg/dL*min, SEM = 4.3 x 10^3, $LepRb^{\Delta AR}$ = 4.3 x 10^4 mg/dL*min, SEM = 3.1 x 10^3, t-test with Welch's correction, P = 0.56, AUC HFD female AR^{flox} = 3.3 x 10^4 mg/dL*min, SEM = 2.5 x 10^3, $LepRb^{\Delta AR}$ = 3.2 x 10^4 mg/dL*min, SEM = 3.4 x 10^3, t-test with Welch's correction, P = 0.79). The GTT data of mice on different diets are not directly comparable because the experiments were done in different cohorts. Males on HFD, however, showed impairment of glucose intolerance compared to normal chow diet, validating the procedure. Due to lack of any difference between genotypes on HFD in both sexes, potential changes in energy homeostasis were not assessed further. Ambulatory activity in male, not female, $LepRb^{\Delta AR}$ mice was increased, specifically during the light phase (Figure 3.7A-D). Despite increased activity, energy expenditure in 24 h, and during light and dark phases was not different in male or female mice (Figure 3.7E-H).

Discussion

In this study we assessed the impact of lack of androgen signaling via AR on LepRb cells, which are a critical population of neurons relevant for both metabolism and reproduction. Consistent with previous studies of AR and LepRb expression (60), we show here that approximately 40-50% of LepRb neurons in the PMv co-express AR, the highest level of co-localization seen in the brain, followed by ~30% colocalization in the mARH. Furthermore, LepRb and AR cells in the pituitary gland and gonads show little to no co-expression, highlighting that androgenic input to LepRb cells occurs primarily in the mARH and PMv. We found that $LepRb^{\Delta AR}$ male mice show increased ambulatory activity, increased serum testosterone, and an exaggerated rise in serum LH in the absence of negative feedback. Female $LepRb^{\Delta AR}$ mice show instead an increased in linear growth, and a greater rise in FSH with OVX. Additionally, lack of AR does not result in upregulation of

ERα in LepRb mARH and PMv neurons, indicating that these populations of neurons are preferentially responsive to androgens rather than estrogens.

LepRb and AR are expressed in many tissues of the HPG axis, including the pituitary gland and gonads (64-69). However, the degree of co-expression of LepRb and AR in the same cells is low, and few cells express $LepRb^{Cre}$ in pituitary and gonads (70). While $LepRb^{Cre}$ and AR coexpression is seen in some Leydig cells, deletion of AR via $LepRb^{Cre}$ in Leydig cells is not likely responsible for increased serum testosterone observed in $LepRb^{\Delta AR}$ male mice. $LepRb^{\Delta AR}$ males show increased serum testosterone when group housed, unchanged testes mass, and are fertile, which does not phenocopy the low testosterone, testicular atrophy, elevated LH and FSH, and infertility seen in Leydig-cell specific ARKO (71). Likewise, female $LepRb^{\Delta AR}$ mice do not mimic ovary-cell specific ARKO mice (72,73), as $LepRb^{\Delta AR}$ females do not show any difference in puberty onset, estrous cyclicity, or fertility. Additionally, pituitary deletion of AR results in reduced FSH with OVX in females (65), which is contrary to the elevation in FSH in OVX female $LepRb^{\Delta AR}$ mice. Therefore, it is unlikely that LepRb specific deletion of AR in the pituitary or gonads would result in the increased LH seen in ORX males or FSH in OVX females. The change in serum testosterone and gonadotropins with gonadectomy may reveal a change in hypothalamic sensitivity to androgens with deletion of AR in LepRb cells, or a different set point for androgenic negative feedback.

Androgens exert negative feedback to the hypothalamus and pituitary gland via AR and ERα (74-76). AR plays a greater role in male negative feedback to the hypothalamus, as males typically have higher levels of circulating androgens compared to females (77). Kisspeptin neurons in the ARH and anteroventral periventricular nucleus stimulate release of gonadotropin releasing

hormone (GnRH) and express sex steroid receptors, including ERα and AR (78,79). Androgenic actions on ARH kisspeptin/neurokinin/dynorphin (KNDy) expressing neurons are important for mediating negative feedback to the HPG axis, and may be indirectly impacted with LepRb-specific deletion of AR. A small population of Kiss1 neurons co-express LepRb or leptin-inducted pSTAT3 in female mice (36,80,81), and up to 42% of Kiss1 neurons co-express *Lepr* mRNA in castrated male mice (82). However, LepRb in Kiss1 neurons is not required for leptin's action in puberty or reproduction in mice (36), and LepRb signaling in Kiss1 neurons only arises in adult life, post-sexual maturation (83). Taken together, this small sub-population of LepRb expressing Kiss1 neurons in the hypothalamus may be indirectly responsible for the changes in LH with ORX and testosterone seen in $LepRb^{\Delta AR}$ males. We observed no changes in *Kiss1*, *Tac2*, or *Pdyn* hypothalamic gene expression in group housed, gonad intact males, further indicating that actions of androgens on LepRb are independent from KNDy neurons.

Alternatively, neurons of the melanocortin system (NPY/AgRP and POMC/CART) have been shown to influence both reproduction and metabolism (39,40,84-87). Leptin promotes an anorexigenic state by stimulating ARH POMC neurons and inhibiting NPY/AgRP neurons (88-90). Androgens have been shown to influence neurons of the melanocortin system, including masculinization of POMC mRNA expression and projections (91,92). However, while most POMC and AgRP/NPY neurons express LepRb (35,88,89,93,94), few POMC neurons express AR in rats (95), and AgRP/NPY neurons are not observed to coexpress AR in post-natal day 10 mice (96). The mechanism by which androgens impact POMC and AgRP/NPY neurons may be indirect and mediated via other populations of AR expressing LepRb neurons. With deletion of AR in LepRb cells, overall food intake and energy expenditure were not changed. Therefore, androgens

may act on additional populations of cells at the level of the hypothalamus to influence the regulation of metabolism and reproduction.

LepRb are expressed in many metabolically relevant tissues, including liver and adipose (97). The degree of co-localization between LepRb and AR, however, is low in these peripheral tissues and the metabolic phenotype of $LepRb^{\Delta AR}$ does not phenocopy metabolic tissue-specific ARKO models, including liver (15) or adipocyte-specific ARKO (17). Both male and female $LepRb^{\Delta AR}$ mice showed no differences in global body fat mass, and glucose homeostasis was not altered on either normal chow or HFD, so it is unlikely that deletion of AR via $LepRb^{Cre}$ in off-target tissues impacted our observed phenotype. Interestingly, female $LepRb^{\Delta AR}$ mice display increased lean mass, while male $LepRb^{\Delta AR}$ mice do not. Neuronal AR have been shown to positively regulate lean muscle mass, as male mice with loss of neuronal AR display decreased hindlimb muscle mass despite increased serum testosterone (98). $LepRb^{\Delta AR}$ females display increased body length, but not increased limb length, indicating an overall increase in axial rather than appendicular skeleton growth.

$LepRb^{\Delta AR}$ male mice show increased ambulatory activity, mainly due to increased activity during the light phase when rodents are typically less active. Male mice with global deletion of AR DNA-binding domain (mimics exon 2 deletion) show decreased activity (99) that is consistent with decreased running wheel activity seen in castrated wild-type males (100,101). However, neuronal-specific AR knockout models provide contrasting results. CaMKIIα-iCre driven ARKO results in decreased activity (98), whereas nestin-Cre driven ARKO males show increased activity, which is correlated with an increase in E2 (19). The differences in activity seen in ARKO mouse models

highlights how the extent, timing, and sites of AR deletion can impact phenotype. In the absence of AR in certain populations of cells, such as LepRb expressing cells, estrogenic signaling is unopposed by androgens, and estrogens are known to increase ambulatory activity (102,103). Leptin increases locomotor activity via hypothalamic targets (104,105), and it is possible that sex steroids may modulate leptin's effect on activity. LepRb$^{\Delta AR}$ males show elevated serum testosterone, which when aromatized to estradiol, can act to increase activity (106). However, this effect is not likely via ARH or PMv LepRb cells, as aromatase expression in these nuclei is low (107) and few LepRb cells express ERα in the ARH and PMv. Activity was increased in LepRb$^{\Delta AR}$ males particularly during the light-phase, which highlights the circadian component of activity which is influenced by gonadal hormones.

Elevated testosterone in LepRb$^{\Delta AR}$ males was only observed in group housed males. This effect was not related to gonadal mass, as testes size was similar compared to control males. The impact of group housing highlights the role of male social hierarchy in rodents. A population of dopamine transporter (DAT)-expressing neurons in the PMv has been implicated in male-male aggression and establishment of male social hierarchy in mice (108). It is possible that AR expression in the PMv could play a role in the establishment of male social hierarchy. Pheromones are known to play a key role in social interaction and behavior in rodents, and exposure to both conspecific and opposite-sex odors result in Fos expression in the PMv of male and female rodents (109,110). PMv LepRb neurons are activated by opposite-sex odors and directly project to GnRH neurons in the pre-optic area (111). A sub-population of PMv LepRb neurons that co-expresses AR is therefore well situated to integrate gonadal signals, pheromone cues, and energy status to regulate the timing and behavior of reproduction.

In summary, our findings demonstrate that deletion of AR from LepRb cells results in sex-specific differences in ambulatory activity, linear growth, testosterone, and gonadotropin levels. Deletion of AR in PMv and ARH neurons may explain this phenotype, revealing a key sexually dimorphic role of metabolically relevant neuronal populations in androgen actions in the brain.

References

1. Davey RA, Grossmann M. Androgen Receptor Structure, Function and Biology: From Bench to Bedside. Clin Biochem Rev 2016; 37:3-15

2. Handelsman DJ. In: Feingold KR AB, Boyce A, et al., ed. *Androgen Physiology, Pharmacology and Abuse.* Vol Updated 2016 Jun 12. December 12, 2016 ed. Endotext.org: MDText.com, Inc., South Dartmouth (MA).

3. Walters KA, Simanainen U, Handelsman DJ. Molecular insights into androgen actions in male and female reproductive function from androgen receptor knockout models. Hum Reprod Update 2010; 16:543-558

4. Schiffer L, Kempegowda P, Arlt W, O'Reilly MW. MECHANISMS IN ENDOCRINOLOGY: The sexually dimorphic role of androgens in human metabolic disease. 2017; 177:R125

5. McEwan IJ BA. In: Feingold KR AB, Boyce A, et al.,, ed. *Androgen Physiology: Receptor and Metabolic Disorders.* Vol Updated 2016 Jun 12. Endotext [Internet]: MDText.com, Inc., South Dartmouth (MA).

6. Brinkmann AO. Molecular Mechanisms of Androgen Action – A Historical Perspective. In: Saatcioglu F, ed. Androgen Action: Methods and Protocols. Totowa, NJ: Humana Press; 2011:3-24.

7. Lyon MF, Hawkes SG. X-linked Gene for Testicular Feminization in the Mouse. Nature 1970; 227:1217-1219

8. De Gendt K, Swinnen JV, Saunders PT, Schoonjans L, Dewerchin M, Devos A, Tan K, Atanassova N, Claessens F, Lecureuil C, Heyns W, Carmeliet P, Guillou F, Sharpe RM, Verhoeven G. A Sertoli cell-selective knockout of the androgen receptor causes spermatogenic arrest in meiosis. Proceedings of the National Academy of Sciences of the United States of America 2004; 101:1327-1332

9. Donovan KA, Walker LM, Wassersug RJ, Thompson LM, Robinson JW. Psychological effects of androgen-deprivation therapy on men with prostate cancer and their partners. Cancer 2015; 121:4286-4299

10. Walters KA, McTavish KJ, Seneviratne MG, Jimenez M, McMahon AC, Allan CM, Salamonsen LA, Handelsman DJ. Subfertile female androgen receptor knockout mice exhibit defects in neuroendocrine signaling, intraovarian function, and uterine development but not uterine function. Endocrinology 2009; 150:3274-3282

11. Lyon MF, Glenister PH. Reduced reproductive performance in androgen-resistant Tfm/Tfm female mice. Proceedings of the Royal Society of London Series B, Biological sciences 1980; 208:1-12

12. Shiina H, Matsumoto T, Sato T, Igarashi K, Miyamoto J, Takemasa S, Sakari M, Takada I, Nakamura T, Metzger D, Chambon P, Kanno J, Yoshikawa H, Kato S. Premature ovarian failure in androgen receptor-deficient mice. Proceedings of the National Academy of Sciences of the United States of America 2006; 103:224-229

13. Lin HY, Xu Q, Yeh S, Wang RS, Sparks JD, Chang C. Insulin and leptin resistance with hyperleptinemia in mice lacking androgen receptor. Diabetes 2005; 54:1717-1725

14. Sato T, Matsumoto T, Yamada T, Watanabe T, Kawano H, Kato S. Late onset of obesity in male androgen receptor-deficient (AR KO) mice. Biochem Biophys Res Commun 2003; 300:167-171

15. Lin HY, Yu IC, Wang RS, Chen YT, Liu NC, Altuwaijri S, Hsu CL, Ma WL, Jokinen J, Sparks JD, Yeh S, Chang C. Increased hepatic steatosis and insulin resistance in mice lacking hepatic androgen receptor. Hepatology 2008; 47:1924-1935

16. Navarro G, Xu W, Jacobson DA, Wicksteed B, Allard C, Zhang G, De Gendt K, Kim SH, Wu H, Zhang H, Verhoeven G, Katzenellenbogen JA, Mauvais-Jarvis F. Extranuclear Actions of the Androgen Receptor Enhance Glucose-Stimulated Insulin Secretion in the Male. Cell metabolism 2016; 23:837-851

17. McInnes KJ, Smith LB, Hunger NI, Saunders PT, Andrew R, Walker BR. Deletion of the androgen receptor in adipose tissue in male mice elevates retinol binding protein 4 and reveals independent effects on visceral fat mass and on glucose homeostasis. Diabetes 2012; 61:1072-1081

18. Yu IC, Lin HY, Liu NC, Sparks JD, Yeh S, Fang LY, Chen L, Chang C. Neuronal androgen receptor regulates insulin sensitivity via suppression of hypothalamic NF-kappaB-mediated PTP1B expression. Diabetes 2013; 62:411-423

19. Raskin K, de Gendt K, Duittoz A, Liere P, Verhoeven G, Tronche F, Mhaouty-Kodja S. Conditional inactivation of androgen receptor gene in the nervous system: effects on male behavioral and neuroendocrine responses. J Neurosci 2009; 29:4461-4470

20. Juntti SA, Tollkuhn J, Wu MV, Fraser EJ, Soderborg T, Tan S, Honda S, Harada N, Shah NM. The androgen receptor governs the execution, but not programming, of male sexual and territorial behaviors. Neuron 2010; 66:260-272

21. Friedman JM, Halaas JL. Leptin and the regulation of body weight in mammals. Nature 1998; 395:763-770

22. Frederich R, Hamann A, Anderson S, Lollmann B, Lowell B, Flier J. Leptin levels reflect body lipid content in mice: evidence for diet-induced resistance to leptin action. Nature Medicine 1995; 1:1311-1314

23. Bates SH, Myers MG. The role of leptin receptor signaling in feeding and neuroendocrine function. Trends in Endocrinology & Metabolism 2003; 14:447-452

24. Myers MG, Münzberg H, Leinninger GM, Leshan RL. The Geometry of Leptin Action in the Brain: More Complicated Than a Simple ARC. Cell metabolism 2009; 9:117-123

25. Hill JW, Elmquist JK, Elias CF. Hypothalamic pathways linking energy balance and reproduction. American Journal of Physiology-Endocrinology and Metabolism 2008; 294:E827-E832

26. Barash IA, Cheung CC, Weigle DS, Ren H, Kabigting EB, Kuijper JL, Clifton DK, Steiner RA. Leptin is a metabolic signal to the reproductive system. Endocrinology 1996; 137:3144-3147

27. Chehab FF, Lim ME, Lu R. Correction of the sterility defect in homozygous obese female mice by treatment with the human recombinant leptin. Nat Genet 1996; 12:318-320

28. Mounzih K, Lu R, Chehab FF. Leptin treatment rescues the sterility of genetically obese ob/ob males. Endocrinology 1997; 138:1190-1193

29. Coleman DL. Obese and diabetes: two mutant genes causing diabetes-obesity syndromes in mice. Diabetologia 1978; 14:141-148

30. Clement K, Vaisse C, Lahlou N, Cabrol S, Pelloux V, Cassuto D, Gourmelen M, Dina C, Chambaz J, Lacorte JM, Basdevant A, Bougneres P, Lebouc Y, Froguel P, Guy-Grand B. A mutation in the human leptin receptor gene causes obesity and pituitary dysfunction. Nature 1998; 392:398-401

31. Farooqi IS, Wangensteen T, Collins S, Kimber W, Matarese G, Keogh JM, Lank E, Bottomley B, Lopez-Fernandez J, Ferraz-Amaro I, Dattani MT, Ercan O, Myhre AG, Retterstol L, Stanhope R, Edge JA, McKenzie S, Lessan N, Ghodsi M, De Rosa V, Perna F, Fontana S, Barroso I, Undlien DE, O'Rahilly S. Clinical and molecular genetic spectrum of congenital deficiency of the leptin receptor. The New England journal of medicine 2007; 356:237-247

32. Hummel KP, Dickie MM, Coleman DL. Diabetes, a new mutation in the mouse. Science 1966; 153:1127-1128

33. Ingalls AM, Dickie MM, Snell GD. Obese, a new mutation in the house mouse. The Journal of heredity 1950; 41:317-318

34. Elias CF, Purohit D. Leptin signaling and circuits in puberty and fertility. Cell Mol Life Sci 2013; 70:841-862

35. Baskin DG, Breininger JF, Schwartz MW. Leptin receptor mRNA identifies a subpopulation of neuropeptide Y neurons activated by fasting in rat hypothalamus. Diabetes 1999; 48:828-833

36. Donato J, Jr., Cravo RM, Frazao R, Gautron L, Scott MM, Lachey J, Castro IA, Margatho LO, Lee S, Lee C, Richardson JA, Friedman J, Chua S, Jr., Coppari R, Zigman

JM, Elmquist JK, Elias CF. Leptin's effect on puberty in mice is relayed by the ventral premammillary nucleus and does not require signaling in Kiss1 neurons. The Journal of clinical investigation 2011; 121:355-368

37. Donato J, Silva RJ, Sita LV, Lee S, Lee C, Lacchini S, Bittencourt JC, Franci CR, Canteras NS, Elias CF. The Ventral Premammillary Nucleus Links Fasting-Induced Changes in Leptin Levels and Coordinated Luteinizing Hormone Secretion. The Journal of Neuroscience 2009; 29:5240-5250

38. Williams KW, Sohn JW, Donato J, Jr., Lee CE, Zhao JJ, Elmquist JK, Elias CF. The acute effects of leptin require PI3K signaling in the hypothalamic ventral premammillary nucleus. J Neurosci 2011; 31:13147-13156

39. Padilla SL, Qiu J, Nestor CC, Zhang C, Smith AW, Whiddon BB, Ronnekleiv OK, Kelly MJ, Palmiter RD. AgRP to Kiss1 neuron signaling links nutritional state and fertility. Proceedings of the National Academy of Sciences of the United States of America 2017; 114:2413-2418

40. Egan OK, Inglis MA, Anderson GM. Leptin Signaling in AgRP Neurons Modulates Puberty Onset and Adult Fertility in Mice. J Neurosci 2017; 37:3875-3886

41. Council NR. Guide for the Care and Use of Laboratory Animals: Eighth Edition. Washington, DC: The National Academies Press.

42. Leshan RL, Bjornholm M, Munzberg H, Myers MG, Jr. Leptin receptor signaling and action in the central nervous system. Obesity (Silver Spring) 2006; 14 Suppl 5:208S-212S

43. Patterson CM, Leshan RL, Jones JC, Myers MG. Molecular mapping of mouse brain regions innervated by leptin receptor-expressing cells. Brain Research 2011; 1378:18-28

44. Krashes MJ, Shah BP, Madara JC, Olson DP, Strochlic DE, Garfield AS, Vong L, Pei H, Watabe-Uchida M, Uchida N, Liberles SD, Lowell BB. An excitatory paraventricular nucleus to AgRP neuron circuit that drives hunger. Nature 2014; 507:238-242

45. Borges BC, Garcia-Galiano D, Rorato R, Elias LLK, Elias CF. PI3K p110beta subunit in leptin receptor expressing cells is required for the acute hypophagia induced by endotoxemia. Mol Metab 2016; 5:379-391

46. Garcia-Galiano D, Borges BC, Donato J, Jr., Allen SJ, Bellefontaine N, Wang M, Zhao JJ, Kozloff KM, Hill JW, Elias CF. PI3Kalpha inactivation in leptin receptor cells increases leptin sensitivity but disrupts growth and reproduction. JCI insight 2017; 2

47. Sadagurski M, Leshan RL, Patterson C, Rozzo A, Kuznetsova A, Skorupski J, Jones JC, Depinho RA, Myers MG, Jr., White MF. IRS2 signaling in LepR-b neurons suppresses FoxO1 to control energy balance independently of leptin action. Cell metabolism 2012; 15:703-712

48. Srinivas S, Watanabe T, Lin CS, William CM, Tanabe Y, Jessell TM, Costantini F. Cre reporter strains produced by targeted insertion of EYFP and ECFP into the ROSA26 locus. BMC developmental biology 2001; 1:4

49. Low KL, Ma C, Soma KK. Tyramide Signal Amplification Permits Immunohistochemical Analyses of Androgen Receptors in the Rat Prefrontal Cortex. J Histochem Cytochem 2017; 65:295-308

50. Silveira MA, Wagenmaker ER, Burger LL, DeFazio RA, Moenter SM. GnRH Neuron Activity and Pituitary Response in Estradiol-Induced vs Proestrous Luteinizing Hormone Surges in Female Mice. Endocrinology 2016; 158:356-366

51. Qiu X, Dowling AR, Marino JS, Faulkner LD, Bryant B, Bruning JC, Elias CF, Hill JW. Delayed puberty but normal fertility in mice with selective deletion of insulin receptors from Kiss1 cells. Endocrinology 2013; 154:1337-1348

52. Garcia-Galiano D, van Ingen Schenau D, Leon S, Krajnc-Franken MA, Manfredi-Lozano M, Romero-Ruiz A, Navarro VM, Gaytan F, van Noort PI, Pinilla L, Blomenrohr M, Tena-Sempere M. Kisspeptin signaling is indispensable for neurokinin B, but not glutamate, stimulation of gonadotropin secretion in mice. Endocrinology 2012; 153:316-328

53. Torsoni MA, Borges BC, Cote JL, Allen SJ, Mahany E, Garcia-Galiano D, Elias CF. AMPKalpha2 in Kiss1 Neurons Is Required for Reproductive Adaptations to Acute Metabolic Challenges in Adult Female Mice. Endocrinology 2016; 157:4803-4816

54. Korenbrot CC, Huhtaniemi IT, Weiner RI. Preputial separation as an external sign of pubertal development in the male rat. Biology of reproduction 1977; 17:298-303

55. Caligioni CS. Assessing reproductive status/stages in mice. Current protocols in neuroscience / editorial board, Jacqueline N Crawley [et al] 2009; Appendix 4:Appendix 4I

56. Green MC, Witham BA. Handbook on genetically standardized JAX mice. 1991;

57. Oyegbile TO, Marler CA. Winning fights elevates testosterone levels in California mice and enhances future ability to win fights. Hormones and Behavior 2005; 48:259-267

58. Scott MM, Lachey JL, Sternson SM, Lee CE, Elias CF, Friedman JM, Elmquist JK. Leptin targets in the mouse brain. J Comp Neurol 2009; 514:518-532

59. Caron E, Sachot C, Prevot V, Bouret SG. Distribution of leptin-sensitive cells in the postnatal and adult mouse brain. Journal of Comparative Neurology 2010; 518:459-476

60. Johnson JA, Calo S, Nair L, IglayReger HB, Greenwald-Yarnell M, Skorupski J, Myers MG, Jr., Bodary PF. Testosterone interacts with the feedback mechanisms engaged by Tyr985 of the leptin receptor and diet-induced obesity. J Steroid Biochem Mol Biol 2012; 132:212-219

61. Kim JS, Rizwan MZ, Clegg DJ, Anderson GM. Leptin Signaling Is Not Required for Anorexigenic Estradiol Effects in Female Mice. Endocrinology 2016; 157:1991-2001

62. Williamson CM, Lee W, Romeo RD, Curley JP. Social context-dependent relationships between mouse dominance rank and plasma hormone levels. Physiology & Behavior 2017; 171:110-119

63. Dubois V, Laurent MR, Jardi F, Antonio L, Lemaire K, Goyvaerts L, Deldicque L, Carmeliet G, Decallonne B, Vanderschueren D, Claessens F. Androgen Deficiency Exacerbates High-Fat Diet-Induced Metabolic Alterations in Male Mice. Endocrinology 2016; 157:648-665

64. O'Hara L, Curley M, Tedim Ferreira M, Cruickshanks L, Milne L, Smith LB. Pituitary androgen receptor signalling regulates prolactin but not gonadotrophins in the male mouse. PloS one 2015; 10:e0121657-e0121657

65. Wu S, Chen Y, Fajobi T, DiVall SA, Chang C, Yeh S, Wolfe A. Conditional knockout of the androgen receptor in gonadotropes reveals crucial roles for androgen in gonadotropin synthesis and surge in female mice. Molecular endocrinology 2014; 28:1670-1681

66. Caprio M, Isidori AM, Carta AR, Moretti C, Dufau ML, Fabbri A. Expression of Functional Leptin Receptors in Rodent Leydig Cells1. Endocrinology 1999; 140:4939-4947

67. Shan L-X, Bardin CW, Hardy MP. Immunohistochemical Analysis of Androgen Effects on Androgen Receptor Expression in Developing Leydig and Sertoli Cells*. Endocrinology 1997; 138:1259-1266

68. Dupuis L, Schuermann Y, Cohen T, Siddappa D, Kalaiselvanraja A, Pansera M, Bordignon V, Duggavathi R. Role of leptin receptors in granulosa cells during ovulation. 2014; 147:221

69. Ryan NK, Woodhouse CM, Van der Hoek KH, Gilchrist RB, Armstrong DT, Norman RJ. Expression of Leptin and Its Receptor in the Murine Ovary: Possible Role in the Regulation of Oocyte Maturation1. Biology of reproduction 2002; 66:1548-1554

70. Allen SJ, Garcia-Galiano D, Borges BC, Burger LL, Boehm U, Elias CF. Leptin receptor null mice with reexpression of LepR in GnRHR expressing cells display elevated FSH levels but remain in a prepubertal state. Am J Physiol Regul Integr Comp Physiol 2016; 310:R1258-1266

71. Xu Q, Lin HY, Yeh SD, Yu IC, Wang RS, Chen YT, Zhang C, Altuwaijri S, Chen LM, Chuang KH, Chiang HS, Yeh S, Chang C. Infertility with defective spermatogenesis and steroidogenesis in male mice lacking androgen receptor in Leydig cells. Endocrine 2007; 32:96-106

72. Sen A, Hammes SR. Granulosa cell-specific androgen receptors are critical regulators of ovarian development and function. Molecular endocrinology (Baltimore, Md) 2010; 24:1393-1403

73. Walters KA, Middleton LJ, Joseph SR, Hazra R, Jimenez M, Simanainen U, Allan CM, Handelsman DJ. Targeted Loss of Androgen Receptor Signaling in Murine Granulosa Cells of Preantral and Antral Follicles Causes Female Subfertility1. Biology of reproduction 2012; 87

74. Tilbrook AJ, de Kretser DM, Cummins JT, Clarke IJ. The negative feedback effects of testicular steroids are predominantly at the hypothalamus in the ram. Endocrinology 1991; 129:3080-3092

75. Scott CJ, Kuehl DE, Ferreira SA, Jackson GL. Hypothalamic sites of action for testosterone, dihydrotestosterone, and estrogen in the regulation of luteinizing hormone secretion in male sheep. Endocrinology 1997; 138:3686-3694

76. Lindzey J, Wetsel WC, Couse JF, Stoker T, Cooper R, Korach KS. Effects of castration and chronic steroid treatments on hypothalamic gonadotropin-releasing hormone content and pituitary gonadotropins in male wild-type and estrogen receptor-alpha knockout mice. Endocrinology 1998; 139:4092-4101

77. Wersinger SR, Haisenleder DJ, Lubahn DB, Rissman EF. Steroid feedback on gonadotropin release and pituitary gonadotropin subunit mRNA in mice lacking a functional estrogen receptor alpha. Endocrine 1999; 11:137-143

78. Smith JT, Dungan HM, Stoll EA, Gottsch ML, Braun RE, Eacker SM, Clifton DK, Steiner RA. Differential Regulation of KiSS-1 mRNA Expression by Sex Steroids in the Brain of the Male Mouse. Endocrinology 2005; 146:2976-2984

79. Kumar D, Periasamy V, Freese M, Voigt A, Boehm U. In Utero Development of Kisspeptin/GnRH Neural Circuitry in Male Mice. Endocrinology 2015; 156:3084-3090

80. Quennell JH, Howell CS, Roa J, Augustine RA, Grattan DR, Anderson GM. Leptin deficiency and diet-induced obesity reduce hypothalamic kisspeptin expression in mice. Endocrinology 2011; 152:1541-1550

81. Louis GW, Greenwald-Yarnell M, Phillips R, Coolen LM, Lehman MN, Myers MG, Jr. Molecular mapping of the neural pathways linking leptin to the neuroendocrine reproductive axis. Endocrinology 2011; 152:2302-2310

82. Smith JT, Acohido BV, Clifton DK, Steiner RA. KiSS-1 Neurones Are Direct Targets for Leptin in the ob/ob Mouse. Journal of Neuroendocrinology 2006; 18:298-303

83. Cravo RM, Frazao R, Perello M, Osborne-Lawrence S, Williams KW, Zigman JM, Vianna C, Elias CF. Leptin signaling in Kiss1 neurons arises after pubertal development. PloS one 2013; 8:e58698

84. Manfredi-Lozano M, Roa J, Ruiz-Pino F, Piet R, Garcia-Galiano D, Pineda R, Zamora A, Leon S, Sanchez-Garrido MA, Romero-Ruiz A, Dieguez C, Vazquez MJ, Herbison AE, Pinilla L, Tena-Sempere M. Defining a novel leptin-melanocortin-kisspeptin pathway involved in the metabolic control of puberty. Mol Metab 2016; 5:844-857

85. Israel DD, Sheffer-Babila S, de Luca C, Jo YH, Liu SM, Xia Q, Spergel DJ, Dun SL, Dun NJ, Chua SC, Jr. Effects of leptin and melanocortin signaling interactions on pubertal development and reproduction. Endocrinology 2012; 153:2408-2419

86. Faulkner LD, Dowling AR, Stuart RC, Nillni EA, Hill JW. Reduced melanocortin production causes sexual dysfunction in male mice with POMC neuronal insulin and leptin insensitivity. Endocrinology 2015; 156:1372-1385

87. Navarro VM, Kaiser UB. Metabolic influences on neuroendocrine regulation of reproduction. Current opinion in endocrinology, diabetes, and obesity 2013; 20:335-341

88. Cowley MA, Smart JL, Rubinstein M, Cerdan MG, Diano S, Horvath TL, Cone RD, Low MJ. Leptin activates anorexigenic POMC neurons through a neural network in the arcuate nucleus. Nature 2001; 411:480-484

89. Elias CF, Aschkenasi C, Lee C, Kelly J, Ahima RS, Bjorbæk C, Flier JS, Saper CB, Elmquist JK. Leptin Differentially Regulates NPY and POMC Neurons Projecting to the Lateral Hypothalamic Area. Neuron 1999; 23:775-786

90. van den Top M, Lee K, Whyment AD, Blanks AM, Spanswick D. Orexigen-sensitive NPY/AgRP pacemaker neurons in the hypothalamic arcuate nucleus. Nat Neurosci 2004; 7:493-494

91. Chowen-Breed J, Fraser HM, Vician L, Damassa DA, Clifton DK, Steiner RA. Testosterone regulation of proopiomelanocortin messenger ribonucleic acid in the arcuate nucleus of the male rat. Endocrinology 1989; 124:1697-1702

92. Nohara K, Zhang Y, Waraich RS, Laque A, Tiano JP, Tong J, Munzberg H, Mauvais-Jarvis F. Early-life exposure to testosterone programs the hypothalamic melanocortin system. Endocrinology 2011; 152:1661-1669

93. Williams KW, Margatho LO, Lee CE, Choi M, Lee S, Scott MM, Elias CF, Elmquist JK. Segregation of acute leptin and insulin effects in distinct populations of arcuate proopiomelanocortin neurons. J Neurosci 2010; 30:2472-2479

94. Wilson BD, Bagnol D, Kaelin CB, Ollmann MM, Gantz I, Watson SJ, Barsh GS. Physiological and Anatomical Circuitry between Agouti-Related Protein and Leptin Signaling*. Endocrinology 1999; 140:2387-2397

95. Fodor M, Delemarre-van de Waal HA. Are POMC neurons targets for sex steroids in the arcuate nucleus of the rat? Neuroreport 2001; 12:3989-3991

96. Kamitakahara A, Bouyer K, Wang CH, Simerly R. A critical period for the trophic actions of leptin on AgRP neurons in the arcuate nucleus of the hypothalamus. J Comp Neurol 2018; 526:133-145

97. Hoggard N, Mercer JG, Rayner DV, Moar K, Trayhurn P, Williams LM. Localization of leptin receptor mRNA splice variants in murine peripheral tissues by RT-PCR and in situ hybridization. Biochem Biophys Res Commun 1997; 232:383-387

98. Davey RA, Clarke MV, Russell PK, Rana K, Seto J, Roeszler KN, How JMY, Chia LY, North K, Zajac JD. Androgen Action via the Androgen Receptor in Neurons Within the Brain Positively Regulates Muscle Mass in Male Mice. Endocrinology 2017; 158:3684-3695

99. Rana K, Fam BC, Clarke MV, Pang TP, Zajac JD, MacLean HE. Increased adiposity in DNA binding-dependent androgen receptor knockout male mice associated with decreased voluntary activity and not insulin resistance. American journal of physiology Endocrinology and metabolism 2011; 301:E767-778

100. Hoskins R. Studies on vigor: II. The effect of castration on voluntary activity. American Journal of Physiology-Legacy Content 1925; 72:324-330

101. Richter CP, Wislocki GB. Activity studies on castrated male and female rats with testicular grafts, in correlation with histological studies of the grafts. American Journal of Physiology-Legacy Content 1928; 86:651-660

102. Roy EJ, Wade GN. Role of estrogens in androgen-induced spontaneous activity in male rats. Journal of comparative and physiological psychology 1975; 89:573-579

103. Ogawa S, Chan J, Gustafsson JA, Korach KS, Pfaff DW. Estrogen increases locomotor activity in mice through estrogen receptor alpha: specificity for the type of activity. Endocrinology 2003; 144:230-239

104. Ribeiro AC, Ceccarini G, Dupre C, Friedman JM, Pfaff DW, Mark AL. Contrasting effects of leptin on food anticipatory and total locomotor activity. PloS one 2011; 6:e23364

105. Coppari R, Ichinose M, Lee CE, Pullen AE, Kenny CD, McGovern RA, Tang V, Liu SM, Ludwig T, Chua SC, Jr., Lowell BB, Elmquist JK. The hypothalamic arcuate nucleus: a key site for mediating leptin's effects on glucose homeostasis and locomotor activity. Cell metabolism 2005; 1:63-72

106. Lightfoot JT. Sex hormones' regulation of rodent physical activity: a review. Int J Biol Sci 2008; 4:126-132

107. Stanić D, Dubois S, Chua HK, Tonge B, Rinehart N, Horne MK, Boon WC. Characterization of Aromatase Expression in the Adult Male and Female Mouse Brain. I. Coexistence with Oestrogen Receptors α and β, and Androgen Receptors. PloS one 2014; 9:e90451

108. Stagkourakis S, Spigolon G, Williams P, Protzmann J, Fisone G, Broberger C. A neural network for intermale aggression to establish social hierarchy. Nature Neuroscience 2018; 21:834-842

109. Yokosuka M, Matsuoka M, Ohtani-Kaneko R, Iigo M, Hara M, Hirata K, Ichikawa M. Female-soiled bedding induced Fos immunoreactivity in the ventral part of the premammillary nucleus (PMv) of the male mouse. Physiology & Behavior 1999; 68:257-261

110. Donato J, Cavalcante JC, Silva RJ, Teixeira AS, Bittencourt JC, Elias CF. Male and female odors induce Fos expression in chemically defined neuronal population. Physiology & Behavior 2010; 99:67-77

111. Leshan RL, Louis GW, Jo YH, Rhodes CJ, Munzberg H, Myers MG, Jr. Direct innervation of GnRH neurons by metabolic- and sexual odorant-sensing leptin receptor neurons in the hypothalamic ventral premammillary nucleus. J Neurosci 2009; 29:3138-3147

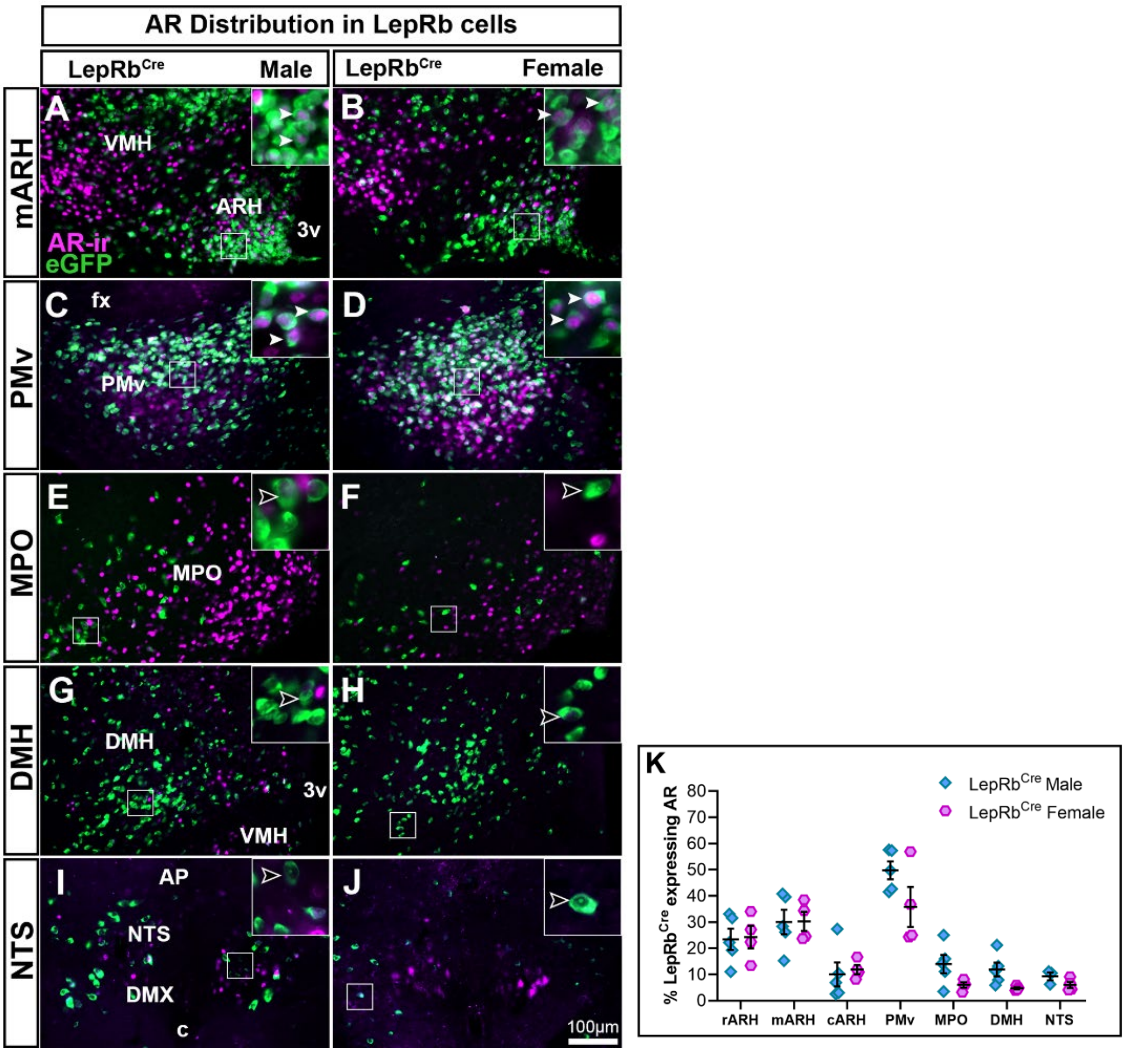

Figure 3.1: Androgen receptor (AR) and leptin receptor (LepRb) are highly colocalized in the mid-arcuate (mARH) and ventral premammillary (PMv) nuclei in male and female brain. A-J, fluorescent images showing colocalization of LepRb^{Cre} (eGFP-L10a, green) and AR immunoreactivity (AR-ir, purple) in the mARH (A-B), PMv (C-D), medial pre-optic area (MPO, E-F), dorsomedial nucleus of the hypothalamus (DMH, G-H), and nucleus of the solitary tract (NTS, I-J). Insets are higher magnification of A-J. K, Scatter plot graph showing percentage of LepRb^{Cre} neurons co-expressing AR (mean ± SEM, n = 5 males and n = 4 females). Three levels of ARH were quantified (rostal, mid/tuberal, and caudal), and images for mARH are presented (A-B). Solid white arrows indicate LepRb cells which co-express AR. Arrows with black center indicate LepRb cells which do not co-express AR. Abbreviations: 3v, third ventricle, AP, area postrema, cARH, caudal arcuate, c, central canal of the medulla, DMX, dorsal motor nucleus of the vagus nerve, fx, fornix, OV, vascular organ of the lamina terminalis, rARH, rostral arcuate, VMH, ventromedial hypothalamus. Abbreviations based on reference brain of the Allen Brain Atlas. Scale bar = 100µm.

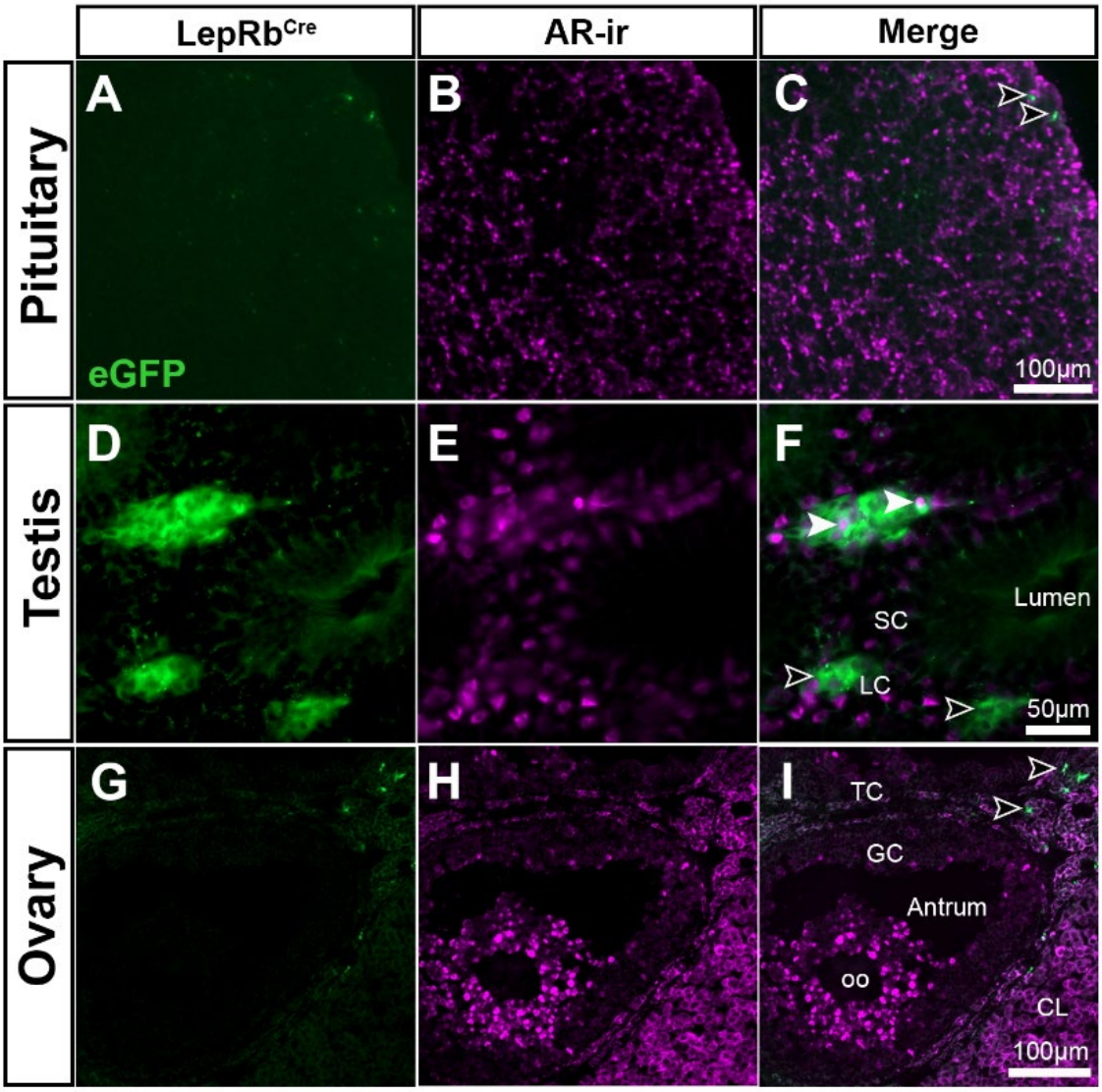

Figure 3.2: Co-expression of androgen receptor (AR) and leptin receptor (LepRb) in the pituitary gland and gonads is very low. A-I, fluorescent images showing $LepRb^{Cre}$ (eGFP-L10a, green, A, D, G) and AR immunoreactivity (AR-ir, purple, B, E, H) expression in the pituitary gland (A-C), testis (D-F), and ovary (G-I). C, F, I, merged images. $LepRb^{Cre}$ expression was low in the pituitary gland (A-C). Female pituitary gland is shown in A-C. $LepRb^{Cre}$ expression in the testes (D-F) was limited to few Leydig cells and virtually absent from Sertoli cells. Ovarian (G-I) $LepRb^{Cre}$ expression was sporadic in ovarian parenchyma, and absent in granulosa and theca cells. Solid white arrows indicate LepRb cells which co-express AR. Arrows with black center indicate LepRb cells which do not co-express AR. Abbreviations: CL, corpus luteum, GC, granulosa cell, LC, Leydig cell, oo, oocyte, SC, Sertoli cell, TC, theca cell. Scale bar = 50µm (F), and 100 µm (C,I).

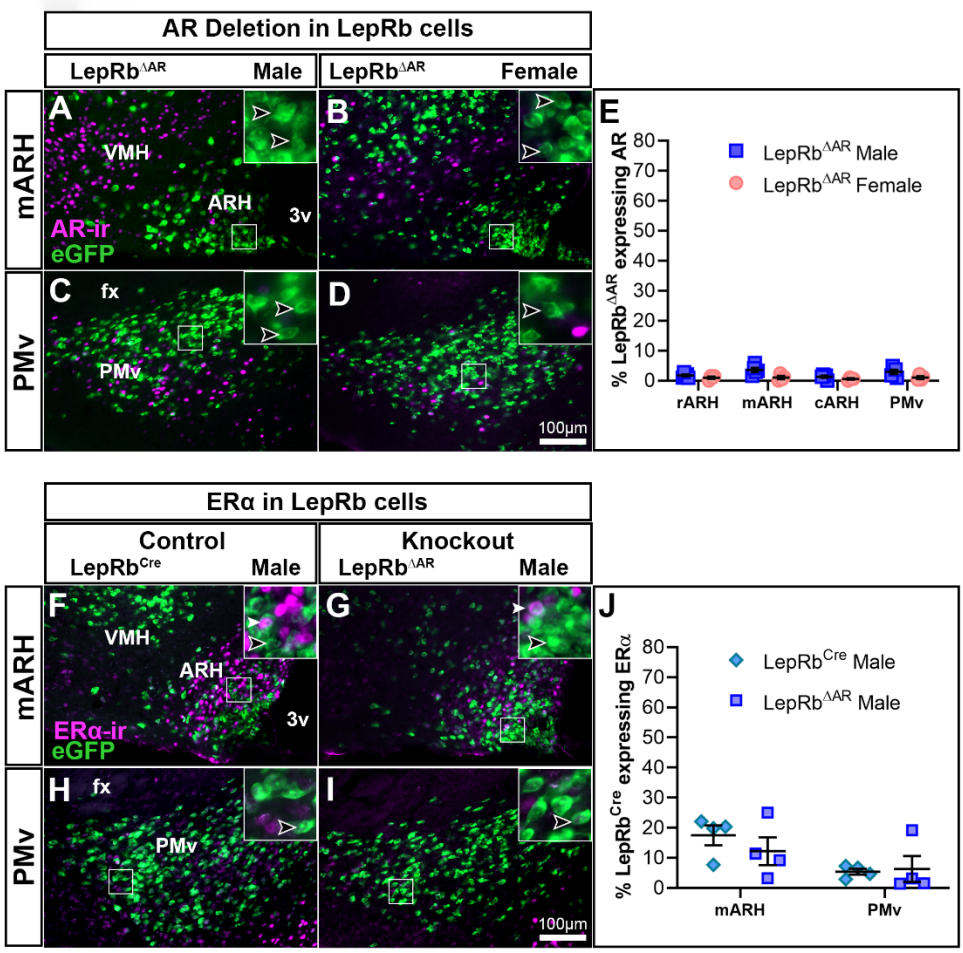

Figure 3.3: Deletion of androgen receptor (AR) in LepRb$^{\Delta AR}$ mice induces no change in estrogen receptor alpha (ERα) expression in leptin receptor (LepRb) expressing cells. A-D, fluorescent images showing AR immunoreactivity (AR-ir, purple) and LepRb$^{\Delta AR}$ (eGFP-L10a, green) expression in mid-arcuate nucleus (mARH, A-B) and ventral pre-mammillary nucleus (PMv, C-D) of a LepRb$^{\Delta AR}$ male (A, C) and female (B, D) hypothalamus. Inset is higher magnification of A-D. E, scatter plot graphs of percentage of LepRb$^{\Delta AR}$ neurons co-expressing AR (mean ± SEM, n = 5 males and n = 4 females, E). Three levels of ARH were quantified (rostal, mid/tuberal, and caudal), and images for mARH shown (A-B). Less than 4% of LepRb$^{\Delta AR}$ express AR in the mARH and PMv in both sexes. Arrows with black center indicate LepRb cells which do not co-express AR. F-I, fluorescent images showing colocalization of LepRb^{Cre} (F, H) and LepRb$^{\Delta AR}$ (G, I) (eGFP-L10a, green) and ERα immunoreactivity (ERα-ir, purple) in mARH (F-G), and PMv (H-I). J, scatter plot graph showing percentage of LepRb^{Cre} neurons co-expressing ERα (mean ± SEM, n = 5 males). Insets are higher magnification of F-I. Solid white arrows indicate LepRb cells which co-express ERα. Arrows with black center indicate LepRb cells which do not co-express ERα. Abbreviations: 3v, third ventricle, fx, fornix, VMH, ventromedial hypothalamus. Abbreviations based on reference brain of the Allen Brain Atlas. Scale bar = 100µm.

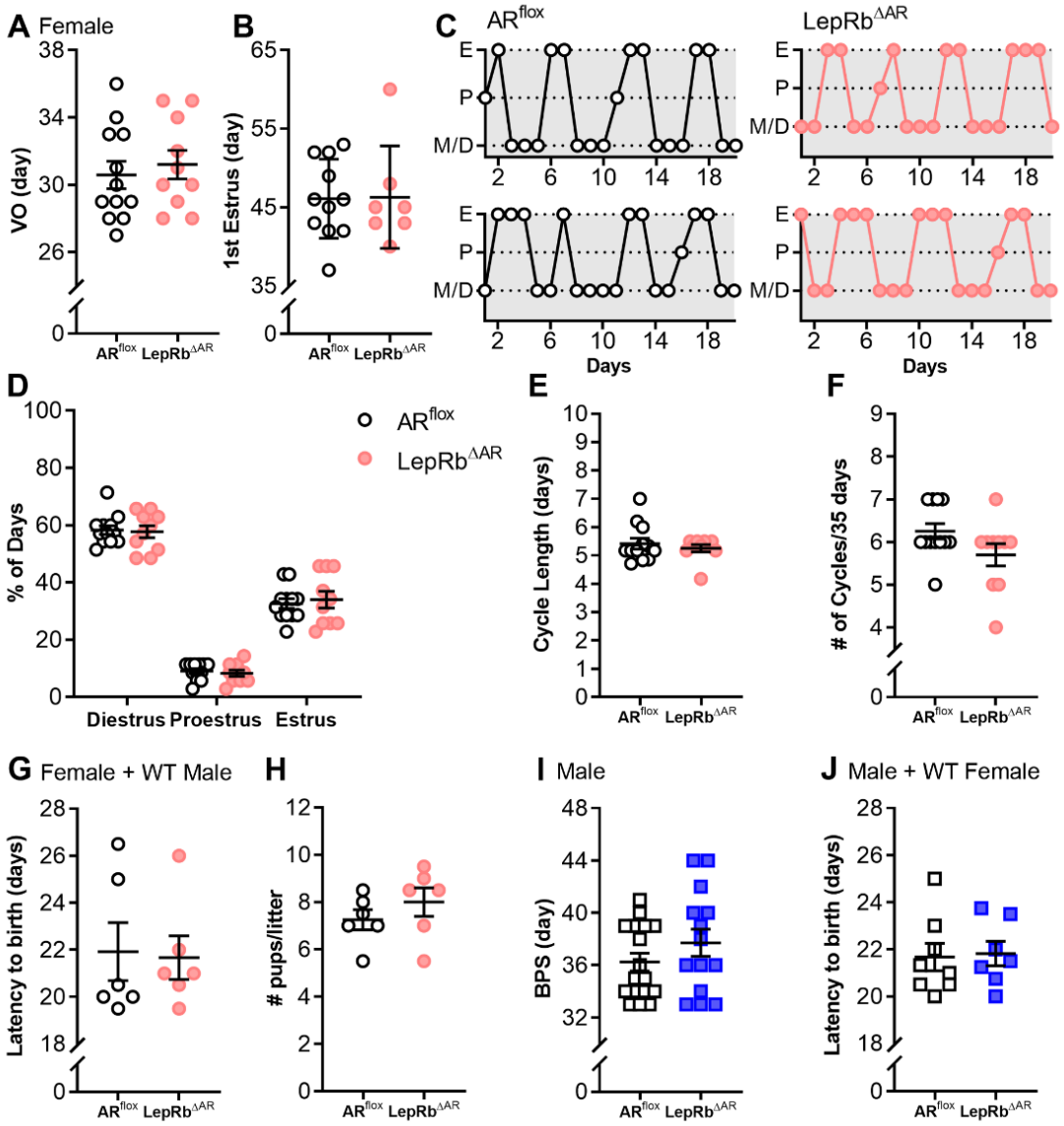

Figure 3.4: Deletion of androgen receptor (AR) in leptin receptor (LepRb) cells does not impact puberty timing and fertility in males and females. A-B, scatter plot graphs of age at vaginal opening (VO), and age at first estrus (B), between AR^{flox} female (n = 11-12) and $LepRb^{\Delta AR}$ (n = 7-10) mice. C, representative cycles shown for AR^{flox} (left panel) and $LepRb^{\Delta AR}$ (right panel). Abbreviations: E, estrus, P, proestrus, M, metestrus, D, diestrus. AR^{flox} and $LepRb^{\Delta AR}$ females show similar percentage of time in each cycle stage (D), typical estrous cycle length (E), and number of cycles per 35 days (F). G-H, $LepRb^{\Delta AR}$ females show typical latency to birth and number of pups per litter when mated with wild-type males (AR^{flox} n = 6, $LepRb^{\Delta AR}$ n = 6). I, day of complete balanopreputial separation (BPS) was not different between AR^{flox} males (n = 17) and $LepRb^{\Delta AR}$ (n = 14). J, latency to birth did not differ in wild-type females mated with AR^{flox} or $LepRb^{\Delta AR}$ males (AR^{flox} n = 8, $LepRb^{\Delta AR}$ n = 7). Mean ± SEM plotted.

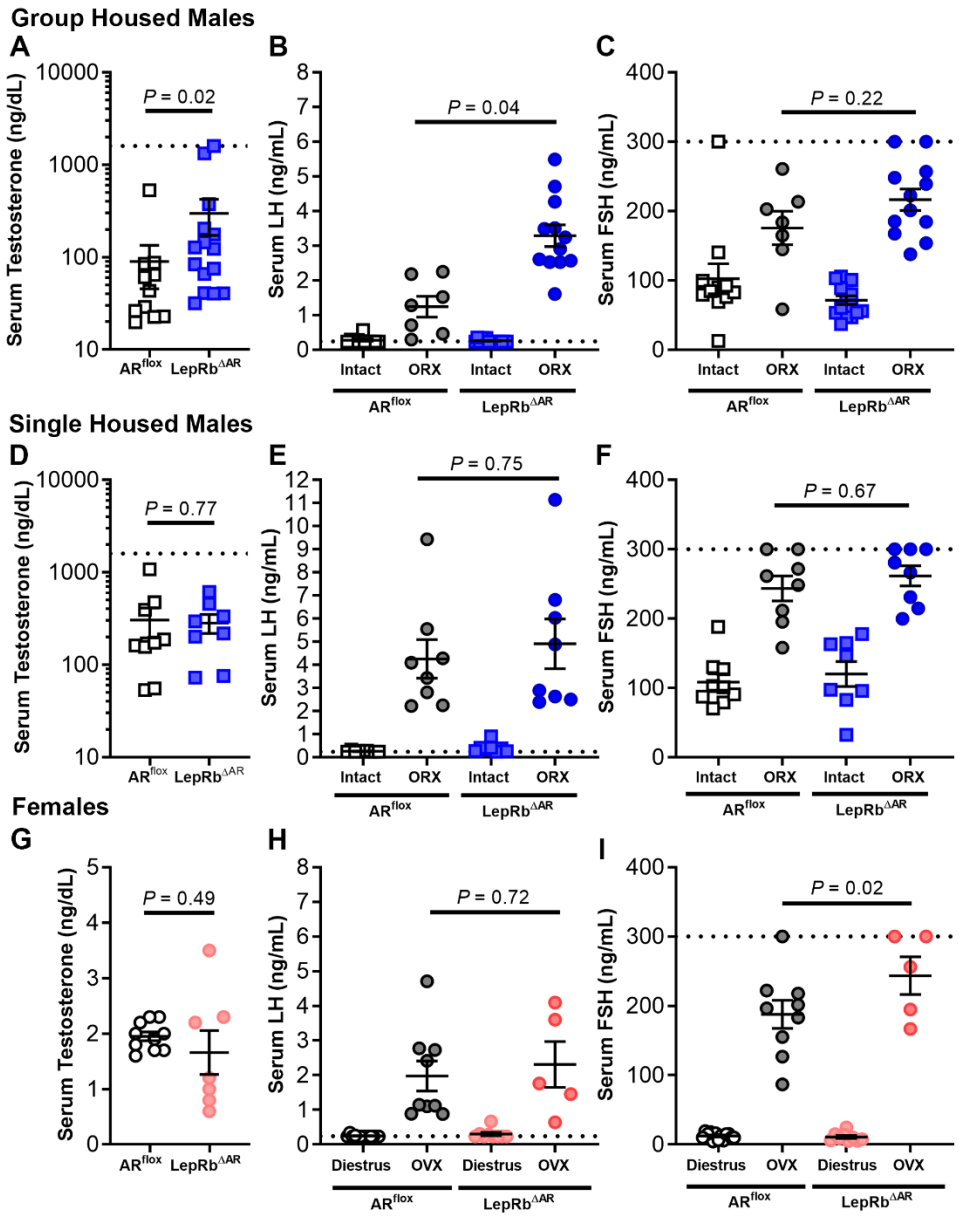

Figure 3.5: LepRb$^{\Delta AR}$ mice display higher testosterone and altered gonadotropin levels in a sexually dimorphic manner. A, scatter plot graph showing serum testosterone (T) in group housed intact AR^{flox} and LepRb$^{\Delta AR}$ males. Serum T levels for males are plotted on a log scale to better illustrate distribution of individual data points. B, serum luteinizing hormone (LH) was significantly different for treatment (intact vs ORX) and genotype (AR^{flox} intact n = 11, ORX n = 7, LepRb$^{\Delta AR}$ intact n = 15, ORX n = 11-12), with LepRb$^{\Delta AR}$ showing higher LH with ORX vs AR^{flox} males. C, serum follicle stimulating hormone (FSH) was not different between genotype or treatment. D-F, scatter plot graphs showing T, LH, and FSH in singled housed intact and ORX males (AR^{flox} intact n = 9, ORX n = 8, LepRb$^{\Delta AR}$ intact n = 8, ORX n = 8). Single-housed male mice did not show significantly different levels of T, LH, or FSH, either intact or ORX. G, serum T was not different between AR^{flox} and LepRb$^{\Delta AR}$ and females. H, serum LH was not different with treatment or genotype in female LepRb$^{\Delta AR}$ compared to AR^{flox} females. I, serum FSH was significantly different for treatment (intact vs OVX), with LepRb$^{\Delta AR}$ females showing elevated FSH with OVX compared to OVX AR^{flox} females. Intact (squares, male) and orchidectomized (ORX, circles, male) male AR^{flox}

(white) and LepRb$^{\Delta AR}$ (blue). AR^{flox} females (white circles intact, grey circles OVX), LepRb$^{\Delta AR}$ (pink circles intact, red circles OVX). Mean ± SEM plotted. Dotted lines indicate detectable limit of the assay.

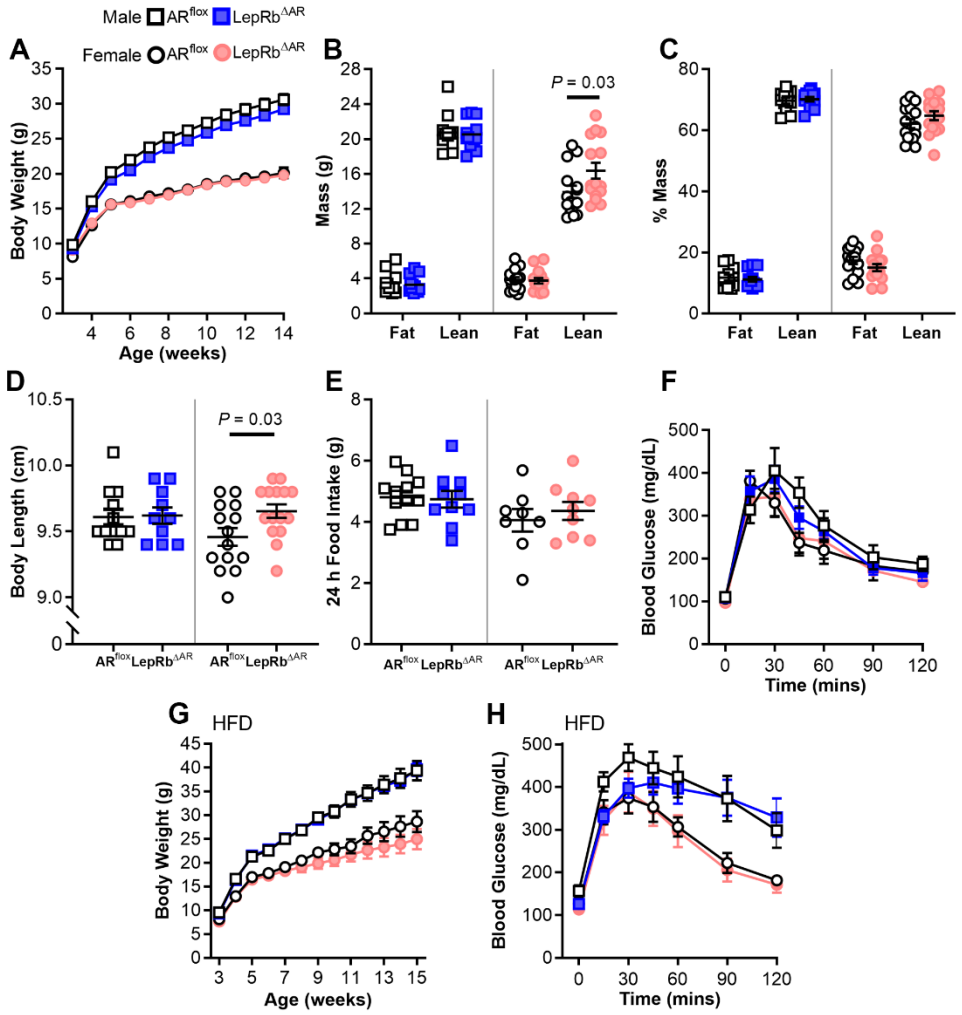

Figure 3.6: Deletion of androgen receptor (AR) in leptin receptor (LepRb) cells results in increased body length in females. A, Scatter plot graphs showing body weight of male AR^{flox} (n =13) and $LepRb^{\Delta AR}$ (n = 11), female AR^{flox} (n = 13) and $LepRb^{\Delta AR}$ (n = 12) mice. B-C, scatter plot graphs showing body composition of male and female AR^{flox} and $LepRb^{\Delta AR}$ mice in total grams of lean and fat mass and percent lean and fat mass. Female $LepRb^{\Delta AR}$ show increased total lean mass but no difference in percentage of lean mass compared to AR^{flox} females. D, scatter plot graph of body length of AR^{flox} and $LepRb^{\Delta AR}$ male and female mice. Female $LepRb^{\Delta AR}$ display greater body length than AR^{flox} females. E, scatter plot graph of average food intake, which was not different in male or female AR^{flox} and $LepRb^{\Delta AR}$ mice. Glucose tolerance test (GTT) for male and female AR^{flox} and $LepRb^{\Delta AR}$ in normal chow (F) and high-fat diet (HFD, H). Body weight of male AR^{flox} (n = 10), $LepRb^{\Delta AR}$ (n = 9), and female AR^{flox} (n = 8), $LepRb^{\Delta AR}$ (n = 7) mice on HFD (G). Male AR^{flox} = white squares, male $LepRb^{\Delta AR}$ = blue squares, female AR^{flox} = white circles, female $LepR^{\Delta AR}$ = pink circles. Mean ± SEM plotted.

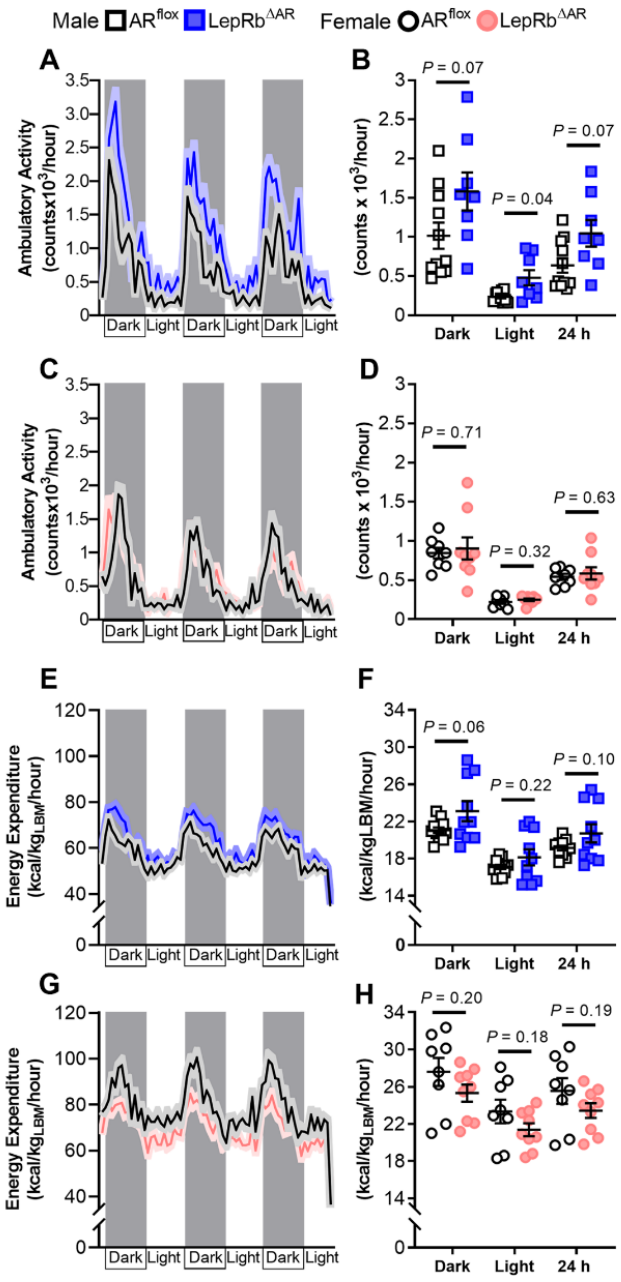

Figure 3.7: Male LepRb$^{\Delta AR}$ mice show increased ambulatory activity in the light phase. A,C, ambulatory activity measured in hourly mean ± SEM over 72 h (males, A, females, C). LepRb$^{\Delta AR}$ males show increased ambulatory activity compared to controls (light phase, mean ± SEM, B). Female ambulatory activity was not different (D). E, G, energy expenditure hourly mean ± SEM over 72 h (males, E, females, G). Energy expenditure was not significantly different in male or female LepRb$^{\Delta AR}$ mice compared to controls (F, H). Male AR^{flox} n = 11, LepRb$^{\Delta AR}$ n = 9, AR^{flox} n = 8, female LepRb$^{\Delta AR}$ n = 9. Mean ± SEM plotted.

CHAPTER 4

Deletion of AR in LepRb Cells Improves Estrous Cyclicity in Prenatally Androgenized Female Mice

Polycystic ovary syndrome (PCOS) is the most common endocrine disorder in people with ovaries who are of reproductive age, and is characterized by hyperandrogenism, oligo/anovulation, and/or polycystic ovaries. Many patients with PCOS also show adverse metabolic phenotypes, including central adiposity, insulin resistance, and glucose intolerance, which can exacerbate reproductive dysfunction. The elevated androgens in PCOS can act upon androgen receptors (AR), which are expressed in many reproductive and metabolic tissues, including the neuroendocrine hypothalamic sites that regulate the hypothalamic-pituitary-gonadal (HPG) axis and energy homeostasis. Yet it is not known which specific populations of neurons are impacted by female androgen excess. We and others have previously shown that AR is highly expressed in LepRb neurons, particularly in the arcuate (ARH) and ventral premammillary nuclei (PMv) of female mice. We hypothesize that leptin-receptor (LepRb) neurons participate in the pathogenesis of PCOS, as LepRb neurons are critical in the central regulation of energy homeostasis, and exert permissive actions on puberty and fertility. We have pre-natally androgenized (PNA) a mouse model of AR deletion specifically in LepRb cells ($LepRb^{\Delta AR}$) and have conducted reproductive and metabolic phenotyping. As previously demonstrated, control PNA females show long periods of acyclicity, whereas $LepRb^{\Delta AR}$ PNA female mice show improved estrous cyclicity. Our findings indicate that a subpopulation of AR/LepRb cells mediate the effects of prenatal androgen excess on female estrous cycles in a mouse model of PCOS-like phenotype.

Introduction

Androgens at physiologic levels are crucial for the adequate functioning of female reproductive and metabolic physiology. Females typically have lower levels of androgens than males, but disorders of androgen excess can lead to reproductive and metabolic dysfunction. Polycystic ovary syndrome (PCOS) is one example of a disorder caused by pathogenic androgen excess. PCOS the most prevalent endocrine disorder among reproductive aged people with ovaries, with a prevalence ranging from 5-20% (1,2). PCOS is a heterogeneous disorder, with diagnostic criteria including oligo/anovulation, polycystic ovarian morphology, and/or hyperandrogenism (3,4). Elevated androgens are key in driving the reproductive, metabolic, and neuroendocrine abnormalities in PCOS patients, that include infertility, increased gonadotropin releasing hormone secretion, abdominal obesity, and insulin resistance (5,6).

Androgens can act on steroid hormone receptors in many tissues via androgen receptors (AR), or estrogen receptors (ERα/β) after conversion to estradiol via aromatase. Androgens acting via AR, however, are critical in driving the pathophysiologic changes seen with female hyperandrogenism. Experimentally, treatment of female animal models with the non-aromatizable androgen dihydrotestosterone (DHT) either prenatally during late embryonic development (7-10), or prepubertally (11-14) leads to a phenotype in adults which mimics that of PCOS. While androgens acting via AR can impact different tissues to cause pathologic change, neuronal AR are key in driving reproductive dysfunction of hyperandrogenic females (15). Mice with neuronal deletion of AR exposed to androgen excess are protected from development of anovulation, polycystic ovaries, and metabolic abnormalities (16). However, it is not clear which population of AR-deleted neurons confers this protection.

We hypothesize that leptin-receptor (LepRb)-expressing neurons participate in the pathogenesis of female hyperandrogenism-induced reproductive dysfunction. Leptin is a hormone produced by white adipose tissue in proportion to the amount of adipose mass, and signals centrally via LepRb. Leptin confers status of peripheral energy stores to hypothalamic sites, permitting energetically demanding processes such as pregnancy and lactation to occur (17). Lack of either leptin or its receptor leads to obesity, diabetes, and infertility. We have previously shown that a subset of LepRb neurons coexpress AR in hypothalamic areas involved in the control of reproduction, and that loss of AR from LepRb neurons has minimal effects in typical female fertility (18). In this study, we examined whether LepRb-specific deletion of AR protects from the development of reproductive dysfunction in a prenatal model of female androgen excess.

Methods

Animal Ethics

All research animals were acquired, used, and maintained in accordance with the National Research Council *Guide for the Care and Use of Laboratory Animals* (19), the US Public Health Service's Policy on Humane Care and Use of Laboratory Animals, and Guide for the Care and Use of Laboratory Animals, as well as federal, state, and local laws. Procedures and protocols were approved by the University of Michigan Committee on Use and Care of Animals (IACUC, Animal Protocol: PRO8712).

Animals

LepRb-Cre (LepRb^{Cre}, JAX® mice, B6.129-*Lepr$^{tm3(cre)Mgmj}$*/J, stock #032457 (20,21)), AR-flox (AR^{flox}, 129-*Ar^{tm1Verh}*/Sv, provided by Dr. S. Marc Breedlove, Michigan State University, with permission from Dr. Karel De Gendt, Catholic University of Leuven, Belgium, UFA ID: 16-UFA03327 (22)), ROSA26-loxSTOPlox-eGFP-L10a (JAX® mice, B6;129S4-*Gt(ROSA)26Sor$^{tm9(EGFP/Rpl10aAmc/}$*J, stock #024750 (23)), ROSA26-loxSTOPlox-ChR2-EYFP (JAX® mice, B6.Cg-*Gt(ROSA)26Sor$^{tm32(CAG-COP4*H134R/EYFP)Hze}$*/J, stock #024109 [24]), and CD-1® IGS (Charles River Laboratories, Crl;CD1(ICR), stock #022) mice were housed in an Association for Assessment and Accreditation of Laboratory Animal Care (AAALAC) accredited facility at the University of Michigan Medical School. Mice were housed in a 12:12 light/dark cycle environment with controlled temperature (21-23°C) and humidity (30-70%). Mice were provided water ad libitum and were fed a phytoestrogen-reduced diet (16% protein, 4.0% fat, 48.5% carbohydrate, Teklad 2916 irradiated global rodent diet, Envigo) or a phytoestrogen-reduced, higher protein and fat diet (19% protein, 9% fat, 44.9% carbohydrate, Teklad 2919 irradiated global rodent diet, Envigo) for breeding and lactating females. Phytoestrogen-reduced diets were used to avoid effects of exogenous dietary estrogens on reproductive or metabolic physiology of experimental mice. Genotyping was performed on DNA extracted from ear samples or tail tips obtained prior to weaning and at termination of experiments (RED Extract-N-Amp Tissue PCR Kit, Cat #XNAT, MilliporeSigma). Primers used for genotyping are listed in Table 4.1.

Table 4.1: Primers used for genotyping

Mice	Primer Sequence	Size (bp)
LepRb^{Cre}	Comm FOR 5' TCC AAG AAG CCT CAA GGT TCC A 3' Wt REV 5' TCG TGT TGA AAT TTC TTC TTT CCA GA 3' Cre REV 5' ACG CAC ACC GGC CTT ATT CC 3'	Wt: 300 Mutant: 200
AR^{flox}	mAR28 5' AGC CTG TAT ACT CAG TTG GGG 3' mAR29 5' AAT GCA TCA CAT TAA GTT GAT ACC 3'	Wt: 860 Flox: 930
R26-loxSTOPlox-eGFP-L10a	FOR 1 5' GAG GGG AGT GTT GCA ATA CC 3' FOR 2 5' TCT ACA AAT GTG GTA GAT CCA GGC 3' REV 5' CAG ATG ACT ACC TAT CCT CCC 3'	Wt: 300 Mutant: 200
R26-loxSTOP-lox-ChR2(H134R)-EYFP	Wt FOR 5'AAG GGA GCT GCA GTG GAG TA 3' Wt REV 5'CCG AAA ATC TGT GGG AAG TC 3' Mut FOR 5' ACA TGG TCC TGC TGG AGT TC 3' Mut REV 5' GGC ATT AAA GCA GCG TAT CC 3'	Wt: 297 Mutant: 253

LepRb-specific deletion of AR (LepRb$^{\Delta AR}$)

As previously described (18), mice with deletion of *Ar* specific to LepRb expressing neurons were generated by crossing *Lepr*^{Cre} mice with AR^{flox} mice (*Ar*$^{fl/fl}$ females and *Ar*$^{fl/Y}$ males). LepRb^{Cre} and LepRb$^{\Delta AR}$ mice were bred with Cre-dependent reporter mice (eGFP-L10a or ChR2-EYFP) to visualize LepRb^{Cre} expressing cells. For scientific rigor and reproducibility, and to generate adequate number of experimental and control mice from the same litter, we performed the same experiment in at least four independent cohorts of animals. Experimental animals were derived from multiple breeding pairs (a minimum of 5, but up to 15 breeding pairs per data set). Each graph shown includes animals derived from different pairs of breeders to account for differences in vivarium conditions.

Prenatal androgenization

To generate PNA female offspring, a LepRb($^{Cre/Wt}$);AR($^{fl/fl}$) female and a CD1 female were paired with a LepRb($^{Cre/Wt}$);AR($^{fl/Y}$) male. Mice that were heterozygous for Cre were mated to generate offspring homozygous for Cre, or wild-type for the *Lepr* gene in order to generate littermate

controls in experimental mice (Figure 4.1A). Timed pregnancy was established by monitoring of vaginal plugs the morning after introduction, and presence of a plug was considered gestational day 1. Males were removed from breeding cages by gestational day 15. On gestational days 16 through 18, pregnant LepRb($^{Cre/Wt}$);AR($^{fl/fl}$) dams were injected subcutaneously with 225 µg of dihydrotestosterone (DHT, 5α-androstan-17β-ol-3-one) in 50 µL of sesame oil. Control dams were injected with sesame oil (vehicle, VEH). All breeding cages included a CD1 dam throughout pregnancy and lactation to provide maternal and nutritional support, in order to increase survival of PNA offspring. Combined litter size was adjusted to 8-10 pups per cage by postnatal day (PND) 10, by culling CD1 offspring or male pups. Androgenization of PNA female offspring was assessed by measurement of anogenital distance (distance from base of the clitoris to midpoint of the anus) with digital calipers at PND 60 (Figure 4.1B). PNA treatment resulted in a significant increase in AGD in both genotypes (two-way ANOVA with Holm-Sidak correction, effect of treatment, $P = 0.001$, $F = 11.57$, $DFn = 1$, $DFd = 59$).

Reproductive Phenotyping

Pubertal onset was monitored daily beginning at PND 14, as advancement in vaginal opening (VO) has been reported with PNA treatment (9,25). Day of VO for PNA females was considered as a reddening of the narrowed and constricted vaginal opening at the base of the clitoris. Body weight was recorded at the time of VO. After VO, females were monitored daily for first estrus via vaginal lavage. First estrus was defined as the presence of predominantly keratinized epithelial cells for two consecutive days following the presence of predominantly leukocytes, or one day preceded by proestrus (26-28). Day of first estrus was monitored up until PND 60.

Adult estrous cyclicity was evaluated for 35 consecutive days beginning at 10 weeks of age by performing daily vaginal lavage. Estrous cycle stage was based on the proportion of leukocytes, epithelial, and keratinized epithelial cells (29). Evaluation of daily vaginal cytology was performed blinded. Estrous cycle length was determined by counting the number of days between the first day of estrous in each cycle, averaged per mouse. Number of cycles completed was considered as the number of complete estrous cycles completed in 35 days. Percentage of time spent in each cycle stage was calculated as the number of days in each stage (diestrus/metestrus, proestrus, or estrus), divided by 35 days.

Metabolic Phenotyping

Body weight of experimental and control mice was measured weekly beginning at weaning (postnatal day 21). Glucose levels were measured in blood samples obtained from tail-tip bleeding in female (n = 7-15 mice/group, 16-17 weeks of age) PNA and VEH LepRb$^{\Delta AR}$ and AR^{flox} mice after an overnight fast (approximately 16 h) using a glucometer (OneTouch Ultra, LifeScan Inc). After fasting blood glucose was measured, mice received an intraperitoneal bolus of D-glucose in sterile saline (2 mg D-glucose/g body weight) at 0 min, and tail tip blood was collected for glucose levels at 15 min intervals for the first hour, and 30 min intervals for the second hour (2 h total). Body composition (fat and lean mass) was quantified in 19-week old female (n = 8-15 mice/group) PNA and VEH LepRb$^{\Delta AR}$ and AR^{flox} mice using an NMR-based device (Minispec LF 90II, Bruker Optics). Body composition measurements were performed at the Michigan Mouse Metabolic Phenotyping Center (MMPC).

Tissue collection

Adult female mice were euthanized during diestrus (morning, 0900-1130 h), as determined by a vaginal lavage with predominately leukocytes (29) and confirmed by uterine weight below 100 mg (30). Mice were deeply anesthetized with isoflurane and euthanized via decapitation. Trunk blood was collected and allowed to clot for 45 mins at room temperature, then centrifuged at 4°C for 20 mins at 3,000 x g, followed by collection of serum which was stored at -20°C. Pituitary glands were quickly collected, frozen on dry ice, and stored at -80°C until RNA extraction.

A separate cohort of mice were deeply anesthetized with isoflurane and transcardially perfused with 0.1M PBS until liver and lungs cleared (about 1 minute), followed by 10% neutral buffered formalin (NBF) for 10 minutes. Perfused ovaries (n = 6-8/group) were transferred to 10% NBF and stored at 4°C until paraffin embedding at the University of Michigan Unit for Laboratory Animal Medicine In-Vivo Animal Core. Ovaries were sectioned at 4 μm in three series, deparaffinized and dehydrated, then stained with hematoxylin and eosin (H&E).

Serum hormone assays

Serum samples (n = 5-6/group) were sent to the University of Virginia Ligand Core for the following assays: ultra-sensitive mouse LH ELISA and mouse anti-Mullerian hormone (AMH) ELISA. LH was measured using an in-house method as previously described(31). The capture monoclonal antibody (anti-bovine LH beta subunit, 518B7, RRID: AB_2665514) was provided by Janet Roser, University of California, and the detection polyclonal antibody (rabbit LH antiserum, AFP240580Rb, RRID: AB_2665533) was provided by A.F. Parlow, National Hormone Peptide Program (NHPP). The HRP-conjugated goat anti-rabbit polyclonal antibody was purchased from DakoCytomation (Glostrup, Denmark; D048701-2). The assay standard was

mouse LH reference prep AFP5306A (NHPP). The limit of quantification (LoQ, lowest concentration that demonstrates accuracy within 20% of expected values) or functional sensitivity = 0.016 ng/mL, intra-assay %CV = 2.2%, inter-assay %CV 7.3% (low QC, 0.13 ng/ml), 5.0% (medium QC, 0.8 ng/ml) and 6.5% (high QC, 2.3 ng/ml). Antibodies used for assays are listed in Table 4.2.

Table 4.2: Antibodies

Peptide/Protein Target	Antibody Name	Cat #	Species Raised In	RRID
LH beta subunit	Anti-bovine LH beta subunit antibody	Janet Roser, University of California, 518B7	Mouse, monoclonal	AB_2756886
LH	Rabbit Anti-LH antiserum	A.F. Parlow, National Hormone and Peptide Program, AFP240580Rb	Rabbit, polyclonal	AB_2665533
Rabbit immunoglobulins	Goat Anti-Rabbit Immunoglobulins/HRP Antibody	Aglient, P0448	Goat, polyclonal	AB_2617138

Quantitative PCR

Pituitary from adult AR^{flox} and $LepRb^{\Delta AR}$ (n = 3/group) mice were homogenized with Qiazol reagent (Qiagen), then total RNA was isolated using the RNeasy Plus Mini Kit (Qiagen), including genomic DNA elimination, according to manufacturer's protocol. First-strand cDNA was synthesized using SuperScript II reverse transcriptase (Invitrogen), oligo(dT), and 1000 ng of RNA. Gene expression was quantified in triplicate samples using quantitative real-time PCR (qPCR) with a CFX-384 Bio-Rad Real-Time PCR detection system. TaqMan Gene Expression MasterMix (Applied Biosystems) was used with primer/probes listed in Table 4.3. Transcript levels were normalized to the housekeeping gene *Actb*. and mRNA expression levels of target genes were determined by comparative cycle threshold (Ct) values, and relative to *Actb* gene copy number was calculated as $2^{-\Delta\Delta Ct}$. No differences were observed in relative expression of *Actb* between experimental groups.

Table 4.3: Primer/Probes used for qPCR

Target Transcript	NCBI Accession #	qPCR Assay	FOR	REV	Taqman Probe
Actb	NM_007393	Mm.PT.39a.22214843.g	5' GATTACTGCTCTGGCTCCTAG 3'	5' GACTCATCGTACTCCTGCTTG 3'	5' CTGGCCTCACTGTCCACCTTCC 3'
Cga	NM_009889	Mm.PT.58.31855537	5' CCTCAGATCGACAATCACCTG 3'	5' AGCATGACCAGAATGACAGC 3'	5' CCCTCAAAAAGTCCAGAGCTTGCAGA 3'
Lhb	NM_008497	Mm.PT.45.5612498	5' CCAGTCTGCATCACCTTCAC 3'	5' GAGGCACAGGAGGCAAAG 3'	5' AGTACTCGGACCATGCTAGGACAGT 3'
Fshb	NM_008045	Mm.PT.45.17694677	5' TTCAGCTTTCCCCAGAAGAG 3'	5' TCCAGCACCAGAATAAGATGC 3'	5' AGCTACGTCCTGTGCAGTCAGC 3'
Pgr	NM_008829	Mm.PT.47.10254276	5' CGCCATACCTTAACTACCTGAG 3'	5' CCATAGTGACAGCCAGATGC 3'	5' AGATTCAGAAGCCAGCCAGAGCC 3'
Esr1	NM_007956	Mm.PT.47.16003033	5' CCTGTTTGCTCCTAACTTGCT 3'	5' GAACCGACTTGACGTAGCC 3'	5' TGCCTTCCACACATTTACCTTGATTCCT 3'
Ar	NM_013476	Mm.PT.47.17416675	5' CTGCCTTGTTATCTAGCCTCA 3'	5' ATACTGAATGACCGCCATCTG 3'	5' ACCACATGCACAAGCTGCCTCT 3'

Microscopy and Image Acquisition

Digital images were acquired using an Axio Imager M2 (Carl Zeiss) with a digital camera (AxioCam, Zeiss) using Zen Pro 2 software (Zeiss), using the same magnification, illumination, and exposure time for each image of the same experiment.

Illustration

Adobe Photoshop and Illustrator software (Adobe Creative Cloud) were used to prepare digital images, including adjusting resolution to 300 dpi, adjustment of image size, addition of annotation and labels. Uniform adjustments were made to every image. Abbreviations are based on the Allen

Mouse Brain Atlas (postnatal day 56, coronal reference atlas, Allen Institute for Brain Science, Allen Mouse Brain Atlas, http://mouse.brain-map.org/static/atlas).

Data Analysis

Ovary sections from one series of H&E-stained slides were imaged at 5× magnification, and every fifth section was imaged for quantification of corpora lutea. All imaging, quantification, and analysis was performed blinded to genotype and treatment.

Statistics

Data are reported as mean ± standard error of the mean (SEM). Analysis was performed using GraphPad Prism software (Version 9). Data is presented as individual values with mean ± standard error of the mean (SEM). Data was analyzed for normal distribution using a Shapiro-Wilk test (significance level alpha 0.05). Non-normal data was log transformed prior to analysis. Two-way ANOVA with multiple comparisons and Holm-Sidak correction was used to analyze data, except for body weight and glucose tolerance test data which two-way ANOVA with repeated measures and Holm-Sidak correction was used. Exact post-hoc *P* values are reported and statistical significance is defined as $P < 0.05$.

Results

$LepRb^{\Delta AR}$ female mice show mild changes in body weight and glucose tolerance

PNA treatment results in mild metabolic changes in female mice (8). We observed that all experimental groups had similar body weight at weaning (Figure 4.2A), and gained similar amounts of weight until 7 weeks of age (Figure 4.2B). At 7 weeks of age, there was a significant

difference in body weight between PNA groups, with LepRb$^{\Delta AR}$ PNA females weighing less than AR^{flox} PNA mice (mean body weight AR^{flox} PNA = 19.71 g, LepRb$^{\Delta AR}$ PNA = 17.82 g, P = 0.01, mean difference 1.90 g, SEM 0.53 g, t = 3.51, DF = 16.57, two-way ANOVA, repeated measures, with Holm-Sidak correction). Additionally, at 8 and 9 weeks of age, LepRb$^{\Delta AR}$ PNA females weighed significantly less than AR^{flox} VEH mice (8 weeks, mean body weight AR^{flox} PNA = 20.73 g, LepRb$^{\Delta AR}$ PNA = 18.40 g, P = 0.04, mean difference 2.3 g, SEM 0.68 g, t =3.42, DF = 9.42, 9 weeks, mean body weight AR^{flox} PNA = 21.21 g, LepRb$^{\Delta AR}$ PNA = 19.01 g, P = 0.02, mean difference 2.2 g, SEM 0.62 g, t =3.53, DF = 11.44, two-way ANOVA, repeated measures, with Holm-Sidak correction). Body weight was not significantly different between groups before or after 7-9 weeks of age. Body composition, including fat and lean mass, was no different between groups at 19 weeks of age (Figure 4.3C). LepRb$^{\Delta AR}$ PNA mice displayed increased blood glucose at15 minutes post-injection during glucose tolerance testing compared to AR^{flox} PNA mice (mean blood glucose AR^{flox} PNA = 295 mg/dL, LepRb$^{\Delta AR}$ PNA = 410 mg/dL, P = 0.01, mean difference = 114 mg/dL, SEM 30 mg/dL, t = 3.75, DF = 16.37, Figure 4.3D). However, area under the curve of GTT was no different between groups (Figure 4.3E).

Knockout of AR from LepRb neurons does not improve delay in sexual maturation with prenatal androgen excess

Previous reports have described an advance in the day of VO in PNA mice. We did not observe a significant difference in day of VO in either PNA or VEH AR^{flox} or LepRb$^{\Delta AR}$ females (Figure 4.3A). Day of VO was similar in all groups (Figure 4.3B). While we did not observe differences in VO, day of first estrus was delayed in both AR^{flox} or LepRb$^{\Delta AR}$ PNA groups compared to AR^{flox} VEH controls (Figure 4.3C). Day of first estrus was also delayed by 8 days in LepRb$^{\Delta AR}$ VEH

females (Figure 4.3D), including the day at which half of LepRb$^{\Delta AR}$ VEH females reached first estrus (delayed by approximately 7 days). Despite this delay, almost all (94%) of LepRb$^{\Delta AR}$ VEH females reached first estrus by PND60. Only 45-50% of females in the PNA groups reached first estrus by PND60, indicating that deletion of AR from LepRb cells was not sufficient in preventing PNA-induced delays in sexual maturity.

Estrous cycles are improved in PNA females with knockout of AR in LepRb neurons

Consistent with our previous findings, VEH LepRb$^{\Delta AR}$ female mice display typical estrous cycles compared to AR^{flox} controls, including similar cycle length, number of cycles, and percentage of time spent in each cycle stage (Figure 4.4A-D). PNA treatment induced acyclicity in AR^{flox} mice, characterized by long periods of anestrus. Compared to VEH, AR^{flox} PNA mice displayed increased cycle length, fewer number of cycles, a greater percentage of days in diestrus, and fewer percentage in estrus. In PNA LepRb$^{\Delta AR}$ mice, cycle length was similar to VEH treated mice, and was significantly different compared to AR^{flox} PNA mice (average cycle length PNA AR^{flox} 9.3 days, PNA LepRb$^{\Delta AR}$ 6.2 days, $P = 0.01$, t = 3.2, DF = 37, Figure 4.4B). PNA LepRb$^{\Delta AR}$ mice also had a similar number of cycles as VEH treated mice, and displayed a significant improvement in number of cycles compared to PNA AR^{flox} (mean number of cycles/35 days PNA AR^{flox} = 3.5, PNA LepRb$^{\Delta AR}$ = 6, $P = 0.005$, t = 3.43, DF = 37, Figure 4.4C). Percentage of days spent in diestrus was significantly improved in PNA LepRb$^{\Delta AR}$ (percentage of days diestrus PNA AR^{flox} = 84.7%, LepRb$^{\Delta AR}$ 69.7%, $P = 0.03$, t = 3.2, DF = 111). Likewise, PNA LepRb$^{\Delta AR}$ mice displayed improvements in percentage of days spent in estrus compared to PNA AR^{flox} mice (percentage of days estrus PNA AR^{flox} = 13.3%, LepRb$^{\Delta AR}$ = 24.2%, $P = 0.03$, t = 2.3, DF = 111). No differences were observed in percentage of days of proestrus in any group (Figure 4.4D).

Pituitary gene expression of gonadotropin subunits and sex steroid receptors

To determine whether changes in pituitary gland gene expression could in part explain the improvement in PNA LepRb$^{\Delta AR}$ estrous cycles, we examined expression of selected genes associated with reproductive neuroendocrine control. No significant differences were observed in gonadotropin subunits *Lhb*, *Fshb*, or *Cga* among experimental groups relative to VEH AR^{flox} mice (Figure 4.5A-C). Relative expression of *Ar* was increased in PNA LepRb$^{\Delta AR}$ compared to both AR^{flox} VEH and PNA mice (mean difference relative expression PNA LepRb$^{\Delta AR}$ vs PNA AR^{flox} = 138%, SEM = 40%, $P = 0.04$, mean difference relative expression PNA LepRb$^{\Delta AR}$ vs VEH AR^{flox} = 152%, SEM = 40%, $P = 0.03$, two-way ANOVA with Holm-Sidak correction, Figure 4.5D). Additionally, sex steroid receptors *Esr1*, and *Pgr* were unchanged (Figure 4.5E-F).

Ovary histology

Ovarian histology was examined for number of corpora lutea (Figure 4.6A-D), an endocrine structure that forms from follicular cells post-ovulation. Ovaries from all experimental groups displayed similar number of corpora lutea per ovary (Figure 4.6E).

Serum LH concentrations

Blood collected at time of sacrifice during the morning of diestrus was analyzed for concentration of serum LH (Figure 4.7). No differences in serum LH were observed between experimental groups.

Discussion

Disorders of androgen imbalance are common, particularly PCOS which is characterized by female androgen excess. Androgens acting via AR can exert significant effects on the central regulation of the neuroendocrine reproductive axis, and have been implicated in the pathogenesis of DHT-induced reproductive and metabolic changes in animal models. However, the specific neuronal populations impacted by androgen excess have not been fully examined. In this study, we have assessed the effect of deletion of AR in LepRb cells in the context of prenatal androgen excess. LepRb expressing neurons represent a metabolically and reproductively relevant hypothalamic population which are also sensitive to androgens, especially those in the ARH and PMv. We have shown that PNA LepRb$^{\Delta AR}$ female mice have improved estrous cycles compared to littermate controls.

LepRb$^{\Delta AR}$ female mice also show mild metabolic changes, including decreased body weight between 7-9 weeks of age. The cause of this temporary difference in body weight is not known, but this is also the period where we observed differences in reproductive maturation. Yet, body weight gain did not differ outside of this period, which is consistent with previous descriptions of PNA female mice that show no difference in adult body weight (8,12). PNA treatment also has been shown to result in glucose intolerance and impairments in pancreatic islet function. While we did not observe glucose intolerance with PNA treatment in our studies, PNA LepRb$^{\Delta AR}$ mice did show increased blood glucose 15 min post-injection during glucose tolerance testing. These differences may represent changes in acute insulin response, and warrant future studies examining pancreatic islet function in PNA LepRb$^{\Delta AR}$ mice.

The PNA mouse model is useful in representing lean PCOS patients, who may develop mild metabolic impairments. However, many people with PCOS are obese (32), and obesity can exacerbate reproductive dysfunction. Therefore, it will be important to study the effects of androgen excess on LepRb neurons in a PCOS-like mouse model that develops a stronger metabolic phenotype. Prepubertal androgen excess (PPA) leads to increased body weight, adiposity, dyslipidemia, and glucose intolerance, in addition to the reproductive PCOS-like features observed in PNA treated mice (12,13). Additional studies involving LepRb$^{\Delta AR}$ and PPA treatment will further elucidate the role of LepRb cells in disorders of female hyperandrogenism.

Previous reports found that PNA female mice have advanced age of VO (9). In our studies, however, we observed uniformly advanced day of VO in all experimental groups. This advancement was likely due to body weight at day of VO, as body weight is a known factor in the initiation of puberty (33). Since our experimental design involved rearing litters with dual dams, offspring were provided with greater nutrition which could explain the advancement of VO. While day of VO was no different, PNA treated mice show a clear delay in day of first estrus, which was not improved in LepRb$^{\Delta AR}$ mice. This suggests that AR in LepRb cells does not play a role in the pubertal deficits with prenatal exposure androgen excess, but may be relevant for adult fertility.

Our AR^{flox} control mice replicate the reported anestrus phenotype seen with PNA treatment, including long periods of diestrus, and fewer completed cycles. PNA LepRb$^{\Delta AR}$ mice displayed improved estrous cycles, although not fully restored to typical cycles observed in VEH treated mice. Since evaluation of estrous cycles via examination of vaginal cytology only indicates relative exposure of vaginal epithelium to fluctuating levels of estradiol, we examined additional markers

of reproductive axis function. Number of corpora lutea, a marker of post-ovulatory ovarian follicles, are either decreased (12,34,35), or unchanged in PNA rodents (9). We did not observe a difference in the number of corpora lutea with PNA treatment. However, other aspect of ovarian health may be affected. For example, increased follicular atresia and greater amount of unhealthy antral follicles are found in PNA ovaries. Prenatal androgen excess has also been shown to deplete the pool of primordial follicles in sheep (36). Therefore, further examination of follicle numbers and markers of morphological health are warranted.

In addition to altered ovarian morphology, PCOS patients and PCOS-like animal models show abnormal neuroendocrine function. Prenatal or peripubertal exposure to androgen excess results in persistently elevated GnRH pulse frequency and impaired hypothalamic sensitivity to the negative feedback effects of progesterone (7,25,37,38). Increased GnRH neuron activity is driven by increased excitatory GABAergic inputs (10,39), particularly by ARH GABAergic neurons which also show reduced progesterone receptor expression (40). Furthermore, the increase in GABAergic inputs to GnRH neurons is AR dependent, and is prevented by treatment with the AR-antagonist flutamide (35). It is possible that AR-expressing LepRb neurons are part of the ARH GABAergic population innervating GnRH neurons. However, a greater portion of LepRb neurons express AR in the female PMv. As opposed to the ARH, the PMv is highly glutamatergic, and PMv LepRb neurons directly innervate GnRH neurons (41). However, glutamatergic inputs to GnRH neurons are not changed with PNA treatment (40). Further studies will be needed to evaluate the impact of PNA on LepRb neuron projections, and whether GABAergic and/or glutamatergic projections are differently affected. Additionally, it will be important to determine if direct projections to GnRH neurons, or indirect projections to upstream reproductively-relevant

neurons (i.e., kisspeptin/neurokinin/dynorphin, and/or agouti-related peptide/neuropeptide Y) are changed in PNA LepRb female mice.

As a consequence of increased GnRH pulse frequency, PCOS patients display altered patterns of gonadotropin release (42,43). LH hypersecretion is present in a majority of people with PCOS (44), and is elevated relative to FSH. However, LH levels in PNA mice show conflicting results. An increase in mean LH at time of sacrifice and increased LH pulses (10,40), or no changes in LH have been described in PNA mice (12,45). In our studies, we did not observe a difference in mean LH at time of sacrifice in gonadally intact diestrus mice. Additionally, we did not observe changes in pituitary gland *Lhb* or *Fshb* transcript levels. It will be interesting to assess pattern of LH pulses and/or LH surge profiles in PNA LepRb$^{\Delta AR}$ mice to determine whether deletion of AR in LepRb cells prevents elevated LH pulse frequency with PNA.

In summary, these studies demonstrate that androgen action via AR in LepRb cells is important for the development of some of the reproductive features of female hyperandrogenism, including anestrus. Future studies will be needed to determine the mechanism of AR action in LepRb neurons, and whether our findings in a rodent model of androgen excess translates to human pathophysiology.

References

1. Azziz R, Carmina E, Chen Z, Dunaif A, Laven JSE, Legro RS, Lizneva D, Natterson-Horowtiz B, Teede HJ, Yildiz BO. Polycystic ovary syndrome. Nature Reviews Disease Primers 2016; 2:16057

2. Lizneva D, Suturina L, Walker W, Brakta S, Gavrilova-Jordan L, Azziz R. Criteria, prevalence, and phenotypes of polycystic ovary syndrome. Fertility and sterility 2016; 106:6-15

3. Revised 2003 consensus on diagnostic criteria and long-term health risks related to polycystic ovary syndrome (PCOS). Human reproduction (Oxford, England) 2004; 19:41-47

4. Dumesic DA, Oberfield SE, Stener-Victorin E, Marshall JC, Laven JS, Legro RS. Scientific Statement on the Diagnostic Criteria, Epidemiology, Pathophysiology, and Molecular Genetics of Polycystic Ovary Syndrome. Endocr Rev 2015; 36:487-525

5. O'Reilly MW, Taylor AE, Crabtree NJ, Hughes BA, Capper F, Crowley RK, Stewart PM, Tomlinson JW, Arlt W. Hyperandrogenemia predicts metabolic phenotype in polycystic ovary syndrome: the utility of serum androstenedione. J Clin Endocrinol Metab 2014; 99:1027-1036

6. Blank S, McCartney C, Marshall J. The origins and sequelae of abnormal neuroendocrine function in polycystic ovary syndrome. Human reproduction update 2006; 12:351-361

7. Roland AV, Moenter SM. Prenatal androgenization of female mice programs an increase in firing activity of gonadotropin-releasing hormone (GnRH) neurons that is reversed by metformin treatment in adulthood. Endocrinology 2011; 152:618-628

8. Roland AV, Nunemaker CS, Keller SR, Moenter SM. Prenatal androgen exposure programs metabolic dysfunction in female mice. The Journal of endocrinology 2010; 207:213-223

9. Witham EA, Meadows JD, Shojaei S, Kauffman AS, Mellon PL. Prenatal exposure to low levels of androgen accelerates female puberty onset and reproductive senescence in mice. Endocrinology 2012; 153:4522-4532

10. Sullivan SD, Moenter SM. Prenatal androgens alter GABAergic drive to gonadotropin-releasing hormone neurons: implications for a common fertility disorder. Proceedings of the National Academy of Sciences of the United States of America 2004; 101:7129-7134

11. Aflatounian A, Edwards MC, Rodriguez Paris V, Bertoldo MJ, Desai R, Gilchrist RB, Ledger WL, Handelsman DJ, Walters KA. Androgen signaling pathways driving reproductive and metabolic phenotypes in a PCOS mouse model. The Journal of endocrinology 2020; 245:381-395

12. Caldwell AS, Middleton LJ, Jimenez M, Desai R, McMahon AC, Allan CM, Handelsman DJ, Walters KA. Characterization of reproductive, metabolic, and endocrine features of polycystic ovary syndrome in female hyperandrogenic mouse models. Endocrinology 2014; 155:3146-3159

13. van Houten EL, Kramer P, McLuskey A, Karels B, Themmen AP, Visser JA. Reproductive and metabolic phenotype of a mouse model of PCOS. Endocrinology 2012; 153:2861-2869

14. Manneras L, Cajander S, Holmang A, Seleskovic Z, Lystig T, Lonn M, Stener-Victorin E. A new rat model exhibiting both ovarian and metabolic characteristics of polycystic ovary syndrome. Endocrinology 2007; 148:3781-3791

15. Walters KA, Gilchrist RB, Ledger WL, Teede HJ, Handelsman DJ, Campbell RE. New perspectives on the pathogenesis of PCOS: neuroendocrine origins. Trends in Endocrinology & Metabolism 2018; 29:841-852

16. Caldwell ASL, Edwards MC, Desai R, Jimenez M, Gilchrist RB, Handelsman DJ, Walters KA. Neuroendocrine androgen action is a key extraovarian mediator in the development of polycystic ovary syndrome. Proceedings of the National Academy of Sciences of the United States of America 2017; 114:E3334-E3343

17. Elias CF, Purohit D. Leptin signaling and circuits in puberty and fertility. Cell Mol Life Sci 2013; 70:841-862

18. Cara AL, Myers MG, Elias CF. Lack of AR in LepRb Cells Disrupts Ambulatory Activity and Neuroendocrine Axes in a Sex-Specific Manner in Mice. Endocrinology 2020; 161

19. Council NR. Guide for the Care and Use of Laboratory Animals: Eighth Edition. Washington, DC: The National Academies Press.

20. Leshan RL, Bjornholm M, Munzberg H, Myers MG, Jr. Leptin receptor signaling and action in the central nervous system. Obesity (Silver Spring) 2006; 14 Suppl 5:208S-212S

21. Patterson CM, Leshan RL, Jones JC, Myers MG. Molecular mapping of mouse brain regions innervated by leptin receptor-expressing cells. Brain Research 2011; 1378:18-28

22. De Gendt K, Swinnen JV, Saunders PT, Schoonjans L, Dewerchin M, Devos A, Tan K, Atanassova N, Claessens F, Lecureuil C, Heyns W, Carmeliet P, Guillou F, Sharpe RM, Verhoeven G. A Sertoli cell-selective knockout of the androgen receptor causes spermatogenic arrest in meiosis. Proceedings of the National Academy of Sciences of the United States of America 2004; 101:1327-1332

23. Krashes MJ, Shah BP, Madara JC, Olson DP, Strochlic DE, Garfield AS, Vong L, Pei H, Watabe-Uchida M, Uchida N, Liberles SD, Lowell BB. An excitatory paraventricular nucleus to AgRP neuron circuit that drives hunger. Nature 2014; 507:238-242

24. Madisen L, Mao T, Koch H, Zhuo JM, Berenyi A, Fujisawa S, Hsu YW, Garcia AJ, 3rd, Gu X, Zanella S, Kidney J, Gu H, Mao Y, Hooks BM, Boyden ES, Buzsáki G, Ramirez JM, Jones AR, Svoboda K, Han X, Turner EE, Zeng H. A toolbox of Cre-dependent optogenetic transgenic mice for light-induced activation and silencing. Nat Neurosci 2012; 15:793-802

25. Dulka EA, Moenter SM. Prepubertal Development of Gonadotropin-Releasing Hormone Neuron Activity Is Altered by Sex, Age, and Prenatal Androgen Exposure. Endocrinology 2017; 158:3943-3953

26. Qiu X, Dowling AR, Marino JS, Faulkner LD, Bryant B, Bruning JC, Elias CF, Hill JW. Delayed puberty but normal fertility in mice with selective deletion of insulin receptors from Kiss1 cells. Endocrinology 2013; 154:1337-1348

27. Garcia-Galiano D, van Ingen Schenau D, Leon S, Krajnc-Franken MA, Manfredi-Lozano M, Romero-Ruiz A, Navarro VM, Gaytan F, van Noort PI, Pinilla L, Blomenrohr M, Tena-Sempere M. Kisspeptin signaling is indispensable for neurokinin B, but not glutamate, stimulation of gonadotropin secretion in mice. Endocrinology 2012; 153:316-328

28. Torsoni MA, Borges BC, Cote JL, Allen SJ, Mahany E, Garcia-Galiano D, Elias CF. AMPKalpha2 in Kiss1 Neurons Is Required for Reproductive Adaptations to Acute Metabolic Challenges in Adult Female Mice. Endocrinology 2016; 157:4803-4816

29. Caligioni C. Assessing Reproductive Status/Stages in Mice. Current protocols in neuroscience / editorial board, Jacqueline N Crawley [et al] 2009:Appendix-4I

30. Silveira MA, Wagenmaker ER, Burger LL, DeFazio RA, Moenter SM. GnRH Neuron Activity and Pituitary Response in Estradiol-Induced vs Proestrous Luteinizing Hormone Surges in Female Mice. Endocrinology 2016; 158:356-366

31. Steyn FJ, Wan Y, Clarkson J, Veldhuis JD, Herbison AE, Chen C. Development of a methodology for and assessment of pulsatile luteinizing hormone secretion in juvenile and adult male mice. Endocrinology 2013; 154:4939-4945

32. Sam S. Obesity and Polycystic Ovary Syndrome. Obesity management 2007; 3:69-73

33. Baker ER. Body weight and the initiation of puberty. Clinical obstetrics and gynecology 1985; 28:573-579

34. Tehrani FR, Noroozzadeh M, Zahediasl S, Piryaei A, Azizi F. Introducing a rat model of prenatal androgen-induced polycystic ovary syndrome in adulthood. Exp Physiol 2014; 99:792-801

35. Silva MS, Prescott M, Campbell RE. Ontogeny and reversal of brain circuit abnormalities in a preclinical model of PCOS. JCI insight 2018; 3

36. Smith P, Steckler TL, Veiga-Lopez A, Padmanabhan V. Developmental Programming: Differential Effects of Prenatal Testosterone and Dihydrotestosterone on Follicular Recruitment, Depletion of Follicular Reserve, and Ovarian Morphology in Sheep1. Biology of reproduction 2009; 80:726-736

37. Foecking EM, Szabo M, Schwartz NB, Levine JE. Neuroendocrine Consequences of Prenatal Androgen Exposure in the Female Rat: Absence of Luteinizing Hormone Surges, Suppression of Progesterone Receptor Gene Expression, and Acceleration of the Gonadotropin-Releasing Hormone Pulse Generator1. Biology of reproduction 2005; 72:1475-1483

38. Chhabra S, McCartney CR, Yoo RY, Eagleson CA, Chang RJ, Marshall JC. Progesterone inhibition of the hypothalamic gonadotropin-releasing hormone pulse generator: evidence for varied effects in hyperandrogenemic adolescent girls. J Clin Endocrinol Metab 2005; 90:2810-2815

39. Berg T, Silveira MA, Moenter SM. Prepubertal Development of GABAergic Transmission to Gonadotropin-Releasing Hormone (GnRH) Neurons and Postsynaptic Response Are Altered by Prenatal Androgenization. J Neurosci 2018; 38:2283-2293

40. Moore AM, Prescott M, Marshall CJ, Yip SH, Campbell RE. Enhancement of a robust arcuate GABAergic input to gonadotropin-releasing hormone neurons in a model of polycystic ovarian syndrome. Proceedings of the National Academy of Sciences of the United States of America 2015; 112:596-601

41. Leshan RL, Louis GW, Jo YH, Rhodes CJ, Munzberg H, Myers MG, Jr. Direct innervation of GnRH neurons by metabolic- and sexual odorant-sensing leptin receptor neurons in the hypothalamic ventral premammillary nucleus. J Neurosci 2009; 29:3138-3147

42. Rebar R, Judd HL, Yen SS, Rakoff J, Vandenberg G, Naftolin F. Characterization of the inappropriate gonadotropin secretion in polycystic ovary syndrome. The Journal of clinical investigation 1976; 57:1320-1329

43. Arroyo A, Laughlin GA, Morales AJ, Yen SS. Inappropriate gonadotropin secretion in polycystic ovary syndrome: influence of adiposity. J Clin Endocrinol Metab 1997; 82:3728-3733

44. Taylor AE, McCourt B, Martin KA, Anderson EJ, Adams JM, Schoenfeld D, Hall JE. Determinants of Abnormal Gonadotropin Secretion in Clinically Defined Women with Polycystic Ovary Syndrome1. The Journal of Clinical Endocrinology & Metabolism 1997; 82:2248-2256

45. Dulka EA, Burger LL, Moenter SM. Ovarian Androgens Maintain High GnRH Neuron Firing Rate in Adult Prenatally-Androgenized Female Mice. Endocrinology 2020; 161

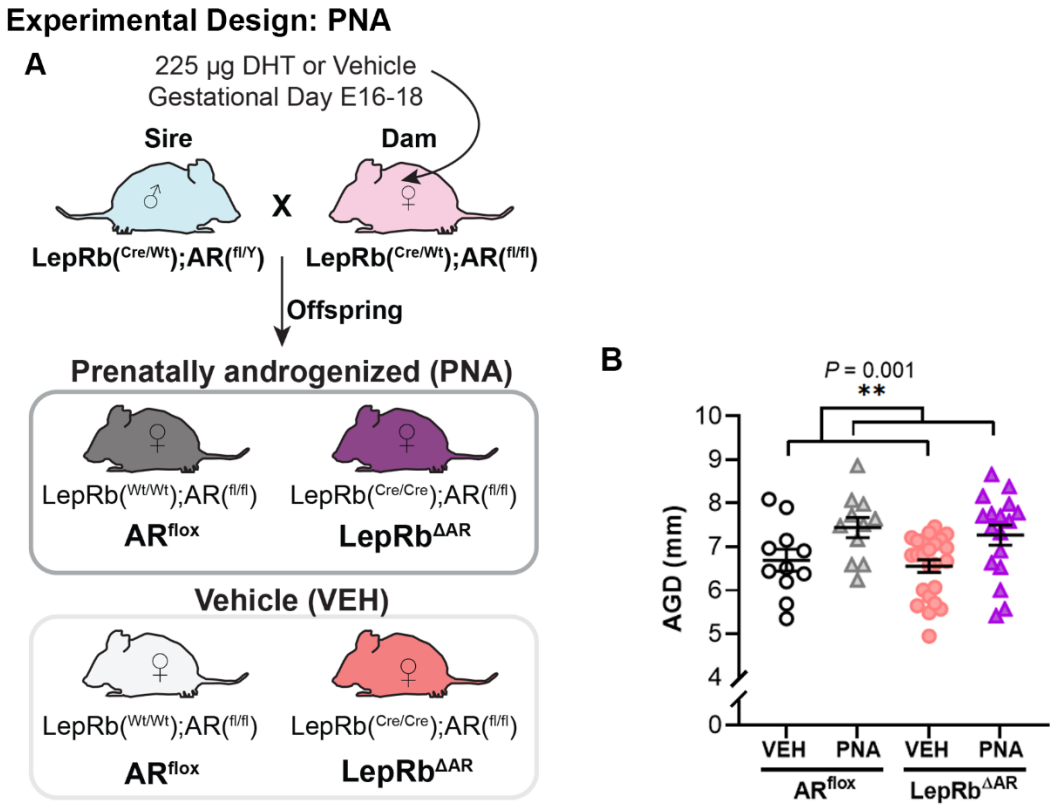

Figure 4.1: Experimental design and validation of prenatal androgenization. A, illustration of experimental setup. A sire and a dam heterozygous for *Lepr*^{Cre} and hemizygous or homozygous for *Ar*^{flox} were mated to generate littermate controls with two copies of *Lepr*^{Cre} (LepRb-specific AR deletion, LepRb$^{\Delta AR}$) and two *Lepr*^{Wt} alleles (AR^{flox}). Dams were treated with dihydrotestosterone (DHT) or oil (vehicle, VEH) on embryonic day (E)16, 17, and 18, and prenatally androgenized (PNA) and control VEH female offspring were used for experiments. B, scatter plot graph showing anogenital distance (AGD) of adult postnatal day 60 mice (mean ± SEM, AR^{flox} VEH n = 11, AR^{flox} PNA n = 11, LepRb$^{\Delta AR}$ VEH n = 24, LepRb$^{\Delta AR}$ PNA n = 17). Effect of treatment was statistically significant (two-way ANOVA with Holm-Sidak correction, effect of treatment, ** = P = 0.001, F = 11.57, DFn = 1, DFd = 59).

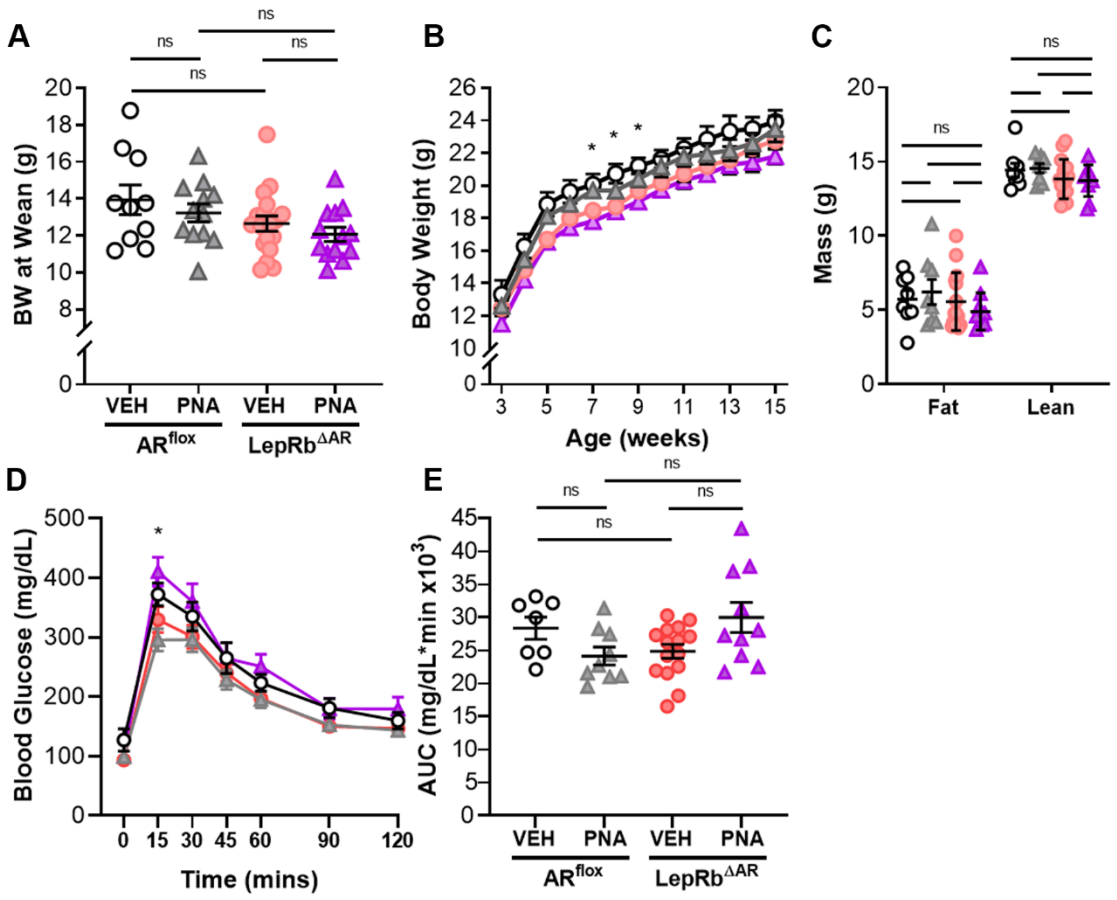

Figure 4.2: Mild changes in body weight and glucose tolerance were observed in LepR$^{\Delta AR}$ PNA mice. A, scatter plot graph of body weight of experimental mice at weaning day/postnatal day 21 (mean ± SEM, AR^{flox} VEH n = 10, AR^{flox} PNA n = 12, LepRb$^{\Delta AR}$ VEH n = 18, LepRb$^{\Delta AR}$ PNA n = 13). B, line graph of weekly body weight from 3 to 15 weeks of age (mean ± SEM, AR^{flox} VEH n = 7, AR^{flox} PNA n = 9, LepRb$^{\Delta AR}$ VEH n = 15, LepRb$^{\Delta AR}$ PNA n = 10). LepR$^{\Delta AR}$ PNA mice weighed significantly less than AR^{flox} PNA mice at 7 weeks (mean difference 1.9 g, SEM = 0.53 g, $P = 0.01$), and less than AR^{flox} VEH mice at 8 weeks (mean difference 2.3 g, SEM = 0.68 g, $P = 0.04$), and 9 weeks (mean difference 2.2 g, SEM = 0.62 g, $P = 0.02$). Body weight gain analyzed by two-way ANOVA with repeated measures and Holm-Sidak correction. C, scatter plot graph of fat and lean mass of 19 week old mice (mean ± SEM, AR^{flox} VEH n = 8, AR^{flox} PNA n = 8, LepRb$^{\Delta AR}$ VEH n = 15, LepRb$^{\Delta AR}$ PNA n = 10). D, line graph showing levels of blood glucose during glucose tolerance testing of 16-17 week old mice (mean ± SEM, AR^{flox} VEH n = 7, AR^{flox} PNA n = 9, LepRb$^{\Delta AR}$ VEH n = 15, LepRb$^{\Delta AR}$ PNA n = 10). LepRb$^{\Delta AR}$ PNA mice show greater blood glucose compared to AR^{flox} PNA mice 15 mins after i.p. injection of glucose (mean difference 114 mg/dL, SEM = 30 mg/dL, $P = 0.01$, two-way ANOVA with repeated measures and Holm-Sidak correction). D, scatter plot graph of area under the curve of glucose tolerance test.

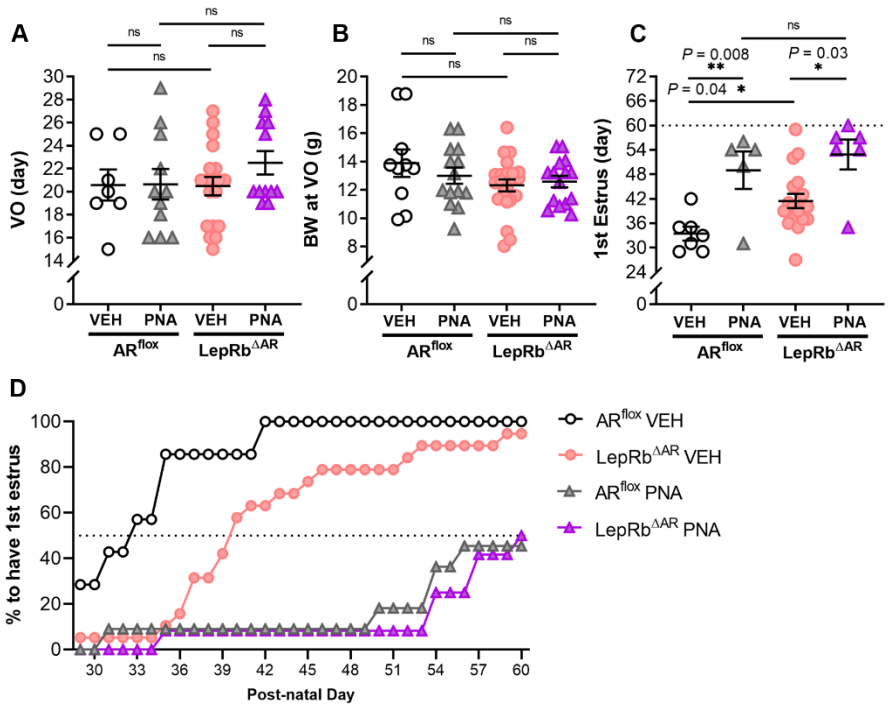

Figure 4.3: LepRb-specific deletion of AR does not impact pubertal timing and does not rescue delayed sexual maturity of PNA mice. A-B, scatter plot graphs of day of vaginal opening (VO) and body weight at day of VO (mean ± SEM, AR^{flox} VEH n = 7, AR^{flox} PNA n = 11, $LepRb^{\Delta AR}$ VEH n = 19, $LepRb^{\Delta AR}$ PNA n = 12). C, scatter plot graph of day of first estrus (mean ± SEM, AR^{flox} VEH n = 7, AR^{flox} PNA n = 5, $LepRb^{\Delta AR}$ VEH n = 18, $LepRb^{\Delta AR}$ PNA n = 6). First estrus was monitored up until postnatal day 60 (dotted line). Day of first estrus was delayed in VEH $LepRb^{\Delta AR}$ vs AR^{flox} mice (mean difference = 8 days, SEM = 1.7 days, $P = 0.04$, two-way ANOVA with Holm-Sidak correction). First estrus was also delayed in AR^{flox} PNA compared to AR^{flox} VEH (mean difference = 15.5 days, SEM = 4.5 days, $P = 0.007$, two-way ANOVA with Holm-Sidak correction), and in $LepRb^{\Delta AR}$ PNA compared to $LepRb^{\Delta AR}$ (mean difference = 11.4 days, SEM = 3.6 days, $P = 0.01$, two-way ANOVA with Holm-Sidak correction). D, percentage of females who had first estrus plotted by postnatal day. Dotted line indicates when 50% of each group had first estrus. 50% of $LepRb^{\Delta AR}$ VEH mice reached first estrus 7 days later than AR^{flox} VEH mice (AR^{flox} VEH 50% reached first estrus = 32.5 days, $LepRb^{\Delta AR}$ VEH 50% reached first estrus = 39.5 days). Note that 50% of mice in both PNA groups showed first estrus around postnatal day 60.

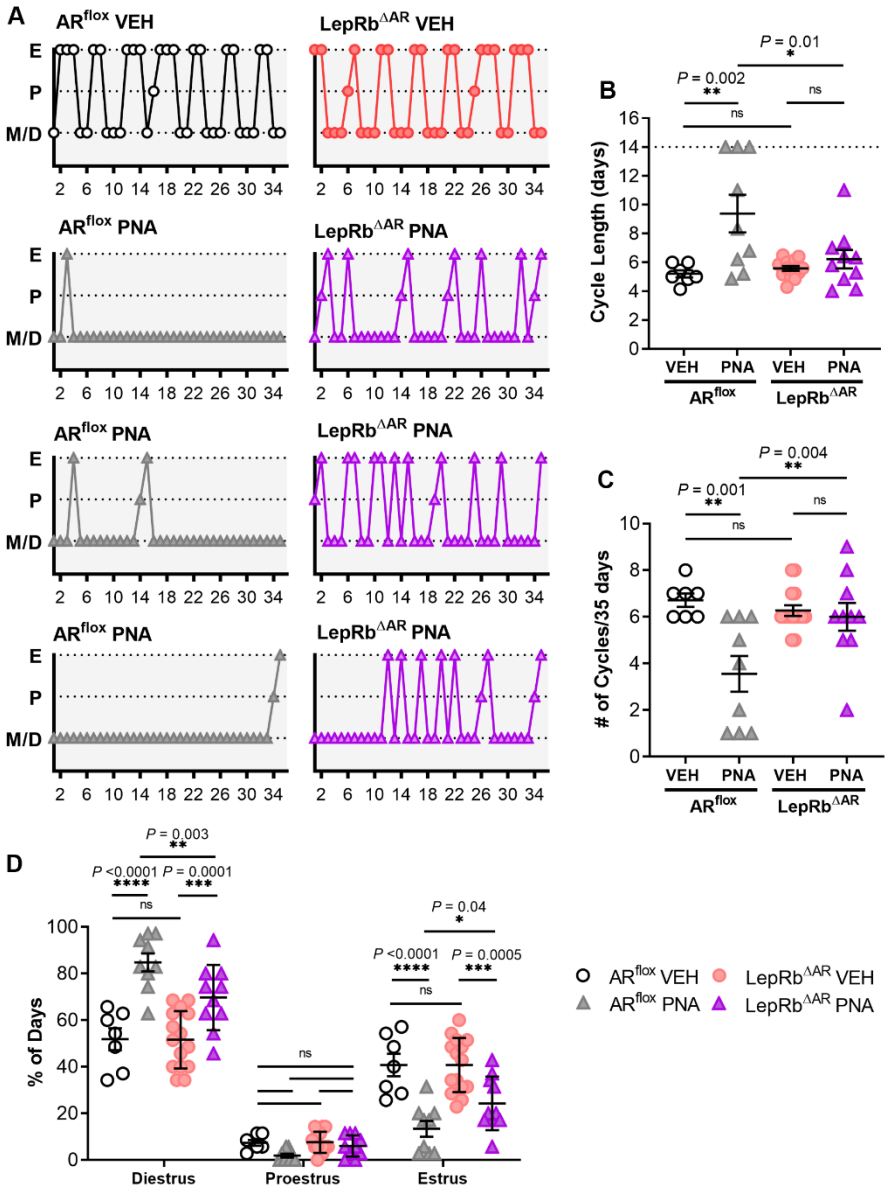

Figure 4.4: Deletion of AR from LepRb cells improves estrous cycles of PNA mice. A, representative cycles shown for experimental and control groups. Littermate controls are shown side by side. M/D = metestrus/diestrus, P = proestrus, E = estrus. B, scatter plot graph of average cycle length (mean ± SEM, AR^{flox} VEH n = 7, AR^{flox} PNA n = 9, $LepRb^{\Delta AR}$ VEH n = 15, $LepRb^{\Delta AR}$ PNA n = 10). AR^{flox} PNA mice had longer cycle length compared to AR^{flox} VEH (mean difference = 4.1 days, SEM = 1.0 days, $P = 0.002$, two-way ANOVA with Holm-Sidak correction). $LepRb^{\Delta AR}$ PNA mice showed improved cycle length compared to AR^{flox} PNA (mean difference = 3.1 days, SEM = 0.9 days, $P = 0.01$, two-way ANOVA with Holm-Sidak correction). C, scatter plot graph of average number of cycles completed in 35 days. AR^{flox} PNA mice completed fewer cycles than AR^{flox} VEH (mean difference = 3.1 cycles, SEM = 0.77 cycles, $P = 0.001$, two-way ANOVA with Holm-Sidak correction). $LepRb^{\Delta AR}$ PNA mice showed improved number of cycles compared to AR^{flox} PNA (mean difference = 2.4 cycles, SEM = 0.71 cycles, $P = 0.005$, two-way ANOVA with Holm-Sidak correction). D, scatter plot graph of percentage of days spent in each cycle stage (mean ± SEM of %metestrus/diestrus, %proestrus, and %estrus). AR^{flox} PNA mice spent greater percentage of days in diestrus and fewer percentage of days in estrus compared to AR^{flox} VEH (%diestrus mean difference =

32%, SEM = 5.0%, P < 0.0001, %estrus mean difference = 27%, SEM = 5.0%, two-way ANOVA with Holm-Sidak correction). $LepRb^{\Delta AR}$ PNA mice showed improvements in percentage of days in diestrus and estrus compared to AR^{flox} PNA (%diestrus mean difference = 15%, SEM = 4.6%, $P = 0.03$, %estrus mean difference = 10%, SEM = 4.6%, $P = 0.04$, two-way ANOVA with Holm-Sidak correction).

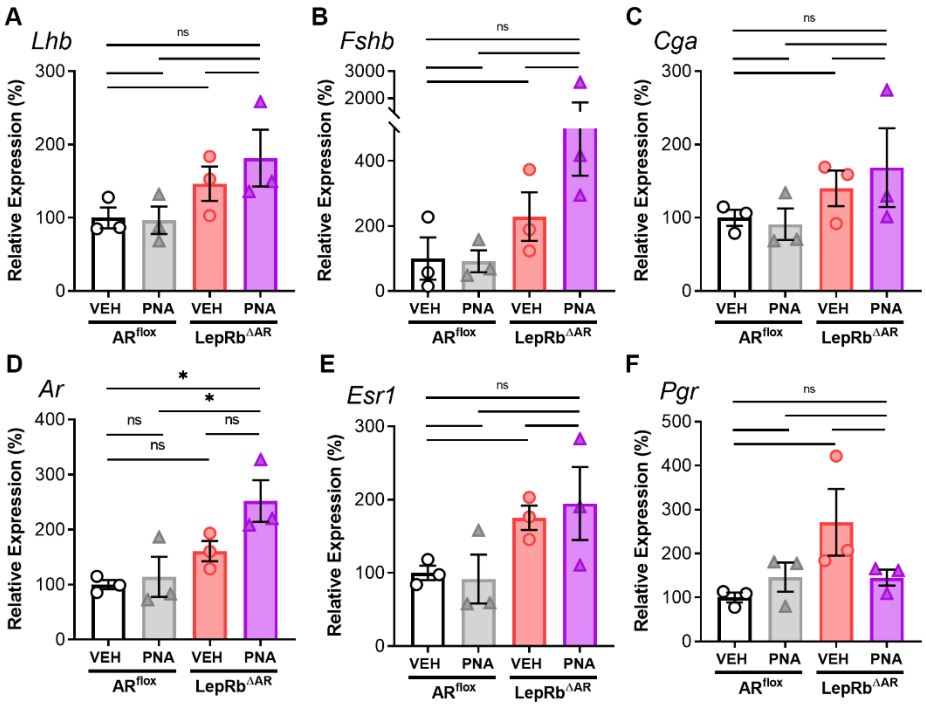

Figure 4.5: Expression of pituitary gland genes in control and experimental mice. A-F, scatter plot graphs of gene expression normalized to housekeeping gene beta-actin (*Actb*), and relative to AR^{flox} VEH. Select genes shown include A, luteinizing hormone, beta subunit (*Lhb*), B, follicle stimulating hormone, beta subunit (Fshb), C, glycoprotein hormones alpha chain (*Cga*), D, androgen receptor (*Ar*), E, estrogen receptor α (*Esr1*), and F, progesterone receptor (*Pgr*). Data presented as mean ± SEM and analyzed by two-way ANOVA with Holm-Sidak correction.

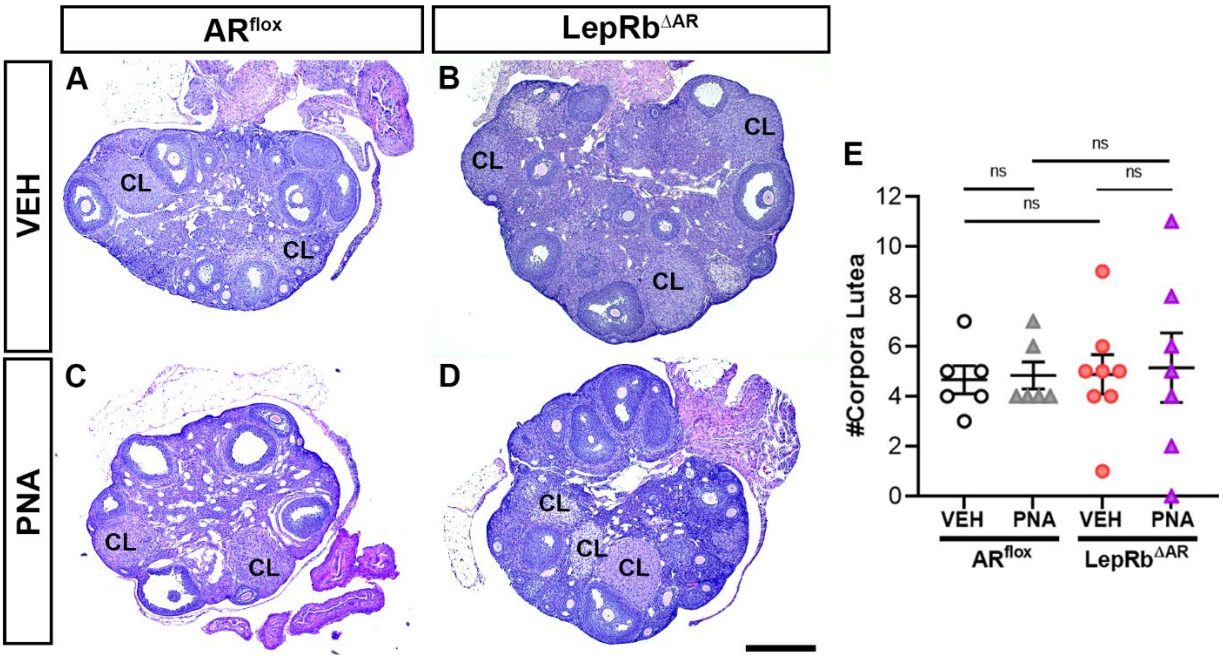

Figure 4.6: Ovarian histology and corpora lutea quantification. A-D, images of histologic hematoxylin and eosin-stained sections of ovaries from VEH AR^{flox} (A), VEH $LepRb^{\Delta AR}$ (B), PNA AR^{flox} (C), and PNA $LepRb^{\Delta AR}$ (D) mice. CL, corpus luteum. Scale bar = 500 µm. E, scatter plot graph of number of corpora lutea per ovary. Data presented as mean ± SEM and analyzed by two-way ANOVA with Holm-Sidak correction. No difference in number of CL was observed between groups.

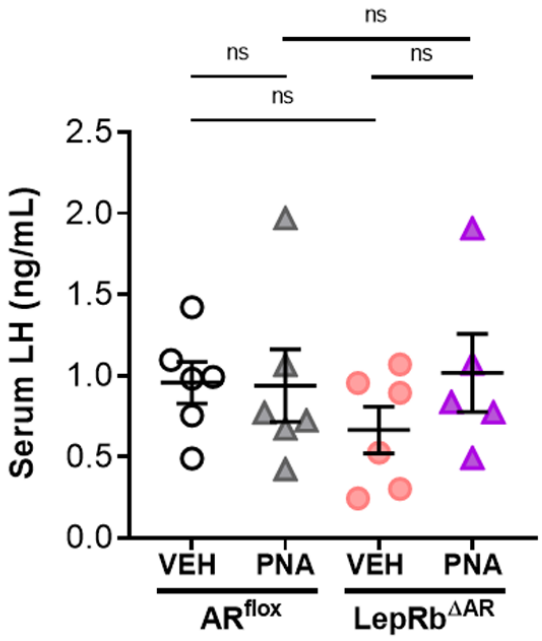

Figure 4.7: Serum LH concentrations. Scatter plot graph of serum levels of luteinizing hormone (LH) at time of sacrifice during the morning of diestrus. Data presented as mean ± SEM and analyzed by two-way ANOVA with Holm-Sidak correction. No difference in serum LH was found between groups.

CHAPTER 5

Conclusions

Overview

Androgens are essential hormones in both male and female physiology, with effects on multiple systems. Imbalance of androgens outside the homeostatic range has both reproductive and metabolic consequences for both sexes. In the second chapter, we show that the brain is a highly androgen-responsive organ, and expresses the androgen receptor (AR) during a critical window of prepubertal development in male and female mice. We further describe brain regions that may preferentially respond to androgens, rather than estrogens. For example, the ventral premammillary nucleus (PMv) shows dense expression of AR in both sexes, yet it is relatively low in ERs, and the enzyme aromatase. Since AR was heavily expressed in areas with known contribution to the regulation of metabolism and reproduction, particularly nuclei that densely express the leptin receptor (LepRb), we conducted a thorough characterization of the expression of AR in LepRb cells in mice. Major coexpression of LepRb and AR was observed in the arcuate (ARH) and PMv of both sexes. Deletion of AR from LepRb cells, causes sex-specific changes in the neuroendocrine reproductive axis, locomotor activity, and body composition. We further evaluated if deletion of AR from LepRb neurons protects female mice from hyperandrogenism-induced reproductive deficits in a model of prenatal androgen excess. We found that deletion of AR from metabolic and reproductively relevant LepRb neurons improved estrous cycles in prenatally androgenized female mice. Our findings highlight that LepRb neurons represent an

important target of androgen action in the brain, particularly with regards to regulation of the hypothalamic-pituitary-gonadal axis and some aspects of metabolic regulation. In previous chapters, I discussed the relevance of all the specific findings of my studies and the contribution to the field. In this chapter, I will focus on the limitations of our studies, propose alternatives and future directions

Limitations of Animal Models and Proposed Alternative Approaches

The Cre/loxP mouse model used in these studies was effective in reducing AR expression in LepRb-Cre cells. However, since LepRb is expressed during embryonic development (1,2), Cre-induced deletion of AR occurred during active periods of neurogenesis and organization of the nervous system. We did not observe a difference in the number of LepRb neurons in $LepRb^{\Delta AR}$ mice, although it is possible other receptors could compensate for the loss of AR (i.e., ERα/β, GPER). Therefore, it is possible that deletion of AR in LepRb neurons in adulthood may induce a stronger phenotype as observed in other hypothalamic systems. For example, mice with embryonic deletion of AgRP only show minor differences in feeding behavior, yet mice with adult deletion of AgRP show drastically reduced food intake, leading to starvation (3). Furthermore, deletion of AR during embryonic development does not allow for the examination of the effects of androgens during different periods of development and maturation. This deficiency became clear when we compared results from distinct experiments. In chapter 3, we observed that $LepRb^{\Delta AR}$ female mice only developed changes in lean mass later in adult life, whereas in chapter 4, $LepRb^{\Delta AR}$ female mice exposed to androgen excess during embryonic development showed improvements in estrous cycles during adulthood. It will be important to determine if AR is deleted from LepRb neurons during DHT treatment, from E16-E18.

Additionally, with deletion of AR from all LepRb-expressing cells, it is difficult to determine the specific nucleus and/or neurons that are responsible for the observed phenotype of LepRb$^{\Delta AR}$ mice. To overcome the limitations of a conditional Cre model, CRISPR (clustered regularly interspaced short palindromic repeats)-Cas9 technology can be used to temporally and spatially refine the deletion of AR. The endonuclease CRISPR-associated protein 9 (Cas9) in the presence of a guide RNA, recognizes the corresponding sequence of target DNA, inducing double-stranded breaks which, when repaired by nonhomologous end-joining, results in genomic insertions or deletions, frame-shift mutations, and knockout of a target sequence (4). Stereotactic delivery of an AAV vector containing guide RNA targeting AR injected into specific hypothalamic nuclei (i.e., ARH or PMv) of LepRb^{Cre};lox-STOP-lox-Cas9 mice (5) will result in excision of AR from only Cas9-expressing LepRb neurons. This approach will restrict deletion of AR to LepRb neurons of specific nuclei in prepubertal or adult mice, allowing for a more precise interpretation of the role of AR in distinct hypothalamic nuclei and their individual contribution to the regulation of metabolism and reproduction. This approach will not allow, however, evaluation of the effects of AR deletion in developing mice.

In our studies, we have used a mouse model with deletion of exon 2 of *Ar*, resulting in a premature stop codon and severely truncated protein. Theoretically, expression of only exon 1 and the N-terminal it encodes, could result in a fragment of AR capable of interacting with other signaling pathways. Ligand-independent activation of AR through the N-terminal domain is possible via MAPK and JAK/STAT3 (6). However, it is unlikely that the AR N-terminal remains in LepRb$^{\Delta AR}$ mice, because the anti-AR antibody used to validate deletion of AR in LepRb-Cre cells targets the

N-terminal of AR (7). We observed a very low percentage of cells expressing Cre-induced reporter gene and AR-ir in LepR$^{\Delta AR}$ mice. While well-defined AR genomic and membrane signaling via alternative pathways is reduced in exon 2 knockouts, novel non-AR receptors that are activated by androgens (i.e., TRPM8, OXER1, GPRC6A, and/or ZIP9) may still allow for androgenic effects. Further work is needed to characterize the multiple pathways by which androgens can modulate intracellular signal transduction, and the specific consequences of each pathway.

Impacts of Androgen Excess in Females

The PNA mouse model replicates many of the reproductive characteristics experienced by patients with polycystic ovary syndrome (PCOS), including acyclicity and altered neuroendocrine output from the HPG axis. Reduced fertility has also been reported in PNA female mice (8,9). However, PNA mice display a narrowed vaginal opening due to timing of androgen excess on development of the external genitalia. The narrowed vaginal opening in PNA females may impact copulation and hinders parturition, preventing analysis of fertility in our model.

A significant portion of PCOS patients also exhibit metabolic abnormalities, including obesity, insulin resistance, and type 2 diabetes. However, these metabolic changes are not replicated with exposure to androgen excess during late fetal development in rodents. Treatment of female mice at PND21 with the non-aromatizable androgen DHT also induces a PCOS-like phenotype in mice (10). These pre-pubertal androgenized (PPA) female mice exhibit acyclicity, anovulation, a polycystic ovary phenotype, and show changes in metabolic physiology, including body mass, adiposity impaired glucose tolerance and dyslipidemia (10-14). The PPA mouse model is useful for studies focused on a subpopulation of PCOS patients with metabolic dysfunction, and may be

more relevant in studies focused on LepRb neurons that are critical in regulation of body mass and adiposity. Determining if LepRb$^{\Delta AR}$ female mice exposed to androgen excess peripubertally show a similar protection in estrous cycles as PNA LepRb$^{\Delta AR}$ mice would be informative and warrants further investigation. Additionally, it would be important to evaluate if deletion of AR from LepRb neurons protects from the increases in body mass and adiposity seen in PPA mice. The PPA mouse model would also allow for evaluation of fertility.

The effects of androgen excess during critical fetal and pubertal windows of development on female reproductive physiology have been well described. However, there are few animal models used to investigate the effects of androgen excess in adult females. Treatment of adult female mice with DHT will allow for the further distinction between the roles of androgens acting during critical windows of permanent developmental organization and pubertal activation compared to actions on adult reproductive and metabolic physiology. This strategy will more closely mimic those who experience androgen excess during adult life, and can distinguish which changes are permanent or reversible.

Potential Mechanisms of AR Action in LepRb-Expressing Cells

While we have shown that deletion of AR from LepRb cells impacts typical physiology, the intracellular mechanism underlying the AR and LepRb interaction has yet to be determined. The LepRb contains an intracellular signaling domain, capable of activating different signaling pathways, including JAK/STAT3 or STAT5, PI3K/AKT, MAPK, and AMPK (15). It has been indicated that T can interact with tyrosine residue 985 of LepRb, which facilitates inhibitory actions through SHP2 and SOCS3 (16). Additionally, AR has the ability to enhance LepRb-

induced STAT3 signaling in vitro (17). Further studies are needed to evaluate if the regulatory mechanisms that exist between AR and LepRb are also observed *in vivo*.

Final Conclusions

I have shown here that LepRb neurons are an important target of androgen action in the hypothalamic control of the reproductive neuroendocrine axis and some aspects of metabolic regulation, and that AR in LepRb neurons may play a role in the pathogenesis of PCOS. Additional work will be needed to characterize the different neurochemical phenotypes of AR-expressing neurons, and to delineate their role in reproductive and metabolic physiology. A complete understanding of the cell-, tissue-, and organ-specific effects of androgens is fundamental for developing better treatments for those experiencing hypo or hyperandrogenism, as well as for gender-affirming hormone therapy designed for transmen taking T, or transwomen taking AR antagonists. Further defining the targets of androgen action via AR in the brain will contribute to a better understanding of the neuroendocrine control of reproduction and metabolism, and will open opportunities for development of therapeutic interventions to overcome disorders of androgen excess or deficiency.

References

1. Hoggard N, Hunter L, Duncan JS, Williams LM, Trayhurn P, Mercer JG. Leptin and leptin receptor mRNA and protein expression in the murine fetus and placenta. Proceedings of the National Academy of Sciences 1997; 94:11073-11078

2. Udagawa J, Hatta T, Naora H, Otani H. Expression of the long form of leptin receptor (Ob-Rb) mRNA in the brain of mouse embryos and newborn mice. Brain Res 2000; 868:251-258

3. Luquet S, Perez FA, Hnasko TS, Palmiter RD. NPY/AgRP Neurons Are Essential for Feeding in Adult Mice but Can Be Ablated in Neonates. Science 2005; 310:683-685

4. Jiang F, Doudna JA. CRISPR–Cas9 Structures and Mechanisms. Annual Review of Biophysics 2017; 46:505-529

5. Platt Randall J, Chen S, Zhou Y, Yim Michael J, Swiech L, Kempton Hannah R, Dahlman James E, Parnas O, Eisenhaure Thomas M, Jovanovic M, Graham Daniel B, Jhunjhunwala S, Heidenreich M, Xavier Ramnik J, Langer R, Anderson Daniel G, Hacohen N, Regev A, Feng G, Sharp Phillip A, Zhang F. CRISPR-Cas9 Knockin Mice for Genome Editing and Cancer Modeling. Cell 2014; 159:440-455

6. Ueda T, Bruchovsky N, Sadar MD. Activation of the Androgen Receptor N-terminal Domain by Interleukin-6 via MAPK and STAT3 Signal Transduction Pathways *. Journal of Biological Chemistry 2002; 277:7076-7085

7. RRID:AB_11156085.

8. Witham EA, Meadows JD, Shojaei S, Kauffman AS, Mellon PL. Prenatal exposure to low levels of androgen accelerates female puberty onset and reproductive senescence in mice. Endocrinology 2012; 153:4522-4532

9. Moore A, Prescott M, Campbell R. Estradiol Negative and Positive Feedback in a Prenatal Androgen-Induced Mouse Model of Polycystic Ovarian Syndrome. Endocrinology 2012; 154

10. Caldwell AS, Middleton LJ, Jimenez M, Desai R, McMahon AC, Allan CM, Handelsman DJ, Walters KA. Characterization of reproductive, metabolic, and endocrine features of polycystic ovary syndrome in female hyperandrogenic mouse models. Endocrinology 2014; 155:3146-3159

11. Caldwell ASL, Edwards MC, Desai R, Jimenez M, Gilchrist RB, Handelsman DJ, Walters KA. Neuroendocrine androgen action is a key extraovarian mediator in the development of polycystic ovary syndrome. Proceedings of the National Academy of Sciences of the United States of America 2017; 114:E3334-E3343

12. van Houten EL, Kramer P, McLuskey A, Karels B, Themmen AP, Visser JA. Reproductive and metabolic phenotype of a mouse model of PCOS. Endocrinology 2012; 153:2861-2869

13. Nohara K, Laque A, Allard C, Munzberg H, Mauvais-Jarvis F. Central mechanisms of adiposity in adult female mice with androgen excess. Obesity (Silver Spring) 2014; 22:1477-1484

14. Kanaya N, Vonderfecht S, Chen S. Androgen (dihydrotestosterone)-mediated regulation of food intake and obesity in female mice. J Steroid Biochem Mol Biol 2013; 138:100-106

15. Villanueva EC, Myers MG, Jr. Leptin receptor signaling and the regulation of mammalian physiology. Int J Obes (Lond) 2008; 32 Suppl 7:S8-12

16. Johnson JA, Calo S, Nair L, IglayReger HB, Greenwald-Yarnell M, Skorupski J, Myers MG, Jr., Bodary PF. Testosterone interacts with the feedback mechanisms engaged by Tyr985 of the leptin receptor and diet-induced obesity. J Steroid Biochem Mol Biol 2012; 132:212-219

17. Fan W, Yanase T, Nishi Y, Chiba S, Okabe T, Nomura M, Yoshimatsu H, Kato S, Takayanagi R, Nawata H. Functional potentiation of leptin-signal transducer and activator of transcription 3 signaling by the androgen receptor. Endocrinology 2008; 149:6028-6036

APPENDIX A

LIST OF ABBREVIATIONS

Name	Abbreviation
Androgen receptor	AR
Androgen receptor knockout	ARKO
Balanopreputial separation	BPS
Corpus luteum/corpora lutea	CL
Dopamine transporter	DAT
Estrus	E
Enhanced green fluorescent protein	eGFP
Estrogen receptor, alpha	ERα
Estrogen receptor, beta	ERβ
Granulosa cell	GC
Hypothalamic-pituitary-gonadal	HPG
Leydig cell	LC
Leptin receptor, b isoform	LepRb
Metestrus/Diestrus	M/D
Oocyte	oo
Proestrus	P
Polycystic ovary syndrome	PCOS
Prenatal androgenization	PNA
Postnatal day	PND
Sertoli cell	SC
Theca cell	TC
Testicular feminization	Tfm
Vehicle treated	VEH
Vaginal opening	VO
Brain Regions	**Abbreviation**
Anterior cingulate cortex, dorsal	ACAd
Anterior cingulate cortex, ventral	ACAv
Nucleus accumbens	ACB
Anterodorsal nucleus of the thalamus	AD
Anterior hypothalamic nucleus	AHN
Alveus	alv
Nucleus ambiguus	AMB
Olfactory nucleus, anterior	AON

Area postrema	AP
Cerebral aqueduct	AQ
Arcuate hypothalamic nucleus	ARH
Anteroventral nucleus of the thalamus	AV
Anteroventral periventricular nucleus	AVPV
Bed nucleus of stria terminalis, principal nucleus	BSTpr
Central canal of the medulla	c
Field CA1	CA1
Field CA2	CA2
Field CA3	CA3
Arcuate hypothalamic nucleus, caudal	cARH
Corpus callosum	cc
Genu of corpus callosum	ccg
Cochlear nuclei	CN
Cortical amygdalar area	COA
Cerebral peduncle	cpd
Dentate gyrus	DG
Dorsomedial nucleus of the hypothalamus	DMH
Dorsal motor nucleus of vagus nerve	DMX
Dorsal nucleus raphe	DR
Dorsal tegmental nucleus	DTN
External medullary lamina of the thalamus	em
Entorhinal area	ENT
Endopiriform	EP
Fasiculus retroflexus	fr
Fornix	fx
Induseum griseum	IG
Intermediate reticular nucleus	IRN
Lateral hypothalamic area	LHA
Lateral olfactory tract	lot
Lateral reticular nucleus	LRN
Lateral septal nucleus, caudodorsal	LSc
Lateral septal nucleus, rostroventral	LSr
Arcuate hypothalamic nucleus, mid/tuberal	mARH
Magnocellular reticular nucleus	MARN
Medial amygdalar nucleus, posterodorsal	MEApd
Medial geniculate complex	MG
Medial lemniscus	ml
Motor cortex	MO
Secondary motor area	MOs
Medial preoptic nucleus	MPN
Medial preoptic area, anterior	MPOa
Medial preoptic area, posterior	MPOp
Medial septal nucleus	MS
Medial vestibular nucleus	MV

Nucleus of the solitary tract	NTS
Optic tract	opt
Olfactory tubercle	OT
Vascular organ of the lamina terminalis	OVLT
Posterior amygdala	PA
Periaqueductal gray, ventrolateral	PAGvl
Parabrachial nucleus	PB
Parafasicular nucleus	PF
Piriform	PIR
Dorsal premammillary nucleus	PMd
Ventral premammillary nucleus	PMv
Presubiculum / Subiculum	PRE/SUB
Pontine reticular nucleus	PRN
Nucleus prepositus	PRP
Principal sensory nucleus of the trigeminal	PSV
Parataenial nucleus	PT
Periventricular hypothalamic nucleus	PV
Paraventricular hypothalamic nucleus	PVH
Paraventricular nucleus of the thalamus	PVT
Pyramid	pyr
Arcuate hypothalamic nucleus, rostral	rARH
Nucleus of reuniens	RE
Rhomboid nucleus	RH
Red nucleus	RN
Subparaventricular zone	SBPV
Suprachiasmatic nucleus	SCH
Ventral spinocerebellar tract	sctv
Subfornical organ	SFO
Septohippocampal nucleus	SH
Stria medullaris	sm
Spinal nucleus of the bulbocavernosus	SNB
Superior olivary complex	SOC
Stria terminalis	st
Subthalamic/ Parasubthalamic, caudal	STN/PSTN
Supramammillary nucleus	SUM
Taenia tecta	TT
Tuberal nucleus	TU
Third ventricle	V3
Fourth ventricle	V4
Facial motor nucleus	VII
Facial nerve	VIIn
Lateral ventricle	VL
Ventromedial hypothalamic nucleus, central	VMHc
Ventromedial hypothalamic nucleus, dorsomedial	VMHdm
Ventromedial hypothalamic nucleus, ventrolateral	VMHvl

Ventral medial nucleus of the thalamus	VMHvl
Vestibular Nucleus	VNC
Ventral posterior complex of the thalamus	VP
Ventral tegmental area	VTA
Hypoglossal nucleus	XII
Zona incerta	ZI
Hormones/Peptides	**Abbreviation**
Agouti-related peptide	AgRP
Anti-Mullerian Hormone	AMH
Cocaine- and amphetamine-regulated transcript	CART
Dihydrotestosterone	DHT
Follicle stimulating hormone	FSH
Gonadotropin releasing hormone	GnRH
Insulin-like growth factor 1	IGF1
Kisspeptin/neurokinin/dynorphin	KNDy
Luteinizing hormone	LH
Neuropeptide Y	NPY
Pro-opiomelanocortin	POMC
Testosterone	T
Methods Related	**Abbreviation**
Association for Assessment and Accreditation of Laboratory Animal Care	AAALAC
Avidin-biotin	AB
Analysis of variance	ANOVA
Area under the curve	AUC
Comprehensive Laboratory Monitoring System	CLAMS
Diethyl pyrocarbonate	DEPC
Dithiothreitol	DTT
Energy expenditure	EE
Enzyme-linked immunosorbent assay	ELISA
Gonadectomy	GDX
Glucose tolerance test	GTT
Haematoxylin and eosin stain	H&E
High fat diet	HFD
Institutional Animal Care and Use Committee	IACUC
Integrated optical density	IOD
Immunoreactivity	ir
Lean body mass	LBM
Liquid chromatography–mass spectrometry	LC/MS
Neutral buffered formalin	NBF
Optimal cutting temperature compound	OCT
Orchidectomy	ORX
Ovariectomy	OVX
Phosphate-buffered saline	PBC

Quantitative polymerase chain reaction	qPCR
Region of interest	ROI
Real-time polymerase chain reaction	RT-PCR
Standard error of the mean	SEM
Sodium chloride-sodium citrate buffer	SSC
Tyramide signal amplification	TSA
Volume carbon dioxide produced	VCO2
Volume oxygen consumed	VO2